University of Strathclyde Science

Metabolomic profiling of the maternal foetal interface and developing foetus during *Toxoplasma gondii* infection

By

Hafiz Muhammad Arshad

A thesis submitted to the University of Strathclyde in partial fulfilment of the requirements for the degree of Doctor of Philosophy

2022

University of Strathclyde

‘I declare that, except where specifically indicated, all the work presented in this thesis is my own and I am the sole author of all the parts.’

Signed:

Date:

Acknowledgements

First and foremost, I would like to thank Allah (SWT) for giving me the strength, knowledge, ability and opportunity to perform this research study.

I would like to express my sincere gratitude to my supervisor, Professor Craig William Roberts, for his continuous support, motivation and enlightening me throughout the process of achieving this scientific milestone. His valuable guidance helped me to go through all hurdles while conducting research and writing the thesis. I could not have imagined having a better supervisor and mentor than him. I am extremely thankful to Dr Gareth Westrop for his invaluable advice, continuous support, and patience during my PhD study. I am out of words to say enough thanks to him for his transferable skills in mass spectrometry and analytical skills regarding metabolomics data.

I offer my heartiest appreciation to the collaborators of this research work, Margarida Borges and her colleagues at the University of Porto, Portugal. Their professional expertise and timely inputs remained very helpful to carry out this study.

My sincere thanks goes to the staff members of the Biological Procedures Unit, whose technical advice on animal care, following the guidance of the Home Office procedures, was a significant contribution towards the fulfilment of this study.

I express my gratitude to fellow members of Robert's laboratory - Stuart Woods, Alemao Carpinteyro, Aisha Abdussalam, Jonathan McGahon and Alonaizan Rasha - for their constructive engagement throughout the process and for making this journey memorable.

I want to extend a heartfelt thanks to my wife Shabana Sheikh, my daughter Bareera, and my son Abdullah, for their understanding of time constraints and unconditional love. I am

incredibly grateful to my father, mother, brother, and sisters for their continuous support and encouragement to follow my dreams.

I am thankful to Bahauddin Zakariya University, Pakistan, for granting leave for this study as well as for their financial support. I am equally thankful to the University of Strathclyde for financial support and for providing excellent resources for this study.

Dedication

This thesis is dedicated to my father for his endless support, love and encouragement.

Abstract

T. gondii infection during pregnancy can cause abortion or congenital disease. Events in the maternal-foetal interface, where immunological changes occur, are critical in determining the pregnancy outcome. Several studies cover the serum biochemical/metabolic changes following *T. gondii* infection, but limited information exists concerning changes to the placental metabolome or the foetus while in utero. For the first time, this study covers the metabolomic profile and potential underlying mechanisms in the maternal-foetal interface, the developing foetus and maternal serum in BALB/c mice in a *T. gondii* congenital infection model. Results demonstrate the highest number of metabolite changes in the maternal serum, however a subset of these changes to tryptophan degradation pathway, arginine metabolic pathway was also found in the maternal-foetal interface and the developing foetus. In addition, some metabolites from microbiome origin including indoxylsulfate and 4-guanidinobutanoate were changed compared with the controls, suggesting the potential of *T. gondii* to change the host microbiome. However, preliminary metagenomics analysis did not demonstrate such changes, albeit in a different model of *T. gondii* infection. Comparison of alterations of metabolites between the developing foetus and the brain from adult mice born to infected mothers was carried out to determine whether the changes observed in early foetal life were still evident in later life. The most significant finding of this study is that increased kynurenine levels are found in early foetal life. This metabolite was found to be increased in the brains of adult mice with congenital *T. gondii* infection, but not in uninfected litter mates exposed to maternal-immune activation. This suggests that raised kynurenine levels in foetuses in utero might be maternally derived and short lived, but ultimately endogenously produced in congenitally infected mice. This metabolite has been implicated in psychoneurological diseases, but the consequences of kynurenine exposure in these circumstances remain to be determined.

Abbreviations

AIDS	Acquired immunodeficiency syndrome
AIM2	Absent In Melanoma 2
APC	Antigen presenting cells
CARD	Caspase recruitment domains
CCAAT	CCAAT-enhancer-binding proteins
CCR5	Chemokine Receptor 5
C-rel	Proto oncogene c-Rel
CSF-1	colony stimulating factor 1
CXCL1	chemokine (C-X-C motif) ligand 1
CXCL4	Platelet factor 4
DC	Dendritic cells
dNK cells	Decidual NK cells
EVTS	Extra-villous trophoblast
GIA	Gestational age
GIRA	Galley Iodine Removal Assembly
GITpases	guanosine triphosphate
IDEOM	identification and evaluation of metabolomics data
IFN	Interferon
IL	Interleukin
IMC	inner membrane complex
ISP1	Implantation serine proteinase 1
ISP3	Implantation serine proteinase 3
IVN	Intravacuolar network
LC3	Microtubule-associated protein 1A/1B-light chain 3
MAPK	mitogen activated protein kinase
MHC	Major histocompatibility complex
MyD88	myeloid differentation primary response 88
NF-KB	Nuclear factor Kappa B

NK cells	Natural killer cells
NLR	Nucleotide-binding/leucine-rich repeat
NLRP1	NLRP1
NMT	N-myristoyl transferase
P2X7R	P2X purinoceptor 7
PAT	Palmitoyl acetyltransferase
pNK cells	Peripheral natural killer cells
PRR	Pattern recognition receptor
PV	Parasitophorous vacuole
ROP	retinopathy of prematurity
ST	Sycytiotrophoblast
T.gondii	Toxoplasma gondii
TgERP	T.gondii embryogenesis related protein
TgFBX01	T. gondii F box protein 1
TH1	Type 1 response
TH2	Type 2 response
TLR	Toll like receptors
TRAF-6	Tumour necrosis factor 6
UNC93B	Unc-93 homolog B1
uNK cells	Uterine NK cells

Table of contents

Contents

List of figures

List of tables

1- Introduction

1.1 Toxoplasma gondii

T. gondii is classified as a single celled coccidian protozoan parasite. It was named after the Gondi, a rodent from North Africa, and was first described by Nicolle and Manceaux in 1908. The parasite was soon recognised as a zoonotic agent. This intracellular parasite can infect humans as well as all warm-blooded animals, including birds and mammals. The parasite is therefore of medical and veterinary importance and for this reason, is one of the most studied unicellular organisms. This is an intracellular holoparasite, hence it must live & reproduce within an animal cell.

Scientifically, this protozoan parasite can be classified as following:

Domain	Eukaryote
Phylum	Apicomplexa
Class	Conoidasida
Order	Eucoccidiorida
Family	Sarcocystidae
Sub-family	Toxoplasmatinae
Genus	Toxoplasma
Species	*Gondii*
Binominal name	*T. gondii*

The zoonotic importance for humans was unclear until the first reports of cases of the congenital toxoplasmosis (Schwartzman et al., 1948). The study of *T. gondii* became more interesting for immunologists, when there was acknowledgement in mid-1970 about the role of *T. gondii* infection in immunocompromised patients.

1.1.1: Morphology

The shape of this parasite is slightly bent and oval with an anterior end and a posterior end. Anterior end is pointed while the posterior end is rounded in shape. The body is covered by two layers of pellicle, with a thickness of 30-50 mμ. there is a special organelle called a conoid consisting of a polar ring with a diameter

of 0.25- 0.30 μ and an interior cone lying into the cytoplasm (Dubey, 2008). The nucleus is in the middle of the body with a size of about 1-2 μ, covered by a very thin doublemembrane and a large nucleolus. In the posterior part of the body, there is a hollow mitochondrion with a diameter of 0.13-0.15 μ, a Golgi complex consisting of very thin fibres of 15-20 mμ lying on the anterior side of the nucleus. Among other cell organelles, there is an endoplasmic reticulum having long tubes of about 15 mμ thickness (Ludvik, 1958).

During its different phases of life, it undergoes various cellular and developmental stages. Each cellular stage has a distinct morphology. These stages are named as tachyzoite, merozoite bradyzoite and sporozoite.

Tachyzoites are a motile and rapidly multiplying stage, responsible for the proliferation of the parasite population. Upon consumption of the tissue cyst or an oocyst (containing bradyzoites and sporozoites, respectively), both these stages convert into the tachyzoites. This process takes place in the intestinal epithelium of the host. Tachyzoites are mainly responsible for the acute type of infection, as it proliferates throughout the body via blood circulation (Kim and Weiss, 2004). These tachyzoites convert into the bradyzoite stage during latent stages of infection.

Bradyzoites are a very slow proliferative stage of the parasite leading to the formation of tissue cysts. Also, tissue cysts measuring 10-100μm in diameter are surrounded by a very thin primary cyst wall and contain hundreds of basophilic bradyzoites (measuring 3-4 by 1-2μm). Upon

ingestion of these tissue cysts, bradyzoites are released and infect epithelial cells of the host (Kim and Weiss,2004).

Merozoites are also a fast replicating stage and is accountable for the population expansion of this protozoan. This replication takes place before sexual reproduction in the feline (cat) intestine. After consumption of a tissue cysts (containing bradyzoites) by the feline host, these bradyzoites convert into the merozoites inside the intestinal epithelial cells (Kim and Weiss, 2004). Following this short period of fast dividing and population growth, these merozoites are converted to non-infectious stages and undergo sexual reproduction, leading to the formation of zygote containing oocysts (Kim and Weiss, 2004). Oocysts are small ovoid stages (10-13 x 9-11µm) and contain two round sporocysts, each containing four elongated sporozoite (Rojas-Pirela et al., 2021). These sporozoites are the residing stage of the parasite within oocysts. Whenever an oocyst is consumed by any warm blooded animal, these sporozoites are released and infect the epithelial cells before consequently converting into the rapidly dividing proliferative stage of tachyzoites (Kim and Weiss, 2004).

1.1.2: Infectious stages

Previously, it has been established that there are three infectious stages of *T. gondii* which were identified as sporozoites, tachyzoites and bradyzoites (Dubey et al., 2005). These infective stages are crescent shaped cells ranging in size from 5µm in length to 2µm in width along with a pointed apical end and a round posterior end. These are bound by a membrane called pellicle and possess a nucleus, mitochondria, golgi complex, ribosomes, endoplasmic reticulum and an apicoplast (Dubey et al., 2005).

Tachyzoites are reported to be present in acute infection and they undergo the effects of a process called endodyogeny which provides the means of fast replication (after every 6-8 hours). They are unique in character as they can invade all vertebrate cells and replicate.

Moreover, this replication takes place in the parasitophorous vacuole. The intracellular growth of this parasite is profoundly influenced and mainly relies on this parasitophorous vacuole (Mordue *et al*. 1999, Angela *et al*. 2007). Surprisingly, tachyzoites have been successfully used to initiate infection via oral administration, but other routes of infection should/are most normally used to induce infection in the murine model e.g., intraperitoneal, subcutaneous or intravenous routes of injection (Edina and Constance, 2017). Tachyzoites are also the likely stages responsible for natural congenital transmission.

In contrast to the above, bradyzoites are prevalent in chronic infection. They are slow replicating and as a result of this replication, vacuoles having bradyzoites mature into thick walled cysts consisting of a number of proteins and glycoproteins. One such glycoprotein, CST1, is believed to play an important role in stability and protection of cyst from the immune response of the host (Zhang, Halonen *et al*. 2001). It is evident from a previous study that bradyzoites can be detected in the brain following 3 days of infection. These are spheroid in brain cells and elongated in muscle cells. With relation to persistency, it was established a long time ago that cysts with sustainable bradyzoites are viable for a long time and in some cases perhaps for the lifetime of the host cells (Ferguson & Hutchison 1987; Frankel 1988).

The sporozoite is an environmental stage present inside mature oocyst. Oocyst are 12 to 13 µm ovoid structures. The parasite is protected from any physical or chemical damage due to the multi-layered structural design of its cell wall. This configuration of the cell walls accounts for the survival of the parasite for longer periods, up to more than a year, in a moist environment (Mai *et al*. 2009).

1.1.3: Life cycle of *T. gondii*

The life cycle of *T. gondii* involves a complex mechanism of various stages. It has since been established that cats are definitive hosts and other warm blooded animals act as an intermediate host. *T. gondii* is classified as a cyst forming coccidian which functions in a prey predator system. This system switches between definitive and intermediate hosts. Sexual reproduction of *T. gondii* occurs within the intestine of the definitive host, while intermediate hosts can only support asexual reproduction. This can be seen as unique since transmission can occur from the intermediate to the definitive hosts via carnivorism, from the definitive hosts to the intermediate or definitive hosts through ingestion of oocyts released in the feces and between intermediate hosts via carnivorism. Importantly, asexual and sexual cycles and transmission dynamics differ in various environments. This arises due to the physical characteristics as well as the structure of intermediate and definitive host populations (Alfonso *et al*.,2006).

1.1.3.1 Definitive hosts

Sexual reproduction occurs in both domestic and wild cats. Following cyst ingestion which is located in tissues of intermediate hosts, gastric enzymes destroy the cyst walls (Mondragon et al., 1998). Subsequently, bradyzoites invade and reside within enterocytes where self-limiting asexual multiplications occur (Mondragon et al., 1998). This results in the formation of merozoites within schizonts (Mondragon et al., 1998). The next step involves sexual development where production of male and female gametes occur. Once fertilization is complete, oocysts produced within enterocytes are freed via cell disruptions (Mondragon et al., 1998). These are then excreted as unsporulated forms within cat faeces (Ferguson et al., 2002). As a result of meiotic reproduction and morphological changes during a process termed sporulation this gives rise to sporulated oocysts which contain two sporocysts (Ferguson et al., 2002). These sporocysts contain four haploid sporozoites. Shedding of oocysts occurs within 3-7 days after tissue cyst ingestion and can continue up to 20 days (Jones and Dubey, 2010). Statistics indicate that infected cats possess the ability to shed more than 100 million oocysts

in their faeces (Jones and Dubey, 2010). These may infect a diverse variety of intermediate hosts such as warm-blooded animals which are then consumed as food.

1.1.3.2 Intermediate hosts

An asexual part of the life cycle of this protozoan takes place in intermediate hosts. Infection normally is initiated by ingestion of tissue cysts or oocysts. Following oocyst ingestion, sporozoites are released. These enter the intestinal epithelium where differentiation occurs into tachyzoites. These then undergo multiple rapid replication via endodyogeny which occurs inside any cell type thus allowing dissemination through the organism. Consequently, tissue cysts appear within 7-10 days following infection and may potentially remain within hosts throughout their life (Robert-Gangneux and Dardé, 2012). This usually occurs within the brain or muscle cells. Following tissue cyst ingestion through sources such as undercooked or raw meat, cysts burst as they migrate through the digestive tract thus resulting in the release of bradyzoites. These bradyzoites then infect the intestinal epithelium of the new host. Rapid differentiation occurs again as the tachyzoite stage resulting in dissemination through the body. A point of interest is that if an acute infection occurs during pregnancy, parasites may cross the placenta and result in the infection of the foetus. This is called as congenital transmission. It has already been concluded that this vertical transmission may result in a severe infection in some species (Duncanson et al., 2001). The life cycle of this parasite is shown in the following figure 1.1.

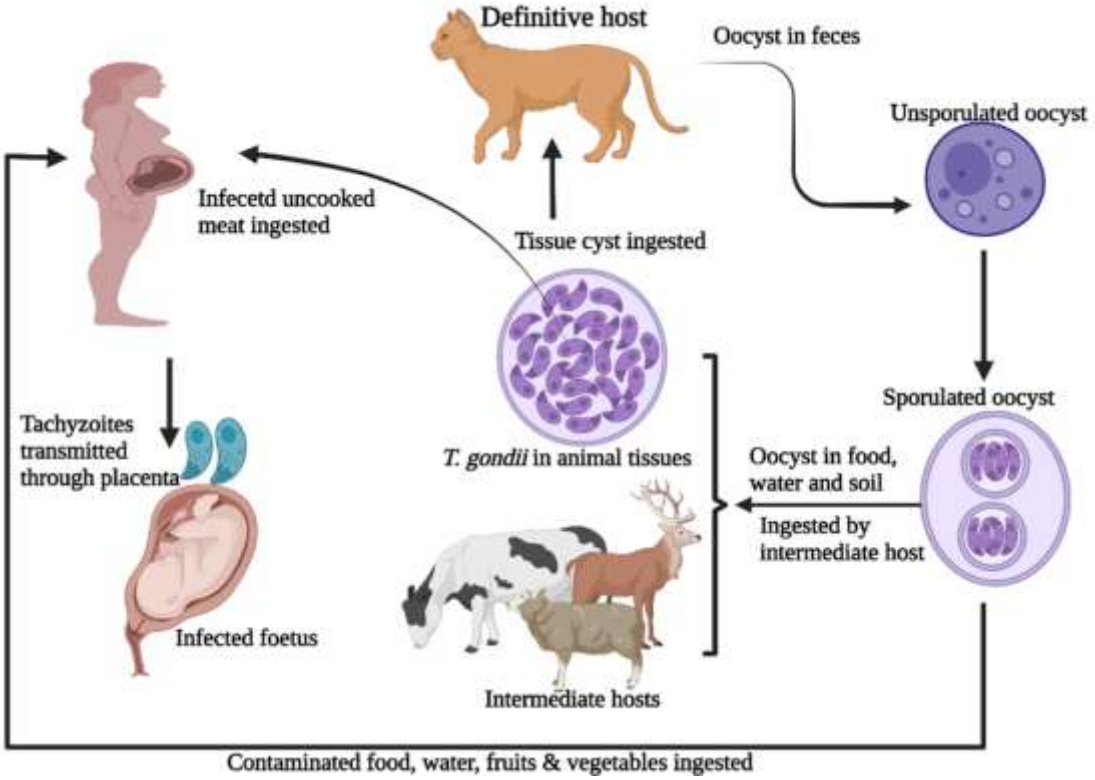

Figure 1.1 Life cycle & transmission of Toxoplasma gondii

The sexual stage of *T. gondii* occurs only inside the definitive host which could be any member of the family Felidae, most probably in cats. After the ingestion of the cysts or oocysts, an asexual followed by a sexual reproduction takes place and oocysts are released.

1.1.3.3 Tachyzoite-Bradyzoite interconversion

An interesting fact reviewed by Lyons and Roberts demonstrated that the infective stages i.e. tachyzoite and bradyzoite (responsible for acute toxoplasmosis and chronic toxoplasmosis, respectively) are interconvertible (Lyons et al., 2002a). Tachyzoites are responsible for the initiation of an acute infection. After almost two weeks of initial infection, these tachyzoites are differentiated into bradyzoites, a very slowly replicating form and they form cysts throughout the body known as tissue cysts. In immunocompromised individuals these tissue cysts may be disrupted and bradyzoite may again converted to tachyzoite which results in disease reactivation (Lyons et al., 2002b). This interconversion and some of the known stimuli responsible for this can be shown in the figure 1.2.

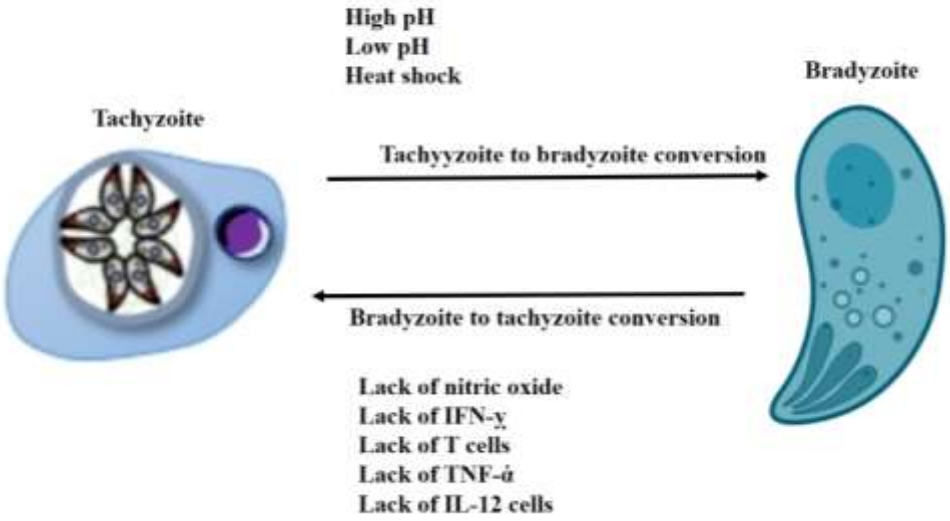

Figure 1. 2 Factors affecting interconversion of bradyzoite and tachyzoites. The process of stage conversion is reversible. Bradyzoites are responsible for chronic disease while tachyzoites are formed in case of disease reactivation (adopted from Lyons et al., 2002b).

It is important to note that the movement of this parasite occurs via a process called gliding activity, with the help of this activity, the parasite penetrates in tissues and different biological barriers of the host (Skariah et al., 2010).

1.2 Toxoplasmosis

The disease caused by *T. gondii* is toxoplasmosis which is considered a multi-faceted disease of animals as well as human beings. This parasite also referred to as mind-altering parasite as it is known to affect the behaviours of rodents which develop a decreased aversion towards cat's urine and become easily preyed (Berdoy et al., 2000). However, the mode of action by which the parasite affects human behaviours is more controversial (Henriquez et al., 2009). In immunocompetent individuals, disease is asymptomatic or symptoms are self-limiting which may include fever and lymphadenopathy and occasionally occur within a few weeks of exposure. Despite disease often being asymptomatic and latent, many studies demonstrate that it can be pathological and even fatal in immunocompromised individuals (Moncada and Montoya, 2012). This is particularly evident in AIDS/HIV patients where it can cause splenomegaly, hydrocephaly, cerebral calcifications, hearing loss, pneumonitis, organ failure, blindness, sometime systemic disease and ultimately death if not treated (Moncada and Montoya, 2012).

1.2.1: How does human infection occur?

It is a well-established fact that the majority of horizontal transmissions to humans is either due to the ingestion of tissue cysts in infected meat or by the ingestion of soil, water or food contaminated with oocysts (Cook et al., 2000). Humans may be unaware of the risks posed or may have difficulty to recall any particular occasion when infection occurred. Thus whether disease was initiated by exposure to infected meat or through ingesting oocysts is often not known. However, to counter this question, the discovery of sporozoite protein, *T. gondii* embryogenesis-related protein (TgERP) was very useful as it allowed serological assays to be developed and it is now known that antibodies to this protein can be detected in serum within 6-8 months of initial oocysts acquired infection (Hill et al., 2011).

1.2.2. Infection through cysts

The infection through cysts may be dependent on the type and consumption of meat. It is well reported that any meat from any warm-blooded animals and birds, if undercooked, is considered a potential hazard and predisposing factor for toxoplasmosis (Awoke et al., 2015). It is estimated in a study conducted in Europe that meat consumption is responsible for 30% to 63% of cases of infection, and as far as soil contact is concerned, it is responsible for 6% to 17% of cases (Cook et al., 2000). The risk of infection for food consumers is hampered due to unavailability of data regarding number of tissue cysts resulting in human infection. In one study of meat processed in a commercial industry, a low risk was reported, due to proper meat treatment procedures, which may lead to low sustainability of cysts (Dubey et al., 2005). Tissue cysts still remain infective for up to 3 weeks in carcasses or in minced meat. It has been reported in a study conducted on cyst viability that deep freezing of meat at -12˚C or even lower than this for at least 3 days is effective for killing of the cysts, depending upon the thickness and size of the piece of meat. This is not always a viable option in all settings. In another study it is also suggested that tissue cysts are instantaneously killed when heated at 67˚C. Survival of cysts at lower temperature is governed by duration of cooking. Tissue cysts stay sustainable on 60˚C for 4 minutes and 50˚C for 10 minutes (Dubey et al., 1990).

1.2.3. Infection through oocysts

It is evident from previous epidemiological studies that environmental conditions play a vital role in oocyst survival e.g., in moist conditions there will be increased rate of survival of the oocyst in hot weather (Dubey, 2005). This is one of the reasons for high prevalence in tropical countries. In France, it was shown in a research conducted that even in temperate climatic conditions, the risk of infection in cats is increased when there was a mix of warm and moist weather (Afonso et al., 2010). Oocysts are resistant to freezing and moderate higher

temperature of water. Most of the water treatment plants adopt chlorination and ozone treatment which is not likely to kill oocysts present in water because these are not killed by physical and chemical treatments applied for the said purpose (Dumètre et al., 2008). *T. gondii* oocysts can also survive in seawater and it is evident by the fact that these oocysts were also detected in many species of shellfish in natural conditions (Putignani et al., 2011). In a study, it is evident that contact with soil is also a strong risk factor and almost 6 to 17% of infections occurred in humans were recognised due to this contaminated soil. Interestingly, this factor was more prevalent in school children which were exposed to contaminated soil (Cook et al, 2000).

It is obvious that contaminated water and soil can act as transfer vehicle for the oocysts to vegetables and fruits which are utilised for human consumption. Such type of contaminated fruits and vegetables if consumed without washing, may expedite the chances of primary infection (Berger et al., 2009, Liu et al., 2009).

1.3 Vertical transmission of *T. gondii* infection

As we know *T. gondii* congenital infection is acquired through placenta during pregnancy. Congenital infection arises from primary acquired maternal infections during the gestation period (Hampton, 2015). Vertical transmission frequency and foetal damage severity occurs based on the pregnancy stage when maternal infection occurs. The placenta plays a significant role within this process since it is a natural barrier and also a target tissue for parasite multiplication. The natural barrier protects the foetus whereas this can also prevent parasite multiplication (Abbasi et al., 2003). Studies have indicated that the placental barrier possesses increased levels of effectiveness during the start of the gestation period. This results in the migration of parasites in less than 10 % of cases during the first trimester (Dunn et al.,1999). However, increased permeability occurs throughout pregnancy thus leading to increased parasite transmission up to 70 %, in some cases equal to or even more than 80%, as the time

leads closer to delivery (Dunn et al., 1999). In case of trans placental transmission occurring during the first trimester of foetal development, it could lead to abortion or major abnormalities. Multiplication of parasites stimulates inflammation and necrosis foci thus resulting in significant abnormalities within the brain and eyes. Also, this leads to destruction or significant white matter remodelling (Remington and Klein, 2001). Blocking of the aqueduct of the Sylvius via infected necrotized foci leads to hydrocephalus of the lateral ventricles. Further calcification of these foci can then occur and is identified via Cranial X ray or transfontanellar echography. Symptoms occur such as mental retardation, deafness, seizures or microcephalus (Remington and Klein, 2001).

With regards to the second trimester, foetal infection can be extremely severe. Through use of echographical ultrasounds this may indicate areas of hyper echogenic mesentery, hepatosplenomegaly or cerebral calcifications. Symptoms presenting at time of birth include epilepsy, anaemia, anaemia, rash, hepatic disorders and pneumonia (Remington and Klein, 2001). It is important to note that although the vast majority of infections arise from primary acquired infections during pregnancy, transmission of parasites may occur not in all cases, but it may range from 30 to more than 80% depending upon the immune status and period of gestation in which infection occurred (Dunn et al., 1999). Inversely, if we consider an immunocompetent individual, then the parasite transmission may rarely occur. These are previously infected females who obtain reinfection of *T. gondii* during gestation (Gavinet et al., 1997, Kodjikian et al., 2004) . In another study conducted in France, it is shown that transmission of this parasite can also be hindered due to placental barrier, and at the end of gestation this parasite can be transmitted into the foetus. In this case foetus is born asymptomatic but congenital infection can be diagnosed after birth if mother was infected with periconceptional infection (Robert-Gangneux and Dardé, 2012). This hypothesis of delayed vertical transmission is also supported by other studies as described by Thulliez that vertical

transmission may be delayed in some women infected during early stages of pregnancy because of the fact that parasite can persist in placenta and at the end of gestation it may move forward to the foetal compartment. This explains why some new born may not show any signs of infection in utero or at the time of birth (Thulliez, 2001).

1.4 Congenital Toxoplasmosis

Disease acquired during pregnancy and associated with transmission of *T. gondii* to the foetus, results in congenital *toxoplasmosis*. It has been reported that the severity and frequency of this infection depends on which stage of the gestation period the mother is infected. In one of the studies conducted at the University of Strathclyde, it has been shown that vertical transmission only occurs in BALB/c mice infected for the first time during pregnancy (Roberts and Alexander, 1992) and the same pattern for pregnant women was established in later studies (Bollani et al., 2013). The most severe expression of this disease is congenital infection occurring in women infected with *T. gondii* for the first time in pregnancy. In congenital transmission of disease, it is well reported that the level of damage depends upon the stage of pregnancy in which the mother was subjected to infection (Shepardson et al., 1999). Initial studies showed that the incidence of congenital toxoplasmosis varies according to the stage of gestation. Infection during the initial stages of pregnancy tends to produce lowest vertical transmission and as a consequence, abortion rates are highest. In contrast to the above, infection occurring during the last trimester will be subjected to highest rates of transmission and lowest incidence of abortion (Roberts & Alexander, 2008). This evidence was a strong base for the justification of around 80% transmission frequency of *T. gondii* infection. One of the key characteristics during early stages of pregnancy with *T. gondii* infection is apoptosis of placental cells and ultimately there will be foetal resorption (Pfaff et al., 2008). A similar pattern of vertical transmission for pregnant women is with probability of 15% at 13 weeks

gestational age (GA), 44% at 26 weeks GA, 71% at 36 weeks ultimately increasing to 90% vertical transmission during last weeks of pregnancy (Bollani et al., 2013).

1.5 Parasite replication

T. gondii is a member of the phylum Apicomplexa, which includes many human pathogens such as *Plasmodium falciparum* and *Cryptosporidium* spp. (Zhang et al., 2019). Apicomplexan parasites share various unique organelles that are essential for maintaining their intracellular lifestyles and causing disease. One of these organelles include the inner membrane complex. (Carlier et al., 2012). The inner membrane complex (IMC) is classified as a unique organelle of apicomplexan parasites that plays significant roles in parasite motility, host cell invasion, and replication (Torres et al., 2021). The IMC is an important organelle that apicomplexan parasites use to maintain their intracellular lifestyle. Many IMC proteins have been identified though few central players that are essential for internal budding have been described and even fewer are conserved across the phylum (Lima et al., 2021). Despite the common functions of the organelle, few IMC proteins are conserved across the phylum and the precise roles of many IMC components remain to be elucidated. The IMC consists of a series of flattened alveoli which together with alveolins have been likened to patches of material stitched together to form a quilt (Megli and Coyne, 2021). During *T. gondii* infection, the alveoli are divided into three rows of rectangular plates along with a single cone-shaped plate called the apical cap at the apical end of the parasites. Studies using detergent fractionation indicates that most IMC proteins localize either to the alveolar membrane or the cytoskeletal network, though many network-associated proteins are likely also to be tethered to the membranes (Torres et al., 2021). Some IMC proteins, such as the GAPM proteins, IMC25, and GAP40, are embedded in the alveoli via transmembrane domains, most are tied to the IMC membrane by myristoylation and/or palmitoylation, which are carried out via a cytoplasmic N-myristoyl transferase (NMT) or a target membrane palmitoyl acyltransferase (PAT) (Guevara

et al., 2021). The IMC plays various important roles in the lytic cycle of *T. gondii*. The IMC houses the glideosome, the actin-myosin motor that provides the required force for gliding motility and host cell invasion (Zhang et al., 2019). The apical cap portion of the IMC has been demonstrated to play a key role in organizing the conoid, a microtubule basket-shaped structure which is critical for the secretion of the micronemes for host cell adhesion. The IMC also serves as the scaffold for forming daughter buds during endodyogeny, the internal budding process of replication in *T. gondii* tachyzoites (Frickel and Hunter, 2021). Endodyogeny begins with the duplication and segregation of the centrosomes and kinetochores subsequently followed by subpellicular microtubule assembly, IMC formation, and daughter cell budding. Newly synthesized or replicated organelles are packaged into the developing IMC scaffold until budding is complete following which the maternal IMC is disassembled and the daughter cells emerge, adopting the maternal plasma membrane. As well as trafficking to the correct organelle subdomain, the timing of expression and recruitment of IMC proteins to the daughter buds during endodyogeny plays an important role in IMC protein functions. These include the AC9/AC10/ERK7 complex, which is essential for invasion and F-box protein TgFBXO1 plays an important role in replication (Mammari et al., 2019b). Subsequently, ISP1 and ISP3, which are dispensable and recruited independently of the cortical microtubules drive bud development. Other proteins such as the cytoskeletal alveolins IMC3 and IMC6, are recruited to daughter buds later in the replication process and other IMC proteins are exclusively recruited to the maternal IMC, after endodyogeny is complete (IMC7, -12, and -14). Formation of the IMC involves precisely timed recruitment of different IMC components to specific subdomains, the exact contribution of each of these components and the importance of correct timing is still not fully understood (Bradley et al., 2005).

Some studies have shown that *T. gondii* IMC (IMC32) that localizes to the body portion of the IMC and is recruited to developing daughter buds early during endodyogeny (Guevara et al.,

2021). IMC32 is required for parasite survival as its conditional depletion leads to a complete collapse of the IMC which is detrimental to the parasite. (Torres et al., 2021). Localization of IMC32 relies on both an N-terminal palmitoylation site and a series of C-terminal coiled-coil domains (Behnke et al., 2010). Through use of deletion analysis and functional complementation, two conserved regions within the C-terminal coiled-coil domains have been identified to play critical roles in protein function during replication. This suggests an essential component of parasite replication which provides a novel target therapeutic intervention of *T. gondii* and related apicomplexan parasites (Guevara et al., 2021).

1.5.1 Cyst Reactivation

T. gondii results in chronic infection that renders the immunocompromised human host susceptible to toxoplasmic encephalitis caused by cyst reactivation in the central nervous system (Torres et al., 2021). Host immunity weakening can result in *T. gondii* multiplication which is assumed to be due to cyst rupture or reactivation. This results in toxoplasmic encephalitis. Currently, therapies target acute stage infection, but do not result in removal of cysts and allows chronic infection with cysts to persist. Parasite molecules that control the development and persistence of chronic infection are poorly understood and Dense granule (GRA) proteins such as GRA12 have been shown to be key virulence factors during acute infection. The dense granule protein GRA12 is a major parasite virulence factor required for parasite survival during acute infection (Pappas et al., 2009). *Toxoplasma* invades a wide variety of nucleated host cells using an arsenal of secreted effectors stored in secretory organelles (Guevara et al., 2021). These secreted effector proteins are released from secretory organelles called rhoptries, micronemes, and dense granules (the organelle containing GRA proteins) in a coordinated fashion to control the parasite's attachment and invasion into host cells, as well as the production of the intracellular parasitophorous vacuole (PV) (Paquet and Yudin, 2018). This parasitophorous vacuole supports parasite survival and replication within

the host cell (Rudzki et al., 2021). Subsequently, the dense granules are secreted into the PV space. This secretion includes a large number of GRA proteins as well as some initial membranous material, which work in conjunction with lipids recruited from the host cell to form an extensive intravacuolar network (IVN) of membranes (Paquet and Yudin, 2018). This produces connections inside the PV between parasites and the limiting PV membrane (PVM) (Paquet and Yudin, 2018).

All IVN-associated GRAs possess the potential to associate with and disassociate from the IVN membranes in the PV space (Torres et al., 2021, Zhang et al., 2019). However, certain GRAs such as GRA2, GRA4, GRA6, GRA9, and GRA12 strongly associate with the IVN membranes via transmembrane interactions, whereas other GRAs such as GRA1 have poor association with the IVN membranes through peripheral membrane interactions. Other GRAs are secreted past the IVN and PV space and associate with the PVM at the host-PV interface or translocate into the host cytosol (GRA18) (Rudzki et al., 2021, Torres et al., 2021). A number of GRAs that translocate past the PVM include GRA16, GRA24, and GRA28, target to and accumulate in the host cell nucleus (Torres et al., 2021).

1.5.2 Prevalence

The distribution of this parasite is worldwide along with the ability to infect virtually all warm blood mammals. However, the domestic cats are known as the only definitive hosts in which parasite undergo sexual reproduction. The other intermediate/secondary hosts are human and rodents in which it undergoes asexual reproduction (Roberts et al., 2001). Notably, studies indicate that *T. gondii* is one of the most prevalent parasites and more than 30% of the world population carries *T. gondii* with infection rate of 77 to 0.8 % (Dubey, 2009). Toxoplasmosis is the infection caused by *T. gondii* and it is important to note that infection rates do vary from

country to country. Prevalence studies carried out in Scotland depicted a positive correlation between increasing age and *T. gondii* sero-positivity with the facts that 56–69 age group had the highest prevalence at 27.2 % (56/206) (95 % CI: 19.5–31.7 %), whilst the lowest prevalence of 6.3 % (25/398) (95 % CI:4.1–9.1 %) was observed in the 17–29 age group (Allison *et al.*, 2016).

A very low seroprevelance (10 to 30 %) has been observed in North America, in Southeast Asia, in Northern Europe and in Sahelian countries of Africa. Moderate prevalence (30 to 50 %) are found in central and southern Europe and a high prevalence have been found in Latin America and in tropical African Countries (Robert-Gangneux and Dardé, 2012). There are many factors which play a vital role in the seroprevelance of the infection in animals e.g., the survival rate of oocysts in the environment is dependent on climatic factors and, therefore, infection rates in meat producing animals also have an important role to play. Initially, this was also reported by Florence and Marie-Laure, 2012) that there is a high prevalence of toxoplasmosis observed in tropical countries with hot and humid environment. Inversely, there is lower prevalence of toxoplasmosis in arid countries. In spite of all these facts, there are many factors which act as a baseline to explain variations in human seroprevelence. These factors include dietary habits, method of cooking meat, quality of water consumed, personal hygiene, cultural, social or economic habits. Poor hygienic conditions and water consumed in any population can be a big source of this disease, because this is linked to waterborne contamination by oocyst ingestion. This is an indication of water as an important source of human infection in areas where there is consumption of unfiltered surface water or where there is contact with fresh water (Jones and Dubey, 2010).

1.6 Toxoplasmosis in pregnancy and sex hormones

The ability of sex and pregnancy related hormones to influence immune events and the severity of *T. gondii* infection is of interest because of the ability of this parasite to develop congenital infection. It was established a very long time ago that the immune response including the inflammatory responses of male and female mice differ during *T. gondii* infection (Roberts et al., 2001). There is further evidence of direct effects of sex hormones on the severity of *T. gondii* infection. One of the initial studies showed that after gonadectomy of mice resistance to infection was observed as compared with exogenous administration of estrogen which aggravated disease in mice (Kittas and Henry, 1979, Roberts et al., 2001) . These studies strongly suggest that sex hormones during *T. gondii* infection have the ability to alter disease outcome.

It is well-established fact that the maternal hormones are markedly altered during pregnancy and this has direct effects on the immune response in the presence of the foetus and foetal antigens. Many of the changes observed, including increased numbers of Treg cells and Th2 cells and associated cytokines are known to be essential for successful pregnancy. However, these changes pose an elevated risk of *T. gondii* infection which is normally controlled with a response dominated by Th1 cells and associated cytokines. Consequently, pregnancy and control of *T. gondii* infection can be seen as antagonistic (Roberts et al., 2001, Robinson and Klein, 2012).

1.6.1 Estradiole

It has been reported in the literature that during different stages of pregnancy (especially 2nd and 3rd trimesters), elevated levels of 17ß-estradiole and progesterone can be observed. These hormones are known to have immunomodulatory properties that antagonise the immune mechanisms that control *T. gondii* multiplication (Al-Warid and Al-Qadhi, 2012). With regards to 17ß-estradiole, this is produced within the ovary, breast, brain and endometrial tissue

(Arevalo et al., 2010). Also known as E2 (Oestrogen), it plays a significant role within the menstrual cycle as well as human reproduction (Arevalo et al., 2010). Other studies have indicated that estrogens have a neuroprotective effect within the brain (Arevalo et al., 2015). One study in particular has demonstrated that the use of pharmacological oestrogen doses results in the likelihood of increased susceptibility of *T. gondii* infection (Pung and Luster, 1986).

1.6.2 Progesterone

In comparison with estrogen, progesterone is located within the ovary and corpus luteum. This is mainly involved in the secondary phase of the menstrual cycle. Progesterone synthesis occurs within the breast, brain and endometria (Shepardson et al., 1999). Cells which are infected with tachyzoites of *T. gondii* have shown that progesterone is unable to regulate parasite replication (Gay-Andrieu et al., 2002). Also, progesterone levels are significantly decreased during pregnancy within sheep after *T. gondii* infection (Fredriksson et al., 1990). Pregnant women with acute toxoplasmosis can have *T. gondii* stimulated via low levels of progesterone and oestrogen (Al-Warid and Al-Qadhi, 2012).

1.6.3 Prolactin

It is reported in one study that prolactin is able to prevent the proliferation of *T. gondii* in cell cultures of murine microglia as well as intracellular growth of toxoplasma in human cell lines and mice (Dzitko et al., 2012). It is also documented by Dzitko and his colleagues that hyper-prolactinemic women may show decreased prevalence for *T. gondii*. In the same study it is also reported that serum human prolactin (shPRL) binds with live RH tachyzoites (type 1) and ME49 (type 2) strains in a particular manner (Dzitko et al., 2013).

1.7 Diagnosis of toxoplasmosis

Some biological, serological or molecular methods are adopted for the diagnosis of toxoplasmosis in humans. Sometimes there may be a combination of some of these procedures. One of the main challenging feature of toxoplasmosis is that it mimics many other parasitic diseases. So identification and characterisation of *T. gondii* antibodies in suspected individuals may help in diagnosis. Many scientific diagnostic tools have been modified to detect immunoglobulin M antibodies (Hill and Dubey, 2002). It is worth noting that during acute infection, IgM and IgG both can be detected in the serum within 1 to 2 weeks. In pregnancy, if only IgG is detected and IgM is not detected, then this is highly likely that infection took place almost 6-12 months before (Many and Koren, 2006).

Some of the specific IgG have the ability to cross the placenta, hence, their presence is not indicative of congenital toxoplasmosis. That is the reason why tests for IgG and IgM antibodies are applied together in new-borns. Almost around 15-55% of the new-borns infected with congenital infection don't show any IgM at birth or during the early months of life (Bollani et al., 2013). So in such circumstances where it is difficult to rule out congenital toxoplasmosis at birth, then there is a follow up serological testing is recommended to construct the proper diagnosis. Maternal IgG antibodies will disappear within 6-12 months (Bollani et al., 2013).

1.7.1 Treatment

Once toxoplasmosis is confirmed, then the drugs of choice most commonly used for treatment in combination comprise sulphadiazine and pyrimethamine and folinic acid. This is the most effective combination of drugs used for the treatment of congenital toxoplasmosis (Bollani et al., 2013). If there is a case of retinochoroiditis, the drug of choice is prednisolone per oral route (Remington and Klein, 2001). Infection of the foetus along with an immunocompromised status of the host is prone to a devastating condition. The drug of choice in this case is the combination of pyrimethamine and sulphadiazine. Despite the fact it is considered as a gold

standard treatment for toxoplasmosis, however, failure rates are still significantly high (Dunay et al., 2018). In another study (Dunay et al., 2018) it was stated that the treatment of maternal infection with the aminoglycoside spiramycin during pregnancy followed by treating with the combination of pyrimethamine and sulphadiazine in cases of confirmed foetal infection, is effective maximally reducing the severe effects of congenital toxoplasmosis.

1.8 Pregnancy and the Maternal Foetal Interface

Pregnancy in mammals is a complex physiological and immunological process involving numerous adaptations to facilitate foetal development. The foetus is semi-allogeneic, being derived from maternal and paternal genes, but yet is allowed to survive in the maternal uterine environment. A detailed outline of different developmental stages from fertilization to the foetus along with the development of the placenta and decidua is described in detail in the following section.

In sexual reproduction, an offspring is formed by the gametes of male and female unlike the somatic cells as in asexual reproduction. As these cells (gametes) undergo meiosis, so they have only one set of the chromosomes and are called haploid. One of the advantage of sexual reproduction is different possibilities of variants among offspring which allows newly desired genes to mix in new individuals. These gametes fuse with each other and this process of fusion is called fertilization. For a successful fertilization of the egg, there are many factors involved for spermatozoa to reach and penetrate into the egg, specially the morphology of the sperm, the host environment of the female reproductive tract, cell to cell interactions, gene expression, and some of the phenotypic traits of the sperm (García-Vázquez et al., 2016). A single celled zygote is formed as a result of fertilization in the oviduct. From a zygote containing the genetic material from both of the parents, it starts to actually develop as an independent individual.

As the main purpose of sexual reproduction is to produce a multicellular organism, so this zygote must produce more cells. To achieve this goal, the process of multiple cleavage, a series of repeated mitotic cell divisions, starts to convert a unicellular zygote into a multicellular zygote. This leads to the morula stage which is a solid mass of blastomere cells as a result of many vertical cleavages. In humans, morula contains sixteen or more blastomere cells. As the number of blastomere cells increases as a result of continuous cleavage, the zygote develops into a stage called blastula having an outer one or two layers of cells called blastoderm and an inner fluid filled cavity blastocoel. Formation of the blastula is indicative of the end of the further cleavage process taking place. Until now it is assumed that the chromosomal genes stay inactive during the process of cleavage.

As the cleavage ends, the embryo needs to go through many changes before it can go to a developed organism. These changes lead to the gastrulation stage. All the developed/adult tissues are derived from three main embryonic layers in the process of gastrulation. The formation of these layers is the start of the division of the developing embryo mass. In mice, the pluripotent tissue is converted into three germ layers, an outer layer ectoderm, the middle one is mesoderm and the inner layer is called endoderm (Bardot and Hadjantonakis, 2020). Skin covering, nervous system and the sense organs originate from the ectoderm. Muscles, gonads and internal skeleton arise from mesoderm. The organs for digestion are made from the endoderm. The process of gastrulation in the mouse takes place in three days mostly from embryonic day E6 to E9. Different cells that originate from the embryonic line in the process of gastrulation are converted into the progenitors of the different organ system as they incline to reposition themselves from the embryonic streak (Bardot and Hadjantonakis, 2020).

For a successful implantation which is necessary for all of the viviparous births, it needs a controlled responses comprising of the apposition of the blastocyst, attachment to the uterine epithelium and decidualization of the uterine stroma. Implantation is a complex process

involving the cross talk between uterus and embryo. A synchronised development of the embryo to the blastocyst stage and the receptivity of the uterus for implantation is essential (Foulk, 2001, Lee et al., 2007) . Many other factors involved in the implantation are the steroid hormones, various cytokines like IL-1, IL-6, CSF-1, transcription factors and many lipid mediators. One of the review studies has suggested that although these factors can influence the frequency of implantation, they are not essential for the implantation (Paria et al., 2001). The outer most covering of the embryo is chorion which acts as a main source of nourishment for the developing embryo. It has the ability to adhere closely to the walls of the uterus and transform into the trophoblasts. These trophoblasts are used for nutrient supply through diffusion to the embryo with the help of blood vessels of the underlying allantois. All these alterations in the decidua and uterus for post implantation give rise to a new organ the placenta made up of tissues of both the maternal side (uterine wall with its blood supply) and the embryonic side (the trophoblast and the allantois with their blood vessels) (Paria et al., 2001). To allow exchange of nutrients and waste products mammals have evolved placentas (which are foetal-derived) that are in direct contact and interact with the maternally derived decidua. Placenta is a very unique tissue in a sense it is only formed in pregnancy. It must have to be expelled after parturition. Development and maintenance of placenta is absolutely essential for a successful outcome of pregnancy. The structure of the placenta varies in different animal species. These types can be broadly categorised as Epitheliochorial (horses, swine and ruminants), Endotheliochorial (dogs and cats) and haemochorial (humans and mice). Although some differences exist between these classes, the broad similarity of the haemochorial placenta of mice, makes them a useful model for human placenta. the types of placentas described above are shown in the following figure 1.3.

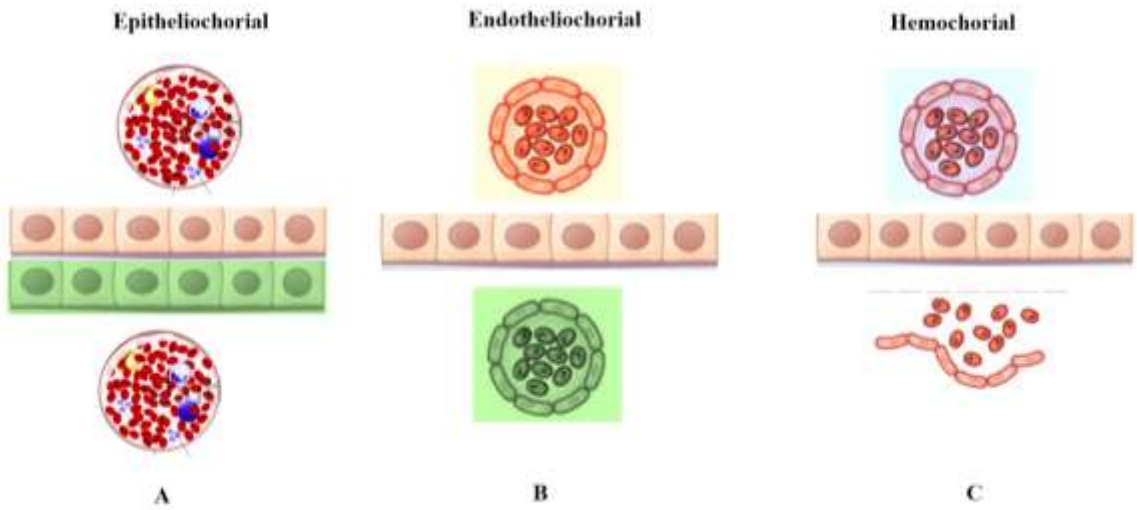

Figure 1.3 Different types of placentas classified on the basis of maternal chorion interface. Modified and adopted from (PrabhuDas et al., 2015).

(A) epitheliochorial placenta, the barrier between maternal blood and the chorion is maternal vascular epithelium and uterine epithelium (green cells). (B) endotheliochorial placenta showing the barrier between maternal blood and chorion is maternal vascular endothelium. (C) hemochorial placenta, maternal blood directly bathes in the villi. Adopted from (PrabhuDas et al., 2015).

In humans, the placenta is the main barrier between maternal and foetal compartments and a main controlling factor of haematogenous spread of invading organisms. For a pregnancy outcome to be successful, immune micro-environment in maternal-foetal interface plays a crucial role to protect the developing foetus as well as to protect from maternal rejection. Placenta consists of specialised epithelial cells knows as trophoblasts. It is derived from outer trophoblast layers of blastocysts during development of conceptus. The inner trophoblast layers of blastocysts are responsible for the developing foetus (Velicky et al., 2016).

All the mammals with haemochorial placenta, consists of two different types of trophoblasts viz; syncytiotrophoblasts (STs) and extra villous trophoblasts (EVTs). STs reside within maternal blood and act as a mediator of nutrients and gas exchange. While EVTs act as an anchor which keep the placenta in the decidua which is in the uterine implantation site, extravillous cytotrophoblastic cells of placenta play a vital role in implantation and the formation of maternal-foetal interface by entering the decidua basalis. It is also an important location for maternal immunity during pregnancy because this is the site where these trophoblasts deal with the maternal immune cells (Robbins et al., 2012). It is also reported in another study that it is a site of bidirectional cell trafficking where foetal cells can pass through placenta and there is an establishment of cell lineages in the mother (Pujal et al., 2012).

1.8.1 Development of maternal-foetal interface

Development of placenta starts with differentiation of trophoblast from trophectoderm. This process starts at day 6 after fertilisation. In the mouse, the process of implantation is manifested in the morula stage in which there are two distinctive cellular populations developed by cell division. Trophectoderm is developed by the outer layer of polarised blastocyst cells, while the inner cell mass is developed from the inner cell layer which is non-polarised (Red-Horse et al., 2004). Extravillous cytotrophoblast cells penetrate into the decidua basalis to arrange the maternal foetal interface. Maternal endometrium is digested enzymatically by the trophoblastic

cells, followed by a hypoxic to normoxia condition in myometrium (Red-Horse et al., 2004). Extravillous trophoblasts actively participate in remodelling of the maternal spiral afferent arteries which increases the vessel diameter and consequently a decrease in blood pressure. This is to ensure enough blood supply for the developing foetus (Whitley and Cartwright, 2009). Villous trophoblasts are held accountable for the formation of chorionic villi, that will increase the contact area for nutrient and gas exchange between foetal red blood cells and maternal blood in intervillous spaces. There are many immunological mechanisms partially composed of these trophoblasts that have been reported (Warning et al., 2011).

During initial phases of a human pregnancy, the uterine mucosa is altered into the decidua, the main foetal placental site for implantation. It is also a site for trophoblast cells to communicate with the maternal cells. This interaction may cause some of the pathological conditions of the pregnancy including preeclampsia and stillbirth.

1.9 Healthy pregnancy and Immune cells at maternal-fetal interface

A successful pregnancy is dependent on the tolerance of the paternal semi-alloantigen genes of the foetus by the maternal immune system. Therefore, to stop foetal rejection by the maternal immune activation, predominantly a Th2 cytokine production over Th1 cytokine production is of utmost importance. During the adaptive immune response, a very high degree of a specific antigen recognition and a subsequent immunological memory are the main components of the acquired immune response. T cells present T-cell receptors that help to identify different antigenic determinants presented on the surface of antigen presenting cells (APC) by major histocompatibility complex (MHC) molecules. To fight against these specific antigens/pathogens presented, immune cells are required that are recruited from the peripheral blood and lymphoid tissues. However, an innate immune system is more a generalised system to protect against any antigen, as it is not selective and specific for the particular antigen or invading organism. These immune cells can be studied in mice as a model to record their

movement and localisation at the maternal-foetal interface. The techniques used for this purpose are flow cytometry, histochemistry and whole mount staining microscopy (Croy et al., 2012). Below is a brief description of immune cells present in maternal-foetal interface and their changing levels in accordance with the needs of the foetus.

1.9.1 Natural Killer cells (NK cells)

These are the cells of innate immune system and cells can be divided into two based on the phenotypes of the surface markers, CD56 ^{dim} CD16^{+} and CD56 ^{high} CD16^{-}. The former contributes to the major portion of the peripheral NK cells (pNK) covering almost 90% of the pNK cells population. These cells have high cytotoxicity and more potent lytic activity against the target cells that are not expressing MHC class 1 molecules. This is also called the missing self-hypothesis (Negishi et al., 2018). With respect to CD56 ^{high} CD16^{-} , these are the major phenotype present in the uterine cells (uNK). uNK cells tend to produce cytokines (IL-1, IL-6, IL-11, IL-15, IFN-ɣ) after entering the decidua basalis. This leads to successful implantation by uNK cells, cell maturation and trophoblast differentiation (Croy *et al.,* 2003). This is the reason why these NK cells function both for cell lysis as well as cytokine production. NK cells are considered to be beneficial for placenta development during early stages of pregnancy. As soon as the implantation is completed, trophoblasts need to enter the extracellular matrix and decidual NK (dNK) cells release certain types of MMPs to assist this process smoothly (Naruse et al., 2009). These MMPs (matrix metalloproteinase) are zinc containing endopeptidases that break down the extracellular matrix proteins e.g collagen.

The uterine bed is prepared for blastocyst implantation by an inflammatory process which is called decidualization. In this process, first of all dendritic cells and uNK cells regulate the differentiation of stromal cells and vascular reactions which is in accordance to spiral artery remodelling. During implantation, there is an increase in the number of DCs and uNK cells at the maternal-foetal interface (Blois et al., 2011). It is reported earlier by Croy *et al.* (2003) that

a decrease in the number of uNK cells in mice gives rise to hypo-cellular and necrotic decidua along with anomalous placental functional structure. Peripheral NK cells act as cytotoxic cells while uNK cells have different phenotypes in comparison to peripheral cells (Croy et al., 2003).

1.9.2 Macrophages

Macrophages are specialised innate cell types involved in the process of phagocytosis of the invading harmful pathogens. They also act as antigen presenting cells that present different types of antigens to the T cells to start an adapted immune response. They have an important immunological role throughout the pregnancy. Macrophages, in general, are divided into two phenotypes that are M1 and M2 (Mills, 2001). It is further established in one study that functional maturation of macrophages have been categorized into M1 & M2 type which is analogous to Th1/ Th2 divergence (Sica and Mantovani, 2012). A detailed numerical and efficient balance is necessary between this M1/ M2 throughout the pregnancy. Macrophages are recruited in response to the seminal fluid antigen after coitus, prominently leading to an inflammatory response (Robertson et al., 1996). It is known that macrophages are present in the endometrium and decidual portion and are able to recognise allogeneic foetal antigens, along with contributing to defence mechanism against any infectious agents.

During the development of the placental phase of trophoblast invasion into the uterine stroma, M1/M2 profile is changed until the pregnancy proceeds to the second trimester. After the formation of the placenta, M2 is a highly expressed phenotype at the maternal foetal interface and it is helpful to prevent foetal rejection (Chabtini et al., 2013).

1.9.3 Dendritic cells (DC)

DCs are important cells as they function as antigen recognition and antigen presenting cell (APC) to the T cells, thus leading to the initiation of the adaptive immune response. There are three types of DCs in human, plasmacytoid DC (pDC), conventional DCs (cDC) and monocyte

derived DCs (Satpathy et al., 2012). In viral infections, the immunity is produced as pDC contribute to produce IFNs, specially IFN-ά, while naïve T-cells are activated by the subtype of cDCs called cDC2, while cDC1 subtype presents foreign antigen to the MHC class I molecules to activate cytotoxic $CD8^+$ T cells (Bozzacco et al., 2007).

DCs can exert both favourable and detrimental special effects during gestation, depending upon the timing of the activation of DCs. In pregnant mice, DCs are captured in decidua, avoiding these DCs to transfer to the clearing out lymph nodes, hence promoting tolerance to the foetus as well as a minimum immune response of the T cells to the allogenic/placental antigens (Collins et al., 2009). However, in the murine model, it is also reported that the paternal seminal antigens are entrapped by DCs and presented to the T cells (Treg cells) present in the reproductive system. This leads to the expansion of the paternal antigen specific Treg cells just before implantation (Saito et al., 2016).

1.9.4 T cells

Adaptive immunity during pregnancy is dependent on B cells and T cells. B lymphocytes give rise to humoral immunity while cellular immunity is mainly mediated by T lymphocytes that are of two types, $CD4^+$ helper Tcells and cytotoxic $CD8^+$ killer Tcells. Whenever a pathogen molecule is recognised and presented on MHC class I molecule, it communicates directly with the $CD8^+$ cytotoxic Tcells, which are proliferated into memory cells and cytotoxic cells that kill the invading antigens. However, an antigen presented by DCs on MHC class II molecules activate $CD4^+$ T helper cells. These cells also proliferate and divided into memory cells and some of these $CD4^+$ cells induce different cytokines (interleukins) through NK cells, macrophages and B cells to send signals to kill the foreign invading organism.

Immunity by these cells is limited in pregnancy and it is necessary to protect foetal allograft from any potential cytotoxic effects of $CD8^+$ T cells and $CD4^+$ Th1/Th17 cells (Saito *et al.*,

2010). In a study conducted by Wegmann *et al.*, 1993, immunomodulatory effect of placenta in Th2 cytokine environment is described for a successful pregnancy. It is also evident that trophoblast cells are responsive to both Th1 and Th2 cytokines (Murphy *et al.,* 2009). It is also established that IL-4, IL-5, IL-9, and IL-13 deficient mice show normal pregnancy, which is suggestive of the fact that a successful pregnancy outcome can occur even in the absence of Th-2 inclined effect (Saito et al., 2010).

Treg cells tend to suppress immune responses against any antigens in different physiological and pathological environments (Allan *et al.,* 2008). There are two subtypes of Treg cells which include from thymic origin and peripheral origin. In humans, there is a reduced expression of Treg cells in implantation failure as well as in case of infertility of unknown origin and recurrent spontaneous abortion (Saito et al., 2010). There is a decreased production of Th17 cells associated with healthy human pregnancy while spontaneous abortions are associated with increased IL-17 production along with infiltration into the decidua (Lee et al., 2012). There is a study suggesting the role of another regulatory molecules, IDO, which suppress differentiation of Th17 (Baban et al., 2009).

1.10 Immunity to *T. gondii*

Resistance to infection relies on the ability of host pattern recognition receptors (PRRs) to detect microorganisms, to stimulate the innate immune system to control initial infection and facilitate the development of protective immunity. *T. gondii* has the ability to invade and replicate within a host cell which involves the injection of ROP effector proteins, production of a parasitophorous vacuole and secretion of GRA proteins into host cytosol (Zhang et al., 2019). Consequently, these processes result in exposure to parasitic material to the host and result in various changes within the host cells which are linked with immune and cellular pathways related to stress (Rastogi *et al.,* 2020). Despite this, their effects on innate recognition of *T. gondii* is yet to be explored fully.

The vast majority of what is known about immunity to *T. gondii* has been determined from murine studies, although much of it is known to be consistent with clinical studies and observations. The innate immune system is necessary for control of parasite growth immediately following infection, although the adaptive immune response is ultimately needed for survival and recovery. *T. gondii* has many pathogens associated molecular patterns (PAMPS), that interact with murine pattern recognition receptors (PRRs) including TLRs.

TLRs are classified as pattern recognition receptors that recognize PAMPs and are important for resistance to various infections. TLRs recognise a wide variety of PAMPS and thus utilise the signalling adaptors MyD88 and TRAF6 to stimulate NF-κB and MAPK signalling, which in turn enhances chemokine and cytokine production. Studies have shown that in mice some proteins such as MyD88 and UNC93B help to promote IL-12 production and resistance to *T. gondii* (Pifer and Yarovinsky, 2011, Wujcicka et al., 2014). UNC93B is classified as an ER-resident protein associated with trafficking of endosomal TLR3, 7, and 9 (Brinkmann et al., 2007). Profilin (a parasite molecule) is a PAMP recognized by murine TLR11/12 and is important in murine recognition of *T. gondii* (Brinkmann et al., 2007). It is important to note here that TLR11 and 12 are not functional in humans. Furthermore murine studies have demonstrated MyD88 independent pathways that also control *T. gondii* showing that there are additional mechanisms in place for identifying *T. gondii* (Pifer and Yarovinsky, 2011). Following the recognition of PAMPS by dendritic cells, macrophages and neutrophils release a number of mediators including TNF-ά and IL-12. These mediators are important in initial control of infection and stimulation of other immune cells. Thus IL-12 stimulates NK cells which release IFN-γ. IFN-γ and TNF-ά can then work in synergy to activate macrophages and induce a number of parasite killing mechanisms.

The importance of these innate mediated mechanisms is evident through the study of SCID mice that lack B and T cells, but can still survive *T. gondii* infection for around 10-15 days depending on infectious dose and parasite strain (Johnson, 1992). However, the adaptive immune response including B cells and especially T cells is necessary for resolution of disease and long-term survival. IL-12 induced in the early stages of infection plays an important role in directing the adaptive immune response as it favours the expansion of Th1 cells rather than Th2 cells. The cells are additional sources of IFN-γ, but also provide IL-2 which is required for the development of cytotoxic CD8 T cells (Sa et al., 2013, Gazzinelli et al., 1991). CD8 T cells can kill infected cells through recognition of parasite peptide displayed on MHC class 1 (Torres-Nagel et al., 1992, Parker et al., 1991, Blackwell et al., 1993, Johnson et al., 1996). It is noteworthy that although in experimental conditions Th2 and Treg cells or their products can antagonise immunity to *T. gondii* infection they are also necessary for recovery as their elimination or neutralisation can exacerbate inflammation and result in death (Gazzinelli et al., 1996). In recent years an increasing list of *T. gondii* secreted proteins have been identified that interfere with the development of many immune responses (Hunter and Sibley, 2012). Studies have shown that in murine models, *T. gondii* is able to stimulate dendritic cells and macrophage production of IL-12 and this is a suggested mechanism to identify directly parasite derived molecules (Bliss et al., 1999). However, it is important to note that *T. gondii* strains differ in their ability to stimulate IL-12, a property which is associated with GRA proteins specially GRA15 and GRA24 (Rosowski *et al.,* 2011).

1.10.1 *T. gondii* mediated activation of the inflammasome

Nod-like receptor (NLR) family members are known to be cytosolic molecules which bind PAMPs and nucleate the assembly of the inflammasome complex, resulting in activation of proteases that enhance inflammatory signals. With regards to toxoplasmosis, this process associates adapter protein apoptosis-associated speck-like protein containing a CARD (ASC),

resulting in caspase-1–mediated processing of IL-1α, IL-1β, and IL-18 to their bioactive forms. This can also result in a form of inflammatory cell death (Snyder and Oberst, 2021). Genome wide association studies have displayed single nucleotide polymorphisms in the N-terminus of NLRP1 with susceptibility to congenital toxoplasmosis and the NLRP3 inflammasome activator P2X7R with clinical toxoplasmosis in immunocompetent patients (Cirelli, 2016). Murine macrophage studies have shown that NLRP1 and NLRP3 play key roles in the detection of *T. gondii* and production of IL-1β and IL-18. Similarly, infecting human monocytes with *T. gondii* stimulates NLRP3 resulting in release of IL-1β, but without inflammatory cell death (Witola et al., 2011).

The vast majority of studies on the inflammasome have investigated the interactions of *T. gondii* with macrophages. However, other studies demonstrate the ability of *T. gondii* to alter the inflammasome pathway and block the stimulation of proapoptotic caspases thus extending the lifespan of infected human neutrophils (Lima et al., 2021). The ability of IFN-γ–primed human macrophages to kill *T. gondii* results in release of parasite DNA into the cytosol which is then recognised by AIM2 to drive host cell apoptosis without IL-1β production in a caspase-8–dependent fashion. Importantly, the caspase-8 enzyme is essential for stimulation of the NF-κB member c-Rel for IL-12 production and resistance to *T. gondii* infection (Fisch et al., 2019).

1.10.2 IFN-γ –mediated antimicrobial effector mechanisms

Recently, it has been discovered that IFN-γ stimulates a series of events which involve recognition, tagging, and disruption of the PV to expose the parasite surface to host effectors. Variations exist in different host species, despite the fact that core processes involved in restriction of *T. gondii* are conserved between cell types and species (Degrandi et al., 2007). It has been shown that in hematopoietic and non-hematopoietic murine cells and human macrophages, control of the parasite is achieved through PV breakage (Clough et al., 2016). For human nonhematopoietic cells, various pathways are implicated in the events that lead to

parasite control that vary with cell type and include non-acidifying autophagy, non–PV targeting GBP1-mediated control, and PV acidification (Selleck et al., 2015). It has been postulated that the autophagy and the ubiquitin–proteasome system involved in cellular housekeeping function to tag proteins for degradation and deal with damaged organelles is required for IFN-γ–mediated clearance of pathogens. Conventional autophagic processes are not linked with control of *T. gondii* but the ability of this machinery to recognize foreign or damaged membranes intersects with the IFN-γ–inducible large GTPases, the immunity-related GTPases (IRGs) and the guanylate-binding proteins (GBPs) to mediate parasite control (Besteiro, 2019). Significant evidence is arising that alteration of the pathways in vivo results in increased susceptibility to *T. gondii*. IFN-γ has been shown to play a significant role in resistance to *T. gondii* infection (Yap and Sher, 1999). Various T cell–dependent, IFN-γ–independent pathways can contribute to parasite control, including the ability of recently activated T cells to express the surface molecule CD40 ligand. CD40 can be expressed on immune and nonimmune cells and signals through CD40 are can stimulate accumulation of the autophagy molecule LC3 around the parasite, vacuole-lysosomal fusion, and death of *T. gondii* (Degrandi et al., 2007).

1.11 Effect of *T. gondii* infection during pregnancy

1.11.1 Effects on implantation

For a healthy pregnancy to occur, this relies on appropriate immune responses from the coitus to post-partum (Mor et al., 2017, Borges et al., 2019). During coitus, seminal plasma is released and contains a wide range of active immunological components such as CXCL8, TFG-beta, Prostaglandin-E and IFN γ (Borges et al., 2019). These immunological components play roles in gene expression changes, recruitment of monocytes, dendritic cells, NK cells and Treg cells. As blastocysts undergo implantation, macrophage activity is essential for the removal of apoptotic maternal uterine cells (Abrahams et al., 2004a, Borges et al., 2019). There is evidence

found in the maternal foetal interface of maternal immune regulation. The decidua development relies on progesterone and is key for implantation. Blastocysts can breach the uterine epithelium which occurs alongside inflammation and alteration of decidual leukocytes as well as NK cells, macrophages and T cells. (Mor et al., 2017, Borges et al., 2019). Implantation can successfully occur depending on levels of cytokines and chemokines such as IL-6, IL-15, GM-CSF, IL-33, CXCL8 as well as activation of signalling pathways such as MAPK, JAK-STAT and PI3K (Suman et al., 2013, Borges et al., 2019). These cytokines are present in the endothelium at this stage and play significant roles in implantation and this provides tolerance to the foetus. *T. gondii* possesses the ability to disrupt early events in pregnancy though limited mechanistic studies have been reported. However, in mouse models, chronic *T. gondii* infection has been shown to induce reproductive failures (Shiadeh et al., 2016). This has been linked to tissue cysts in *T. gondii* within the brain and other organs resulting in damage to the hypothalamic-pituitary-gonadal axis leading to changes in the female oestrus cycle (Stahl et al., 1994). Further studies have suggested that acute *T. gondii* infection stimulates transient changes in systemic expression of various immune mediators which then in turn have the ability to impact normal immune changes during pregnancy (Liu et al., 2014).

1.11.2 Effect on the developing placenta, decidua and foetus:

As pregnancy progresses, various alterations occur within the maternal immune system which provides fetoplacental development and averts foetal rejection (Borges et al., 2019). For a successful pregnancy to occur, this requires specific regulation and balance of maternal immune responses within the decidua and placenta. Immune regulation permits growth and ensures protection of the semi-allogeneic foetus, expressing paternal major histocompatibility antigens from maternal immune rejection (Svensson-Arvelund et al., 2015, Borges et al., 2019). Disruption of this immune regulation via extrinsic factors as occurs in infection, can alter pregnancy maintenance resulting in adverse gestational outcomes. With regards to *T. gondii*

infection, this can have significant effects on the systemic maternal cellular immune responses thus affecting normal immune mechanisms occurring at the maternal foetal interface leading to effects on pregnancy. Various *T. gondii* strains with varying levels of virulence can infect decidual immune cell populations and the placenta which is known to be a prime anatomical location to change immune responses at the maternal foetal interface (Borges et al., 2019). Contrastingly, immunomodulation during pregnancy may help the development of *T. gondii* suited environments. These type of environments includes lots of TH2 and Treg cells which can help *T. gondii* escape from the immune response. Consequently, this results in increased maternal pathology and increased chances of congenital transmission (Rezende-Oliveira et al., 2012).

1.11.3 Effect of *T. gondii* infection on the placenta

Trophoblasts are classified as epithelial cells that constitute the foetal placenta whereas cytotrophoblasts act as stem cells for other trophoblast cell types: the syncytiotrophoblast and extravillous trophoblasts. Syncytiotrophoblast produces a multinucleated cell layer that is in direct contact with maternal blood these permitting intimate interactions between the mother and foetus. Extravillous trophoblasts can invade maternal tissues and essentially these cells operate in a protective manner to protect the foetus from harmful substances (Rezende-Oliveira et al., 2012). Also, this allows the passage of nutrients and factors important for foetal development. Immune responses within the placenta also provide protection from infection and help with maternal tissue remodelling which is significant for foetus development (Carlier et al., 2012, Borges et al., 2019). Trophoblasts stimulate the production of various anti-inflammatory mediators such as TFG beta, IL-10 and Fas ligand (Abrahams et al., 2004b). However, they also can initiate signals which initiate foetal rejection. T *gondii* does not have TLR3 ligands but does possess ligands that can activate TLR2, 4 and 11 supporting that trophoblasts can operate as immune regulators and affect differentiation and migration of

immune cells (Mor and Kwon, 2015). Infection with *T. gondii* could stimulate TLR-mediated trophoblast inflammatory or apoptotic responses. During *T. gondii* infection, it has been shown that these cells switch from protective to aggressive phenotypes thus promoting foetal rejection (Koga et al., 2009). Trophoblast have been linked to parasite transmission to the foetus due to their location between the maternal and foetal blood circulations systems thus leading to infection with *T. gondii*. Some studies using Bewo cells (human trophoblast cell line) in vitro have indicated that trophoblast susceptibility to *T. gondii* is enhanced in response to increased concentrations of macrophage inhibitory factor (Barbosa et al., 2014). However, treatment of Bewo cells with TFG-beta or IL-10 stimulated *T. gondii* proliferation. Similar studies found that the addition of IFN-γ to Bewo cells did not reduce *T. gondii* proliferation unless IL-10 or TFG-beta was neutralized with specific antibodies (Barbosa et al., 2015). Increased levels of trophoblast apoptosis and necrosis occurring after *T. gondii* infection depends on IFN- γ which is deemed to be a major factor in determining pregnancy outcome in pregnant women infected with *T. gondii* (Robbins et al., 2012). Contrastingly, IL-10 reduces *T. gondii* infected trophoblast apoptosis levels. IFN-gamma can possess a dual function if trophoblast invasion is significantly high as demonstrated in *T. gondii* infection. This can be either inhibiting parasite infection or stimulating its removal, though adhesion of infected monocytes to trophoblasts, could also stimulate placental and foetal infection. Trophoblasts possess the ability to regulate monocyte activity controlling *T. gondii* infection thus promoting pregnancy maintenance (Barbosa et al., 2014). Interaction between trophoblast cells and maternal-foetal immune cells such as macrophages determines *T. gondii* survival and putative vertical transmission (Barbosa et al., 2014).

1.11.4 Effect of *T. gondii* on the decidua

The decidua arises from the proliferation and differentiation of stromal endometrial cells into decidual stromal cells via decidualization. These cells are required for embryo implantation,

placentation and modulation of local immune cell functions which are required for maternal/foetal tolerance and protection against interferons (Borges et al., 2019). Decidual stromal cells are stimulated by TLR signalling and produce G-CSF, IL-6, TNF-alpha, IL-8, CXCL1 and CXCR4 (Vacca et al., 2015, Borges et al., 2019). Chemokines such as IL-8, CXCL1 stimulate T cell recruitment, monocytes and peripheral NK cells controlling the activation profile at the decidua (Vacca et al., 2015, Borges et al., 2019). Decidual stromal cells can contribute to successful pregnancies or miscarriages depending on the decidua environment (Xu et al., 2012). Though the *T. gondii* tropism is not clearly understood, the decidua/trophoblasts interface is deemed to be highly vulnerable to infection after parasite dissemination via maternal leukocytes (Robbins et al., 2012, Borges et al., 2019). Currently, there is no description regarding the association between DSC and *T. gondii* infection.

1.11.5 Decidual immune cells and *T. gondii* infection

The decidua is classified as a highly dynamic tissue made of various maternal immune cell types and is maintained by placental-derived factors. Mouse studies have indicated a significant role for CCR5 and RANTES in abortion resulting from *T. gondii* infection (Svensson-Arvelund et al., 2015, Borges et al., 2019). It is suggested that loss of embryo arises from changes in decidual and trophoblastic function stimulated by recruitment of macrophages, DCs and T cells in response to enhanced levels of CCR5 and RANTES within implantation units from *T. gondii* infected mice (Nishimiura, 2017). Proteomic analysis of *T. gondii* infected human decidual immune cells display altered levels of proteins involved in immune tolerance, foetal intrauterine growth and trophoblast invasion which are important processes occurring during pregnancy (Nishimura et al., 2017). One study demonstrated reduced levels of IL-1beta and increased levels of granzyme A and CCAAT enhancer-binding protein were discovered in *T. gondii* infected decidual immune cells in comparison with uninfected ones (Nishimura et al., 2017). Consequently, this would result in an altered immune balance at the maternal-foetal

interface and restrict decidualization, placenta development and foetus development. Increased levels of granzyme A suggests increased levels of NK and cytotoxic T-cells thus affecting decidualization and foetus development. These studies suggest that by altering pathways related to decidual immune responses, *T. gondii* infection can have a negative impact on pregnancy outcome (Zhang et al., 2018).

Recent studies have demonstrated that *T. gondii* can modify the immune profile of decidual cells and invade and multiply within uterine decidual NK cells (Zhang et al., 2018). As well as increasing IFN- γ secretion by decidual NK cells, *T. gondii* is also associated with increased levels of trophoblast apoptosis via caspase 3 and 8 mediated pathways (Mammari et al., 2019a). Also, *T. gondii* infection increases expression of human dNK cell activating receptor thus stimulating increased levels of higher cytotoxic activity of decidual NK cells towards trophoblast cells. These modulations can also contribute to abnormal pregnancy outcomes (Zhang et al., 2018, Borges et al., 2019).

In vitro studies have shown that *T. gondii* infected human decidual dendritic cells produce IL-12 which increases the cytotoxicity of decidual NK cells as shown by increased expression of NKG2D and IFN- γ production. Increased levels of IL-12 and IFN- γ levels favours a Th1 response thus inhibiting Th2 cells and resulting in pregnancy disruption (Yu et al., 2017).

Increased Treg cells have a positive correlation with the placental enzyme indoleamine-2-3 dioxygenase (IDO) and tryptophan 2,3-dioxygenase (TDO) during pregnancy and is linked to maternal tolerance (Yu et al., 2017). IDO expression is stimulated by IFN- γ and converts L-tryptophan which is an essential amino acid during pregnancy into kynurenine which thus favours expansion of Treg cells (Yu et al., 2017). These events are quite significant due to the fact that reduced levels of kynurenine and other downstream metabolites of tryptophan degradation as well as decreased transcripts for indoleamine-2-3 dioxygenase (IDO)

(indoleamine-2-3 dioxygenase) and tryptophan 2,3-dioxygenase (TDO) have been linked to foetal growth restriction (Chaudhry et al., 2014). Moreover, IDO levels are increased in the placenta during acute *T. gondii* infection at late gestation (Yu et al., 2017). Recent studies have suggested a decrease of Treg/Th17 ratio in *T. gondii* infected pregnant mice was reported thus indicating a role for this imbalance in *T. gondii*-induced embryo loss. Decrease in maternal T-reg cells have been reported to inhibit foetal tolerance and is associated with pregnancy complications (Pfaff et al., 2008, Borges et al., 2019).

1.12 Aims and Objectives

Recent work has explored how *T. gondii* affects the immune response at the maternal foetal interface (Borges et al., 2019). It has been known for some time now that the immune response stimulates certain metabolic processes including degradation of tryptophan and changes to arginine metabolism that are important to control of *T. gondii* infection. This link has been further bolstered by recent large scale metabolic studies for many immunological situations including *T. gondii* infection (Hargrave et al., 2019). Changes to metabolism, in particular tryptophan have also been described as important for pregnancy (Badawy, 2015). How *T. gondii* affects metabolism at the maternal foetal interface and in the developing foetus have not been studied. Logically changes at these sites could have profound effects on the outcome of pregnancy and the health of any surviving offspring. Therefore, the overall aim of the work described in this thesis is to better understand the effect of *T. gondii* infection on the metabolism of pregnant mice, the maternal foetal interface and the developing foetus. Specific objectives are:

1. To determine how *T. gondii* infection affects the metabolic profile of the decidua, placenta and foetus of *T. gondii* infected mice.
2. To look for commonalities in metabolic profiles of foetuses derived from *T. gondii*-infected mice with the metabolic profile of brain tissue derived from adult mice infected with *T. gondii* in utero.
3. Confirmation of identification of different metabolites of interest detected in this study.
4. To determine how *T. gondii* infection alters the microbiota of the intestine.

2- Materials and Methods

2.1 Mice and infections

For experiments described in chapter 3 and 4, BALB/c mice were obtained from Charles River (L'Arbresle, France) and were bred and maintained in the animal facility at the Department de Ciencias Biologicas Faculdade de Farmacia, Universidad do Porto, Portugal. BALB/c virgin females, aged 8-12 weeks, were selected as a model of congenital toxoplasmosis and housed with fertile males (1 male/ 2 females/ cage). For each female, day 1 of pregnancy was set as the day when vaginal plug became apparent, designated day 1 of pregnancy. Mice were infected on day 7 of gestation, each mouse was infected intraperitoneally (i.p.) with 5×10^3 viable tachyzoites of Me49 strains of *T. gondii*. Mice were sacrificed 7 and 6 days post-infection (corresponding to day 14 and day 13 of gestation) for chapter 3 and chapter 4, respectively. It is worth mentioning here that this animal model yields similar pattern of results with regard to foetal infection as described by Roberts and Alexander (1994).

In chapter 3 a total of 4 litters were obtained (2 from control mice, resulted in 13, 13 and 14 extracts for decidua, placenta and foetus, respectively) and 2 from infected mice, resulted in 10, 10 and 9 extracts for decidua, placenta and foetus, respectively). In chapter 4, a total of 13 litters were obtained (6 from control mice, resulted in 24 foetal placental units and 7 from infected mice, resulted in 21 foetal placental units).

The studies described in chapter 3 was designed mainly to focus on the metabolomics profile of the maternal foetal interface, hence the major tissues involved in this interface, the decidua, the placenta and the developing foetus were dissected and metabolites extracted for comparative investigation. The studies described in chapter 4 focused solely on foetus tissue. All samples from these three tissues were extracted at the University of Porto, Portugal and shipped to SIPBS, University of Strathclyde on dry ice.

The studies described in chapter 5 was carried out to confirm the identification of some important metabolites. The inclusion of the metabolites in this study was based on the links with *T. gondii* infection. A software called ToxID was used to compare the relative abundance against retention time as well as relative abundance against *m/z* mass of the metabolites. A RAW file and a configuration file were used as input files to obtain an output file. This output file contains information regarding chemical formula, *m/z* mass, retention time and peak intensity. Many metabolites were compared with their commercial standards regarding their relative abundance against retention time and *m/z* mass.

A comparison was made between the metabolomic profiles of the developing foetus from the infected mothers and the brains taken from the adult mice born to the infected mothers. The metabolomic profile of brain from adult mice born to infected mothers was previously carried out in the laboratory (Abdelsalam, 2019). There were 19 brain extracts with confirmed infection status and 29 extracts were exposed to maternal infection. Infection status was confirmed through seropositive evaluation of IgG1 and IgG2 levels in the serum of offsprings.

BALB/c mice (6-8 weeks) used in the metagenomic experiments in chapter 7 were bred in house at the University of Strathclyde. All mice were kept in Biological Procedures Unit facility, under the project license I59901CD7. The metagenomics study was carried out with a reasonable sample size (based on the fact that these can be analysed statistically), with a 5% level of significance. Out of the total 40 mice, the male and female ratio was 50:50 (n = 20 for each sex). And within each sex, there were three different groups according to the experimental design viz;

Uninfected group (n= 5 each for male and female).

Infected group (n= 10 each for male and female).

Control brain group (n=5 each for male and female).

2.1.2 *Toxoplasma* infection

The uninfected group was used as control and the infected group was gavaged with *Toxoplasma gondii* infection with 10 cysts of Me49 strain at day 0, while the control brain group was named because that was gavaged with brain homogenised with PBS solution.

2.1.3 Mice caging

Mice were co-housed as 5 mice per cage that contains bedding, ad libitum access to food (pellets feed) and water 24/7. A constant temperature was set into the room where these cages were kept with a 12 hours' light and dark cycle.

2.1.4 Daily weight gain/loss

All the mice from each group were weighed at day 0 and their 20% cut-off weight was calculated as a standard procedure. Subsequently, weighing of all the mice from all groups was a daily routine to access their health and suffering level closely. The body weight cut-off values of 20% for each mouse determine a baseline for the severity of distress and pain of animals used in experimental research. Hence, all mice used in this research were subjected to national regulation and operated on the principle of 3Rs – reduce, refine, replace. These regulations govern the use of animals in any trials and as soon as any mouse reaches this 20% cut-off value, those were humanely killed to avoid further suffering and discomfort.

2.2 Preparation and extraction of tissues for metabolomics analysis

After carefully collecting, dissecting and weighing the required three tissues (decidua, placenta and foetus), the samples were immediately placed in ice-cold 0.1% formic acid before proceeding with the metabolite extraction procedures involved in metabolomics analysis.

2.2.1 Metabolite extraction

Extraction of polar and non-polar metabolites was achieved using a two-step extraction protocol used with chloroform, methanol and deionized water. Tissues samples were removed from the formic acid solution and added to a pre-chilled 15 ml polypropylene tube containing 4 ml/g tissue sample of ice-cold methanol (Fisher, Optima LC/MS grade) and 0.85 ml/g ice-cold deionized water. Homegenisation of the tissue sample was carried out, keeping the sample chilled in an ice-bucket. 4ml/g cold chloroform (Fisher chemicals) and 2ml/g dH_2O were then added and the homogenate was vortexed for 60 seconds. Samples were allowed to partition on ice for 10 minutes. After this, samples were centrifuged at 12000 xg for 15 minutes at 4°C to produce a biphasic mix. The upper polar layer was removed from each extract and transferred to a 1.5 ml HPLC vials with a 0.2 ml insert. Metabolites are present in the upper layer, while the lower layer contains mostly extraction solvents. These samples were then stored at -80°C.

These samples were dispatched on dry-ice to the University of Strathclyde, where these samples/extracts were received and stored at -80ºC, before metabolomics study using the LCMS technique. This workflow is summarised as a schematic diagram in the following figure 2.1.

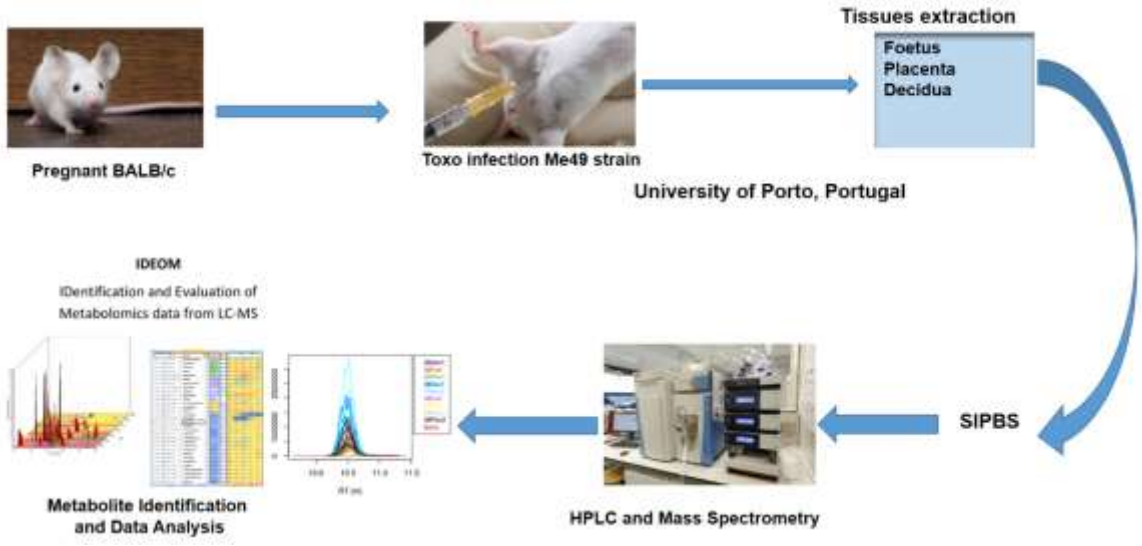

Figure 2.1 Schematic diagram of the workflow for the metabolomics profiling carried out in this study.

2.2.2 LCMS analysis

Samples were processed by running on the LC-MS by Dr Gareth Westrop at Strathclyde University. This consisted of an Accela 600 HPLC system combined with an Exactive (Orbitrap) mass spectrometer, Thermo Fisher Scientific (Bremen, Germany). Two complementary columns were used for the HPLC step;

1- ZIC-pHILIC column (150 mm × 4.6 mm; 3.5 μm, Merck, Germany.
2- Reversed-phase C18-PFP column (150 mm × 4.6 mm; 3.5 μm, Hichrom).

The reason to use both these columns was to enhance the coverage of the detected peaks, as ZIC-pHILIC column is hydrophilic thus ensuring detection of hydrophilic metabolites whereas C18-PFP is a hydrophobic column resulting in the detection of hydrophobic metabolites. In both of these systems, the volume of injection was 10 μl and the flow rate was adjusted to 0.3 ml/min. The ZIC-pHILIC column was eluted using two mobile phases A and B. In mobile phase A, 20 mM ammonium carbonate with pH 9.2, and mobile phase B, acetonitrile (ACN). The concentration of A was slowly increased from 20% to 80% over 30 min and then held at 92% for 5 mins, after that it was equilibrated at 20% for 5 minutes. The mobile phases for the reverse phase column were: A, 0.1% (v/v) formic acid in H_20; B, 0.1% (v/v) formic acid in ACN. Mobile phase A was decreased from 95% to 10% over 30 min and then it is held at 10% for 5 min. Samples were analyzed by LCMS and different metabolites detected were identified with the help of their accurate mass and comparing their retention time with that of the authentic standards used.

2.2.3 Data Retrieval

There are two types of ionic molecular modes that are positive mode and negative mode. These ionic modes depend on the gain or loss of the protons. The data from both of these ionic mode were processed separately. The output from the LCMS are RAW files which contain data from positive and negative modes and these RAW files were organised into separate folders for each of the treatment groups. For an initial organisation of the data, RAW files containing data were transferred to a server to convert this raw data into csv files. RAW data files were first converted to the mzXML format using msconvert (ProteoWizard), this splits the data according to the polarity, generating separate positive mode and negative mode mzXML files from each RAW file. Peaks in each file were identified and extracted by XCMS to generate a peakML file and peaks from replicate samples were aligned using mzMatch.R. All peaks from replicate samples were combined in a single peakML file. This file was converted to a csv file containing retention times, accurate masses and peak intensities for each peak in all the samples. This csv file was imported into IDEOM (identification and evaluation of metabolomics data from LCMS) for further analysis**.** IDEOM is an excel template with macros with the following features (Creek et al., 2012):

- With small data sets, IDEOM can process the raw files with msconvert, XCMS and mzMatch as described above. For speed and convenience, these steps were routinely carried out on a server using a script written by Dr G. Blackburn, before uploading the csv file into IDEOM.
- An additional automated filtering and annotation procedure was used to remove artifacts from the LCMS data.
- Identification of peaks was carried out using a procedure based on exact mass and retention time, with annotation of confidence level (the excel spreadsheets in IDEOM software have the confidence level of true identification of metabolites ranging from 1-

10, The assigned level of confidence to each of the peaks selected is based on how accurately the m/z mass and retention times are matched with that of the authentic standards of any particular metabolite. So all the peaks/chromatograms ≥ 6 confidence level were selected while all the remaining peaks were excluded from the further analysis).

- Data analysis and visualization tools to enable biological interpretation of results are also available. IDEOM has an extensive data base of metabolites which is used to calculate retention time based on physico chemical properties (also in the database) and the conditions of LC. The retention times of a panel of authentic standards are also incorporated in the calculation using a multivariate linear regression model.

A software ToxID 2.1 was used to process raw data files of metabolite standards solutions (Thermo Fisher Scientific Inc., Hemel Hempstead, UK). After evaluation of the extracted ion chromatograms, retention times of the standards were used to compare with the tested molecules. Initial processing of RAW data carried out on a server using mzMatch R created a CSV file with a table of peak intensities, accurate mass and retention times for all features identified for all samples which were imported to IDEOM v19 for metabolite identification. This identification was based on accurate mass and retention time. IDEOM gives two levels of identifications that are confirmed identification and putative identifications. The former is accurate mass and retention time matching with that of an authentic standard (difference ≤ 5%). While a putative identification is accurate mass and retention time matching the retention time calculated in IDEOM (difference ≤ 50%).

For the details of all the standards used in chapter 3 and 4, see appendix 2.

All the data obtained were subjected to further statistical analysis for multivariate analysis in a software called SIMCA® version 16.0.1. The main features of this software include

- Import data from multiple file formats
- Review, plot and explore data interactively to identify important correlations
- Click individual data points to reveal underlying contributions
- Examine relationships between variables
- Quickly identify the most important factors and interactions
- Implement Python scripts to automate your workflows
- Investigate and diagnose the root causes of problems
- Predict yield, quality and future behaviour
- Communicate results effectively using the automated report generator
- Seamlessly integrate your optimized models into SIMCA®-online

In the current studies, different features of this programme were used including workset, model selection and diagnostics & interpretation to perform multivariate analysis. For an overview of the data, PCA-X model was chosen.

Another software for the initial analysis of data is called metaboanalyst software (version 5). This is a user-friendly, streamlined metabolomics data analysis tool and accepts a wide variety of metabolomics data types produced by metabolomics studies along with KEGG orthologs (KO) and a list of genes, thus supporting integrative analysis with metagenomics and transcriptomic. Metaboanalyst has 12 modules which are classified into 4 general categories as follows:

- Exploratory statistical analysis
- Functional enrichment analysis
- Data integration & systems biology
- Data processing & utilities

At this stage in project, exploratory statistical analysis was used.

The csv files containing identified metabolites exported from IDEOM v19 were subjected to multivariate analysis through SIMCA. The main components of this analysis were principal component analysis (PCA) and orthogonal partial least square discriminant analysis (OPLS-DA). These two were performed to observe major trends in different data sets from all of the three tissues in experiment 1 data set shown in chapter 3. Different statistical parameters are inbuilt in this software to determine the level of significance between different variables. Metaboanalyst was used for further analysis of different features obtained from the data set including volcano plots, which gives us an initial screening of different variables and their significance based on log 2FC and –log10 P. The details of each segment discussed here can be seen in the results section.

2.2.4 Glasgow Polyomics Data analysis

For LCMS analysis, samples/ extracts from this large set of the experiment were sent to Glasgow polyomics under the project number 2162 dated 6th of July,2021. These extracts were mainly analyzed by Erin Manson, a member of the Glasgow polyomics staff. The RAW files obtained were received in the SIPBS, University of Strathclyde where all further steps of analysis were carried out. An analysis in PiMP was also carried out in Glasgow polyomics uploaded online on a server. After getting the raw data from polyomics, further analysis of the data was carried out as discussed above for experiment 1. However, it is worth mentioning here that there was an additional information of MS^2 fragmentation data available in this analysis while Strathclyde mass spec data was lacking this information.

2.3 Metagenomic analysis

2.3.1. Faecal pellets collection

Faecal pellets were collected after every week starting from day 0 through day 21. The collection was possible only by monitoring each individual mouse until defecate under natural conditions. The freshly excreted faecal pellets (n= 3-5) were collected in cryotubes and immediately snap-frozen in dry ice until transferred to -80˚C freezer for storage till further processing. It is worth mentioning here that there were no visible changes that can be seen by the naked eye regarding colour, consistency or size of the pellets amongst different groups.

In this experimental design, faecal pellets were supposed to be collected for 5 different time points (days 0,7,14,21 and 28), but keeping in view the circumstances of the weight loss of some of the infected mice from both sexes, only 4 time-point collections (days 0, 7, 14 and 21) were made and all the mice were humanely killed and their blood samples directly from the heart were collected. These blood samples were subjected to centrifugation at 13,000 rpm for 10 minutes at a temperature of 4˚C to collect plasma samples. These plasma samples were stored at -80˚C for future use.

2.3.2 Faecal DNA extraction

DNA was extracted from the faecal pellets with the help of QIAamp® PowerFecal® DNA Kit, catalog No.12830-5, Number of Preps 50 (Qiagen).

2.3.2.1 DNA extraction protocol

Faecal pellets equivalent to around 0.25 grams were added to the dry bead tube. 750 µl of Bead Solution was added to the dry bead tube and gently vortexed to mix. 60 µl of Solution C1 added and inverted several times or vortexed very briefly. This tube is heated at 65°C for 10 minutes and after securing the bead tubes horizontally with the help of the vortex adapter tube holder,

tubes were vortexed at maximum speed for 10 minutes. Then the tubes were centrifuged at 13,000 x g for 1 minute. After centrifugation, the supernatant was transferred to a clean 2 ml collection tube. 250 µl of solution C2 was mixed and vortexed briefly before incubation at 4°C for 5 minutes. Then again the tubes centrifuges at 13,000 x g for 1 minute. Avoiding the pellet, up to 600 µl of supernatant was transferred to a clean 2 ml collection tube. Then 200 µl of solution C3 was mixed and vortexed briefly before incubation at 4°C for 5 minutes. Again, the tubes were again centrifuged at 13,000 x g for 1 minute. Up to 750 µl of the supernatant again transferred to a clean 2 ml collection tube. 1200 µl of solution C4 was added to the supernatant and vortexed for 5 seconds. 650 µl of supernatant was loaded onto a spin filter and centrifuged at 13,000 x g for 1 minute. Then 500 µl of Solution C5 was added and centrifuged for 1 minute at 13,000 x g. Flow through was discarded and centrifuged again for 1 minute at 13,000 x g. The Spin Filter was placed in a clean 2 ml collection tube. A 100 µl of solution C6 added to the centre of the white filter membrane. Alternatively, sterile DNA-Free PCR Grade Water or TE buffer can also be used for elution from the silica spin filter membrane at this step. The tubes were centrifuge at 13,000 x g for 1 minute and discarded the spin filter basket. The DNA in the tube is now ready for downstream application.

2.3.2.2 Quantification and assessment of DNA purity

The concentrations and purity of the extracted DNA was measured a nanodrop spectrophotometer using 260/280 and 260/230 absorbance ratios (Nanodrop 1000 Spectrophotometer, Thermo Fisher Scientific, Waltham, MA). Extracted DNA was run on 1% agarose gel to evaluate the DNA signals regarding the concentrations of DNA. After quantification and assessment of DNA Samples, these were stored at -80°C until further sequencing analysis. Followings are the images of DNA gel electrophoresis (DNA extracted

from faecal pellets at different time points) along with the concentration of DNA in tabulated form for each time point examined. (Fig. 2.2 to 2.5, Table 2.1 to 2.4)

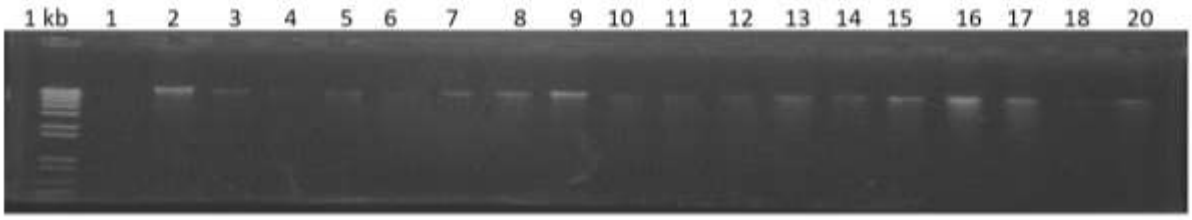

Figure 2. 2 shows pre-infection (Day-0) faecal DNA concentration on 1% agarose gel electrophoresis.

Table 2. 1 The concentration and 260/280 ratio of the extracted DNA extracted at day 0. Light blue represents control group members, red indicates infected samples while blue shows samples from the control group gavaged with control brain in PBS.

Sample	Image number	Conc (ng/ul)	260/280
D0-M2	2	5.2	1.4
D0-M3	3	19	1.3
D0-M5	5	12.9	1.55
D0-M8	8	53.5	1.75
D0-M9	9	104.6	1.66
D0-M15	15	53.6	1.72
D0-M16	16	68.3	1.75
D0-M17	17	13.9	1.48
D0-M20	20	12.8	1.64

	Control
	Infecetd
	Control brain

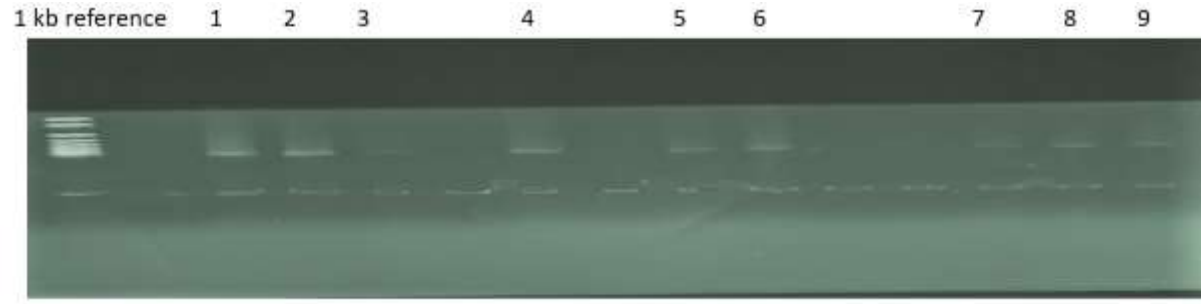

Figure 2. 3 Shows day 7 post-infection faecal DNA concentration on 1% agarose gel electrophoresis.

Table 2. 2 The concentration and 260/280 ratio of the DNA extracted on day 7. Light blue represents control group members, red indicates infected samples while blue shows samples from the control group gavaged with control brain in PBS.

Sample	Image number	Conc (ng/ul)	260/280
D7-M1	1	46	1.65
D7-M2	2	24.9	1.64
D7-M3	3	19.3	1.45
D7-M6	4	19.7	1.53
D7-M7	5	15.2	1.49
D7-M8	6	22	1.38
D7-M16	7	29.3	1.63
D7-M17	8	38.3	1.68
D7-M18	9	20.9	1.44

	Control
	Infecetd
	Control brain

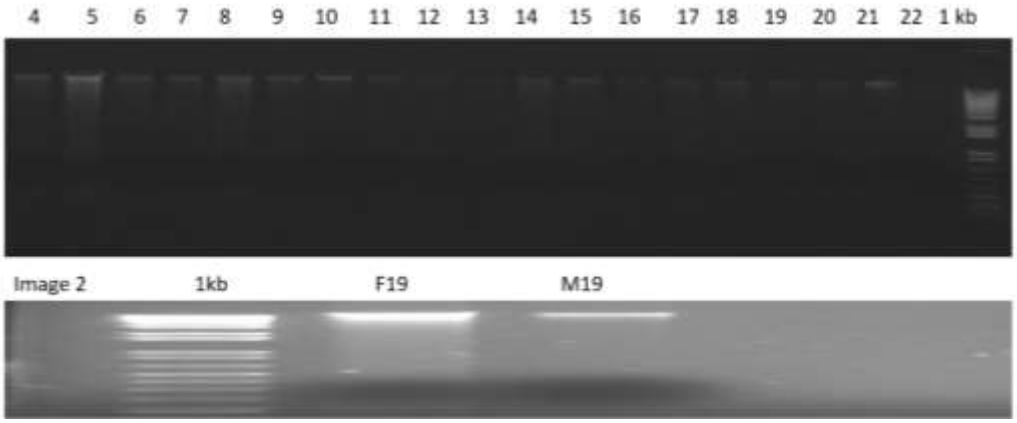

Figure 2. 4 Shows day 14 post-infection fecal DNA concentration on 1% agarose gel electrophoresis.

Table 2. 3 showing the concentration and 260/280 ratio of the DNA extracted on day 14. Light blue represents control group members, red indicates infected samples while blue shows samples from the control group gavaged with control brain in PBS.

Sample	Image number	Conc (ng/ul)	260/280
D14-M2	17	21.5	1.87
D14-M3	7	17	1.8
D14-M5	9	28	1.81
D14-M7	14	35.2	1.83
D14-M11	8	49.4	1.83
D14-M12	18	24.9	1.89
D14-M16	19	10.8	1.78
D14-M17	20	7.8	1.86
D14-M19	Image 2	17.1	1.38

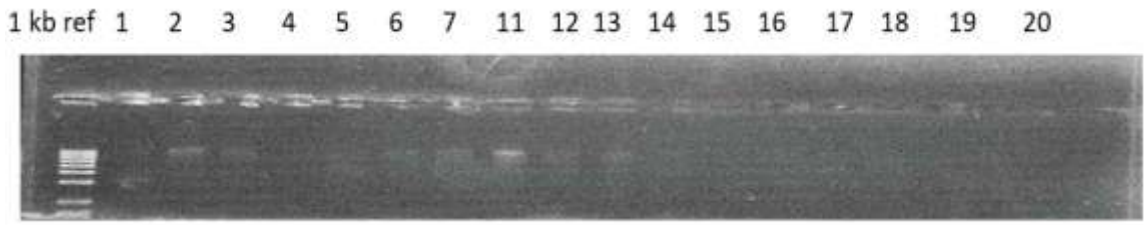

Figure 2. 5 Day 21 post-infection faecal DNA concentration on 1% agarose gel electrophoresis.

Table 2. 4 showing the concentration and 260/280 ratio of the DNA. Light blue represents control group members, red indicates infected samples while blue shows samples from the control group gavaged with control brain in PBS.

Sample	Image number	Conc (ng/ul)	260/280
D21-M1	1	16.8	1.65
D21-M2	2	21.4	1.65
D21-M5	5	17.2	1.55
D21-M7	7	24.5	1.55
D21-M11	11	32.8	1.71
D21-M13	13	21.9	1.69
D21-M17	17	12.3	1.57
D21-M19	19	14.4	1.64
D21-M20	20	12.3	1.68

DNA extraction from days 0, 7, 14 and 21 were carried out using the same faecal DNA isolation kit. These DNA samples were sent off to Novogene (HK) Company Ltd for further sequencing analysis to evaluate the changes in the biological ecosystem.

3- Metabolomics profile of the maternal foetal interface infected with *T. gondii*

Abstract

Congenital toxoplasmosis is a serious risk to the developing foetus. Despite a large volume of literature available for *T. gondii infection* in adulthood, very little is known about the effects of infection on the developing foetus and the maternal foetal interface. Less still is known about the how metabolism is affected at these sites. The primary objective of this chapter is to determine whether *T. gondii* infection alters the metabolism of the maternal foetal interface and the developing foetus and to understand the consequences of these changes for mother and foetus. BALB/c, mice were infected with tachyzoites of the Me49 strain intra-peritoneally on day 7 of pregnancy and decidua, placenta and foetus were collected on day 14 of pregnancy. Following preparation of metabolite extracts, LCMS was performed followed by analysis of raw data into IDEOM. Multivariate analysis was performed using SIMCA version 16.0.1 along with metaboanalyst version 5. For graphical representation of data, Graph Pad Prism version 9 is used. Based on accurate mass and retention time, a total of 290, 323, and 287 metabolites were confidently identified from decidua, placenta and foetus, respectively. A number of these metabolites were identified as being altered in the maternal foetal interface and foetuses of mice infected with *T. gondii* in comparison to tissues form control mice ($P<0.05$). Significantly, these metabolites include citrulline, proline, kynurenine and 1-methylnicotinamide. Kynurenine was upregulated in infected mice in comparison to controls ($P<0.05$) in foetus while downregulated in placenta and decidua ($P<0.05$) whereas citrulline, and 1-methylnicotinamide were downregulated in the foetus, placenta and decidual extracts in comparison to controls ($P<0.05$). In addition, some of the metabolites (indoxylsulfate and 4-guanidinobutanoate) most probably originating from microbiome sources are also observed to be downregulated in all 3 tissues examined ($P<0.05$), indicating a significant change in the microbiome of the maternal foetal interface in *T. gondii* infected mice. In conclusion**,** the work described here has for the first time identified various metabolites as being altered in maternal foetal interface and the developing

foetus of mice infected with *T. gondii.* Alteration of these pathways could have consequences for the success of pregnancy and the development of the foetus and provides an insight into how the maternal metabolism could affect the developing foetus. Notably, the results demonstrate that maternal *T. gondii* infection induces metabolic changes to the foetus in utero. The consequences of these changes for post-natal health and development requires further investigation.

3.1 Introduction

T. gondii is an intracellular protozoan parasite that causes toxoplasmosis infection. This parasite can pass through the intestinal epithelium and break biological barriers e.g., placenta and blood-brain barrier. By passing these barriers, *T. gondii* can cause severe pathologies such as neurological, ocular and congenital toxoplasmosis (Silveira et al., 2001). If the primary infection with *T. gondii* occurs for the first time during late pregnancy, it may result in the severe consequences of vertical transmission to the foetus, leading to congenital toxoplasmosis (Roberts and Alexander, 1992). There is a considerable volume of literature available describing how *T. gondii* contributes to neural and ocular toxoplasmosis in both adult and congenital acquired disease. However, our knowledge regarding congenital toxoplasmosis and how it affects the maternal foetal interface and the developing foetus is still minimal. By keeping in view the potential to fill this gap with regards to the maternal foetal interface and the developing foetus infected with *T. gondii*, a global metabolomics approach was adopted. Metabolomics is the study of small molecules within cells, bio fluids, tissues, or any organ under consideration. Despite having great potential to aid our understanding of biological processes and disease, metabolomics is still considered an emerging science among the omics techniques. There is growing evidence of literature available detailing metabolomics profiling of physiological and pathological pregnancies. The tissues or bio fluids that can be evaluated in pregnancy are from the mother (serum, vaginal fluid or any other biological fluid), the foetus (amniotic fluid, umbilical cord blood) and the new born (plasma, placenta, urine, saliva or other bio fluids available (Vassilies et al., 2013). In addition, metabolite extracts can be made from available tissue or tissue biopsies. Metabolomics profiles of these tissues, fluids or organs reflect the biochemical changes occurring and provide clues about their underlying reasons and consequences. Therefore, in this study foetus, placenta and decidua obtained from BALB/c mice infected with *T. gondii* tachyzoites during pregnancy was subjected to metabolomics

profiling in comparison with these tissues obtained from uninfected control pregnant BALB/c mice.

3.2. Aims and Objectives

The aims of the studies described herein is to determine if *T. gondii* infection alters metabolism of the maternal foetal interface and the foetus of infected mice. To achieve this, the BALB/c murine model of congenital toxoplasmosis is an ideal fit. Vertical transmission of infection only occurs in BALB/c infected for the first time during pregnancy and thus emulates this characteristic of congenital toxoplasmosis in humans (Roberts and Alexander, 1992).

Specific objectives are:

(i) to use LCMS to identify the metabolites present in decidua, placenta and the foetuses from control non-infected BALB/c mice and compare these with metabolites present in these tissues from BALB/c mice infected with *T. gondii* during pregnancy.

(ii) to use this information to determine biochemical pathways and processes affected in these tissues by *T. gondii* infection.

3.3 Results

3.3.1 Metabolomics profile of maternal foetal interface in mice infected with *T. gondii*

This research project is collaborative, so all of the steps for mice rearing, housing, mating, and pregnancy diagnosis were performed by Margarida Borges and colleagues at the University of Porto, Portugal. After confirmation of pregnancy, infection with *T. gondii* Me49 strain was used and samples from the placenta, foetus and decidua were collected from pregnant *T. gondii* infected and pregnant uninfected mice. There was a total of 4 BALB/c pregnant mice used in this study. 2 of these mice were infected with Me49 strain of *T. gondii* on day 7 of pregnancy and tissues harvested on day 14 of pregnancy. The remaining 2 mice served as controls from which healthy tissues were obtained on day 14 of pregnancy.

The details of samples/extracts from each of the tissue is displayed (Table 3.1)

Table 3. 1 No. of samples/units for each mouse in each tissue.

	Uninfected		Infected	
	Mouse 1	Mouse 2	Mouse 1	Mouse 2
Decidua	5	8	8	2
Placenta	5	8	8	2
Foetus	6	8	7	2

Those samples were stored at -80^{o}C and shipped to SIPBS on dry ice and further processed for metabolites extraction and LCMS analysis. An untargeted metabolomics approach was adopted to evaluate different biochemical pathways and metabolite alterations in the decidua, placenta and foetus. For an overview of the data obtained from the IDEOM software and the metabolic variations in all three tissues under examination, a multivariate analysis was performed to observe the distribution/ groupings and an overall trend of the different extracts involved in the infected and control groups.

3.3.2 Multivariate analysis

To start with an overall visualisation of the data and the groups under investigation, two components principle component analysis (PCA) plot and a cross-validated orthogonal partial least square discriminant analysis (OPLS-DA) plot were used. PCA illustrates separation or distinct/non-distinct grouping between infected and uninfected groups. This separation is based on the peak intensity of different variables in infected and uninfected groups involved in this experiment. The OPLS-DA plot is a supervised pattern recognition process that differentiates between groups and permits the identification of metabolites associated with any treatment given in this experiment. To further identify the significant metabolites, volcano plots for each of the tissues were obtained from Metaboanalyst version 5.0 (an online software) which

provides a user-friendly and streamlined metabolomics data analysis. The plots were analysed both from the two columns used i.e., ZIC-pHILIC column which is the primary column along with the ACE C18-PFP column used to augment the coverage of metabolites identified in the primary column. All the significant metabolites are shown in their relevant tissue sections along with their formula, mass, retention time, log2 fold change (threshold 1.5) and –log10 P values (Section 3.3.3, 3.3.4, 3.3.5). LC-MS based metabolomics analysis was utilised to detect the global metabolomic profiles of the decidua, placenta and foetus of maternally infected mice with *T. gondii*. Lipid profile was excluded from this analysis because LC-MS system settings used for this analysis are not suitable for lipid analysis. Analysis of the PCA outputs indicated that both infected and non-infected decidua, placenta and foetus produced distinct groups. On the other hand, OPLS-DA was facilitated the identification of which metabolites and thus which metabolic pathways are undergoing the most alterations with maternal *T. gondii* infection. Metabolites identified included amino acids and carbohydrates which have been implicated in various biological processes and pathways. It is important to note that other metabolites have also been identified though not to an extensive scale as amino acids and carbohydrates. The detailed results of each tissue are as under in their relevant section.

3.3.3 Decidua

The following results below indicate the PCA plots from the pHILIC column as well as the C18-PFP column. The PCA plots were produced to distinguish between the two groups (infected and uninfected) based on the relative variables. The pHILICcolumn is hydrophilic thus ensuring detection of hydrophilic metabolites whereas C18-PFP is a hydrophobic column resulting in detection of hydrophobic metabolites. C18-PFP also includes a pentafluorophenol (PFP) group that binds aromatic amino acids and their derivatives, including dopamine and serotonin. Furthermore, a volcano plot was produced to analyse the significant metabolites based on their log 2-fold change with a threshold of 1.5 and -log10 P-value of $\geq$ 1.3. Analysis was taken for the decidua as well as the placenta and the developing foetuses.

Different metabolites detected using pHILIC and C18-PFP columns were evaluated for multivariate analysis, the resultant PCA and OPLSDA plots for the decidual extracts infected with *T. gondii* compared with the uninfected control extracts are shown in the following figures 3.1 and 3.2.

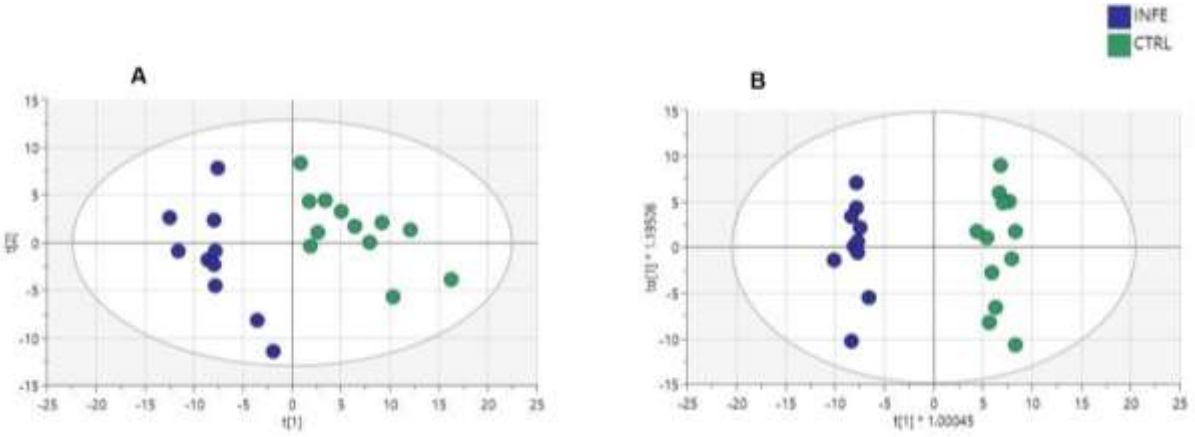

Figure 3. 1 Multivariate Analysis of Decidua using pHILIC column. (A) PCA score plot indicates separation between decidual extracts from infected with T. gondii and uninfected control group, **(B)** Orthogonal Partial Least Square Discriminant Analysis (OPLS-DA) plot shows an excellent separation between decidual extracts from infected with T. gondii group and uninfected control groups. Each data point in A & B represents one mouse decidua sample.

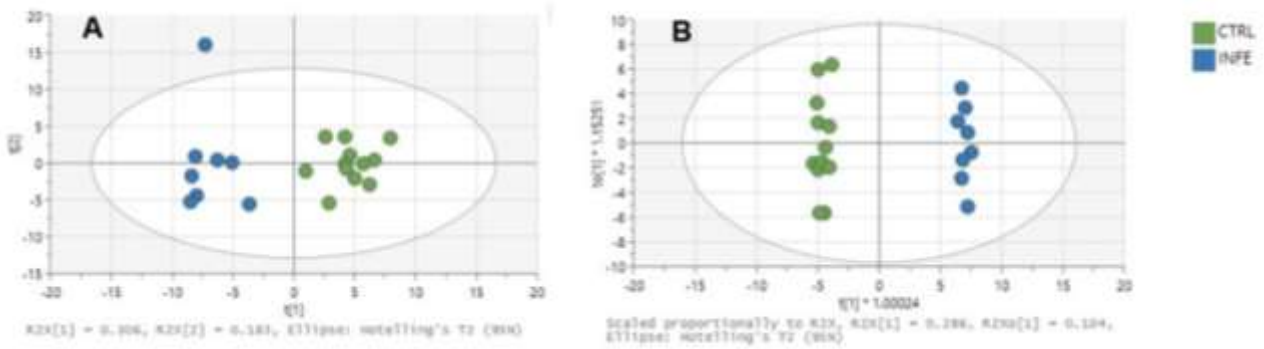

Figure 3. 2 Multivariate Analysis of Decidua using C-18 PFP column. (A) PCA score plot shows separation between decidual extracts infected with T. gondii and uninfected control group, **(B)** Orthogonal Partial Least Square Discriminant Analysis (OPLS-DA) plot shows an excellent separation between decidual extracts from infected with T. gondii and uninfected control groups. Each data point in A & B represents one mouse decidua sample.

A further analysis to determine different metabolites with a significant change, volcano plots analysis was carried out shown in the following figure 3.3 below.

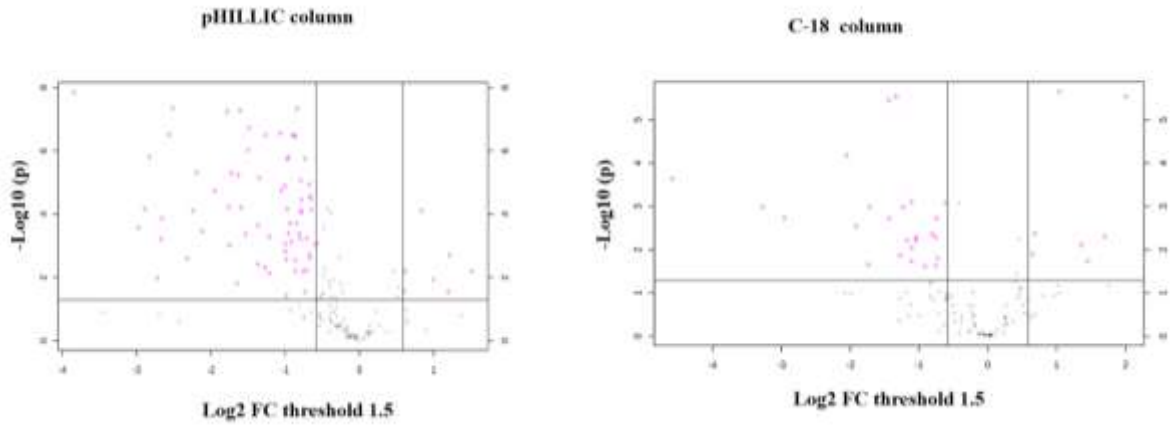

Figure 3. 3 represents volcano plots for the analysis of significant metabolites in Decidua with pHILLIC column and C-18 PFP column. The X-axis shows fold change and Y-axis is indicative of significance. Each pink dot represents a particular significantly increased/decreased metabolite with log2 fold change threshold 1.5 and –log10 P >1.3, while all the black dots correspond to different metabolites below the significance threshold.

Table 3. 2 LC-MS analysis of decidua extracts congenitally infected with *T. gondii* using the pHILIC column: Metabolites that show a significant change (> Log2-fold change (threshold 1.5) in peak intensity and P < 0.05) using metaboanalyst. Fold change (FC) values are shown as log2 and P values as –log10. Retention times (RT) are also shown in minutes. Significantly increased metabolites (log2 FC (threshold 2) ≥ 1.0, log2 FC (threshold 1.5) ≥ 0.60, -log10 P >1.3) are marked as dark red and bright red, respectively. A significant decrease (log2 FC (threshold 2) ≤ -1.0, log2 FC (threshold 1.5) ≤ 0.60, -log10 P >1.3) is represented by a dark blue and light blue colour, respectively. The identity of metabolites highlighted in yellow were confirmed by matching their retention times with those obtained for authentic standards under the same conditions.

Mass	RT(*min*)	Formula	Metabolites	VIP	log2(FC)	-Log10 P
231.07	14.65	C9H13NO6	N-Succinyl-L-glutamate 5-semialdehyde	1.06	1.52	2.19
158.07	12.87	C6H10N2O3	4-Methylene-L-glutamine	1.02	1.21	2.70
580.04	18.05	C15H22N2O18P2	UDP-glucuronate	0.81	1.20	1.54
286.06	15.82122	C7H15N2O8P	5'-Phosphoribosylglycinamide	1.02	0.99	1.94
267.10	8.798256	C10H13N5O4	Adenosine	1.21	0.84	4.12
132.05	11.47593	C4H8N2O3	N-Carbamoylsarcosine	1.02	0.62	2.19
240.12	13.82981	C10H16N4O3	Homocarnosine	0.86	0.61	1.56
105.04	15.20266	C3H7NO3	L-Serine	1.14	-0.59	3.06
131.06	9.020336	C5H9NO3	L-Glutamate 5-semialdehyde	1.25	-0.65	4.15
146.11	24.00281	C6H14N2O2	L-Lysine	1.28	-0.65	4.49
204.09	11.16595	C11H12N2O2	L-Tryptophan	1.12	-0.67	2.60
181.07	12.5223	C9H11NO3	L-Tyrosine	1.30	-0.67	4.57
398.14	15.87697	C15H22N6O5S	S-Adenosyl-L-methionine	1.03	-0.67	2.74
75.03	15.06258	C2H5NO2	Glycine	1.29	-0.68	4.95
136.05	8.540666	C8H8O2	Phenylacetic acid	1.18	-0.71	3.23
384.12	13.13307	C14H20N6O5S	S-Adenosyl-L-homocysteine	1.11	-0.71	2.24
149.05	11.21522	C5H11NO2S	L-Methionine	1.36	-0.73	5.75
147.05	10.77301	C5H9NO4	O-Acetyl-L-serine	0.85	-0.74	1.54
170.00	14.70124	C3H7O6P	D-Glyceraldehyde 3-phosphate	1.05	-0.76	2.19
164.05	8.421009	C9H8O3	Phenylpyruvate	1.31	-0.78	4.45
148.05	9.976453	C9H8O2	trans-Cinnamate	1.28	-0.79	4.05
132.09	25.47095	C5H12N2O2	D-Ornithine	1.33	-0.79	5.07
130.11	19.89209	C6H14N2O	N-Acetylputrescine	1.14	-0.79	3.23
446.06	15.70266	C11H20N4O11P2	CDP-ethanolamine	1.19	-0.81	3.39
115.06	12.34717	C5H9NO2	L-Proline	1.44	-0.84	7.34
229.09	14.28907	C9H15N3O2S	Ergothioneine	1.21	-0.85	3.71
119.06	13.87997	C4H9NO3	L-Threonine	1.40	-0.87	6.46
158.04	13.06366	C4H6N4O3	Allantoin	1.08	-0.87	2.22
109.0198	14.44623	C2H7NO2S	Hypotaurine	1.01	-0.87	2.54
131.09	10.51255	C6H13NO2	L-Leucine	1.39	-0.88	6.49
165.08	9.977262	C9H11NO2	L-Phenylalanine	1.41	-0.89	6.49
134.02	15.086	C4H6O5	(S)-Malate	1.17	-0.92	3.13
167.04	14.92073	C3H9N3O3S	Taurocyamine	1.20	-0.94	3.71
176.03	16.38429	C6H8O6	D-Glucuronolactone	1.17	-0.96	3.39
258.08	12.28824	C10H14N2O6	(1-Ribosylimidazole)-4-acetate	1.35	-0.96	5.80
103.10	18.89349	C5H13NO	Choline	1.34	-0.97	5.75
167.06	7.969169	C8H9NO3	Pyridoxal	1.25	-0.97	4.17
159.07	7.466535	C10H9NO	Indole-3-acetaldehyde	1.07	-0.98	2.57
589.08	16.73262	C16H25N5O15P2	GDP-L-fucose	0.90	-0.98	1.43

Log2 FC Threshold 2	Increase	≥ 1.0	
Log2 FC Threshold 1.5	Increase	≥ 0.6	
Log2 FC Threshold 1.5	Decrease	≤ -0.6	
Log2 FC Threshold 2	Decrease	≤ -1.0	

254.06	14.85876	C7H14N2O6S	5-L-Glutamyl-taurine	1.13	-1.00	3.06
208.08	12.81	C10H12N2O3	L-Kynurenine	1.14	-1.00	2.83
168.03	11.99	C5H4N4O3	Urate	1.29	-1.00	4.90
152.03	10.95	C5H4N4O2	Xanthine	1.31	-1.05	4.74
117.05	15.19	C3H7N3O2	Guanidinoacetate	1.41	-1.06	6.54
536.05	15.44	C14H22N2O16P2	UDP-D-xylose	1.05	-1.21	2.15
182.08	13.42	C6H14O6	D-Sorbitol	1.10	-1.21	3.29
188.13	25.73	C7H16N4O2	Homoarginine	1.38	-1.27	6.49
376.14	8.38	C17H20N4O6	Riboflavin	1.01	-1.28	2.32
188.15	21.47	C9H20N2O2	N6_N6_N6-Trimethyl-L-lysine	1.34	-1.35	5.16
314.05	14.54	C8H15N2O9P	5'-Phosphoribosyl-N-formylglycinamide	1.21	-1.36	3.65
301.06	14.47	C8H16NO9P	N-Acetyl-D-glucosamine 6-phosphate	1.03	-1.37	2.43
160.12	22.85	C7H16N2O2	N6-Methyl-L-lysine	1.41	-1.49	6.73
103.06	14.93	C4H9NO2	4-Aminobutanoate	1.38	-1.50	6.02
129.04	10.45	C5H7NO3	L-1-Pyrroline-3-hydroxy-5-carboxylate	1.18	-1.53	3.37
162.05	19.57	C6H10O5	3-Ethylmalate	1.29	-1.59	4.21
136.06	22.96	C7H8N2O	1-Methylnicotinamide	1.43	-1.61	7.27
142.07	12.70	C6H10N2O2	Ectoine	1.28	-1.63	5.24
607.08	14.46	C17H27N3O17P2	UDP-N-acetyl-D-glucosamine	1.07	-1.65	1.82
284.08	11.59	C10H12N4O6	Xanthosine	1.34	-1.72	5.30
663.11	13.69	C21H27N7O14P2	NAD+	1.19	-1.75	3.02
240.02	15.75	C6H12N2O4S2	L-Cystine	1.23	-1.76	4.24
175.10	15.38	C6H13N3O3	L-Citrulline	1.44	-1.78	7.25
75.07	22.03239	C3H9NO	(R)-1-Aminopropan-2-ol	1.31	-1.95	4.73
111.04	10.99	C4H5N3O	Cytosine	1.20	-2.12	3.46
264.10	19.42	C12H16N4OS	Thiamin	1.35	-2.19	5.32
102.03	10.64	C4H6O3	(S)-Methylmalonate semialdehyde	1.26	-2.25	4.12
105.08	18.01	C4H11NO2	Diethanolamine	1.02	-2.32	2.61
145.09	14.62	C5H11N3O2	4-Guanidinobutanoate	1.41	-2.52	7.36
180.05	8.14	C6H12O4S	5-Methylthio-D-ribose	1.40	-2.57	6.51
290.12	16.19	C10H18N4O6	N-(L-Arginino)succinate	1.18	-2.66	3.87
194.08	10.41	C7H14O6	1-O-Methyl-myo-inositol	1.18	-2.67	3.22
156.05	7.73	C6H8N2O3	4-Imidazolone-5-propanoate	1.03	-2.72	1.98
139.07	7.85	C6H9N3O	L-Histidinal	1.36	-2.83	5.80
306.03	10.25	C9H11N2O8P	2'_3'-Cyclic UMP	1.27	-2.90	4.17
337.07	11.61	C10H16N3O8P	5-Hydroxymethyldeoxycytidylate	1.21	-2.98	3.57
153.09	7.44	C7H11N3O	4-(beta-Acetylaminoethyl)imidazole	1.45	-3.84	7.84

Table 3. 3 LC-MS analysis of decidua extracts congenitally infected with *T. gondii* using the C-18 column: Metabolites that show a significant change (> Log2-fold change (threshold 1.5) in peak intensity and P < 0.05) using metaboanalyst. Fold change (FC) values are shown as log2 and P values as –log10. Retention times (RT) are also shown in minutes. Significantly increased metabolites (log2 FC (threshold 2) ≥ 1.0, log2 FC (threshold 1.5) ≥ 0.60, -log10 P >1.3) are marked as dark red and bright red, respectively. A significant decrease (log2 FC (threshold 2) ≤ -1.0, log2 (FC threshold 1.5) ≤ 0.60, -log10 P >1.3) is represented by a dark blue and light blue colour, respectively. The identity of metabolites highlighted in yellow were confirmed by matching their retention times with those obtained for authentic standards under the same conditions.

Mass	RT	FORMULA	Metabolites	VIP	log2(FC)	-Log10 P
289.15	12.33	C13H23NO6	3-Methylglutarylcarnitine	1.55	2.00	5.54
321.10	8.53	C11H19N3O6S	gamma-L-Glutamyl-L-cystei	1.26	1.70	2.31
101.11	3.82	C10H26N4	Spermine	1.14	1.45	1.74
267.10	8.00	C9H17NO8	Neuraminic acid	1.21	1.36	2.12
141.02	5.37	C2H8NO4P	Ethanolamine phosphate	1.59	1.04	5.65
324.04	5.96	C9H13N2O9P	UMP	1.23	0.68	2.37
230.02	5.63	C5H11O8P	D-Ribose 5-phosphate	1.16	0.64	1.90
103.10	5.27	C5H13NO	Choline	1.36	-0.61	3.08
103.06	5.69	C4H9NO2	4-Aminobutanoate	1.16	-0.73	1.81
217.13	8.55	C10H19NO4	O-Propanoylcarnitine	1.35	-0.75	2.73
90.03	7.32	C3H6O3	(S)-Lactate	1.30	-0.76	2.28
109.02	5.42	C2H7NO2S	Hypotaurine	1.05	-0.76	1.63
229.09	5.77	C9H15N3O2S	Ergothioneine	1.29	-0.81	2.36
121.02	5.61	C3H7NO2S	L-Cysteine	1.09	-0.91	1.62
208.08	12.81	C10H12N2O3	L-Kynurenine	1.29	-1.04	2.28
191.06	12.94	C10H9NO3	5-Hydroxyindoleacetate	1.27	-1.05	2.21
259.18	38.80	C13H25NO4	Hexanoylcarnitine	1.25	-1.11	2.05
136.04	5.70	C5H4N4O	Hypoxanthine	1.38	-1.11	3.10
129.04	7.37	C5H7NO3	4-Oxoproline	1.15	-1.11	1.73
152.03	7.94	C5H4N4O2	Xanthine	1.22	-1.18	2.21
168.03	7.05	C5H4N4O3	Urate	1.38	-1.23	2.99
112.03	6.87	C4H4N2O2	Uracil	1.21	-1.28	1.87
132.09	4.79	C5H12N2O2	L-Ornithine	1.57	-1.34	5.54
106.03	5.91	C3H6O4	D-Glycerate	1.34	-1.43	2.73
175.10	5.43	C6H13N3O3	L-Citrulline	1.56	-1.44	5.46
239.10	7.25	C9H13N5O3	Dihydrobiopterin	1.33	-1.72	2.99
166.07	11.59	C6H14O3S	hexanesulfonate	1.17	-1.74	1.66
161.07	6.34	C6H11NO4	L-2-Aminoadipate	1.31	-1.92	2.55
176.09	12.50	C10H12N2O	Serotonin	1.47	-2.05	4.18
255.11	12.52	C12H17NO5	N-D-Glucosylarylamine	1.34	-2.96	2.73
193.07	37.89	C10H11NO3	Phenylacetylglycine	1.39	-3.27	2.99
144.12	39.52	C8H16O2	[FA (8:0)] octanoic acid	1.43	-4.59	3.64

3.3.4 Placenta

The following results below indicate the PCA plots from the pHILIC column as well as the C18-PFP column carried out for the extracts of the placenta. The PCA plots were produced to distinguish between the two groups (infected and uninfected) based on the relative variables. The pHILICcolumn is hydrophilic thus ensuring detection of hydrophilic metabolites whereas C18-PFP is a hydrophobic column resulting in detection of hydrophobic metabolites. C18-PFP also includes a pentafluorophenol (PFP) group that binds aromatic amino acids and their derivatives, including dopamine and serotonin. Furthermore, a volcano plot was produced to analyse the significant metabolites based on their log 2-fold change with a threshold of 1.5 and -log10 P-value of ≥ 1.3.

Different metabolites detected using pHILIC and C18-PFP columns were evaluated for multivariate analysis, the resultant PCA and OPLSDA plots for the decidual extracts infected with *T. gondii* compared with the uninfected control extracts are shown in the following figures 3.4 and 3.5.

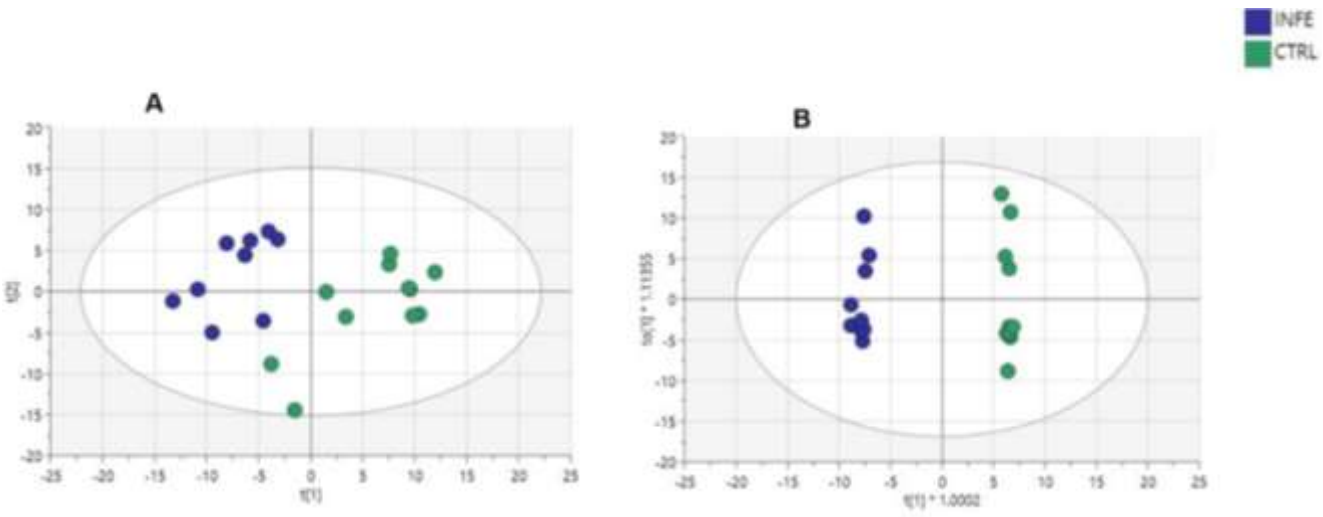

Figure 3. 4 Multivariate Analysis of Placenta using pHILIC column. (A) PCA score plot shows a separation (not tightly grouped) between placental extracts maternally infected with *T. gondii* group and uninfected control group, **(B)** Orthogonal Partial Least Square Discriminant Analysis (OPLS-DA) plot shows a clear separation between placental extracts maternally infected with *T. gondii* group and uninfected control groups. Each data point in A & B represents one mouse placenta sample.

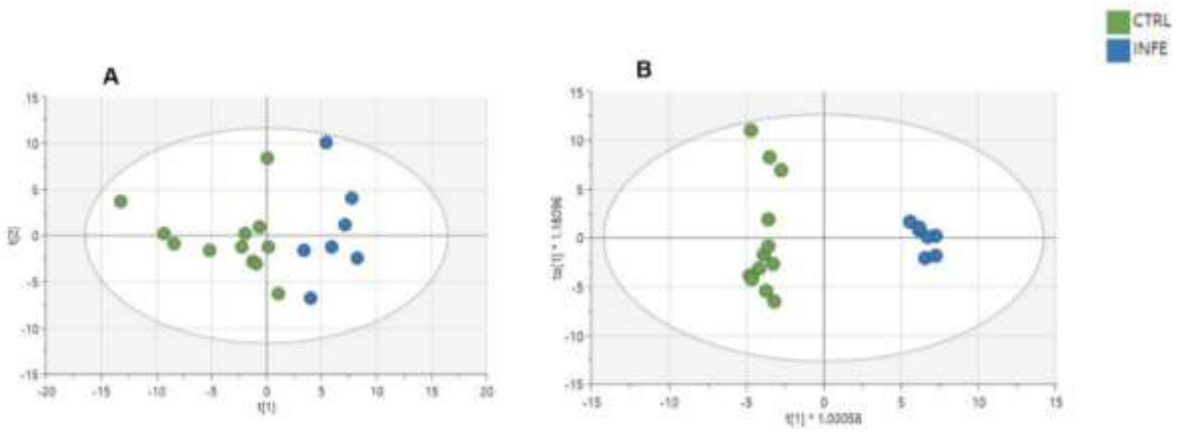

Figure 3. 5 Multivariate Analysis of Placenta using C18-PFP column. (A) PCA score plot shows a separation (distributed amongst four quadrants of the plot) between placenta extracts maternally infected with *T. gondii* group and uninfected control group, **(B)** Orthogonal Partial Least Square Discriminant Analysis (OPLS-DA) plot shows a clear separation between infected and control groups. Each data point in A & B represents one mouse placenta sample.

As evident from the Figures 3.4 and 3.5 above, there are separate groups of each class (infected and uninfected control) showing the status of infection. This classification is based on multiple variables (metabolites) distribution.

Based on these observations shown in the PCA plots above (Fig. 3.4, 3.5), it was necessary to examine which metabolites are the cause of this class/cluster formation in PCA plots. This was carried out with the help of the volcano plots shown in the following Figure 3.6.

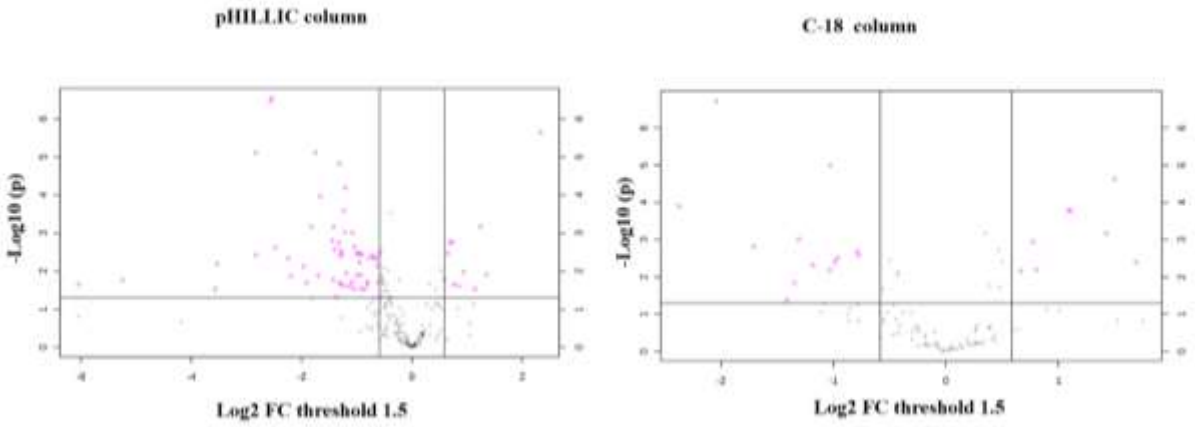

Figure 3. 6 represents volcano plots for the analysis of placental important metabolites with log2 fold change and –log10 p by pHILIC column and C18-PFP column. The X-axis shows fold change and Y-axis is indicative of significance. Each pink dot represents a particular significantly increased/decreased metabolite with log2 fold change threshold 1.5 and –log10 >1.3, while all the black dots correspond to different metabolites below the significance threshold.

The volcano plots shown above represented many metabolites that are changed significantly in placental extracts. The details of these metabolites can be seen in the following Table 3.4.

Table 3. 4 LC-MS analysis of placenta extracts using the pHILLIC column. Metabolites that show a significant change (>Log2-fold change (threshold 1.5) in peak intensity and P < 0.05) using metaboanalyst. Fold change (FC) values are shown as log2 and P values as –log10. Retention times (RT) are also shown in minutes. Significantly increased metabolites (log2 FC (threshold 2) ≥ 1.0, log2 FC (threshold 1.5) ≥ 0.60, -log10 P >1.3) are marked as dark red and bright red, respectively. A significant decrease (log2 FC (threshold 2) ≤ -1.0, log2 (FC threshold 1.5) ≤ 0.60, -log10 P >1.3) is represented by a dark blue and light blue colour, respectively. The identity of metabolites highlighted in yellow were confirmed by matching their retention times with those obtained for authentic standards under the same conditions.

Mass	RT (Min)	Formula	Metabolites	VIP	log2(FC)	-Log10 P
128.06	10.16	C5H8N2O2	5_6-Dihydrothymine	1.56	2.34	5.65
250.06	13.53	C8H14N2O5S	gamma-L-Glutamyl-L-cysteine	1.13	1.35	1.90
125.06	9.15	C5H7N3O	5-Methylcytosine	1.44	1.25	3.16
166.05	12.23	C5H10O6	L-Arabinonate	0.98	1.14	1.52
88.05	12.93	C4H8O2	(R)-Acetoin	1.25	0.94	1.98
267.10	8.81	C10H13N5O4	Adenosine	0.85	0.85	1.61
240.12	13.83	C10H16N4O3	Homocarnosine	1.07	0.76	1.65
113.06	9.44	C4H7N3O	Creatinine	1.23	0.73	2.76
132.05	11.47	C4H8N2O3	N-Carbamoylsarcosine	1.39	0.69	2.76
169.08	12.52	C7H11N3O2	N(pi)-Methyl-L-histidine	1.20	0.65	2.46
189.06	13.37	C7H11NO5	N-Acetyl-L-glutamate	1.11	0.59	1.78
149.05	11.21	C5H11NO2S	L-Methionine	1.25	-0.59	2.46
219.11	8.48	C9H17NO5	Pantothenate	0.76	-0.60	1.31
144.10	26.77	C5H12N4O	4-Guanidinobutanamide	1.23	-0.61	1.71
196.06	12.89	C6H12O7	D-Gluconic acid	1.34	-0.66	2.32
116.01	15.20	C4H4O4	Fumarate	1.26	-0.68	2.34
103.10	18.88	C5H13NO	Choline	1.39	-0.72	2.42
229.09	14.30	C9H15N3O2S	Ergothioneine	1.33	-0.78	2.34
182.06	8.54	C9H10O4	3-(4-Hydroxyphenyl)lactate	1.26	-0.80	1.72
130.11	19.87	C6H14N2O	N-Acetylputrescine	1.23	-0.81	1.65
121.02	14.71	C3H7NO2S	D-Cysteine	1.11	-0.86	1.52
160.08	13.72	C6H12N2O3	N-gamma-Acetyldiaminobutyrate	1.38	-0.91	2.42
175.05	13.83	C6H9NO5	N-Acetyl-L-aspartate	1.15	-0.92	1.53
348.05	14.78	C10H13N4O8P	IMP	1.13	-0.92	1.90
168.03	11.99	C5H4N4O3	Urate	1.29	-0.95	2.23
117.05	15.19	C3H7N3O2	Guanidinoacetate	1.32	-0.98	2.46
158.04	13.07	C4H6N4O3	Allantoin	1.42	-1.00	2.46
455.15	15.77	C20H21N7O6	5_10-Methenyltetrahydrofolate	1.03	-1.04	1.52
152.03	10.91	C5H4N4O2	Xanthine	1.47	-1.04	2.64
167.06	7.99	C8H9NO3	Pyridoxal	1.37	-1.08	3.01
208.08	10.51	C10H12N2O3	L-Kynurenine	1.17	-1.08	1.71
459.19	13.56	C20H25N7O6	5-Methyltetrahydrofolate	1.12	-1.12	1.59
239.10	12.16	C9H13N5O3	Dihydrobiopterin	1.24	-1.19	1.95
175.10	15.39	C6H13N3O3	L-Citrulline	1.58	-1.21	4.19

314.05	14.53	C8H15N2O9P	5'-Phosphoribosyl-N-formylglycinamide	1.15	-1.21	1.62
160.12	22.84	C7H16N2O2	N6-Methyl-L-lysine	1.47	-1.22	3.01
112.03	8.29	C4H4N2O2	Uracil	1.51	-1.23	3.59
162.10	22.36	C6H14N2O3	N6-Hydroxy-L-lysine	1.42	-1.26	2.45
132.09	22.44	C5H12N2O2	L-Ornithine	1.34	-1.29	2.53
159.07	7.48	C10H9NO	Indole-3-acetaldehyde	1.28	-1.31	2.40
605.08	17.34	C16H25N5O16P2	GDP-mannose	1.28	-1.31	1.69
559.07	14.13	C15H23N5O14P2	Phosphoribosyl-AMP	1.28	-1.32	2.74
188.13	25.75	C7H16N4O2	Homoarginine	1.62	-1.32	4.81
240.02	15.74	C6H12N2O4S2	L-Cystine	0.98	-1.37	1.32
364.04	17.08	C10H13N4O9P	Xanthosine 5'-phosphate	1.23	-1.40	2.57
136.06	22.97	C7H8N2O	1-Methylnicotinamide	1.50	-1.42	3.16
663.11	13.68	C21H27N7O14P2	NAD+	1.26	-1.42	1.78
182.08	13.43	C6H14O6	D-Sorbitol	1.31	-1.45	2.79
105.08	18.02	C4H11NO2	Diethanolamine	1.52	-1.66	3.96
607.08	14.44	C17H27N3O17P2	UDP-N-acetyl-D-glucosamine	1.30	-1.70	1.89
103.06	14.95	C4H9NO2	4-Aminobutanoate	1.66	-1.75	5.11
264.10	19.45	C12H16N4OS	Thiamin	1.51	-1.83	3.16
589.08	16.73	C16H25N5O15P2	GDP-L-fucose	1.27	-1.91	1.69
194.08	10.43	C7H14O6	1-O-Methyl-myo-inositol	1.26	-1.96	2.13
743.07	16.08	C21H28N7O17P3	NADP+	1.26	-2.19	1.86
75.07	22.00	C3H9NO	(R)-1-Aminopropan-2-ol	1.35	-2.24	2.33
290.12	16.18	C10H18N4O6	N-(L-Arginino)succinate	1.43	-2.48	2.62
284.08	11.58	C10H12N4O6	Xanthosine	1.73	-2.53	6.54
180.05	8.15	C6H12O4S	5-Methylthio-D-ribose	1.68	-2.56	6.46
145.09	14.61	C5H11N3O2	4-Guanidinobutanoate	1.61	-2.83	5.11
404.00	15.70	C9H14N2O12P2	UDP	1.40	-2.83	2.42
185.99	16.01	C3H7O7P	3-Phospho-D-glycerate	1.31	-3.52	2.19
156.05	7.72	C6H8N2O3	4-Imidazolone-5-propanoate	1.20	-3.57	1.52
443.03	17.18	C10H15N5O11P2	GDP	1.28	-5.25	1.76
427.03	14.21	C10H15N5O10P2	ADP	1.22	-6.05	1.65

Table 3. 5 LC-MS analysis of placenta extracts using the C18-PFP column: Metabolites that show a significant change (> Log2-fold change (threshold 1.5) in peak intensity and P < 0.05) using metaboanalyst. Fold change (FC) values are shown as log2 and P values as –log10. Retention times (RT) are also shown in minutes. Significantly increased metabolites (log2 FC (threshold 2) ≥ 1.0, log2 FC (threshold 1.5) ≥ 0.60, -log10 P >1.3) are marked as dark red and bright red, respectively. A significant decrease (log2 FC (threshold 2) ≤ -1.0, log2 (FC threshold 1.5) ≤ 0.60, -log10 P >1.3) is represented by a dark blue and light blue colour, respectively. The identity of metabolites highlighted in yellow were confirmed by matching their retention times with those obtained for authentic standards under the same conditions.

Mass	RT(*min*)	Formula	Metabolites	VIP	log2(FC)	-Log10 P
250.06	6.93	C8H14N2O5S	gamma-L-Glutamyl-L-cysteine	0.90	1.69	2.40
113.06	5.40	C4H7N3O	Creatinine	1.23	1.42	3.18
104.05	10.29	C4H8O3	2S-hydroxy-butanoic acid	0.97	1.11	3.78
145.16	4.09	C7H19N3	Spermidine	0.51	1.09	3.78
324.04	5.91	C9H13N2O9P	UMP	1.23	0.80	2.19
141.02	5.37	C2H8NO4P	Ethanolamine phosphate	1.59	0.77	2.95
183.07	5.38	C5H14NO4P	Choline phosphate	0.83	0.66	2.16
106.03	5.85	C3H6O4	D-Glycerate	1.34	-0.77	2.59
152.03	7.93	C5H4N4O2	Xanthine	1.22	-0.99	2.40
175.10	5.44	C6H13N3O3	L-Citrulline	1.56	-1.03	5.00
111.99	5.69	CH5O4P	Hydroxymethylphosphonate	0.99	-1.03	2.19
136.04	5.61	C5H4N4O	Hypoxanthine	1.38	-1.18	2.32
132.09	4.82	C5H12N2O2	L-Ornithine	1.57	-1.31	3.02
168.03	7.04	C5H4N4O3	Urate	1.38	-1.35	1.84
240.02	5.34	C6H12N2O4S2	L-Cystine	0.98	-1.41	1.38
284.08	10.79	C10H12N4O6	Xanthosine	1.06	-2.04	6.72
255.11	12.49	C12H17NO5	N-D-Glucosylarylamine	1.34	-2.37	3.90

3.3.5 Foetus

In contrast to the decidua and placenta, multivariate analysis of foetus extracts showed an outlier which can be seen out of the 95% confidence range in the plot shown below as F10 in figure 3.7 (A).

In theory, analysis of the PCA plot normally shows this type of an outlier, which can be expected out of every 15-20 extracts/samples, but it needs to be evaluated for fair representative distribution of variables/metabolites between infected and control groups. This can be evaluated through loading plot analysis as shown next to PCA plots (B). Following this, loading plot analysis was carried out to confirm the presence of an outlier. Subsequently, the PCA plot and OPLS-DA plot were produced to show the distribution of the metabolites based on the variables after removal of the outlier.

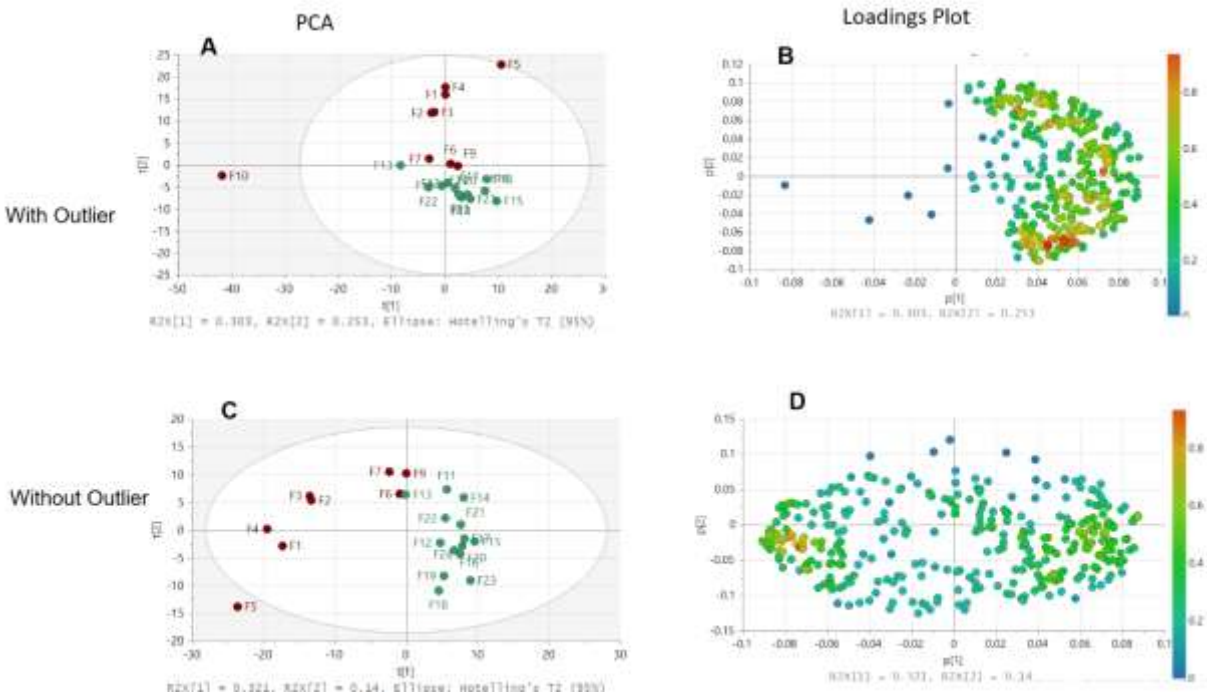

Figure 3. 7 Detection of an outlier in samples from Foetus through multivariate analysis techniques. (A) represents PCA score plot between infected and uninfected foetuses with an outlier F10 out of confidence range (95%) and the corresponding loadings plot **(B)** shows the unequal distribution of variables amongst tested two groups. When the outlier is excluded **(C)** it affects PCA scores as well as an excellent distribution of variable metabolites in corresponding loading plot **(D)**. This phenomenon can also be seen in figure 3.8 for further confirmation of detecting an outlier.

Following this, a total ionic current plot of all the samples from the foetuses was analysed for further confirmation of the outlier. This plot represents the total ionic current value for each of the extracts.

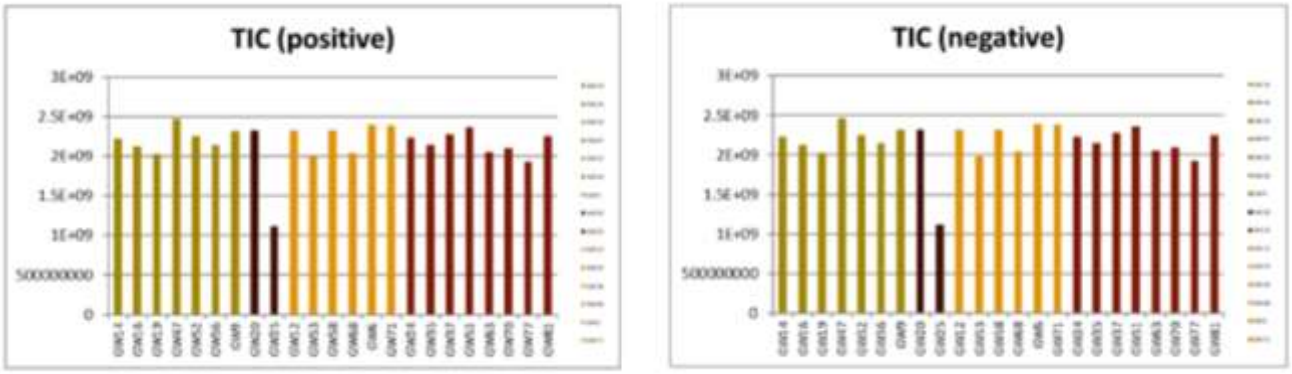

Figure 3. 8 Detection of an outlier in samples from Foetus through total ionic current (TIC) value analysis both for ESI positive and negative modes. As shown in the previous figure 3.7, F10 is an outlier that corresponds to G25 (a name given to the corresponding foetal unit/ sample) in the current figure, which clearly shows an abnormal total ionic current in this unit as compared to all other foetal units from either of the group. Each GW number represents a foetal unit.

So, this outlier was excluded from further analysis after confirmation on the basis of loading plot and TIC value. Following this, multivariate analysis was carried out as shown in the PCA and OPLSDA plots in the following figure 3.9 and 3.10 for pHILIC column and C18-PFP columns respectively.

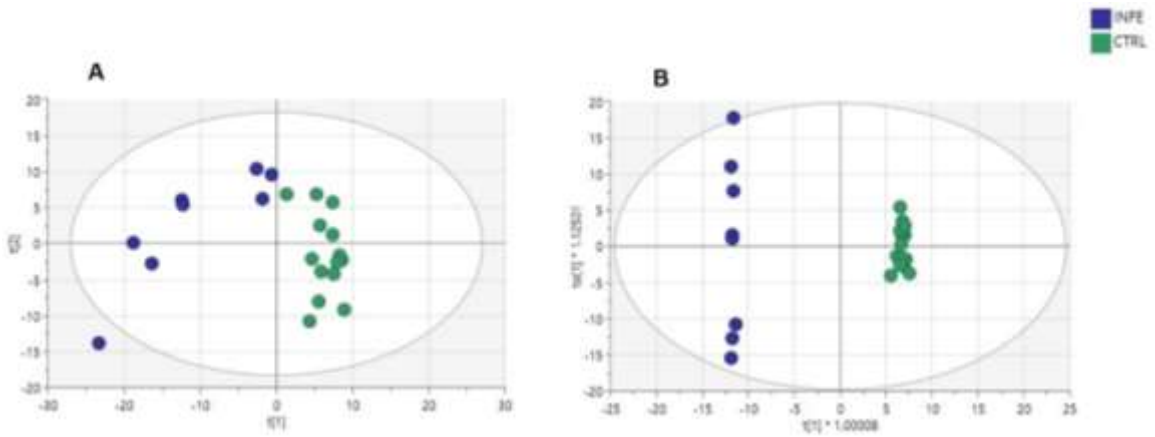

Figure 3. 9 Multivariate Analysis of Foetus using pHILIC column. (A) PCA score plot shows a grouped separation (some of the infected foetal units are more likely to be uninfected group). **(B)** Orthogonal Partial Least Square Discriminant Analysis (OPLS-DA) plot shows clear separation between infected and uninfecteds control but also there are two separate clusters in between the infected group. Each data point in A & B represents one mouse foetal sample.

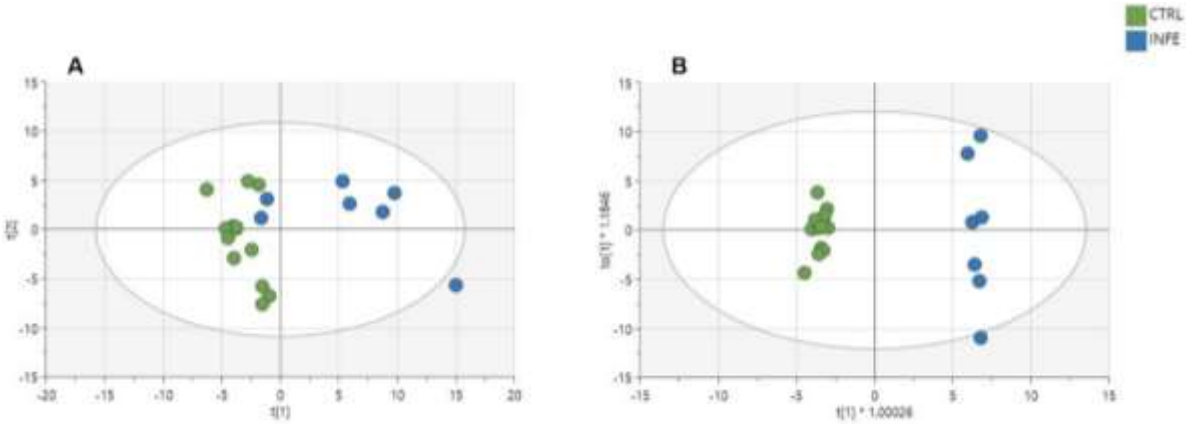

Figure 3. 10 Multivariate Analysis of Foetus using C18-PFP column. (A) PCA score plot shows two distinct groups of infected foetuses as shown in separation (some of the infected foetal units are more like the uninfected group. **(B)** The orthogonal Partial Least Square Discriminant Analysis (OPLS-DA) plot shows distinct separation but the infected group has two separate clusters in between the infected group. Each data point in A & B represents one mouse foetal sample.

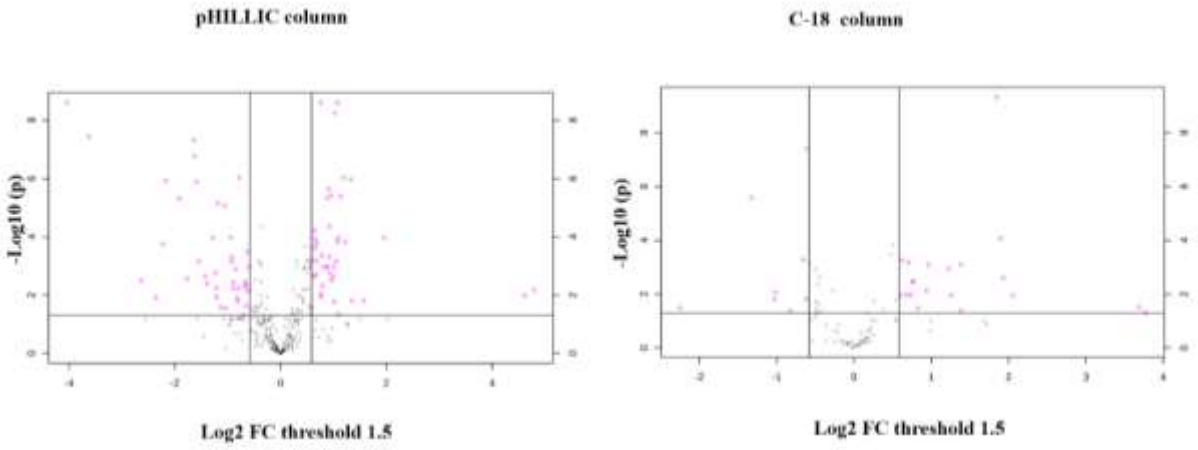

Figure 3. 11 represents volcano plots for foetal extracts with log2 fold change and –log10 P values by (A) pHILLIC column and (B) C-18 PFP column. The X-axis shows fold change and Y-axis is indicative of significance. Each pink dot represents a particular significantly increased/decreased metabolite with log2 fold change threshold 1.5 and –log10 >1.3, while all the black dots corresponds to different metabolites below the significance threshold.

Table 3. 6 LC-MS analysis of foetus extracts using the pHILIC column: Metabolites that show a significant change (Log2-fold change with a threshold of 1.5) in peak intensity and P < 0.05) using metaboanalyst. Fold change (FC) values are shown as log2 and P values as –log10. Retention times (RT) are also shown in minutes. Significantly increased metabolites (log2 FC (threshold 2) ≥ 1.0, log2 FC (threshold 1.5) ≥ 0.60, -log10 P >1.3) are marked as dark red and bright red, respectively. A significant decrease (log2 FC (threshold 2) ≤ -1.0, log2 (FC threshold 1.5) ≤ 0.60, -log10 P >1.3) is represented by a dark blue and light blue colour, respectively. The identity of metabolites highlighted in yellow were confirmed by matching their retention times with those obtained for authentic standards under the same conditions.

Mass	RT(*min*)	Formula	Metabolites	VIP	log2(FC)	-Log10 P
159.09	7.81	C6H10N2O3	4-Methylene-L-glutamine	1.16	4.62	1.97
153.09	7.44	C4H8O2	(R)-Acetoin	1.42	1.96	3.97
364.04	17.06	C10H13N5O3	Deoxyadenosine	1.05	1.57	1.81
284.08	11.59	C8H14N2O5S	gamma-L-Glutamyl-L-cysteine	1.17	1.35	1.80
255.11	8.85	C4H9O7P	D-Erythrose 4-phosphate	1.50	1.32	5.96
75.07	10.73	C2H7O4P	2-Hydroxyethylphosphonate	1.39	1.21	3.82
167.98	16.50	C4H8N2O3	N-Carbamoylsarcosine	1.53	1.18	6.03
139.07	7.83	C5H7N3O	5-Methylcytosine	1.49	1.13	5.39
145.09	14.63	C5H7NO3	L-1-Pyrroline-3-hydroxy-5-carboxylate	1.02	1.09	1.34
309.99	16.19	C3H9O6P	sn-Glycerol 3-phosphate	1.40	1.09	3.97
161.07	10.69	C7H11N3O2	N(pi)-Methyl-L-histidine	1.59	1.08	8.60
443.03	17.07	C2H6O4S	2-Hydroxyethanesulfonate	1.41	1.07	3.83
290.12	16.20	C7H15O10P	D-Sedoheptulose 7-phosphate	1.28	1.05	3.17
105.08	18.00	C8H16NO9P	D-Glucosamine	1.57	1.02	8.24
363.06	18.14	C4H7N3O	Creatinine	1.11	1.01	1.77
427.03	14.44	C6H13O10P	6-Phospho-D-gluconate	1.28	1.00	2.96
243.15	8.15	C10H12N2O3	L-Kynurenine	1.47	0.96	5.43
152.03	16.64	C9H13N2O9P	UMP	1.27	0.96	2.51
253.10	7.66	C9H12N2O5	Deoxyuridine	1.24	0.93	2.75
118.03	8.05	C6H9N3O2	L-Histidine	1.43	0.92	4.35
246.13	13.65	C7H7ClO5	5-chloro-2-methyl-maleylacetate	1.27	0.92	3.30
112.03	8.30	C6H13O9P	D-Glucose 6-phosphate	1.48	0.91	5.65
334.07	15.45	C12H24N2O8	Procollagen 5-(D-galactosyloxy)-L-lysine	1.26	0.88	2.97
387.04	18.21	C11H15N3O6	N4-Acetylcytidine	1.45	0.88	5.33
152.03	10.92	C6H14N2O2	D-Lysine	1.31	0.87	2.97
589.08	16.73	C7H15N3O3	L-Homocitrulline	1.29	0.79	2.97
127.04	10.48	C10H14N5O6P	dAMP	1.23	0.79	2.31
152.06	7.39	C9H8O2	trans-Cinnamate	1.32	0.78	3.36
136.04	9.83	C9H14N3O8P	CMP	1.20	0.76	2.03

132.09	22.42	C7H14N2O3	N-Acetylornithine	1.37	0.68	3.76
145.04	10.26	C6H12N2O2	L-isoglutamine	1.29	0.68	3.18
269.09	15.73	C5H14NO6P	sn-glycero-3-Phosphoethanolamine	1.22	0.67	2.71
536.05	15.44	C6H13NO4	1-deoxynojirimycin	1.38	0.67	3.91
158.06	9.55	C11H21NO5	Hydroxybutyrylcarnitine	1.39	0.64	4.21
322.06	12.37	C8H20NO6P	sn-glycero-3-Phosphocholine	1.30	0.64	3.61
188.12	12.52	C10H16N2O3S	Biotin	1.21	0.63	2.65
244.09	8.60	C8H16N2O3	N2-Acetyl-L-lysine	1.27	0.59	3.22
257.10	13.95	C10H15N2O8P	dTMP	1.04	0.59	1.57
247.14	11.12	C7H10O4	2-Isopropylmaleate	1.31	-0.60	2.97
163.08	15.32	C14H22N2O16P2	UDP-D-xylose	1.35	-0.62	3.49
215.06	15.15	C10H12FN5O3	5'-deoxy-5'-fluoroadenosine	1.15	-0.63	2.14
144.09	23.03	C5H7NO4	2-Oxoglutaramate	1.07	-0.65	1.63
174.10	13.08	C5H12N2O2	L-Ornithine	1.13	-0.67	2.44
323.05	15.20	C5H4N4O	Hypoxanthine	1.51	-0.79	6.02
148.05	9.97	C7H8N2O2	N1-Methyl-2-pyridone-5-carboxamide	1.14	-0.80	2.23
331.07	12.30	C4H5N3O2	5-Amino-4-imidazole carboxylate	1.01	-0.82	1.91
189.11	14.70	C16H25N5O15P2	GDP-L-fucose	1.26	-0.84	2.89
146.11	14.69	C5H4N4O2	Xanthine	1.18	-0.89	2.43
285.10	8.08	C10H17N3O9S2	glutathione-sulfite	1.12	-0.90	2.23
324.15	23.04	C9H19O11P	sn-glycero-3-Phospho-1-inositol	1.36	-0.93	3.30
260.03	16.18	C4H4N2O2	Uracil	1.26	-0.93	3.15
206.00	15.85	C9H18N4O4	N2-(D-1-Carboxyethyl)-L-arginine	1.39	-0.95	3.98
155.07	14.35	C4H6O4	Succinate	1.12	-1.04	1.54
228.07	7.99	C12H15NO5	N-Acetylvanilalanine	1.45	-1.06	5.07
324.04	14.49	C5H4N4O2	6-8-Dihydroxypurine	1.10	-1.13	1.58
208.08	10.51	C12H21NO4	Tiglylcarnitine	1.44	-1.18	5.14
276.03	16.77	C10H15N5O10P2	ADP	1.22	-1.22	2.24
113.06	9.45	C10H14N5O8P	Guanosine 3'-phosphate	1.18	-1.22	1.93
301.06	14.24	C4H11NO2	Diethanolamine	1.20	-1.24	2.76
290.04	15.53	C10H18N4O6	N-(L-Arginino)succinate	1.36	-1.29	3.97
126.00	10.37	C10H15N5O11P2	GDP	1.23	-1.39	2.40
169.08	12.53	C6H11NO4	L-2-Aminoadipate	1.21	-1.43	2.65
172.01	14.02	C5H12O11P2	D-Ribose 1_5-bisphosphate	1.31	-1.55	3.16
129.04	10.02	C5H11N3O2	4-Guanidinobutanoate	1.52	-1.63	6.77
125.06	9.20	C6H9N3O	L-Histidinal	1.54	-1.64	7.32
132.05	11.48	C3H5O6P	Phosphoenolpyruvate	1.18	-1.77	2.57
126.01	14.01	C3H9NO	Trimethylamine N-oxide	1.48	-1.91	5.33
200.01	15.96	C12H17NO5	N-D-Glucosylarylamine	1.50	-2.17	5.92
250.06	13.47	C10H12N4O6	Xanthosine	1.39	-2.23	3.75
251.10	8.01	C10H13N4O9P	Xanthosine 5'-phosphate	1.16	-2.35	1.91
88.05	12.93	C7H11N3O	4-(beta-Acetylaminoethyl)imidazole	1.55	-3.62	7.43
158.07	10.01	C7H13NO3	3-Dehydrocarnitine	1.60	-4.04	8.60

Table 3. 7 LC-MS analysis of foetus extracts using the C-18 column: Metabolites that show a significant change (> Log2-fold change (threshold 1.5) in peak intensity and P < 0.05) using metaboanalyst. Fold change (FC) values are shown as log2 and P values as –log10. Retention times (RT) are also shown in minutes. Significantly increased metabolites (log2 FC (threshold 2) ≥ 1.0, log2 FC (threshold 1.5) ≥ 0.60, -log10 P >1.3) are marked as dark red and bright red, respectively. A significant decrease (log2 FC (threshold 2) ≤ -1.0, log2 (FC threshold 1.5) ≤ 0.60, -log10 P >1.3) is represented by a dark blue and light blue colour, respectively. The identity of metabolites highlighted in yellow were confirmed by matching their retention times with those obtained for authentic standards under the same conditions.

Mass	RT(*min*)	Formula	Metabolites	VIP	log2(FC)	-Log10 P
195.09	16.50	C10H13NO3	L-Tyrosine methyl ester	1.04	3.77	1.31
163.07	10.94	C6H13NO2S	S-Methyl-L-methionine	1.11	3.68	1.51
145.16	4.11	C7H19N3	Spermidine	1.21	2.06	1.95
250.06	6.90	C8H14N2O5S	gamma-L-Glutamyl-L-cysteine	1.28	1.93	2.60
88.05	18.12	C4H8O2	Butanoic acid	1.45	1.89	4.06
289.13	6.65	C11H19N3O6	Ophthalmicacid	1.58	1.85	9.32
267.10	7.91	C9H17NO8	Neuraminic acid	1.05	1.39	1.39
104.05	10.38	C4H8O3	2S-hydroxy-butanoic acid	1.35	1.38	3.09
121.02	5.61	C3H7NO2S	L-Cysteine	1.15	1.26	1.95
176.03	6.21	C6H8O6	Ascorbate	1.33	1.23	2.94
228.07	8.23	C9H12N2O5	Deoxyuridine	1.35	0.97	3.09
309.11	6.27	C11H19NO9	N-Acetylneuraminate	1.21	0.94	2.13
165.08	14.21	C9H11NO2	L-Phenylalanine	1.09	0.83	1.49
208.08	12.83	C10H12N2O3	L-Kynurenine	1.27	0.77	2.46
323.05	5.63	C9H14N3O8P	CMP	1.27	0.76	2.46
274.01	6.14	C6H11O10P	6-Phospho-2-dehydro-D-gluconate	1.15	0.73	1.97
203.12	6.27	C9H17NO4	O-Acetylcarnitine	1.33	0.71	3.18
260.03	5.83	C6H13O9P	D-Fructose 6-phosphate	1.19	0.68	1.97
158.04	5.68	C4H6N4O3	Allantoin	1.37	0.62	3.27
187.17	4.82	C9H21N3O	N1-Acetylspermidine	1.09	0.60	1.97
257.10	5.40	C8H20NO6P	Choline	1.55	-0.61	7.41
116.01	10.46	C4H4O4	Fumarate	1.05	-0.62	1.81
109.02	5.44	C2H7NO2S	Hypotaurine	1.28	-0.66	3.29
160.04	6.10	C6H8O5	2-Oxoadipate	1.07	-0.82	1.37
152.03	7.90	C5H4N4O2	Xanthine	1.11	-1.01	2.07
341.13	6.27	C12H23NO10	Lactosamine	1.14	-1.03	1.80
132.09	4.86	C5H12N2O2	L-Ornithine	1.49	-1.33	5.58
133.02	5.76	C4H7NO2S	L-thiazolidine-4-carboxylate	1.08	-2.26	1.49

3.3.6 Alterations in different metabolic pathways in the maternal foetal interface of mice congenitally infected with *T. gondii*.

Metabolic pathways identified in all of the three tissue extracts were scrutinized for variations following maternal infection with *T. gondii*. Not all metabolites were found to be altered the same way in the different tissues examined in the maternal foetal interface. However, there are some metabolic pathways and downstream metabolites that were altered significantly that are discussed in the relevant pathways/origin section below.

3.3.6.1 Arginine metabolism.

Arginine is utilised in the biosynthesis of proteins and also plays a significant role in cell division, immune function, wound healing and release of hormones. Arginine is typically found on the outside of the protein and is involved in hydrogen bonding and salt bridges (Morris Jr, 2007). It is a known precursor for nitric oxide synthesis thus playing a key role in regulating blood pressure and immune functions. The side chain of arginine is amphipathic due to the fact that at physiological pH, this contains a positively charged polar guanidinium group at the end of the hydrophobic aliphatic hydrocarbon chain (Armstrong et al., 2016). Residues of arginine can be deaminated resulting in production of citrulline via post translational modifications such as citrullination. The importance of this process is underlined in foetal development and is a normal part of the immune process as well as gene expression control and auto immune diseases. With regards to *T. gondii*, it has been shown that *T. gondii* lacks the enzymes required for de novo arginine biosynthesis and lack of arginine results in cyst formation (Weckman et al., 2019).

Metabolomics profile of the maternal foetal interface revealed the ability of *T. gondii* to alter the arginine metabolism. Different alterations in this pathway and resultant changes in different metabolites are shown in the figure 3.12.

Metabolic pathway for arginine:

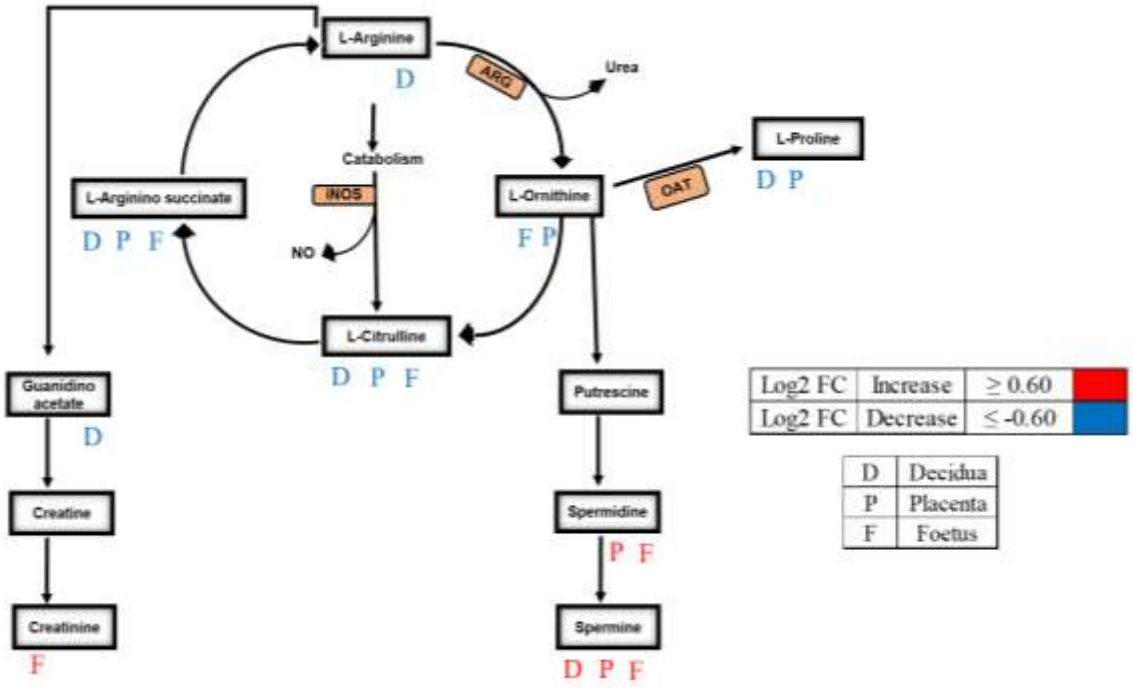

Figure 3. 12 Arginine and proline metabolic pathway and the related products showing interactions between different metabolites in arginine metabolic cycle and with other pathways. Letter D below the rectangle box represents decidua, P is indicative of the placenta and letter F is representative of foetus. A significant log2 fold change threshold 1.5 increase is shown by red colour and blue colour indicates a significant decrease with log2 fold change threshold 1.5.

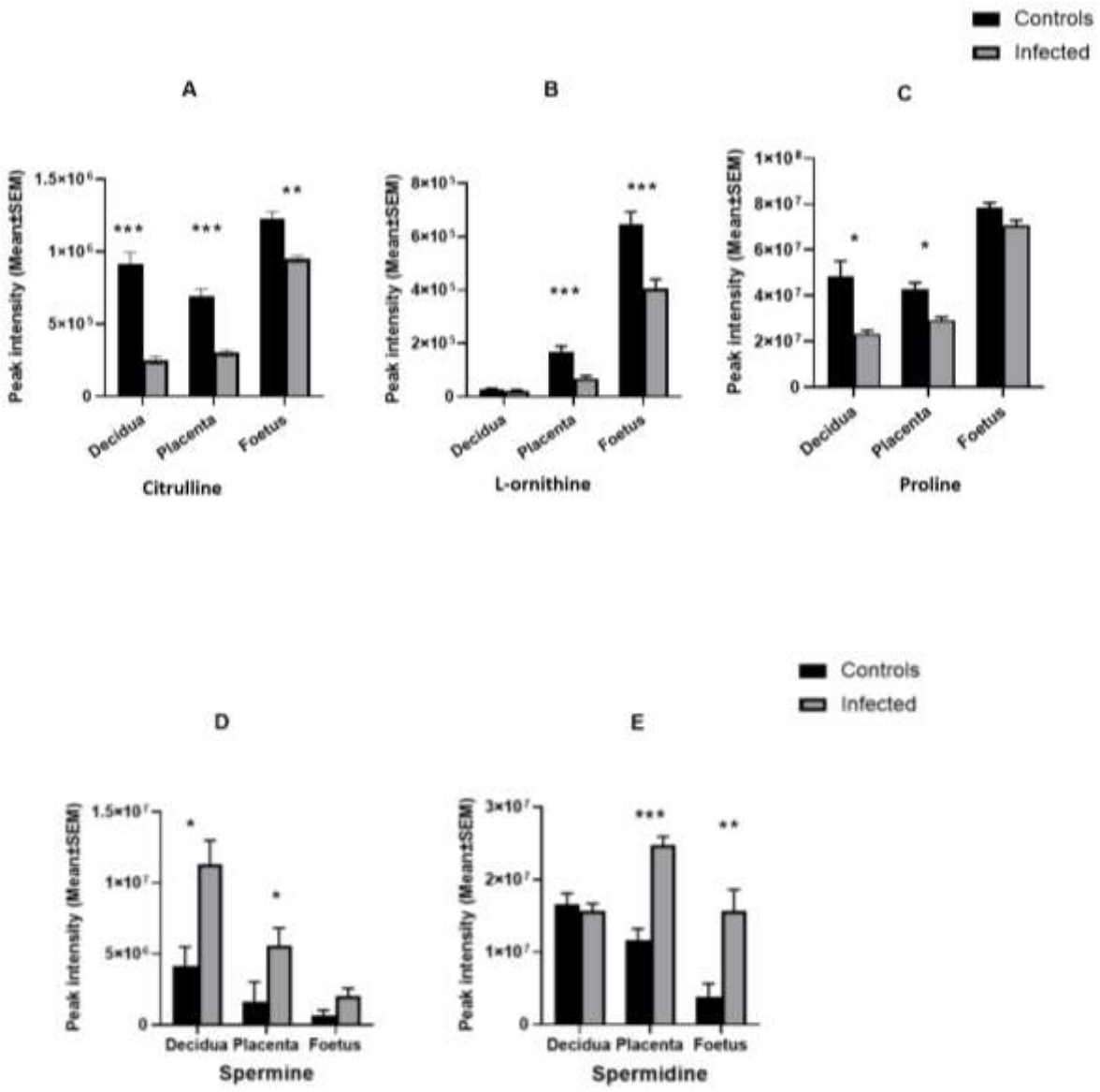

Figure 3. 13 arginine metabolic pathway. Metabolites detected in this important pathway are represented in graphical form. Decidual and placental extracts (n= 13 and 10 for uninfected and infected, respectively, Foetal extracts (n= 14 and 09 for uninfected and infected). Student´s t-test was performed to determine significance ($p < 0.05$) where *p <0.05, **p <0.001 ***p <0.0001 are significant compared to the control uninfected.

(A) Represents the average peak intensity values of citrulline in each of the three tissues.

(B) Represents the average peak intensity values of L-ornithine in each of the three tissues.

(C) Represents the average peak intensity values of proline in each of the three tissues.

(D) Represents the average peak intensity values of spermine in each of the three tissues.

(E) Represents the average peak intensity values of spermidine in each of the three tissues.

The results above (Fig. 3.13) show metabolites identified in the arginine metabolic pathway in the decidua, placenta and foetus from mice maternally infected with *T. gondii*. Mice infected with *T. gondii* displayed statistically significant decreased levels of citrulline, within the decidua (p <0.00001), placenta (p <0.00001) and the developing foetus (p= 0.00016) compared to the uninfected control tissues/ extracts from the pregnant mothers. Analysis of L-ornithine expression found that decreased levels of L-ornithine in both the placenta and foetus (p= 0.0008 and 0.0003, respectively) from infected mice relative to control mice. However, in the decidua, there were no significant changes observed in the expression levels of L-ornithine in infected mice when compared with that of uninfected control mice. A significant decreased levels of proline were noted in all of the three tissues, but it was statistically significant only in the decidual extracts (p=0.023). Spermine levels were increased in decidua and placenta (p= 0.007, 0.041 respectively) of infected mice relative to the uninfected control mice. An increased level of spermine was also observed in the developing foetus although the difference was not statistically significant (p= 0.056). However, spermidine levels were increased in placenta and the developing foetus with a statistical significance (p=0.000, p=0.012, respectively). However, there were no significant change in the expression levels of spermidine in the decidual extracts compared with the control. The data obtained indicate that *T. gondii* infection increases flux through the arginine pathways resulting in reduced levels of citrulline, ornithine and proline while increasing levels of spermine and spermidine within the decidua, placenta and the developing foetus.

3.3.6.2 Tryptophan degradation pathway

Tryptophan is an alpha amino acid utilised in the biosynthesis of proteins. This contains an alpha-amino group, alpha carboxylic acid group and a side chain indole thus tryptophan is classified as a non-polar aromatic amino acid. Tryptophan is important for the maternal protein

synthesis and the foetal development. Alteration of tryptophan metabolic pathway during the pregnancy impairs foetal programming leading to the developmental programming of kidney disease and hypertension in adult offsprings (Baban et al., 2009). Tryptophan is also a precursor of serotonin. *T. gondii* is a tryptophan auxotroph and induction of indolamine dioxygenase (IDO) as part of an immune response has been shown to degrade tryptophan and curtail the growth of *T. gondii* (Floc'h et al., 2011). It has been demonstrated that *T. gondii* infection alters the intestinal microbiota and disturb tryptophan for its metabolism.

Metabolomics profile of the maternal foetal interface in this study indicated the ability of *T. gondii* to alter the tryptophan degradation pathway. Different alterations in this pathway and the resultant changes in different metabolites are shown in the figure 3.14.

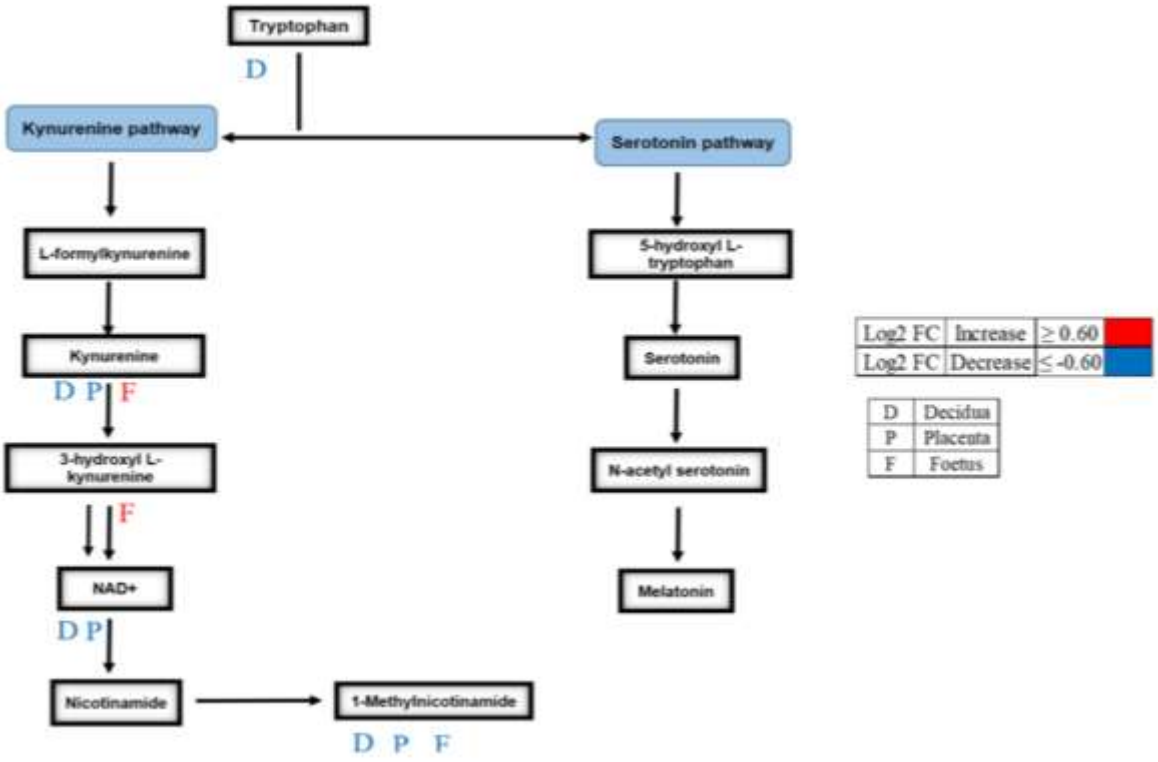

Figure 3. 14 Tryptophan degradation pathway showing interactions between different metabolites in tryptophan metabolic cycle along with interactions with other pathways. Letter D below the rectangle box represents decidua, P is indicative of the placenta and letter F is representative of foetus. A significant log2 fold change threshold 1.5 increase is shown by red colour and blue colour indicates a significant decrease with log2 fold change threshold 1.5. Double arrow from 3-hydroxl-L-kynurenine to NAD+ indicate that multiple reactions are involved.

Significantly decreased levels of kynurenine are seen in the decidua and placenta of infected mice in comparison with control uninfected mice (p= 0.004, 0.0055 respectively). However, increased levels of kynurenine (p= 0.0006) are seen in the foetuses from infected mice in comparison with control mice. The trend of an alteration in the kynurenine levels in an opposite direction in the developing foetus from the decidua and the placenta is indicated in the figure 3.15. The foetuses from infected mice also had increased levels of 3-hydroxyl L-kynurenine relative to control uninfected mice (p= 0.003). Together these results demonstrate the build-up of tryptophan degradation products in the foetus during *T. gondii* infection.

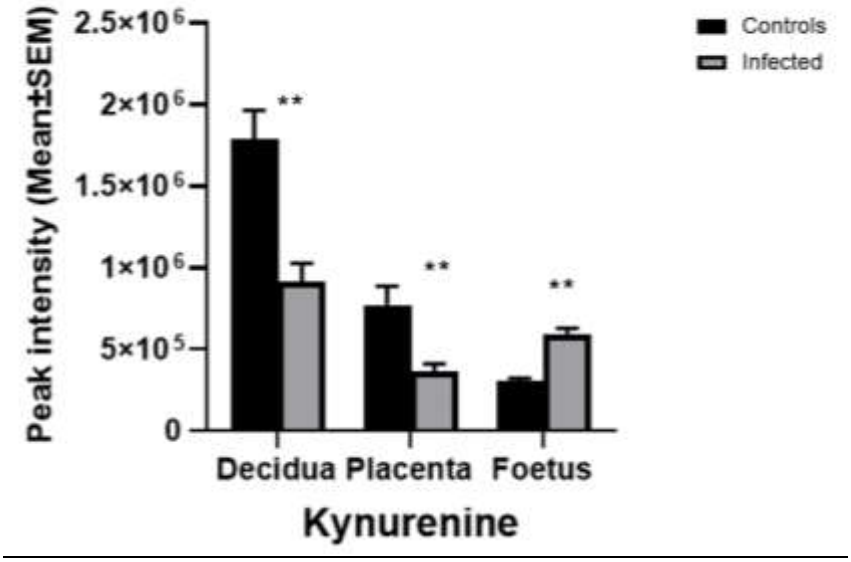

Figure 3. 15 Tryptophan degradation pathway. Represents the average peak intensity values (Mean ± SEM) of kynurenine in each of the three tissues examined for metabolomics profile. Decidual and placental extracts (n= 13 and 10 for uninfected and infected, respectively), Foetal extracts (n= 14 and 09 for uninfected and infected). Student´s t-test was performed to determine significance ($p < 0.05$) where *$p < 0.05$, **$p < 0.001$ ***$p < 0.0001$ are significant compared to the control uninfected.

3.3.6.3 Potential Microbial metabolites

Microbial metabolites are classified as metabolic intermediate molecules which are produced by microorganisms during and after their growth. Microbial metabolisms can be classified according to three principles such as how the organism obtains carbon for synthesising cell mass, how it obtains reducing equivalents utilised in energy conservation or biosynthetic reactions and how organisms obtain energy for living and growing (Krautkramer et al., 2021). During *T. gondii* infection, studies have shown that the microbial population is potentially affected and as a result, there is an alteration of the metabolic profile. The expression of these microbial metabolites were examined in this study.

The following results below show different microbial metabolites identified as being altered in the decidua, placenta and the developing foetus of the mice maternally infected with *T. gondii*. These microbial metabolites include indole, indoxyl, Indoxylsulfate, 4-guanidinobutanoate and trimethylamine N-oxide (Fig. 3.17 and 3.19).

The biosynthesis pathway for indoxyl and indoxylsulfate from tryptophan is altered by the activity of the microbiome. The production of indole is affected by tryptophanase expressing gastrointestinal tract bacteria in the gut, which ultimately affects the production of indoxyl and indoxylsulfate (Figure 3.16).

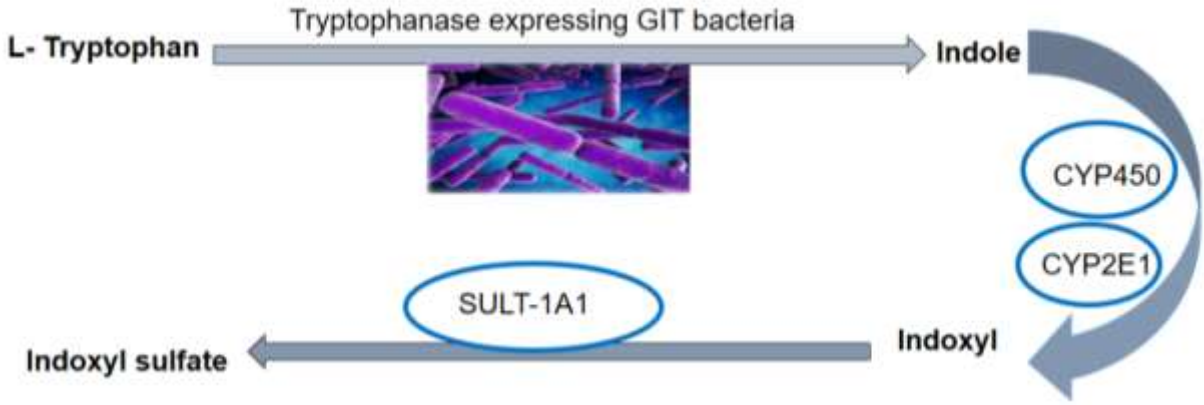

Figure 3. 16 Origin of indoxyl and indoxylsulfate (IS) as a result of the tryptophan utilisation by tryptophanase expressing Gastro intestinal bacteria in the gut. Conversion of tryptophan to indole takes place in the gut by the activity of microbiome, and indole is converted to indoxyl by the enzymatic reactions (mainly cytochromes) in the liver, and then with the help of sulfotransferase enzyme it is converted to indoxylsulfate.

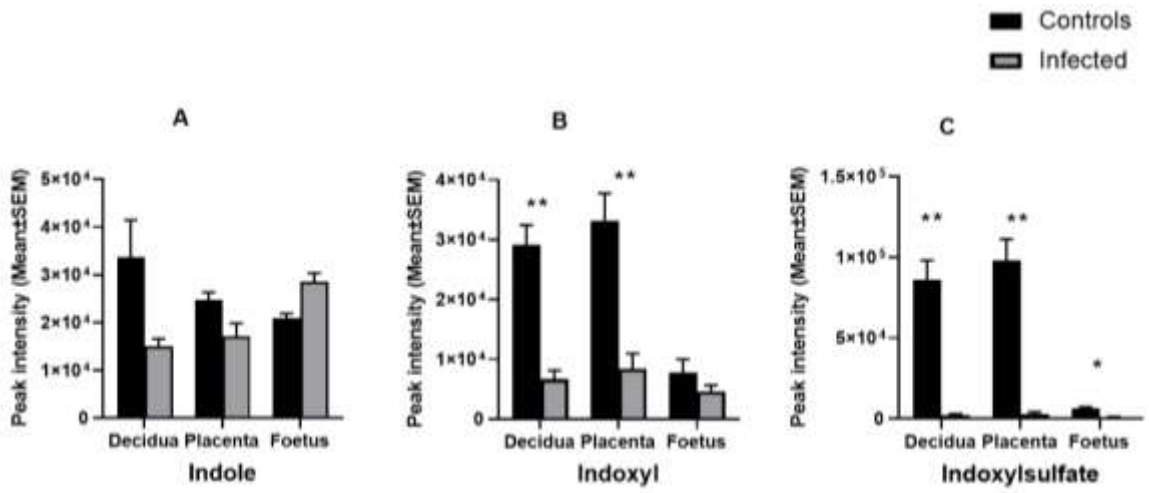

Figure 3. 17 Potential microbial metabolites detected in this study. Decidual and placental extracts (n= 13 and 10 for uninfected and infected, respectively, Foetal extracts (n= 14 and 09 for uninfected and infected). Student´s t-test was performed to determine significance ($p < 0.05$) where *$p < 0.05$, **$p < 0.001$ ***$p < 0.0001$ are significant compared to the control uninfected.

(A) Represents the average peak intensity values of indole in each of the three tissues.

(B) Represents the average peak intensity values of indoxyl in each of the three tissues.

(C) Represents the average peak intensity values of indoxysulfate in each of the three tissues.

The data obtained indicate that *T. gondii* infection decreased conversion of tryptophan to indoxyl and indoxylsulfate in the decidua, placenta and the developing foetus as these metabolites were detected at lower levels in these tissues from infected mice (Indoxyl: p=0.001, 0.001 and 0.32, respectively and Indoxylsulfate: (p=0.001, 0.003 and 0.042, respectively). Although indole levels were increased in the developing foetus and reduced levels were noted in the decidua and placenta, these differences were not statistically significant. Furthermore, reduction of 4-guanidinobutanoate in the decidua, placenta and the foetus is observed (p= 0.000, 0.001 and 0.001, respectively). The biosynthesis of guanidinobutanoate takes place in the presence of *Pseudomonas aeruginosa* in arginine catabolic pathway (Figure 3.18). These data indicate that *T. gondii* infection has the ability to alter the microbiome of the host.

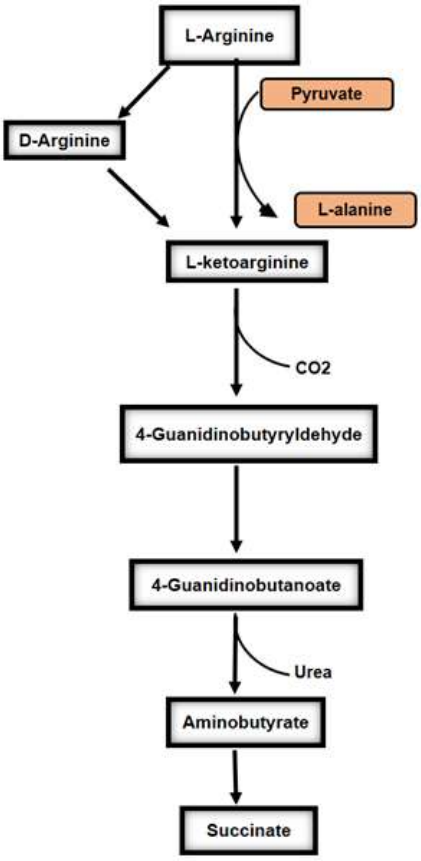

Figure 3.18 Arginine catabolic pathway in Pseudomonas aeruginosa. Origin of guanidinobutanoate as a result of pseudomonas aeruginosa (PAO1) reactions in the L-arginine metabolic pathway.

There is significant decrease in the levels of trimethylamine N-oxide are noted in the decidua, placenta and the developing foetus (p = 0.0001, p= 0.0000 and p= 0.0002, respectively in mice infected with *T. gondii* relative to control mice. The data indicates that *T. gondii* infection of pregnant mice results in reduced levels of the microbial metabolites required for further processes and pathways arising from the different pathways.

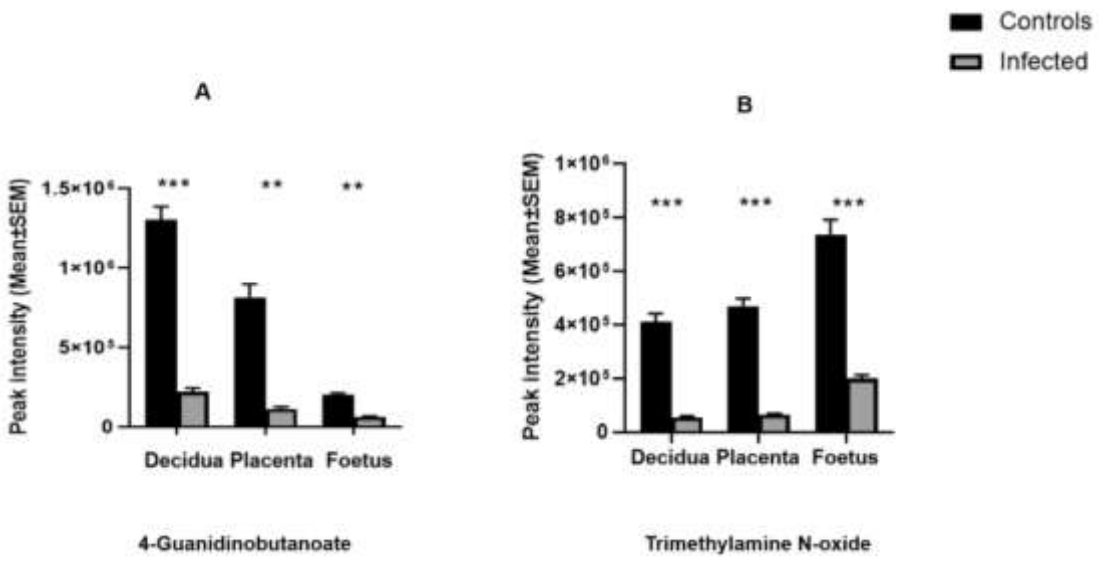

Figure 3. 19 Potential microbial metabolites detected in this study. Decidual and placental extracts (n= 13 and 10 for uninfected and infected, respectively, Foetal extracts (n= 14 and 09 for uninfected and infected). Student´s t-test was performed to determine significance ($p < 0.05$) where *$p < 0.05$, **$p < 0.001$ ***$p < 0.0001$ are significant compared to the control uninfected.

(A) Represents the average peak intensity values of guanidinobutanoate in each of the three tissues.

(B) Represents the average peak intensity values of trimethylamine N-oxide in each of the three tissues.

3.4 Conclusion

The results presented in this chapter demonstrate that there are significant alterations in the metabolism detectable at the maternal foetal interface and foetuses of pregnant mice infected with *T. gondii*. During this study, an untargeted approach was utilised to identify metabolites that are influenced by *T. gondii* infection in the decidua, placenta and the developing foetus. Two types of columns, a pHILIC and a C18-PFP were used to increase the coverage of the metabolites detected. As detailed in previous studies, this approach was used to identify a wide range of metabolites which could be altered during *T. gondii* infection. PCA of LCMS outputs from both pHILIC and C18-PFP columns provided separation of infected and non-infected mice within the decidua, placenta and the developing foetuses. This permitted data to be analysed via OPLS-DA to identify metabolites associated with *T. gondii* infection with VIP values. These scores were used in conjunction with p values obtained using IDEOM. The results obtained here identified various metabolites which are deemed to be associated with congenital *T. gondii* infection within the decidua, placenta and foetus. These metabolites which were identified have been implicated in pathways such as tryptophan degradation, arginine metabolism and different microbial metabolites as part of the microbiome. Significantly increased or decreased levels of individual metabolites implicated in these pathways were seen in the decidua, placenta and foetus. Interestingly, the pathways mentioned above have been previously implicated in previous studies as potentially having a role in congenital toxoplasmosis. However, it is important to note that the metabolites identified here are based on a very small sample size (14 foetal placental units from 2 infected and 9 foeto-placental units from 2 control uninfected mice). Thus, on this basis, it was important to repeat the experiment in a larger sample size. In the following chapter, a larger sample size will be used, but only examining the change in metabolomics profile in the developing foetus and serum. This is due to the fact that the greatest changes are seen in the foetus thus making it a target for further exploration and analysis. Serum

was chosen on the basis that the effect of *T. gondii* on the biochemical composition of host body fluids is largely unknown. *T. gondii* although operating intracellularly has been detected in body fluids. Therefore, the next chapter will explore the changes of metabolomics profile in the foetus and serum in a much larger sample size to identify metabolomics changes in congenital *T. gondii* infection.

4- Metabolomic profile of the developing foetus and the maternal serum infected with *T. gondii* during pregnancy

Abstract

In the previous chapter, the effect of *T. gondii* infection on the metabolomics profile of the maternal foetal interface and the developing foetus of mice infected with *T. gondii* was examined. The results indicated that the maternal infection induce significant metabolomics changes in the decidua, placenta and the developing foetus. Changes to the metabolome of the foetus indicate that maternal infection and potentially congenital infection could influence foetal development and potentially have long lasting post-natal effects. Here, the effect of maternal infection on the foetal metabolome is further studied in a larger cohort of mice and comparison is made between the metabolomics profile of the maternally infected foetus and maternal serum of mice infected with *T. gondii*. The primary objective of this study was to determine whether *T. gondii* infection alters the metabolomics profile of the developing foetuses of mice infected with *T. gondii* tachyzoites during pregnancy and by comparing this with the metabolomics profile of maternal serum gain insight into maternal and foetal metabolism.

A total of 13 BALB/c pregnant mice were selected for this study, 7 mice were infected on day 7 of pregnancy and 6 left uninfected as a control group. After metabolite extraction and separation with a pHILIC column, the raw data files were analysed in IDIOM software v19 to obtain all the detected peaks and chromatograms. Following manual curation and elimination of lipids and peptides and other metabolites which could not be identified with high confidence, the remaining metabolites were evaluated and compared between infected and non-infected groups. Kynurenine was found to be significantly raised in the developing foetuses and sera from infected mothers compared with control mothers. Other metabolites, including citrulline, proline, ornithine, tryptophan, 1-methylnicotinamide, 4-guanidinobutanoate, and indoxysulfate were found to be significantly reduced in foetuses from infected mothers and maternal serum. Urate was found to increase in the maternal serum of infected mice, but not significantly in the

foetus. Degradation of tryptophan and a resultant increase in kynurenine has been linked previously with the *T. gondii* infection. However, these data along with the results of the previous chapter demonstrate that kynurenine levels within the foetus are directly affected by maternal infection. Many metabolites, including those linked to arginine metabolism, are altered in the maternal serum and the foetus and might reflect *T. gondii* induced metabolic changes that occur in both the mother or alternatively that these metabolites are actively transported from the mother to the foetus. Notably, 4-guanidinobutanoate, and indoxylsulfate which are reliant on the metabolism of the microbiome are reduced in maternal serum and the developing foetuses suggesting that *T. gondii* mediated effects on the maternal microbiome affect foetal exposure to these. Overall these data demonstrate that maternal infection with *T. gondii* induces significant changes to the foetal metabolome. Notably, increased levels of foetal kynurenine have been suggested to have serious life-long consequences including an increased likelihood of developing schizophrenia. The consequences for the foetus due to changes to the other metabolites remain to be determined but could provide insight into the pathogenesis and management of congenital *T. gondii* infection.

4.1 Introduction

Previously, examination of the metabolomics profiles of the decidua, placenta and the developing foetus in chapter 3 revealed alterations of metabolites and identified various pathways where a number of metabolites were affected. Out of these three tissues investigated in the previous chapter, the greatest changes occurred within the foetus. Notably, changes to tryptophan degradation pathway, arginine metabolic pathway and purine metabolic pathways were found to be affected by maternal *T. gondii* infection. These changes occurring in gestation could have significant effects to the success of pregnancy, development of the foetus and life-long health of the offspring. Therefore, the studies described in this chapter focus on verification of these results obtained from the foetus in a larger cohort of mice infected maternally with *T. gondii*. In the past, there are many studies detailing the profiling the metabolome of acute and chronic *T. gondii* infections (Halama et al., 2014, Xia et al., 2015, Chun-Xue et al., 2018), however, to date there is a lack of literature/study covering the metabolomics profiles of the developing foetus and maternal foetal interface, to the best of my knowledge. Inclusion of maternal serum provided insight into changes occurring in the mother following infection and allow potential insight into how the maternal and foetal metabolomes interact.

To achieve these goals, the raw data obtained after liquid chromatography mass spectrometry was manually curated and subjected to multivariate analysis for quality control and to give insight into metabolites and metabolic pathways altered during *T. gondii* infection. During multivariate analysis, two components principle component analysis (PCA) plot and a cross-validated orthogonal partial least square discriminant analysis (OPLS-DA) plot were used. PCA and OPLS-DA were used to differentiate between groups and allowed the identification of metabolites associated with infection. To further identify the significant metabolites, volcano plots for each of the tissues were obtained from Metaboanalyst version 5.0 (online software),

which provides a user-friendly and streamlined metabolomics data analysis. Investigation of these metabolites and their pathways can then be subsequently investigated in the context of disease. For a graphical representation of data, graph Pad prism software version 9 was used.

4.2 Aims and Objectives

The aim of the studies described herein is to verify and extend the studies in the previous chapter that found that *T. gondii* infection alters metabolism of the foetus. Specific objectives are: (i) to use LCMS to identify the metabolites present in a large cohort of foetuses and maternal serum from infected BALB/c mice and compare these with metabolites present in these tissues from control non-infected BALB/c mice. (ii) to use this information to determine biochemical pathways and processes that are affected in these tissues by *T. gondii* infection. (iii) to compare the results obtained in this study with those obtained in the previous study.

4.3 Metabolomics profile of the foetus and serum of the mice infected with *T. gondii* during pregnancy

In this study, an untargeted metabolomics approach was undertaken to evaluate changes in biochemical pathways and metabolite variations in the foetus and serum from mice infected and control mice during pregnancy. A ZIC-pHILIC column was utilised to identify the maximum number of polar metabolites. In the previous chapter that detailed metabolomic changes in the foetus, decidua and placenta, there was a total of 4 BALB/c pregnant mice, 2 uninfected control and 2 mice were infected. The results obtained demonstrated that the developing foetuses showed the greatest number of changes within the metabolomic profile of all the tissues examined. However, in the previous chapter, a small number of mice were utilised for a preliminary analysis. Herein, for statistical purposes a larger sample size was used. Furthermore, in this chapter, there will also be a focus on the metabolomics profile of maternal serum to see if the results obtained previously are occuring at the same level and distribubtion in the maternal serum and the developing foetus.

The control group consisted of a total of 6 mice from which serum and tissue was collected at day 13 of pregnancy. A total of 24 foetuses were obtained in this control group and the corresponding maternal serum was collected from five of these uninfected control mice. Similarly, In the infected group, 7 mice were infected with tachyzoites of *T. gondii* Me49 strain at day 7 of pregnancy and were killed at day 13 to collect foetuses and maternal serum. A total of 21 foetuses were obtained and maternal serum was collected from five mice. Details of these extracts can be seen in Table 4.1. The samples/extracts described in Table 4.1 were processed for metabolite extraction. LC-MS was carried out by Glasgow Polyomics to characterise and confirm the metabolites of interest in the developing foetus and the maternal serum.

Table 4. 1 No. of samples/units for each individual mouse in each tissue (Infected, Control)

Infected

Maternal Mouse ID	Foetus	Maternal Serum
Inf-1	6	0
Inf-2	1	0
Inf-3	1	1
Inf-4	4	1
Inf-5	3	1
Inf-6	4	1
Inf-7	2	1
Total extracts	21	5

Control

Maternal Mouse ID	Foetus	Maternal Serum
C-1	6	1
C-2	1	1
C-3	1	1
C-4	6	1
C-5	5	1
C-6	5	0
Total extracts	24	5

Following LC-MS of the extracts by Glasgow Polyomics, raw data was obtained and further analysed through IDEOM. The analysis of the raw data identified a significant number of peaks/chromatograms which were rejected based on certain criteria (see criteria below).

After manual curation, the final number of selected metabolites for the developing foetuses were 395 whereas the maternal serum had 399 metabolites that were included in the analysis after manual curation (Table 4.2).

Table 4. 2 Statistics of the developing foetus and the maternal serum extracts.

Foetus	
Peaks identified	855
Rejected *	496
Selected Metabolites	359
≥ 1.5 Fold Change	57

Serum	
Peaks identified	1281
Rejected *	882
Selected Metabolites	399
≥ 1.5 Fold Change	104

The rejection of metabolites/ peaks was based on our selection criteria:

1- Lipids: after carefully screening all of the metabolites, the peaks representing the lipids were rejected manually from the dataset. The reason for this rejection is that the column used in this analysis is not optimised/suitable for accurate lipid identification.

2- Peptides: simple peptides were also removed. Certain peptides (e.g. glutathione) have biological activity, but most are merely short-lived intermediates of protein degradation.

3- Low confidence level in IDEOM: the excel spreadsheets in IDEOM software have the confidence level of true identification of metabolites ranging from 1-10, The assigned level of confidence to each of the peaks selected is based on how accurately the m/z mass and retention times are matched with the calculated mass and predicted retention time of any particular metabolite. Highest confidence values are obtained when the measured retention time matches that of an authentic standard in a standard mix run in the same batch. All the peaks/chromatograms ≥ 6 confidence level were selected while all the remaining peaks were excluded from the further analysis.

4- Peak shape: there could be many shapes and styles of peak representing different metabolites, but ideally, only symmetrical and smooth peaks with high peak intensity

are selected for further analysis for accurate identifications. Some peaks are relatively zig-zag on slopes of peak with relatively low peak intensity. Similarly, the peaks with high back grounds and some peaks which do not match with retention time windows, these all are rejected to avoid any misleading identification. Here, in the figure below (Fig 4.1), are some of the examples shown for ideal/selected and rejected peaks.

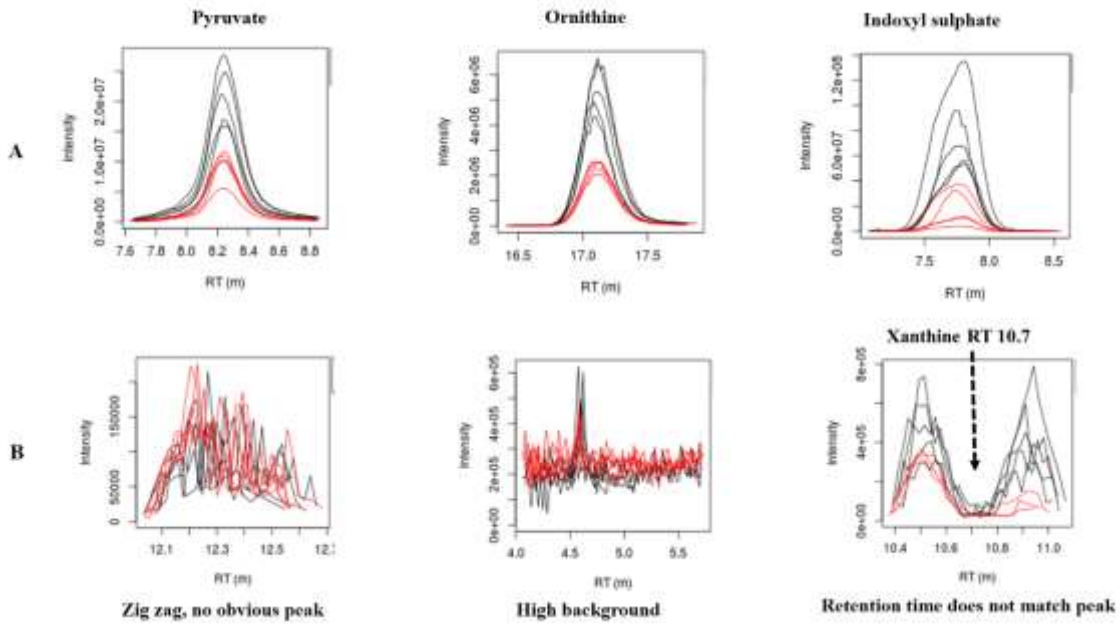

Figure 4. 1 represents different peak shapes and criteria for selection.

Row A shows the types of peaks selected on the basis of criteria mentioned above in description.

Row B is representative of three different criteria (no peak shape, high background noise and retention time is not matching with peak) for the rejection of peaks/metabolites to include in further analysis.

After all this manual curation discussed above, the selected metabolites were then investigated for further multivariate analysis via PCA and Orthogonal Partial Least Square Discriminant Analysis (OPLS-DA) to evaluate the differences between the infected and the uninfected control group.

4.3.1 Multivariate analysis of the maternal serum

Below, the PCA plot and OPLS-DA was produced by SIMCA software to evaluate the differences between the uninfected control and infected groups in the maternal serum based on the different variables. The PCA plot indicated a clear distribution of the two groups, so it can be further evaluated by OPLS-DA plots. As discussed previously, OPLS-DA was not a suitable model for the foetal extracts based on the PCA score plots of the two different groups. The OPLS-DA model plot is a supervised pattern recognition allowing identification of metabolites linked with the *T. gondii* infection in this analysis. A volcano plot was also produced to determine the significantly altered metabolites. The X axis in volcano plot indicates log2 fold change whilst Y axis depicts the -Log10 p-values. All pink dots correspond to one significant metabolite described in the volcano plot below. Full identification of significant metabolites associated with different changes observed in the maternal serum are listed below in Table 4.3.

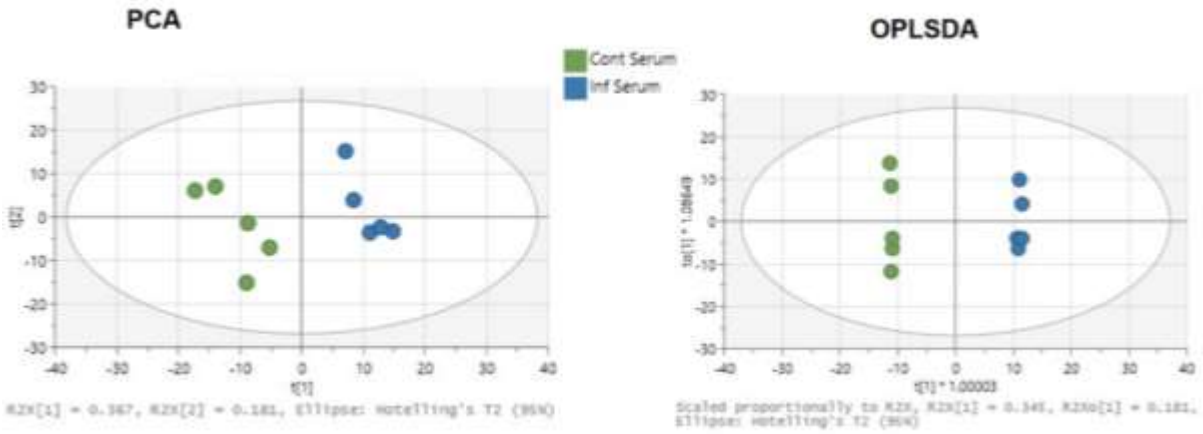

Figure 4. 2 Multivariate Analysis of Serum extracts (A) PCA score plot clearly shows two separated groups of the infected and control group, **(B)** Orthogonal Partial Least Square Discriminant Analysis (OPLS-DA) plot shows an excellent separation between infected and control groups. Each data point in A & B represents one mouse serum sample.

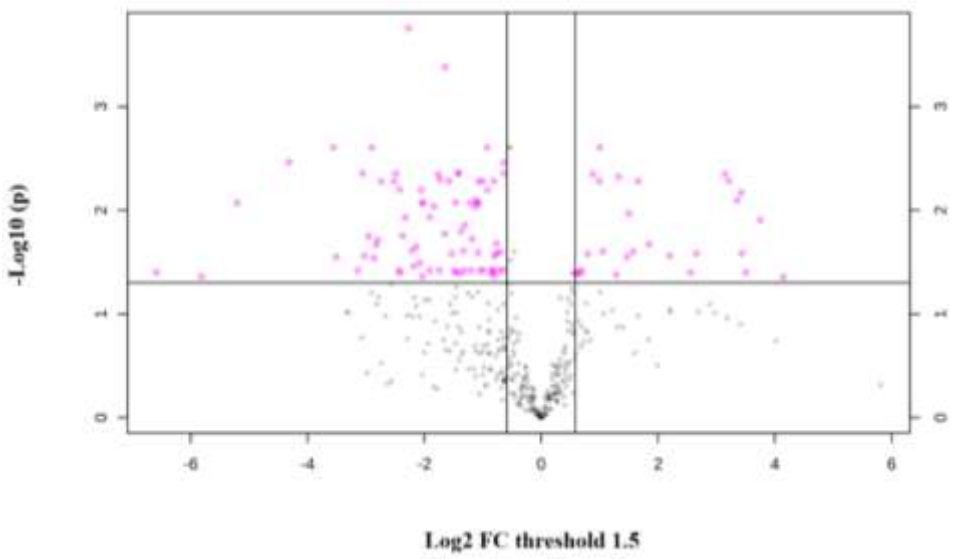

Figure 4. 3 shows volcano plot for the analysis of significant metabolites in serum with log2 fold change threshold 1.5 and –log10 P values. X-axis shows fold change and Y-axis is indicative of significance. Each blue and red dot indicative of significantly decreased and increased metabolites, respectively.

Table 4. 3 Significant metabolites detected by volcano plot in the serum as detected by volcano plot. Significantly increased metabolites marked as red, dark red (Log2 FC threshold 2) and light red (Log2 FC threshold 1) while significantly decreased metabolites represented by blue colour, dark blue (Log2 FC threshold 2) and light blue (Log2 FC threshold 1.5).

Mass	RT (*min*)	Formula	Metabolites	log2(FC)	-Log10 P
309.11	11.37	C11H19NO9	Deoxyguanosine	3.75	1.91
167.06	7.80	C8H9NO3	Urocortisol	3.50	1.40
168.04	10.38	C8H8O4	Adenine	3.21	2.28
138.03	4.78	C7H6O3	12alpha-Hydroxyamoorstatin	3.15	2.35
88.10	20.39	C4H12N2	(S)-Methylmalonate semialdehyde	2.66	1.58
192.03	13.86	C6H8O7	4-Hydroxyphenylacetaldehyde	2.56	1.40
166.05	11.44	C5H10O6	5_6-Dihydrothymine	2.20	1.56
131.11	20.41	C5H13N3O	Phenylacetaldehyde	1.85	1.67
149.05	7.08	C8H7NO2	Thymine	1.66	2.28
232.11	11.32	C9H16N2O5	Indole-3-ethanol	1.57	1.60
199.12	9.51	C10H17NO3	Cytosine	1.50	1.97
174.02	10.58	C6H6O6	Urate	1.47	1.55
208.08	9.80	C10H12N2O3	L-Kynurenine	1.40	-1.35
184.07	4.53	C9H12O4	Deoxycytidine	1.33	2.32
192.03	13.86	C6H8O7	D-Glutamine	1.29	1.38
132.05	10.73	C4H8N2O3	Methylimidazoleacetic acid	1.08	1.60
208.08	9.80	C10H12N2O3	Uracil	1.00	2.61
190.05	10.09	C7H10O6	N-Acetyl-beta-alanine	1.00	2.28
213.06	8.28	C9H11NO5	(S)-1-Pyrroline-5-carboxylate	0.89	2.35
398.14	12.75	C15H22N6O5S	Dodecanoic acid	0.79	1.58
116.05	7.08	C5H8O3	D-Gluconic acid	0.68	1.42
117.08	10.09	C5H11NO2	N2-Acetyl-L-aminoadipate	0.68	1.40
167.06	7.80	C8H9NO3	N-Acetylneuraminate	0.61	1.39
116.05	7.08	C5H8O3	D-Glucarate	0.50	1.40
204.09	10.48	C11H12N2O2	(R)-Lactate	-0.64	2.36
153.04	7.11	C7H7NO3	L-Valine	-0.64	2.46
117.08	10.09	C5H11NO2	L-1-Pyrroline-3-hydroxy-5-carboxylat	-0.64	1.42
104.02	10.21	C2H4N2O3	N6-Acetyl-L-lysine	-0.70	1.59
132.01	13.52	C4H4O5	Guanidinoacetate	-0.72	1.42
88.10	18.20	C4H12N2	1-O-methyl-β-D-glucuronate	-0.76	1.58
129.04	9.55	C5H7NO3	Pyruvate	-0.76	1.68
134.02	12.94	C4H6O5	Monomethyl sulfate	-0.80	1.37
210.04	13.48	C6H10O8	L-Arginine	-0.81	1.56

152.05	7.10	C8H8O3	2-(Acetamidomethylene)succinate	-0.81	2.28
130.03	8.53	C5H6O4	Orotate	-0.83	1.42
159.05	10.08	C6H9NO4	L-Alanine	-0.84	1.42
102.03	8.47	C4H6O3	Isopyridoxal	-0.85	1.39
136.04	21.94	C7H8N2O	1-methylnicotinamide	-0.91	-1.31
161.08	4.09	C10H11NO	Cytidine	-0.92	2.61
75.03	12.92	C2H5NO2	D-Glucose 6-sulfate	-0.99	1.42
262.01	14.49	C9H10O7S	Carnosine	-1.00	2.28
146.02	12.80	C5H6O5	1H-Imidazole-4-ethanamine	-1.04	1.42
182.06	8.83	C9H10O4	LL-2_6-Diaminoheptanedioate	-1.07	2.28
117.08	10.09	C5H11NO2	5_6-Dihydrouracil	-1.07	2.07
174.11	19.57	C6H14N4O2	N-gamma-Acetyldiaminobutyrate	-1.08	1.59
102.03	7.10	C4H6O3	Choline	-1.10	2.07
174.05	7.10	C7H10O5	L-Ornithine	-1.12	2.09
167.06	7.80	C8H9NO3	L-Lysine	-1.13	2.04
217.14	15.46	C9H19N3O3	N-Formimino-L-glutamate.1	-1.18	1.72
132.04	11.62	C5H8O4	L-Threonine	-1.20	1.42
130.06	6.96	C6H10O3	L-Proline	-1.21	2.07
246.13	11.77	C9H18N4O4	L-Methionine	-1.31	1.86
116.01	11.33	C4H4O4	1-thio-β-D-glucose	-1.32	1.42
147.05	9.87	C5H9NO4	O-Propanoylcarnitine	-1.33	1.61
145.09	12.54	C5H11N3O2	3-Methoxy-4-hydroxyphenylethyleneg	-1.37	1.80
208.08	9.80	C10H12N2O3	N6-Methyl-L-lysine	-1.42	2.36
117.06	9.30	C8H7N	2-hydroxy-2-methylbutyronitrile	-1.42	2.36
132.01	13.52	C4H4O5	(R_R)-Tartaric acid	-1.45	1.40
158.06	9.93	C7H10O4	Isopyridoxal.1	-1.47	2.07
88.05	7.15	C4H8O2	5-Guanidino-2-oxopentanoate	-1.49	1.42
147.05	12.12	C5H9NO4	3-tert-Butyl-5-methylcatechol	-1.53	1.58
213.01	7.79	C8H7NO4S	Indoxylsulfate	-1.56	-1.57
190.05	13.66	C7H10O6	N5-(L-1-Carboxyethyl)-L-ornithine	-1.58	2.28
191.06	7.39	C10H9NO3	Homostachydrine	-1.65	3.38
216.11	8.09	C9H16N2O4	Deoxyinosine	-1.65	1.77
198.05	7.92	C9H10O5	L-Tryptophan	-1.73	2.30
190.08	10.00	C8H14O5	Methyloxaloacetate	-1.74	1.42
197.11	7.04	C10H15NO3	Ngamma-Monomethyl-L-arginine	-1.77	2.35
102.03	8.47	C4H6O3	Arecoline	-1.84	2.04

126.01	8.56	C2H7O4P	L-Citrulline	-1.91	1.93
84.02	9.78	C4H4O2	Iminodiacetate	-1.91	1.42
116.05	7.08	C5H8O3	N-Acetyl-L-glutamate	-2.02	2.07
174.05	7.10	C7H10O5	gamma-Glutamyl-gamma-aminobutyra	-2.03	1.36
130.06	4.53	C6H10O3	5-Methyltetrahydrofolate	-2.04	2.07
152.05	9.42	C8H8O3	Heliotridine	-2.06	2.20
131.06	8.88	C5H9NO3	L-Pipecolate	-2.07	1.49
113.06	9.09	C4H7N3O	Indoxyl	-2.13	1.65
145.09	12.54	C5H11N3O2	4-guanidinobutanoate	-2.17	-1.67
219.11	8.37	C9H17NO5	Succinate	-2.18	1.46
130.11	17.23	C6H14N2O	Phenylpropanoate	-2.21	1.61
205.07	7.80	C11H11NO3	1-O-Methyl-myo-inositol	-2.27	3.76
179.08	12.55	C6H13NO5	4-Nitroaniline	-2.32	1.93
189.06	11.68	C7H11NO5	4-Coumaryl alcohol	-2.37	1.75
134.02	12.94	C4H6O5	Hypoxanthine	-2.41	1.40
136.05	7.08	C8H8O2	Stachydrine	-2.43	2.20
244.09	8.45	C10H16N2O3S	N2-(D-1-Carboxyethyl)-L-arginine	-2.44	1.42
109.05	9.00	C6H7NO	N2-(D-1-Carboxyethyl)-L-lysine	-2.49	2.36
180.04	7.93	C9H8O4	3-Dehydroxycarnitine	-2.52	2.28
183.09	8.37	C9H13NO3	3-beta-D-Galactosyl-sn-glycerol	-2.74	2.28
174.10	11.35	C7H14N2O3	N-Formyl-L-methionine	-2.80	1.71
240.12	11.66	C10H16N4O3	sn-glycero-3-Phosphocholine	-2.82	1.67
176.03	12.44	C6H8O6	5-Acetamidopentanoate	-2.87	1.54
224.08	11.43	C10H12N2O4	Phenylethyl alcohol	-2.90	2.61
175.10	12.89	C6H13N3O3	L-Histidinal	-2.95	1.75
115.06	11.13	C5H9NO2	N-Ribosylnicotinamide	-3.03	1.56
195.05	7.15	C9H9NO4	Xanthosine	-3.06	2.36
187.12	7.10	C9H17NO3	Tyramineglucuronide	-3.14	1.42
130.03	10.98	C5H6O4	Nicotinate D-ribonucleoside	-3.51	1.55
220.08	9.35	C11H12N2O3	Hippurate	-3.56	2.61
236.08	9.10	C11H12N2O4	5-Methoxyindoleacetate	-4.32	2.47
131.09	9.76	C6H13NO2	2-Hydroxyethylphosphonate	-5.20	2.07
158.06	9.93	C7H10O4	Bis(2-ethylhexyl)phthalate	-5.82	1.36
102.03	8.47	C4H6O3	alpha-Methylstyrene	-6.59	1.40

4.3.2 Multivariate analysis of the foetus

Below, the PCA plot was produced by SIMCA software to evaluate the differences between uninfected control and the infected groups in the developing foetuses on the basis of different variables. The PCA plot indicates improper distribution of the two groups (Figure 4.4). The samples do not form very tight groups indicating a high degree of variation within the group. Ideally, both groups should be separated, however there is a large overlap with some samples from the infected group closer to the uninfected control group. Previous studies using this model of *T. gondii* infection have demonstrated that *T. gondii* DNA cannot be amplified in all foetuses, suggesting that not all the foetuses become infected (Brito et al., 2020). This is in keeping with the results found here that also suggests that some of these foetal units did not develop infection. Since the PCA (Fig.4.4) was unable to separate the two groups, further investigation using OPLS-DA plots was not performed. There is no definitive way of determining which of the pre-term foetuses were infected and which were not. However, to gain potential insight the utility of 2-dimensional hierarchical clustering to discriminate between infected and non-infected samples was explored (Section 4.3.2.1, Fig. 4.5, 4.6, 4.7). Firstly, this analysis was performed with maternal serum where infection status was clear (Fig. 4.5). Secondly, the validity of this approach was tested using a data set previously obtained in the laboratory consisting of brain metabolic profiles from adult mice that were originally born to control mothers or mothers infected with *T. gondii* during pregnancy. Importantly since these mice were adults when euthanized, their infection status was determined by serology (Abdelsalam, 2019) (Fig. 4.6). Finally, the analysis was performed on the samples derived from the pre-term foetuses (Fig 4.7).

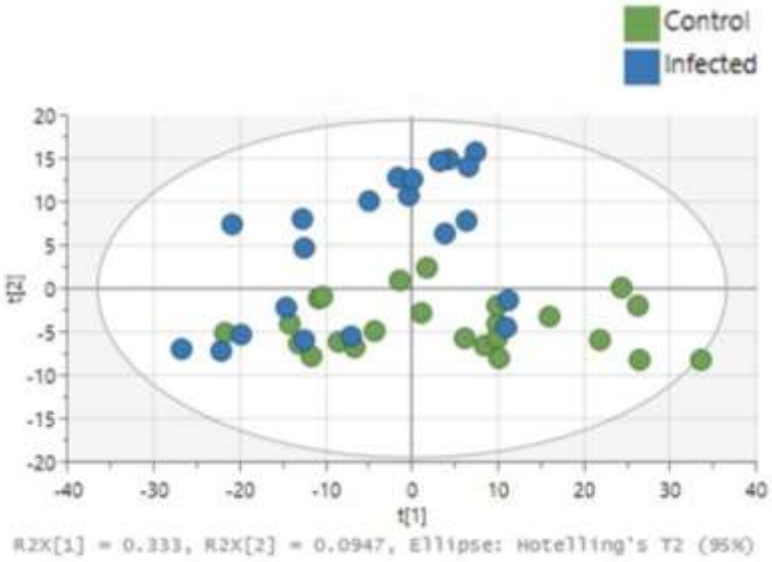

Figure 4. 4 Multivariate Analysis of Foetus (A) PCA score plot shows a homogenous distribution of the samples derived from infected mothers with those derived from the control group. It is worth noting that some samples derived from infected mothers cluster with samples from control mothers. Each data point represents one mouse foetal sample.

4.3.2.1 Hierarchical clustering to determine the likely infection status of foetuses

As determined by the PCA plot for the foetal extracts (Fig.4.4), the tested groups overlap, making a homogenous distribution of the foetal extracts rather than two separate clusters for the infected and the uninfected/control groups. This type of distribution in this particular type of PCA plot suggests that some of the foetal samples from infected mothers are only exposed and did not develop an infection. A previous study, using this same model of infection also reported that *T. gondii* DNA cannot be amplified in all the foetuses born to infected mothers suggesting that not all the foetuses become infected (Brito et al., 2020). As briefly discussed in section 4.3.2, previously, another data set of metabolomics profile from the brains of mice born to control mothers and of mothers infected while pregnant was produced in the laboratory (Abdelsalam, 2019). These samples were obtained from the brains of these mice at approximately 10 weeks of age and serology used to determine which mice were infected in utero. This dataset previously obtained from the brain and the current data set from the developing foetus were each separately analysed by hierarchical clustering to determine how efficiently this model can identify the corresponding class.

4.3.2.2. Dendrogram

A dendrogram is a mathematical diagram showing a tree used in different contexts like phylogenetic, hierarchical clustering, and computational biology. In phylogenetic studies, it represents the evolutionary relationship amongst many biological observations. That is the reason it is also called a phylogenetic tree. In hierarchical clustering, this diagram illustrates the cluster organization produced by the corresponding analysis, while in computational biology, dendrogram represents the clustering of genes or samples under investigation. An important use of a dendrogram is to find a way to allocate different samples to the relevant clusters. Dendrograms are interpreted based on the height/ horizontal line distance at which

any of the two samples/extracts are united together. The dendrograms shown here are made based on the average peak intensity values of the variables/ metabolites.

Initially, analysis of the samples from the brains of adult mice derived from control mothers or mothers infected during pregnancy was performed as three groups of mice (control/uninfected, infected and exposed/uninfected) had already been confirmed by the seropositive evaluation of IgG1 and IgG2.

Keeping in view the potential efficacy of the hierarchical clustering model mentioned above, it was applied to the maternal serum to serve as a control, as the infection status was very much definitive in this data set. This method was able to separate the samples into 2 clear clusters that corresponded with the infection status of the mice (Figure 4.5).

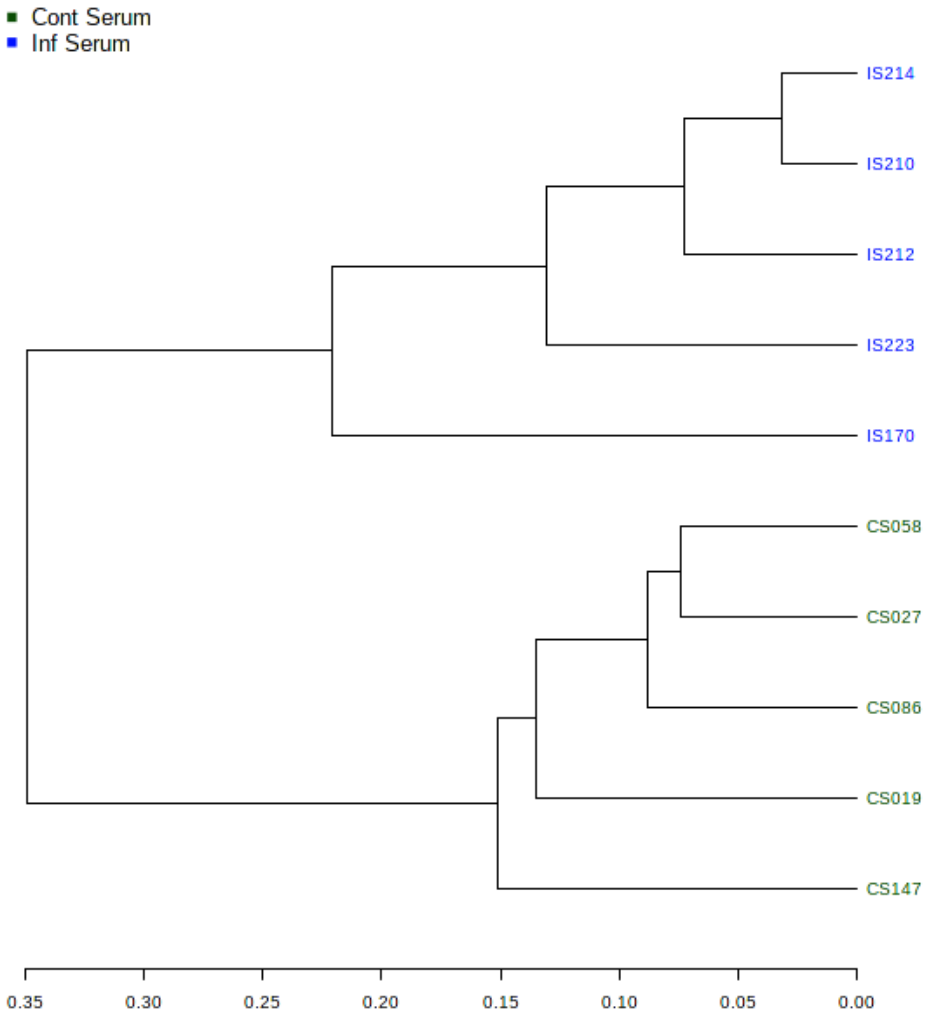

Figure 4. 5 Dendrogram showing hierarchical clustering between maternal infected serum and maternal control serum samples. X-axis shows a horizontal line representing the distance between plot matrix while right Y axis shows the clustering between three groups.

Similarly, a hierarchical clustering analysis of brain metabolites from adult mice born to infected and non-infected mothers was carried out to determine if the dendrogram successfully matched the infection status, as we knew the infection status by serological testing. This analysis did not result in clear separation of the infected and uninfected brain extracts from the mice born to infected mothers. In addition, mice born to non-infected mothers formed a distinct group in the dendrogram demonstrating that this method could not reliably even discriminate brains from congenitally infected and non-infected mice (Figure 4.6).

Notwithstanding the results above, hierarchical clustering was performed on the foetal extracts. The dendrograms indicate that there are some samples from the infected class clustering with that of the extracts from uninfected control foetal class. These samples include all the samples from mother 1 (IF032, IF037, IF040, IF043, IF046, IF049) and mother 2 (IF062) (Figure 4.7). This is in agreement with the PCA plot shown for the extracts from the foetuses derived from the infected mothers and uninfected control mothers (Figure 4.4). This suggests that the hierarchical clustering is strongly influenced by the mother from which the foetuses were derived. The metabolic profiles of maternal serum, the corresponding class representation in the PCA and dendrogram all demonstrate that the mothers were all successfully infected (Figure 4.2 and figure 4.5). Based on these observations, hierarchical clustering cannot conclusively identify the preterm foetuses derived from infected mothers or the foetuses only exposed to the maternal infection that did not develop *T. gondii* infection. The hierarchical clustering model worked perfectly in the maternal serum samples but the reasons for not leading to a firm conclusion in case of the foetal extracts is still not known. So the analysis was carried out by comparing all the foetuses from infected mothers compared with the foetuses from uninfected control mothers.

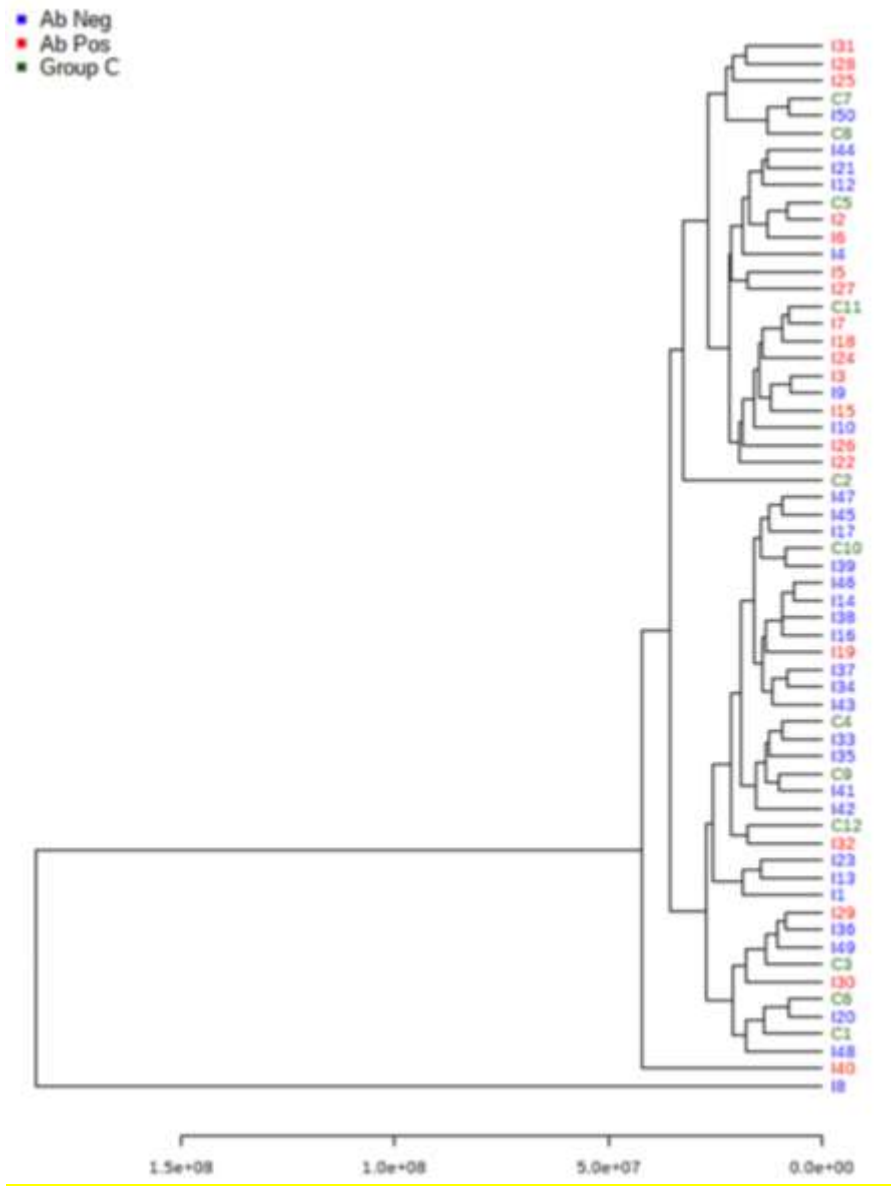

Figure 4. 6 Dendrogram showing hierarchical clustering between adult mice derived from infected mothers and control mothers during pregnancy. X-axis shows a horizontal line representing the distance between plot matrix while right Y axis shows the clustering between three groups.

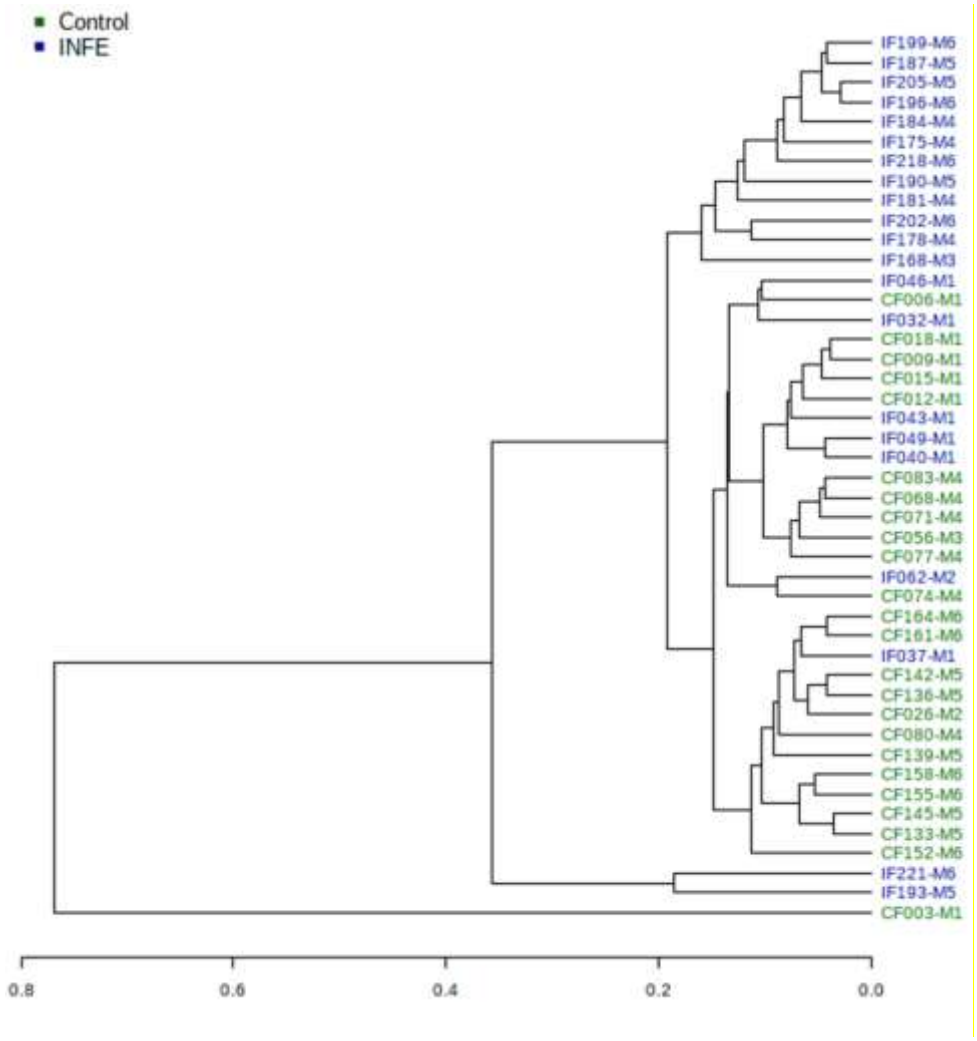

Figure 4. 7 represents a dendrogram showing hierarchical clustering between pre-term foetus from infected mothers and the pre-term foetuses from control mothers. X-axis shows a horizontal line representing the distance between plot matrix while right Y axis shows the clustering between the groups. Sample name represents infected or uninfected control class along with the corresponding mother. E.g, IF032-M1 shows infected foetus sample number 032 from mother 1.

4.3.2.3 Comparison of metabolites from all foetuses from infected mothers in comparison with foetuses from non-infected mothers

As the hierarchical clustering was unable to confidently identify those foetuses that were likely infected and those that were not likely infected born to infected mothers, further analysis of metabolites was performed treating all foetuses derived from infected mothers as a single variable. A volcano plot was produced to analyse the significant metabolites. In volcano plots, the X axis indicates log2-fold change with a threshold of 1.5 whilst Y axis depicts the - Log10 p value. All pink dots correspond to one significant metabolite described in the volcano plot below. All of the metabolites changing significantly in the volcano plot are represented with all of their details in table 4.4.

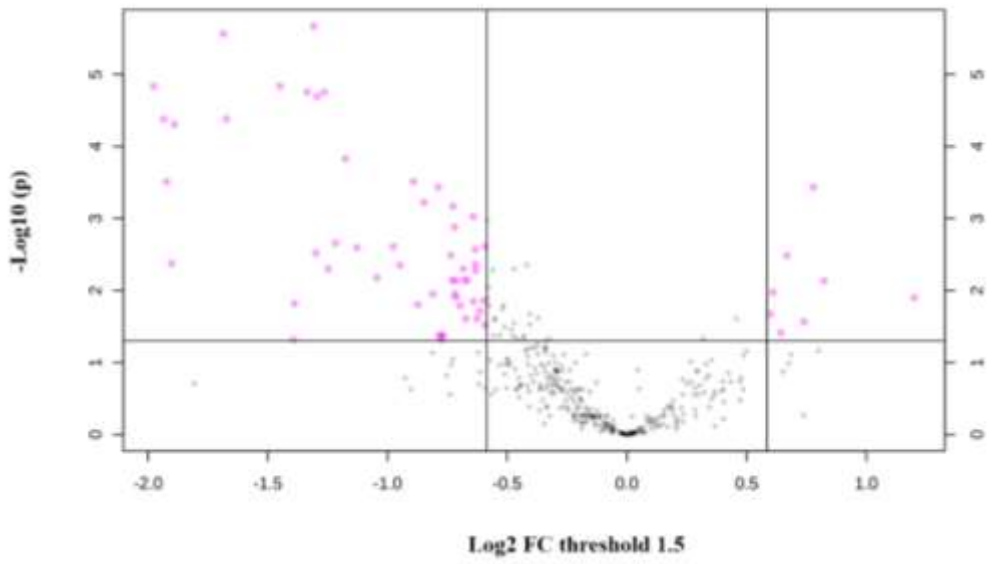

Figure 4. 8 Volcano plot for the analysis of significant metabolites in Foetus with log2 fold change threshold 1.5 and –log10 P values. X-axis shows fold change and Y-axis is indicative of significance. Each pink dot is representative of a metabolite that is significantly increased or decreased by log2 fold change with a threshold of 1.5 in samples derived from infected mothers relative to samples derived from uninfected control mothers.

Table 4. 4 Metabolites significantly altered in the developing foetuses derived from infected mothers. Significantly increased metabolites marked as red (dark red and light red) and significantly decreased metabolites represented by blue colour (dark blue and light blue).

Mass	RT	FORMULA	Metabolites	log2(FC)	-Log10 P
159.09	7.81	C6H10N2O3	(R)-3-Hydroxybutanoate	1.20	1.90
153.09	7.44	C4H8O2	Hydroxybutyrylcarnitine	0.82	2.14
364.04	17.06	C10H13N5O3	L-Homocysteine	0.78	3.43
284.08	11.59	C8H14N2O5S	Thymine	0.74	1.57
255.11	8.85	C4H9O7P	L-Kynurenine	0.67	2.49
75.07	10.73	C2H7O4P	AMP	0.64	1.41
167.98	16.50	C4H8N2O3	N(pi)-Methyl-L-histidine	0.61	1.98
139.07	7.83	C5H7N3O	5-Hydroxyindoleacetate	0.60	1.68
145.09	14.63	C5H7NO3	D-Fructose	-0.59	2.61
309.99	16.19	C3H9O6P	Pyruvate	-0.59	1.52
161.07	10.69	C7H11N3O2	5-6-Dihydrouridine	-0.60	1.86
443.03	17.07	C2H6O4S	5-Methylthio-D-ribose.1	-0.61	1.71
290.12	16.20	C7H15O10P	D-Glucose 6-phosphate	-0.63	1.61
105.08	18.00	C8H16NO9P	2-Hydroxy-2_4-pentadienoate	-0.63	2.36
363.06	18.14	C4H7N3O	5'-methylthioformycin	-0.63	2.28
427.03	14.44	C6H13O10P	sn-glycero-3-Phosphocholine	-0.63	2.57
243.15	8.15	C10H12N2O3	L-Glutamate 5-semialdehyde	-0.64	1.85
152.03	16.64	C9H13N2O9P	N-Formimino-L-glutamate	-0.64	3.03
253.10	7.66	C9H12N2O5	N_N-Dimethylglycine	-0.67	2.14
118.03	8.05	C6H9N3O2	Phosphodimethylethanolamine	-0.67	1.61
246.13	13.65	C7H7ClO5	1-deoxyxylonojirimycin	-0.68	2.14
112.03	8.30	C6H13O9P	5_6-Dihydrothymine.1	-0.68	2.30
334.07	15.45	C12H24N2O8	L-Cystathionine	-0.70	1.79
387.04	18.21	C11H15N3O6	Homoarginine	-0.71	1.90
152.03	10.92	C6H14N2O2	L-Methionine S-oxide	-0.71	2.14
589.08	16.73	C7H15N3O3	5'-deoxyribose	-0.72	1.95
127.04	10.48	C10H14N5O6P	sn-Glycerol 3-phosphate	-0.72	2.88
152.06	7.39	C9H8O2	L-Methionine	-0.73	3.17

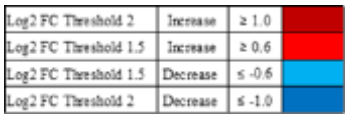

136.04	9.83	C9H14N3O8P	D-Sedoheptulose 7-phosphate	-0.73	2.14
132.09	22.42	C7H14N2O3	5-Guanidino-2-oxopentanoate	-0.74	2.49
145.04	10.26	C6H12N2O2	N-Acetyl-L-aspartate	-0.77	1.37
269.09	15.73	C5H14NO6P	6-Phospho-D-gluconate	-0.77	1.38
536.05	15.44	C6H13NO4	L-Pipecolate	-0.78	1.32
322.06	12.37	C8H20NO6P	Tiglylcarnitine	-0.79	3.43
188.12	12.52	C10H16N2O3S	sn-glycero-3-Phosphoethanola	-0.81	1.95
244.09	8.60	C8H16N2O3	(Z)-4-Hydroxyphenylacetaldel	-0.85	3.22
257.10	13.95	C10H15N2O8P	4-Guanidinobutanoate	-0.87	1.80
247.14	11.12	C7H10O4	D-Erythrose	-0.89	3.51
163.08	15.32	C14H22N2O16P2	Urea-1-carboxylate	-0.95	2.35
215.06	15.15	C10H12FN5O3	3-Hydroxyanthranilate.1	-0.98	2.61
144.09	23.03	C5H7NO4	N-D-Glucosylarylamine	-1.04	2.18
174.10	13.08	C5H12N2O2	1-O-Methyl-myo-inositol	-1.13	2.60
323.05	15.20	C5H4N4O	L-Hypoglycin	-1.18	3.83
148.05	9.97	C7H8N2O2	1-Methylnicotinamide	-1.22	2.66
331.07	12.30	C4H5N3O2	Methyloxaloacetate	-1.25	2.30
189.11	14.70	C16H25N5O15P2	Isopyridoxal	-1.26	4.75
146.11	14.69	C5H4N4O2	N-Acetyl-D-quinovosamine	-1.29	4.69
285.10	8.08	C10H17N3O9S2	2-Oxoglutaramate	-1.30	2.52
324.15	23.04	C9H19O11P	Homostachydrine	-1.31	5.67
260.03	16.18	C4H4N2O2	4-Nitroaniline	-1.34	4.75
206.00	15.85	C9H18N4O4	L-Citrulline	-1.39	1.82
324.04	14.49	C5H4N4O2	Trimethylamine N-oxide	-1.67	4.38
208.08	10.51	C12H21NO4	Stachydrine	-1.69	5.57
276.03	16.77	C10H15N5O10P2	D-Ribose	-1.89	4.31
113.06	9.45	C10H14N5O8P	Indoxylsulfate	-1.90	2.38
301.06	14.24	C4H11NO2	Hippurate	-1.92	3.51
290.04	15.53	C10H18N4O6	Phenylamil	-1.93	4.38
126.00	10.37	C10H15N5O11P2	1-butanesulfonate	-1.98	4.84

4.3.2.4 Comparison of metabolomics profile of the foetuses from both experiments

An overall analysis and comparison of all the foetal metabolites detected in the experiments described here and in chapter 3 was carried out. Caution needs to be exercised in comparing these data sets as for the first experiment foetuses were extracted at day 14 of pregnancy (day 7 of maternal infection) and for the second experiment day 13 of pregnancy (day 6 of maternal infection). Furthermore, the second experiment used an updated more modern mass spectrometer. However, there are still 145 metabolites in common which are detected in both of the experiments. A total number and overlapping of all the metabolites within these two experiments can be seen as follows (figure 4.9).

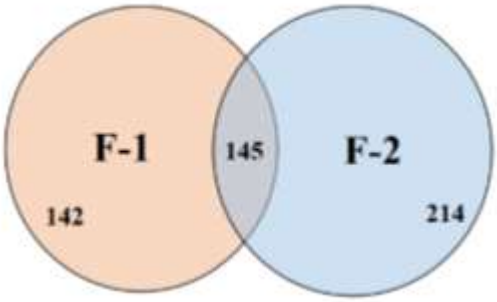

Figure 4. 9 Venn diagram shows the total number of metabolites and overlapping that were detected in foetuses from both of the experiments. (F1 represents foetuses from previous chapter 3, while F2 indicates the developing foetuses derived from the infected mothers from chapter 4).

A similar comparison was performed for the metabolites that were significantly increased or decreased by log2 FC with a threshold of 1.5 or more (Figure 4.10). There are more significant changes observed in foetal extract from experiment 1 (chapter 3) in comparison with experiment 2 (chapter 4). Further details of the metabolites significantly increased/decreased can be seen in the following table 4.5 and 4.6.

A comparison of both experiments demonstrated that there are many differences in both the numbers of metabolites as well as some specific metabolites that are differentially expressed between these two experimental settings. The reasons underlying this variation could reflect the differences in the experimental timings, the instrument used for analysis or the actual variability in this complex biological system. The current study analyses metabolites based on the comparison of the peak intensity values, which can be highly variable between different experimental batches, different instruments and different parameters and different pre-processing methods adopted (Traquete et al., 2021). Despite these inconsistencies between the two experiments, a number of metabolites are consistently found to be altered including L-kynurenine, hydroxybutyrylcarnitine, 4-guanidinobutanoate, indoxylsulfate and trimethylamine N-oxide.

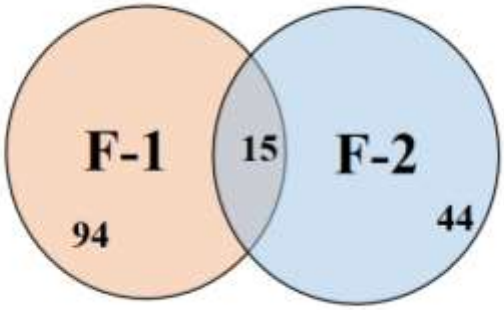

Figure 4. 10 Venn diagram showing only the number of significantly changing metabolites and overlapping in between foetuses that were detected in foetuses from both of the experiments. (F1 represents foetuses from previous chapter 3, while the number of metabolites from the developing foetuses detected in the current chapter are denoted by F2.)

Table 4. 5 significantly changing metabolites in the developing foetal extracts from both of the experiments. Criteria for significance is log2 fold change with a threshold of 1.5. Number of significantly increased metabolites are shown by red, while a significantly reduced expression of metabolites is indicated by blue colour.

	Log2 FC (1.5)	Log2 FC (1.5)	Total
Foetus-1	62	47	109
Foetus-2	8	51	59

Following the Venn diagram (Fig. 4.10) above, here are the common metabolites with a significantly high/ reduced expression in both experiments shown in the following table 4.6.

Table 4. 6 Metabolites significantly affected by infection and detected in both of the experiments from foetal extracts. Foetus-1 and foetus-2 in the table represent the data sets of foetal extracts from chapter 3 and chapter 4, respectively. Significantly increased metabolites marked as red (dark red and light red) and significantly decreased metabolites represented by blue colour (dark blue and light blue).

Common between F1-F2	Foetus-1		Foetus-2	
Metabolites	log2(FC)	-Log10 P	log2(FC)	-Log10 P
sn-Glycerol 3-phosphate	1.09	3.97	-0.72	2.88
N(pi)-Methyl-L-histidine	1.08	8.60	0.61	1.98
D-Sedoheptulose 7-phosphate	1.05	3.17	-0.73	2.14
6-Phospho-D-gluconate	1.00	2.96	-0.77	1.38
L-Kynurenine	0.96	5.43	0.67	2.49
D-Glucose 6-phosphate	0.91	5.65	-0.63	1.61
N_N-Dimethylglycine	0.76	8.60	-0.67	2.14
sn-glycero-3-Phosphoethanolamine	0.67	2.71	-0.81	1.95
Hydroxybutyrylcarnitine	0.64	4.21	0.82	2.14
sn-glycero-3-Phosphocholine	0.64	3.61	-0.63	2.57
2-Oxoglutaramate	-0.65	1.63	-1.30	2.52
Tiglylcarnitine	-1.18	5.14	-0.79	3.43
4-Guanidinobutanoate	-1.63	6.77	-0.87	1.80
Trimethylamine N-oxide	-1.91	5.33	-1.67	4.38
N-D-Glucosylarylamine	-2.17	5.92	-1.04	2.18
Indoxylsulfate	-2.64	3.13	-1.90	2.38

Log2 FC Threshold 2	Increase	≥ 1.0	
Log2 FC Threshold 1.5	Increase	≥ 0.6	
Log2 FC Threshold 1.5	Decrease	≤ -0.6	
Log2 FC Threshold 2	Decrease	≤ -1.0	

4.4 Significant changes between foetus and the maternal serum

The following Venn diagram displays the overlap of significantly changing metabolites detected by volcano plots between the developing foetus maternally infected with *T. gondii* and the maternal serum. The criteria for the significance shown in the figure below is log2 fold change with a threshold of 1.5 and a –log *p* is ≥ 1.3.

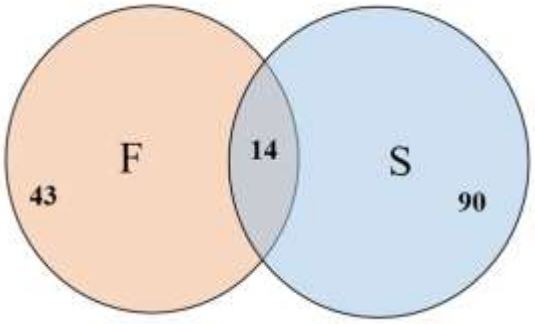

Figure 4. 11 Venn diagram showing the overlap of significant metabolites detected by volcano plots between the foetus and maternal serum.

Following the figure above, a detailed statistics of the number of metabolites either significantly increased or decreased is shown in the following Table 4.7.

Table 4. 7 Represents significantly increasing/decreasing the number of metabolites in the developing foetus and the maternal serum.

Tissue	Log2-FC (2)↑	Log2-FC (1.5)↑	Log2-FC (2)↓	Log2-FC (1.5)↓	Total
Foetus	**1**	**7**	**18**	**31**	**57**
Serum	**20**	**6**	**15**	**63**	**104**

In the foetus maternally infected with *T. gondii*, a total of 57 metabolites were showing a significant alteration in their peak intensity levels compared with the uninfecetd control foetuses. These metabolites were further divided based on the log2 fold change with a threshold of 2 and log2 fold change with a threshold of 1.5. The reason for this subdivision is to enhance the coverage of the metabolites being altered with a statistical significance.

Table 4. 8 Metabolites significantly affected by T. gondii infection and detected in common between the maternal serum and the developing foetal extracts. Significantly increased metabolites marked as red (dark red and light red) and significantly decreased metabolites represented by blue colour (dark blue and light blue).

	Foetus		Maternal serum	
Metabolites	**log2(FC)**	**-Log10 P**	**log2(FC)**	**-Log10 P**
1-Methylnicotinamide	-1.22	2.66	0.91	1.31
4-Guanidinobutanoate	-0.87	1.80	2.17	1.67
4-Nitroaniline	-1.34	4.75	2.32	1.93
5-Guanidino-2-oxopentanoate	-0.74	2.49	1.49	1.42
Hippurate	-1.92	3.51	3.56	2.61
Homostachydrine	-1.31	5.67	1.65	3.38
Indoxylsulfate	-1.90	2.38	1.56	1.57
L-Citrulline	-1.39	1.82	1.91	1.93
L-Kynurenine	0.67	2.49	1.40	1.35
L-Methionine	-0.73	3.17	1.31	1.86
L-Pipecolate	-0.78	1.32	2.07	1.49
Methyloxaloacetate	-1.25	2.30	1.74	1.42
Pyruvate	-0.59	1.52	0.76	1.68
Thymine	0.74	1.57	1.66	2.28

Log2 FC Threshold 2	Increase	≥ 1.0	
Log2 FC Threshold 1.5	Increase	≥ 0.6	
Log2 FC Threshold 1.5	Decrease	≤ -0.6	
Log2 FC Threshold 2	Decrease	≤ -1.0	

Considering the results from the analysis or maternal serum and foetal extracts, a number of pathways were identified as being most affected. Notably, tryptophan metabolism, purine metabolism and arginine metabolism are found to have multiple metabolites altered due to infection. In addition, metabolites that are associated with the microbiome (4-guanidinobutonate and indoxylsulfate) are also seen to be affected by maternal infection

4.5 Metabolites detected in tryptophan degradation pathway

The following results below show different metabolites identified in the tryptophan degradation pathway in the foetus maternally infected with *T. gondii* and the maternal serum. The metabolites identified were tryptophan, kynurenine, 3-hydroxyanthranilate and 1-methylnicotinamide. Importantly, significantly increased levels of kynurenine were seen in the developing pre-term foetuses (p = 0.041) and maternal serum (p = 0.0006) in comparison with control uninfected samples (Fig. 4.13). Analysis of the tryptophan expression showed a decreased level of tryptophan in the foetuses derived from mice infected with *T. gondii* as well as maternal serum (p = 0.0400 and p = 0.00006) in comparison with control uninfected foetus and maternal serum. Similar results for both metabolites were obtained in both of the developing foetus and the maternal serum where decreased levels of tryptophan and increased levels of kynurenine were recorded (Fig. 4.13). Similarly, there were significantly decreased levels of 1-methylnicotinamide in the foetuses derived from mice infected with *T. gondii* (p = 0.005) and although this metabolite was decreased in maternal serum of *T. gondii* infected mice as compared with control uninfected serum, this difference was not significant (p = 0.060) (Fig. 4.13). The maternal serum from the infected mice also had increased levels of L-formyl kynurenine in comparison with the maternal serum from the control uninfected mice (p=0.0007). Another metabolite 3-hydroxyl L-kynurenine was found to be increased in the maternal serum according to the fold change value but not p-value (p=0.08). Similarly, some of the metabolites are found to be significantly increased only in the foetuses including and 3-hydroxyanthranilate (p=0.0001) (Fig. 4.12, 4.13).

Other metabolites derived from tryptophan degradation pathway including some indole derivatives, indoxyl (p = 0.003), indole-3-acetate (p = 0.03), and 5-methoxyindoleacetate (0.00007) were significantly reduced in maternal infected serum while indole-3-ethanol (p = 0.004) was found to be increased significantly in maternal infected serum, however all these

metabolites were not detected in the foetal extracts. Similarly, few metabolites from nicotinate and nicotinamide metabolic pathway including Nicotinate D-ribonucleoside (p= 0.01), N-Ribosylnicotinamide (p= 0.01), 6-Hydroxynicotinate (p= 0.02), were found to be altered to a significantly low levels in maternal serum infected with *T. gondii*, however these were not detected in the foetus derived from the infected mothers compared with the uninfected control mothers.

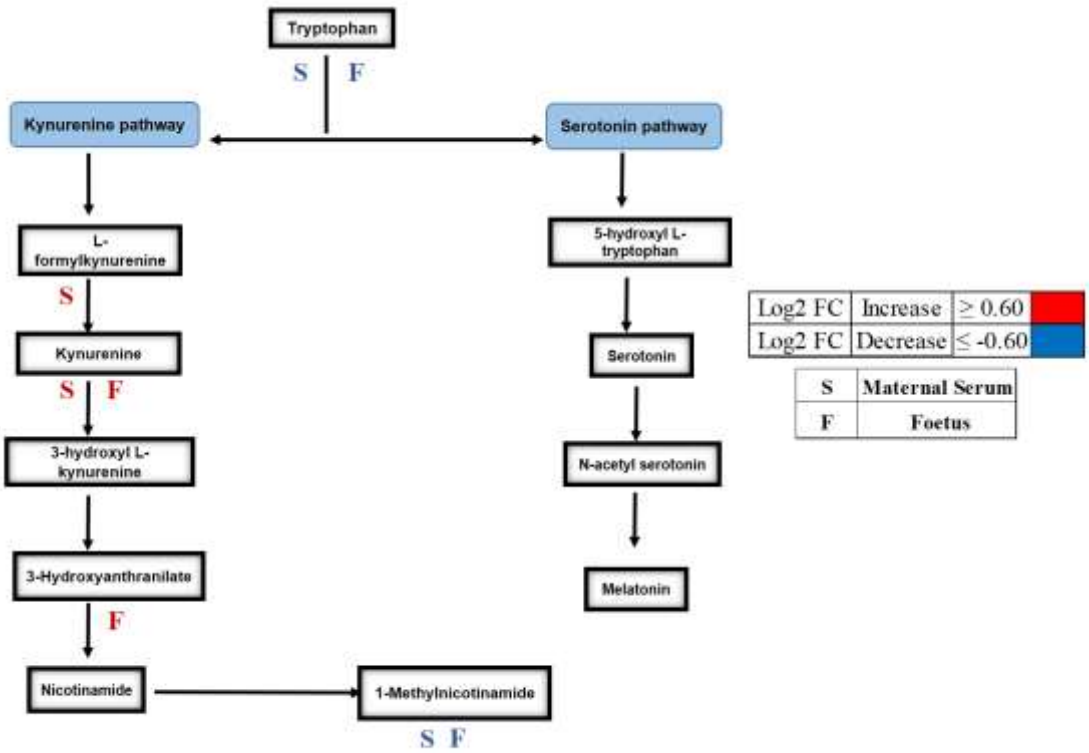

Figure 4.12 Tryptophan degradation pathway showing interactions between different metabolites in tryptophan metabolic cycle along-with interactions with other pathways. Letter S below the rectangle box represents maternal serum, letter F is representative of the foetus. A significant log2 fold change threshold 1.5 increase is shown by red colour and blue colour indicates a significant decrease of log2 fold change with a threshold of 1.5.

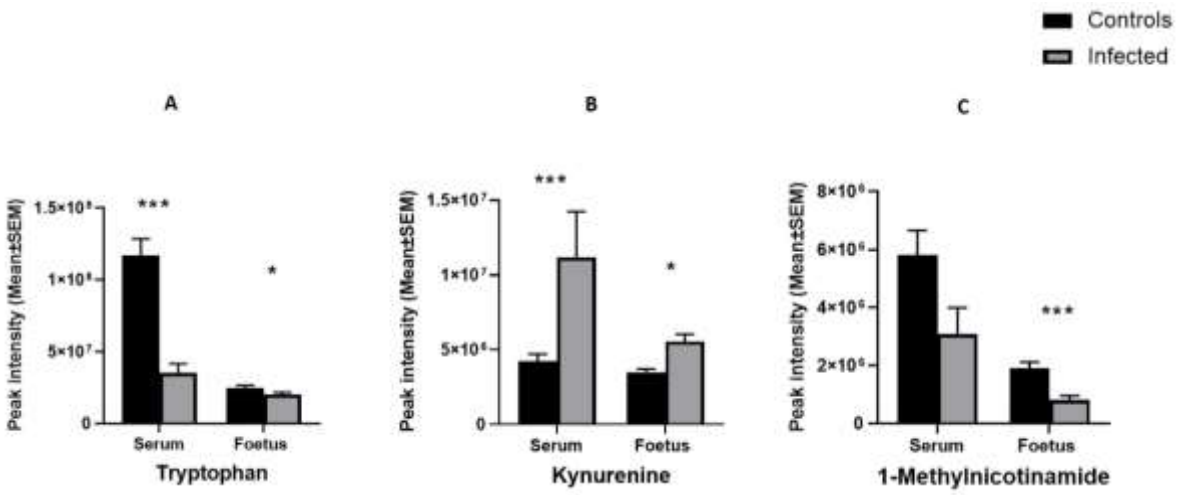

Figure 4. 13 represents different metabolites detected in tryptophan degradation pathway in the foetus maternally infected with T. gondii and the maternal serum. Foetal extracts (n= 24 and 21 for uninfected and infected, respectively, Maternal serum extracts (n= 5 each for uninfected and infected). Student´s t-test was performed to determine significance ($p < 0.05$) where *$p < 0.05$, **$p < 0.001$ ***$p < 0.0001$ are significant compared to the control uninfected.

A- shows peak intensity value (Mean± SEM) of tryptophan in serum and foetus

B- shows peak intensity value (Mean± SEM) of kynurenine in serum and foetus

C- shows peak intensity value (Mean± SEM) of 1-methylnicotinamide in the developing foetus and the maternal serum.

4.6 Metabolites detected in arginine metabolism pathway

The following results below show different metabolites identified in the arginine metabolic pathway in the foetus maternally infected with *T. gondii* and the maternal serum. Three important metabolites identified as being altered consistent with the previous results are citrulline, ornithine and proline (Chapter 3, Fig 3.12, 3.13). With regards to citrulline, the foetus derived from mice infected with *T. gondii* displayed statistically significant decreased levels as compared to control uninfected foetus (p = 0.042) (Fig. 4.14). Similar differences were seen in the maternal serum from the infected mice. There is a significant decrease in the peak intensity concentration of citrulline in the maternal serum from infected mice as compared to the control uninfected maternal serum (p = 0.00007) (Fig. 4.14). Decreased levels of ornithine were found in the foetuses from mice infected with *T. gondii* in comparison to the developing foetuses from control uninfected mice. Although this difference is not significant statistically the decrease of ornithine is in agreement with the results discussed in previous chapter. However, in the maternal serum, a statistically significant decrease in levels of ornithine expression is noted (p = 0.00008). Finally, decreased levels of proline were noted in the maternal serum from infected mice (p = 0.0004) (Fig. 4.14). Although a decrease was noted in proline levels in the foetuses from infected mice compared with the control uninfected foetus, this difference was not statistically significant (p = 0.074). So for both proline and ornithine, we can conclude that there is no change in the levels of peak intensity of infected extracts when compared with the uninfected control extracts of the foetuses. The data obtained indicates that *T. gondii* infection causes reduced levels of citrulline, ornithine and proline within foetuses derived from infected mothers and the maternal serum thus suggesting that the arginine metabolism pathway is disrupted during *T. gondii* infection. There is a strong possibility of an increased flux through the arginine pathway.

Some metabolites related to glutamate and proline and therefore arginine metabolism were found to be altered significantly only in one of the tissues examined. These metabolites, N-acetyl ornithine, N-acetyl glutamate and L-glutamate were found to be significantly decreased in the maternal serum when compared with that of the uninfected control serum (p = 0.0072, 0.000 and 0.0531, respectively). Similarly, one of the metabolites, L-glutamate 5-semialdehyde was significantly decreased only in the foetuses of mice infected with *T. gondii* when relative to foetuses derived from uninfected control mice (p = 0.0053).

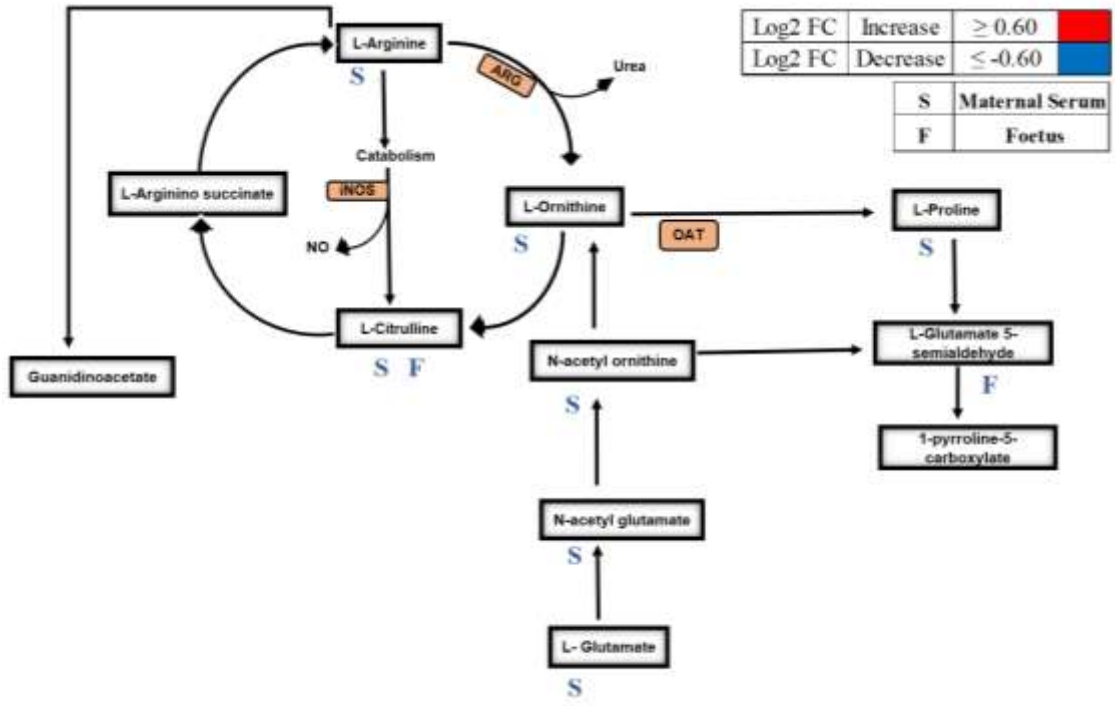

Figure 4. 14 Arginine metabolic pathway showing interactions between different metabolites along with interactions with other pathways. Letter S below the rectangle box represents maternal serum, letter F is representative of foetus. A significant log2 fold change threshold 1.5 increase is shown by red colour and blue colour indicates a significant decrease with log2 fold change threshold 1.5.

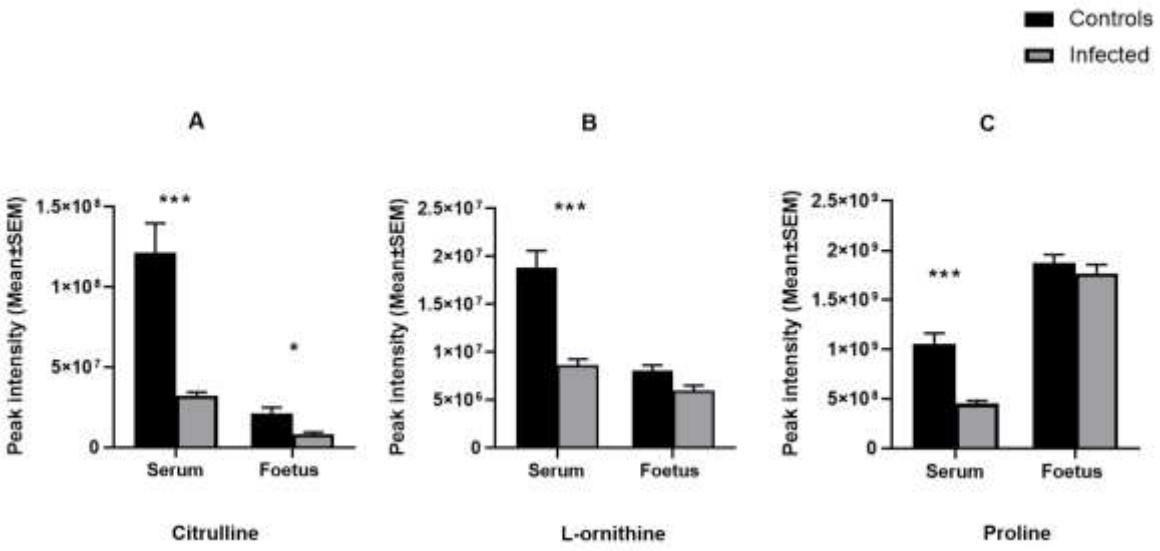

Figure 4. 15 represents different metabolites detected in arginine metabolic pathway in the foetus and maternal serum. Foetal extracts (n= 24 and 21 for uninfected and infected, respectively, Maternal serum extracts (n= 5 each for uninfected and infected). Student´s t-test was performed to determine significance ($p < 0.05$) where *$p < 0.05$, **$p < 0.001$ ***$p < 0.0001$ are significant compared to the control uninfected.

A- shows peak intensity value (Mean± SEM) of citrulline in maternal serum and the developing foetus

B- shows peak intensity value (Mean± SEM) of ornithine in maternal serum and developing foetus

C- shows peak intensity value (Mean± SEM) of proline in maternal serum and developing foetuses

4.7 Metabolites associated with or dependent on microbiome

The following results show different microbial metabolites identified as being altered in the foetus and the maternal serum in mice infected with *T. gondii* during pregnancy. These microbial metabolites include indole, indoxylsulfate and 4-guanidinobutanoate. These metabolites have also been implicated in the tryptophan degradation pathway. Decreased levels of indoxylsulfate were seen in the foetuses derived from infected mice and the maternal serum in infected mice compared to foetuses derived from uninfected control mice and control maternal serum ($p = 0.003$ and 0.002, respectively). Reduced levels of 4-guanidinobutanoate were also seen in the developing foetuses and maternal serum of infected mice (Fig 4.17B). These observations indicate that *T. gondii* infection in mice during pregnancy results in reduced levels of these metabolites most probably arising from the effects of the infection on microbial population. However, this needs to be verified through metagenomics studies.

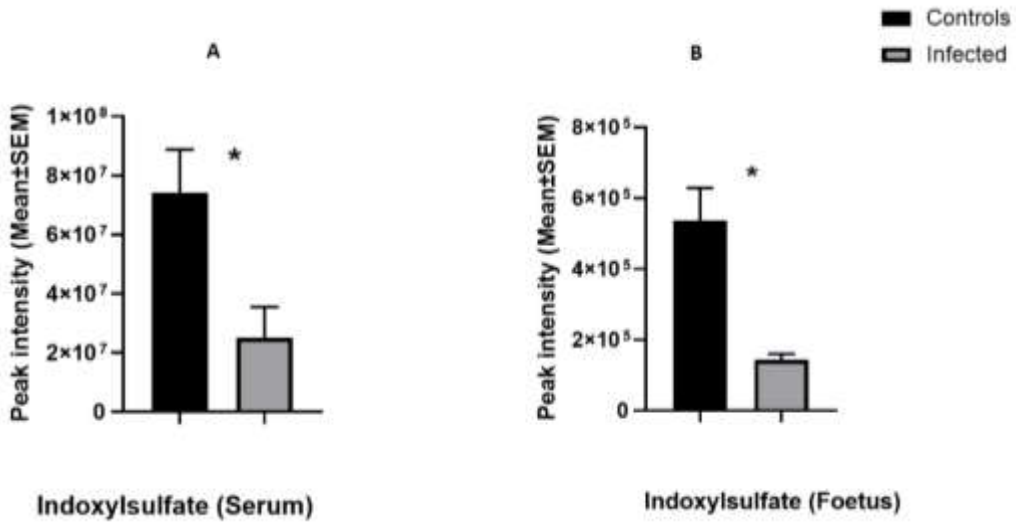

Figure 4. 16 represents metabolite indoxylsulfate detected in both tissues. Foetal extracts (n= 24 and 21 for uninfected and infected, respectively, Maternal serum extracts (n= 5 each for uninfected and infected). Student´s t-test was performed to determine significance ($p < 0.05$) where *$p < 0.05$, **$p < 0.001$ ***$p < 0.0001$ are significant compared to the control uninfected.

A- shows peak intensity value (Mean± SEM) of indoxylsulfate in serum

B- shows peak intensity value (Mean± SEM) of indoxylsulfate in foetus

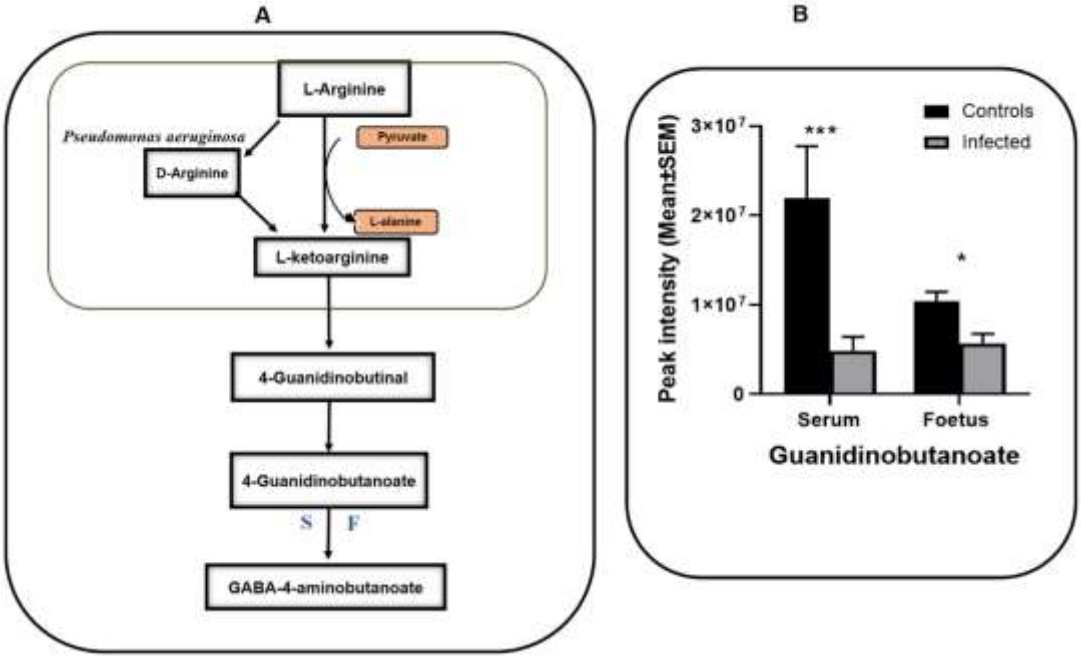

Figure 4. 17 Arginine catabolic pathway in microbiome.

(A) Origin of guanidinobutanoate as a result of pseudomonas aeruginosa (PAO1) reactions in the L-arginine metabolic pathway.

(B) shows peak intensity value (Mean± SEM) of guanidinobutanoate in the maternal serum and foetus. Foetal extracts (n= 24 and 21 for uninfected and infected, respectively, Maternal serum extracts (n= 5 each for uninfected and infected). Student´s t-test was performed to determine significance ($p < 0.05$) where *$p < 0.05$, **$p < 0.001$ ***$p < 0.0001$ are significant compared to the control uninfected.

Statistically significant decreased levels of guanidinobutanoate are seen in the maternal serum, maternally infected foetus and as well as in the infected mice compared to control ($p = 0.0006$ and 0.0071, respectively). High levels of reduction of guanidinobutanoate are also seen in the foetus ($p = 0.0002$) and serum ($p = 0.020$).

4.8 Conclusion

Building on from the results in the previous chapter, here the results once again indicate that infection of mice with *T. gondii* during pregnancy induces significant alterations in maternal metabolism that is easily detected in the serum. In addition, changes to the metabolism of the foetuses is also evident. During this study, an untargeted approach was utilised to identify metabolites that are influenced by *T. gondii* infection in the foetus and the maternal serum. Raw data was obtained commercially via Glasgow Polyomics to characterise and confirm the metabolites of interest in the foetus and serum. Hydrophilic interaction liquid chromatography was undertaken on Dionex Ultimate 3000 RSLC system using a ZIC-pHILIC column. This approach was used to identify a wide range of metabolites which could be altered during *T. gondii* infection. Raw data that was obtained from Glasgow Polymics was analysed using IDEOM v19. Multivariate analysis was performed with PCA and OPLS-DA to identify metabolites associated with *T. gondii* infection in maternal serum or their foetuses. The results obtained here identified various metabolites that through association highlight a number of metabolic pathways such as trytophan degradation, arginine metabolism and purine degradation as those most affected due to the infection. In addition, a number of microbial metabolites that are known to be affected by the microbiome were found to be affected in maternal serum and foetal extracts. Notably, most metabolic changes were found in the maternal serum but a subset of these were found to also be affected in the foetus. A few metabolites were only noted to change in the foetus that are shown in the following figure 4.18.

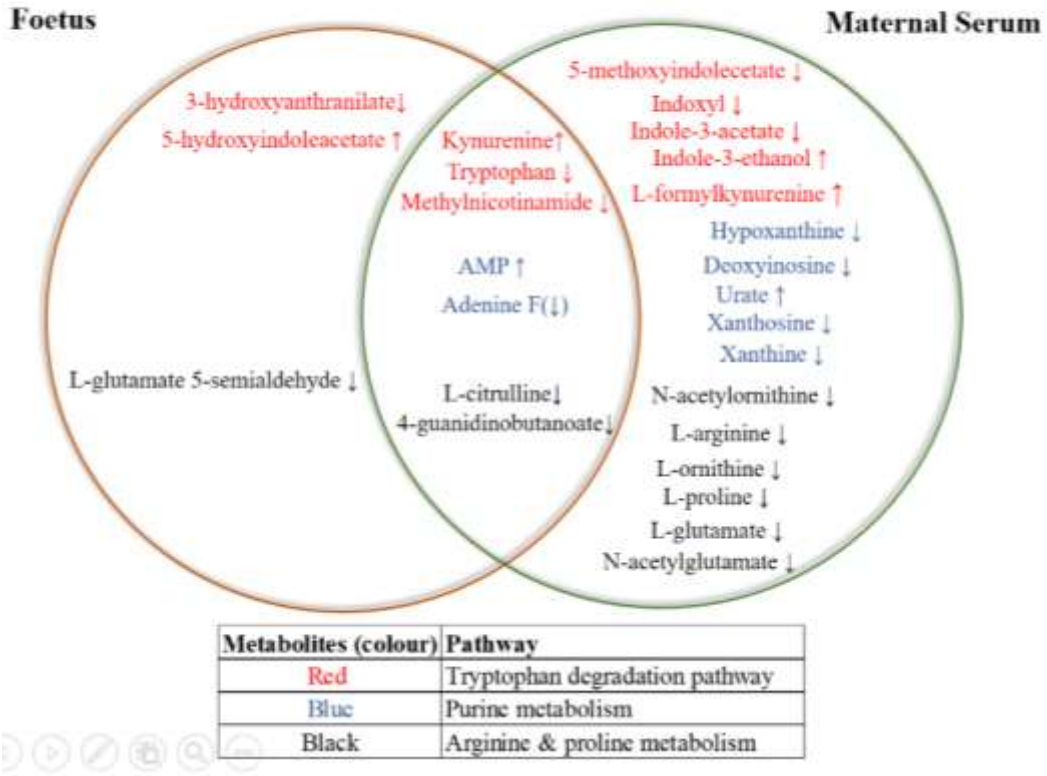

Metabolites (colour)	Pathway
Red	Tryptophan degradation pathway
Blue	Purine metabolism
Black	Arginine & proline metabolism

Figure 4.18 Venn diagram showing an overlap of different metabolites between maternal serum and the foetal extracts. Some of the metabolites can be seen as being altered significantly only in foetal extracts or in the maternal serum affected by *T. gondii*. While some of the metabolites that are changed significantly in both of the tissues examined also shown in the diagram.

It is important to note that there were more and sometimes different metabolites detected as being significantly different following infection in this chapter that were found as such in the previous chapter. This could be attributed to a number of factors including the larger sample size being used this time and the increased sensitivity for the HPLC system and chromatography column used. In addition, in the studies described in this chapter foetuses were extracted at day 6 post infection as opposed to day 7 post infection.

However, in both chapters, a number of pathways were consistently seen to be affected. Importantly in this chapter the simultaneous analysis of maternal serum allows potential insight into the contribution of maternal metabolism in affecting foetal metabolites. Tryptophan metabolism was found to be affected in both maternal and foetal samples. Tryptophan was found to be reduced and kynurenine raised in both maternal serum and foetal samples. In addition, formyl kynurenine was raised in maternal serum but not significantly raised in foetal extracts. Overall, this suggests that maternal degradation of tryptophan could result in raised kynurenine levels in the foetus although a contribution from foetal metabolism cannot be ruled out. The observation that foetal kynurenine levels were raised following maternal infection is important as this metabolite has been associated with the polyIC administration in models of maternal immune activation which results in schizophrenia like behaviour in rodents (Clark et al., 2019).

Purine metabolism was found to be significantly altered in maternal serum with evidence of degradation of purines and the accumulation of urate. In contrast purine intermediates were not seen to be significantly depleted in the foetal samples and no evidence of urate accumulation was seen. However, adenine levels were significantly lower in the foetal extracts from infected mice than control foetal extracts, but increased in maternal serum from infected mice. These changes to purine metabolism could have adverse effects of pregnancy as high urate levels

have been associated with gestational hypertension and pre-eclampsia in humans (Martell Claros, 2017).

Maternal arginine and citrulline levels were found to be reduced following infection. This could have adverse effects on pregnancy as arginine is an essential amino acid in pregnancy and is required not only for foetal growth and placental vascular development. Reduced intake of L-arginine due to protein malnutrition and depletion of endogenous L-arginine due to the maternal infection e.g. malaria have been associated with pre-eclampsia and poor pregnancy outcomes (Weckman et al., 2019). Conversely arginine and citrulline supplementation has been shown to be beneficial (Weckman et al., 2019).

Indoxylsulfate levels were seen to be decreased in both foetus and serum. In the previous chapter, this was also observed and although indole which is eventually converted to indoxylsulfate was raised in this chapter, this difference was not significant. Two possibilities could account for the observed difference in indoxylsulfate. Firstly, it could be hypothesised previously that this change in metabolomics profile arises from a change in the microbiome, converting tryptophan to indole. Secondly, *T. gondii* infection could alter metabolism of indole in the liver, rather than the microbiome and consequently affect the levels of indoxyl and indoxylsulfate. This needs to be further evaluated exclusively in the future as this is only a hypothetical reason.

Guanidinobutanoate levels were found to be decreased in both maternal serum and foetal extracts from infected mice. As this metabolite is dependent of the host microbiome, it suggests *T. gondii* induced changes to the microbiome. The implications of this change for the outcome of pregnancy is not known.

Overall the results from the current chapter demonstrate that *T. gondii* induces a number of metabolic changes to maternal serum and foetuses. A number of the observed changes could

have adverse outcomes to pregnancy. The observation that kynurenine levels are increased in the foetus at an early stage of pregnancy is important as this metabolite has been suggested to have implications for the development of psychoneurological disease in later life (Clark et al., 2019).

5- Confirmation of metabolites identification

Abstract

In the previous chapters 3 and 4, the metabolomics profile of the maternal foetal interface, the developing foetus and maternal serum were discussed in detail. A significant number of metabolites and the associated perturbed pathways were identified in relation to *T. gondii* infection. However, the identification of some metabolites had to be considered putative as it was based on accurate mass and retention time, but not compared with standards. Confirming the true identity of any given metabolite/s is paramount to accurately interpret the acquired data set. The primary objective of this study was to confirm the most important/interesting metabolites from the large number of metabolites detected discussed in previous chapters 3 and 4. Any downstream analysis of the results obtained without accurate identification could lead to a false-positive or false-negative interpretation. Metabolites selected for this study were Indoxylsulfate, kynurenine, 4-guanidinobutanoate, 1-methylnicotinamide, indole, carnitine and urate. This study was carried out by evaluating the relative abundance of the molecules against retention time and m/z mass using ToxID software. Results demonstrated that retention times and m/z mass for authentic standards and putative metabolites were all within an accepted 20% variation indicating these metabolites had been accurately identified.

5.1 Introduction

The metabolome is the accumulation of all the metabolites in any given biological system. It reflects a cell's or organism's physiological state under any physiological or pathological environment. Most of the metabolites are not encoded in any of the organism's genome, but it is the metabolic state of the enzymes expressed and the availability of substrates that determines these. That is the reason the early identification of the metabolites detected is of utmost importance. Otherwise, the results may lead us to false-positive or false-negative interpretation. There are a large number of metabolites produced by the organisms that are investigation in any study. However, a large volume of xenometabolites, food-derivatives, drugs and other metabolites might also be present in the same system (Witting and Böcker, 2020).

Keeping in view the co-existing situations of the metabolites, identification represents the most encountered bottleneck to analyse the metabolomics data based on the LC-MS. Interestingly, a study to accurately identify the metabolites reported that only 1.8% of the total spectra can be annotated in an untargeted metabolomics approach. This is the concept of dark matter of metabolomics; according to this concept, a large part of the metabolomics data exists as unidentified metabolic molecules (da Silva et al., 2015). However, there is an ongoing discussion on how many detected features in LC-MS truly represent the metabolites and how many features are being observed for a single metabolite (Mahieu and Patti, 2017). Features may represent adducts or fragmentation derivatives of metabolites generated during sample preparation or analysis by LC-MS. Adducts are positive molecular ions (original molecule + a proton), while fragments are –ve molecular ions (molecule – proton). Fragments are generated by two processes, the first one is the mass spec process of ionisation in which fragments are formed while the second process is tandem MS (MS^2) that uses a collision CID technique, in

which metabolites are accelerated & forced to collide with a neutral molecule or gas e.g. argon (Ar) and different metabolites are generated through this collision process.

It is very common to detect thousands of features from different biological samples in any untargeted metabolomics data set. However, interpretation of data is complicated owing to the presence of unidentified metabolites that are measured in any given experimental setting. In a study conducted on metabolites detected in *E.coli* with a global metabolomics profiling, there were thousands of features/peaks arising from the analyte, but after curation of unwanted features and cleaning of the data from the same analyte, the number of features were reduced to almost 90% (Witting and Böcker, 2020). On the basis of the results, an alternative approach on thoroughly annotated datasets used as a reference to untargeted metabolomics was proposed by the authors, that is creDBIe database (http:// creDBIe.wustl.edu), containing the accurate *m/z* mass ratio, retention time and fragmentation data along with the annotation of all the features (Mahieu and Patti, 2017).

In the current study, the IDEOM software was used that uses data from KEGG, HMDB and lipid maps in its database of biological molecules likely to be present. The database includes accurate *m/z* mass and calculated RT for the column and running conditions used for LC-MS. It also screens for adducts and fragments to remove non-biological features. In spite of all these limitations and bottlenecks presented in metabolomics data, a downstream biochemical analysis needs a high degree of accuracy to identify the actual metabolites to avoid any false positive or negative biological interpretation of the results.

Putative identification using accurate mass only is not sufficient because of the reasons described above. That is why a comparison of the retention time of authentic standards with that of the putative metabolites run under the same conditions was carried out in the current study. Alternatively, a fragmentation analysis by tandem MS or MS^2 can be used. This is

important and more desirable when the metabolite is not commercially available. It is worth mentioning here that in the current study, MS^2 analysis was included in the data set described in chapter 4, as this MS^2 fragmentation information is available in the data set obtained from the Glasgow Polyomics, however, the fragmentation information was not available in the data set processed and analysed at the University of Strathclyde.

Metabolite identification can be made based on different levels, e.g., looking for the accurate mass (m/z) and isotope pattern (both can be used to derive molecular formula) and analysis of tandem MS data (Sumner et al., 2007). Tandem MS gives information about structure and retention time also relates to structure because it depends on physical and chemical properties of the molecule (which is determined by structure). However, if we look only at accurate mass of metabolites, it does not give us precise information about the structure and identity of the metabolite under question. For example, if we search a mass of 378.1678 Da and ten ppm mass accuracy in ChemSpider, it will give us thousands of results linked to this mass (>9500). Similarly, if we search for an exact chemical formula of $C_{20}H_{26}O_7$, it will result in around 300 different chemical structures and molecules (Williams, 2008). So by having all the above information from literature and past experiences of other authors, we can confidently say that the only accurate mass cannot genuinely provide information about its precise identification rather than its molecular formula only. This information will try to locate a small molecule based on its mass and the results will bring up many putatively correct labels and many false identities (Witting and Böcker, 2020). However, a comparison of the retention time of the given sample with that of the authentic standards is more accurate and convincing method for the true identification of the metabolites in untargeted spectrum of the metabolomics. Tandem mass spectrometry is applied for a partial structural identity. Until now, most of the identifications were based on the reference standards included in some spectral libraries e.g., mzCloud, Human metabolome database (HMDB) (Wishart et al., 2018). These reference libraries are still

in use to identify different compounds. However, the more accurate identifications for MS data is the comparison of tandem MS and RT information for a biological sample and the chemical standard under the same type of conditions. There are many compounds that do not have their standards available or the number of compounds present in these libraries are considerably less compared to the total metabolites detected in many MS data analysis.

In the recent past, different MS^2 libraries regarding genome-scale metabolic models were calculated, and there is less than 40% of metabolites in the models that have ≥ 1 reference spectra from authentic compound standards. Another strategy to accurately identify metabolites was developed and implemented in the recent past called an in silico approach, allowing searching in Pub-Chem, ChemSpider, MAGMa, CFM-ID, Mass Frontier and CSI:FingerID, which are all molecular structure databases (Dührkop et al., 2015, Ridder et al., 2012, Ruttkies et al., 2016, Wolf et al., 2010). These databases are much larger than the spectral libraries; therefore, the coverage of the metabolites according to their molecular structures is much broader. PubChem can aid as a substitution of a wide-ranging structural database containing more than 100 million entries (Witting and Böcker, 2020). Regarding CFM-ID and CSI-FingerID, these are of interest to help identify different compounds; however, they are dependent on the input of the training set of data. To determine the structural identity of any new metabolite with training data sets presents a considerable degree of complexity.

There are many stages of metabolite identifications defined above, leading to the second-highest level of metabolomics standard initiative (MSI). It can still lead to many false-positive labellings of the compounds under investigation. To expand the quality of identification of any given compound, a combination of different parameters, e.g., mass, fragmentation pattern, and retention time of a compound standard should be measured and compared to the metabolites/compounds under investigation (Witting and Böcker, 2020).

5.2 Aims and objectives

The aim of the study described here was to confirm the identification of different metabolites detected in the previous chapters. As the identity of metabolites in MS data is putative, it is of utmost importance to ensure the confirmed identification of any compound of interest so that any false positive/ negative biological interpretation can be avoided.

5.3 RT dimensions for the identification of metabolites

Retention time is a valuable tool to maximize the assessment of accurate identification of a metabolite. As different metabolomics experimentation does not apply the standardized protocols, the mass of a metabolite is a consistent property and it is the same across different methodologies and experimentation systems. (Witting and Böcker, 2020). Different chemical solvents used and chemistries of different columns can produce different RTs of the same metabolites, even with the same settings different instruments may read different RTs of the same metabolites (Witting and Böcker, 2020). These variations in RTs can also be observed in the current data, which is in line with the available literature cited above.

A software Thermo ToxID was used, a sample file (Raw file containing the data) and a configuration file are used as input files to generate an output file. This output file is a PDF file containing all the information regarding the chemical name, formula, detected *m/z* mass, ppm, expected and actual retention time along with the peak intensity value. A sample of the ToxID file used in the current analysis is shown as follows (Figure 5.1).

Your Company
Summary Report

Raw File Name: C:\Users\yqb17218\Desktop\STDRD-POLYOMIC-DESKTOP - Copy\GW_SU_0001.raw
Config File Name: C:\Users\yqb17218\Desktop\STDRD-POLYOMIC-DESKTOP - C...\STRATH-STD1-NEG.csv
Sample Name: Laboratory:
Acquistion Start Time: June 23,2021 01:55:42

Screening Conditions: Based on Exactive screening method. Accurate mass window (ppm): 40, Addacts: H+, NH4+, Na+, RT window (min): 30.00. The Delta, Actual RT and intensity are reported based on the adduct labeled with "*".

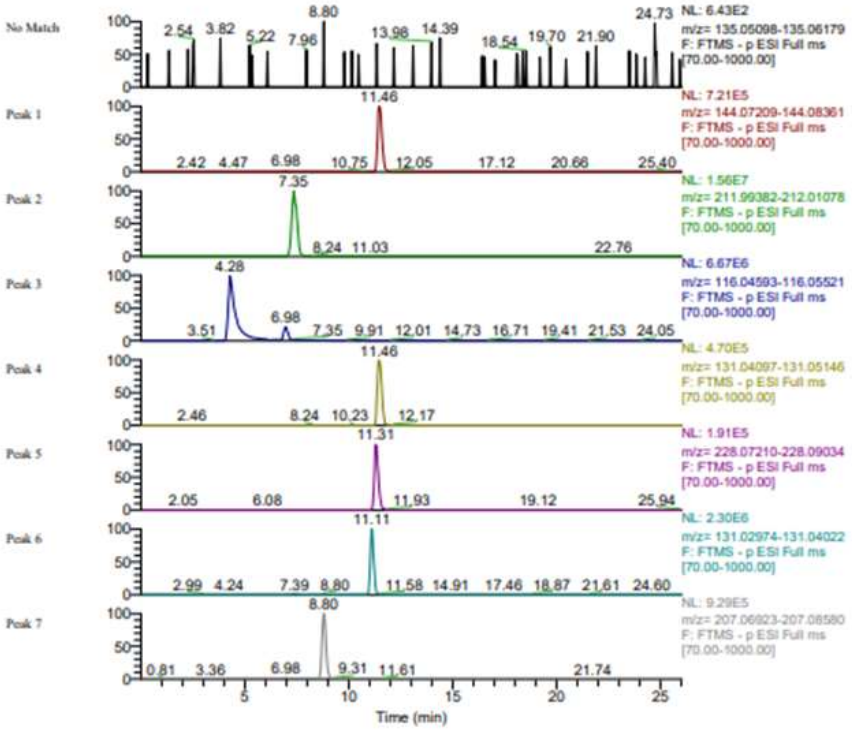

#	Comp. Index	Compound Name	Formula	Detected m/z	Delta (ppm)	Expected RT	Actual RT	Intensity	Adducts			Fragments		
									H+	NH4+	Na+	1	2	3
N	1	1-methylnicotinamide	C7H8N2O	-	-	10.00	-	-	N	-	-	-	-	-
1	2	4-guanidinobutanoate	C5H11N3O2	144.07780	-0.3	10.00	11.46	720727	Y*	-	-	-	-	-
2	3	Indoxylsulphate	C8H7NO4S	212.00256	1.2	10.00	7.35	15646948	Y*	-	-	-	-	-
3	4	Indole	C8H7N	116.05052	-0.4	10.00	4.28	6662767	Y*	-	-	-	-	-
4	5	Asparagine	C4H8N2O3	131.04620	-0.1	10.00	11.46	469515	Y*	-	-	-	-	-
5	6	Ergothionine	C9H15N3O2S	228.08156	1.5	10.00	11.31	191060	Y*	-	-	-	-	-
6	7	Glutarate	C5H8O4	131.03496	-0.2	10.00	11.11	2294314	Y*	-	-	-	-	-
7	8	Kynurenine	C10H12N2O3	207.07773	1.0	10.00	8.80	928454	Y*	-	-	-	-	-

Figure 5. 1 A PDF file used for the chemical information generated through ToxID software.

Thermo ToxID software was used to extract chromatograms that show a plot of relative abundance against the retention time of the molecules meant to be analysed.

A software Thermo Xcalibur (qual browser) was used to generate mass spectrum and total ion current chromatograms from the sample RAW file. The data is searched for peaks corresponding to the *m/z* mass of the metabolites of interest. Consequently, there are two chromatogram plots generated that correspond to each other, one represents the relative abundance against retention time, and the other one shows a plot of relative abundance against *m/z* mass. A model chromatogram panel can be seen in the following figure 5.2.

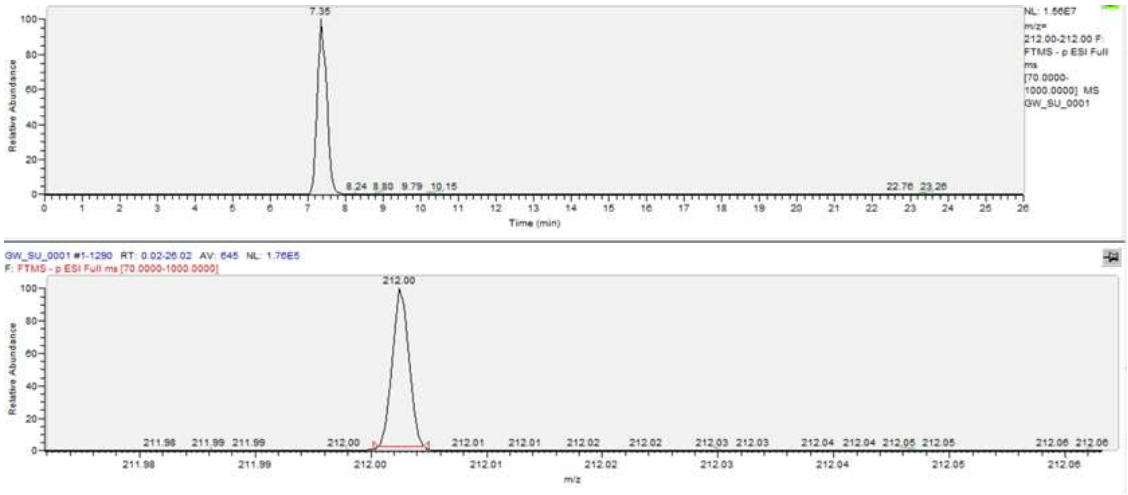

Figure 5. 2 shows two chromatogram plots generated from the Thermo Xcalibur qual browser. (A) represents the relative abundance against retention time, and the (B) shows a plot of relative abundance against m/z mass.

5.4 Results

There are different putative metabolites that were consistently found to be altered significantly during *T. gondii* infection and have been already discussed in detail in the previous chapters (Chapters 3 and 4). These metabolites include citrulline, proline, ornithine, arginino succinate, spermine, spermidine, kynurenine, tryptophan, urate, indole, indoxyl, indoxylsulfate, 4-guanidinobutanoate, trimethylamine N-oxide, creatinine. Out of these, some of the metabolites were available commercially and it was possible to confirm the putative identification by matching their retention times with those obtained for authentic standards of the same molecules under the same conditions. The standard samples were made for these available metabolites and run with the original samples.

To confirm identifications of the metabolites detected in the untargeted metabolomics spectrum in the previous chapter, a pool from the replicates of original serum samples was made by mixing an equal aliquot from each serum sample. Samples from the developing foetus and maternal serum were run at the same time and with the identical conditions in the data shown in chapter 4. If the metabolite in the serum sample is confirmed it follows that the corresponding metabolite in the foetus is also confirmed because they have the same accurate mass and retention time. These pooled samples were run against the mix of authentic standards to compare the retention time of the various metabolites of interest in this study.

The following results below indicate some of the important metabolites and their confirmed identifications, these metabolites were selected because these were found to be significantly altered in different tissues infected with *T. gondii*, discussed in detail in chapter 3 and 4.

5.4.1 Indoxylsulfate

This is an important microbial metabolite altered with a statistical significant decrease throughout the different batches of extracts, different LC-MS machines and time period of analysis. The detailed analysis for the confirmation is shown in the following table 5.1 and figure 5.3.

Table 5. 1 represents the chemical formula, m/z mass, retention time along with delta ppm for indoxylsulfate of each of the samples examined.

Sample	Formulae	m/z mass	RT (*min*)	Delta ppm	Mode
Standard	$C_8H_6O_4NS$	212.0025	7.35	1.12	Negative
Pooled serum sample	$C_8H_6O_4NS$	212.0027	7.68	1.36	Negative

The table shows the detailed description of the metabolites extracted from the Thermo Xcalibur qual browser. The chemical formula of indoxylsulfate is $C_8H_7O_4NS$, however, it is detected in negative ion mode, so there is a loss of proton reflected in the chemical formula shown in the table above. The *m/z* mass for the standard sample and the pooled samples were 212.0025 and 212.0027, respectively with a delta ppm of 1.12 and 1.36 as shown in the table above. The retention times are shown in the following chromatograms taken from the Thermo Xcalibur qual browser.

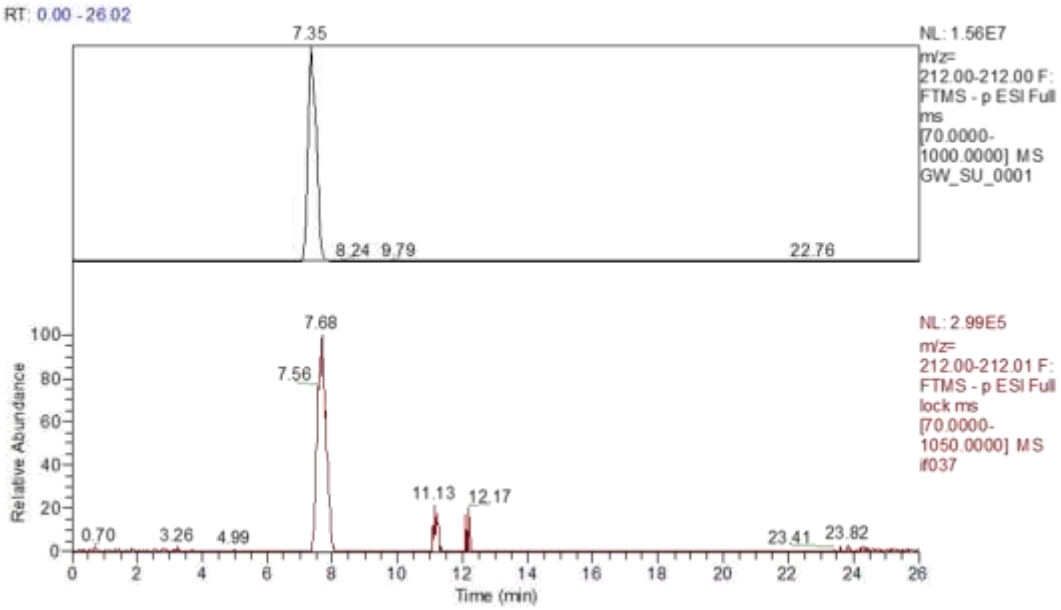

Figure 5. 3 Retention time information of Indoxylsulfate. There are two panels showing plots of relative abundance against time. The extracted ion chromatograms of m/z 212 correspond to retention times of 7.35 for the standard used (chromatograms shown in the top panel) while a retention time of 7.68 is shown in the bottom panel for the pooled serum sample. The molecule in the pooled serum sample (bottom panel) has the same retention time as the indoxylsulfate. There are some other small peaks shown in the bottom panel that represents some other molecules/ features in the spectrum and their corresponding m/z masses do not match with that of the indoxylsulfate.

5.4.2 Kynurenine

This is an important metabolite altered with a statistically significant decrease in the decidua and placenta, while it was increased significantly in the developing foetus and the maternal serum infected with *T. gondii*. Owing to the findings of the current study regarding the kynurenine as discussed in the previous chapter 4, the detailed analysis for its confirmed identification was carried out that is shown as in the following table 5.2 detailing its chemical properties and figure 5.2 showing chromatograms for its retention time against the authentic standards used.

Table 5. 2 represents the chemical formula, m/z mass, retention time along with delta ppm for kynurenine of each of the samples examined.

Sample	Formulae	m/z mass	RT (*min*)	Delta ppm	Mode
Standard	$C_{10}H_{13}O_3N_2$	209.0918	8.82	-0.903	Positive
Pooled serum sample	$C_{10}H_{13}O_3N_2$	209.0921	8.75	0.054	Positive

Table 5.2 shows the detailed description of kynurenine extracted from Thermo Xcalibur qual browser. The chemical formula of kynurenine is $C_{10}H_{12}O_3N_2$. It is detected in positive mode, so there is a gain of proton reflected in the chemical formula shown in the table above. The *m/z mass* for the standard sample and the pooled samples was 209.09.0918 and 209.0921, respectively with a delta ppm of – 0.903 and 0.056 as shown in the table above. The retention times are shown in the following chromatograms taken from the Thermo Xcalibur qual browser (Figure 5.4).

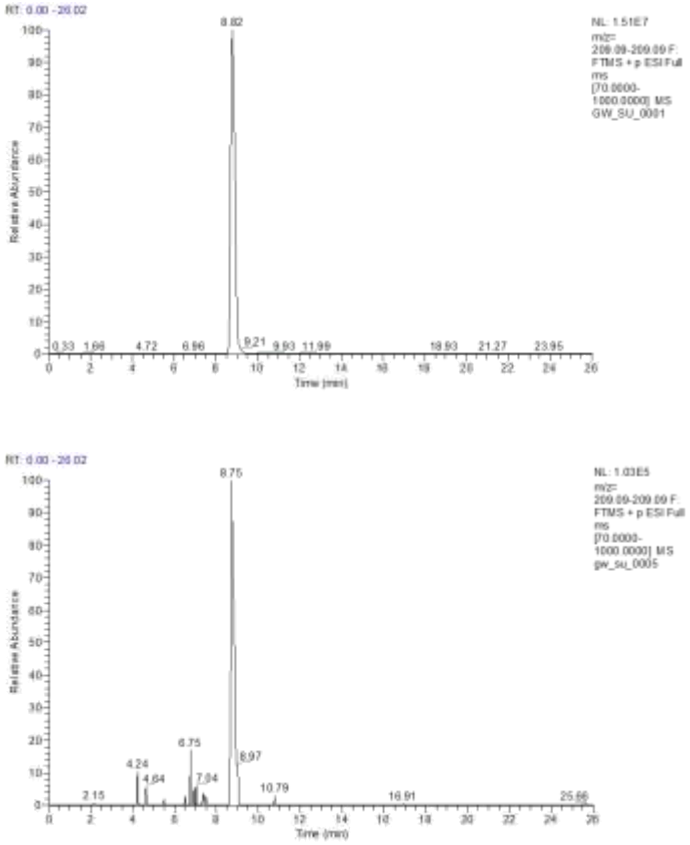

Figure 5. 4 Retention time information of kynurenine. Extracted ion chromatogram of m/z 209.09 shows plots of relative abundance against time, corresponding to a retention time of 8.82 (authentic standard in the top panel) and a retention time of 8.75 for the pooled serum sample shown in the bottom panel.

The chromatogram representing only authentic standard shows a single and clear peak for the standard used. However, in the pooled sample, there are some other small peaks representing some other molecules detected within the selected window for the retention time shown in minutes.

5.4.3 4-Guanidinobutanoate (4-GB)

This is another important microbial metabolite altered with a statistical significance, was found decreased in infected tissues extracts throughout the different batches of extracts, different LC-MS machines and time period of analysis. The analysis detailing its chemical properties and plots of relative abundance against retention time (minutes) showing chromatograms for the confirmation is shown in the following table 5.3 and figure 5.5.

Table 5. 3 represents the chemical formula, m/z mass, retention time along with delta ppm for 4-guanidinobutanoate of each of the samples examined.

Sample	Formulae	m/z mass	RT (*min*)	Delta ppm	Mode
Standard	$C_5H_{12}O_2N_3$	146.0923	11.52	-0.432	Positive
Pooled serum sample	$C_5H_{12}O_2N_3$	146.0924	11.45	0.252	Positive

Table above shows the detailed description of 4-guanidinobutanoate extracted from Thermo Xcalibur qual browser. The chemical formula of 4-guanidinobutanoate is $C_{10}H_{11}O_3N_2$. It is detected in the positive mode, so there is a gain of proton reflected in the chemical formula. The *m/z* mass for the standard sample and the pooled samples were 146.0923 and 146.0924, respectively with a delta ppm of – 0.432 and 0.252 as shown in the table above. The retention times are shown in the following chromatograms taken from the Thermo Xcalibur qual browser (Figure 5.5).

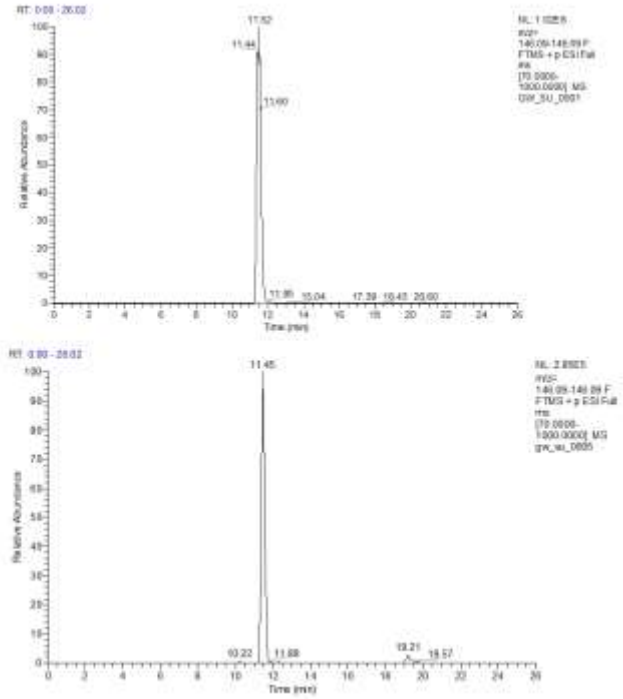

Figure 5. 5 Retention time information of 4-guanidinobutanoate. Extracted ion chromatogram of m/z146.092 shows plots of relative abundance against time, and these plots/chromatograms correspond to a retention time of 11.52 (authentic standard in the top panel) and a retention time of 11.45 for the pooled serum sample shown in the bottom panel.

5.4.4. 1-Methylnicotinamide

This is an important metabolite altered with a statistically significant decrease in the decidua, placenta and the developing foetus infected with *T. gondii*. Similarly, it showed the same trend in the maternal serum infected with *T. gondii*. However, in a previous study in the same laboratory, 1-methylnicotinamide was found to be altered with a significant increase in the brain of the mice born to the mothers infected with *T. gondii* (Abdelsalam, 2019). Owing to these findings of the current study, a detailed analysis for the confirmed identification was carried out that is shown in the following table 5.4 detailing its chemical properties and figure 5.4 showing chromatograms for its retention time against the authentic standard used.

Table 5. 4 represents the chemical formula, m/z mass, retention time along with delta ppm for 1-methylnicotinamide of each of the samples examined.

Sample	Formulae	m/z mass	RT (*min*)	Delta ppm	Mode
Standard	$C_7H_8ON_2$	137.0709	9.49	0.15	Positive
Pooled serum sample	$C_7H_8ON_2$	137.0709	9.48	0.442	Positive

The peak for 1-methylnicotinamide was found in the positive ion mode with a delta ppm of –0.15 and 0.442 for the authentic standard and the pooled serum sample, respectively. The *m/z* mass for both of the standard and the pooled serum samples used was measured 137.0709 (Figure 5.6).

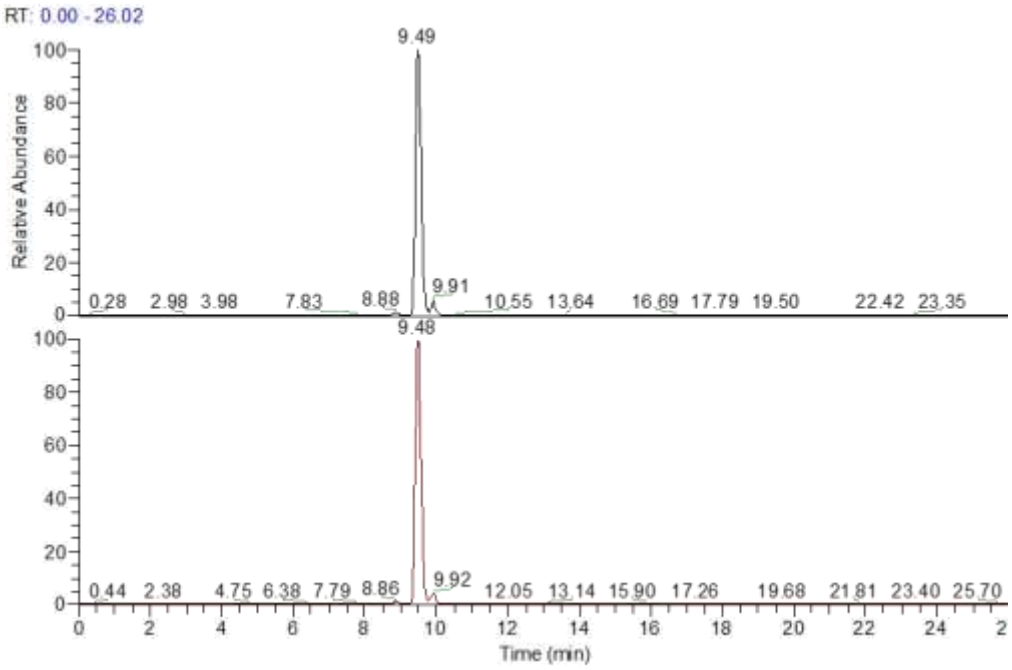

Figure 5. 6 Retention time information of 1-methylnicotinamide. Extracted ion chromatogram of m/z137.07 shows plots of relative abundance against time and these plots/chromatograms correspond to a retention time of 9.49 (authentic standard in the top panel) and a retention time of 9.48 for the pooled serum sample shown in the chromatogram in the bottom panel.

5.4.5 Indole

This is an important microbial metabolite produced with the action of the tryptophanase expressing gastrointestinal bacteria e.g., *Escherichia coli.* This metabolite was found altered with a statistically significant decrease in the decidua and placenta. In contrast, it was found to be significantly increased in the developing foetus infected with *T. gondii* in the first experiment (Chapter 3). It showed the same trend in the second experiment (Chapter 4), but the difference was not statistically significant. The reason for this derivative to include in the confirmation of identification analysis was due to its ultimate conversion into indoxylsulfate. The detailed analysis for the confirmation is shown in the following table 5.5 and figure 5.7.

Table 5. 5 represents the chemical formula, m/z mass and retention time for indole of each of the samples examined.

Sample	Formulae	m/z mass	RT (*min*)	Delta ppm	Mode
Standard	C_8H_8N	118.0651	8.82	-0.049	Positive
Pooled serum sample	C_8H_8N	118.0651	9.5	0.459	Positive

The table shows the detailed description of the metabolite extracted from the thermos Xcalibur qual browser. The chemical formula for indole is C_8H_7N. However, it is detected in positive ion mode, so there is an addition of proton reflected in the chemical formula shown in the table above. The *m/z* mass of both the standard sample and the pooled samples was 118.0651 with a delta ppm of – 0.049 and 0.459, respectively. The retention times are shown in the following chromatograms taken from the Thermo Xcalibur qual browser (Figure 5.7).

.

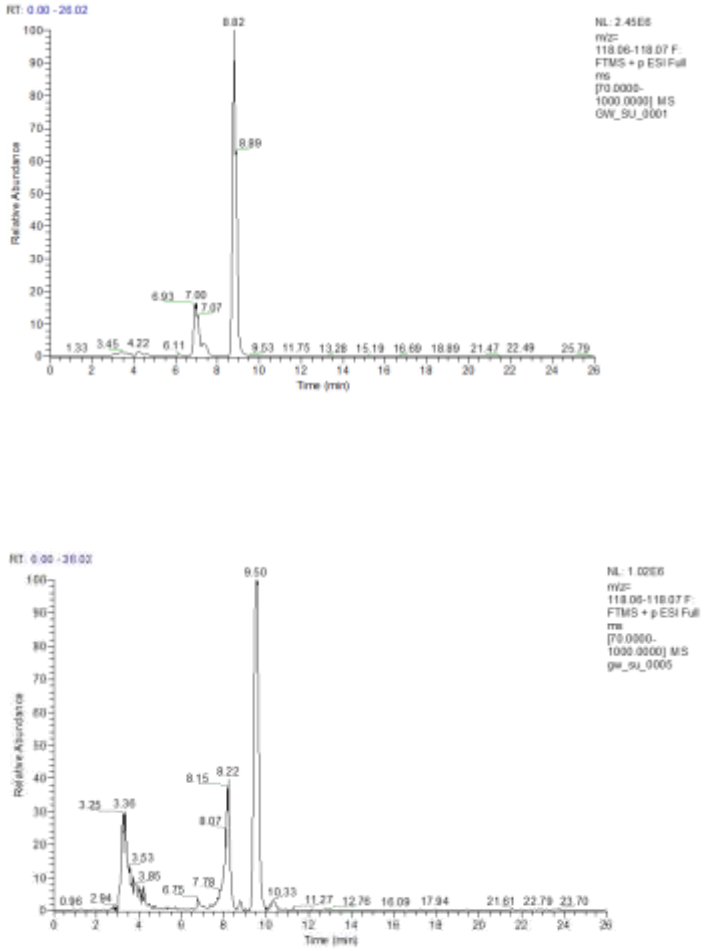

Figure 5. 7 Retention time information of indole. There are two panels showing plots of relative abundance against time. The extracted ion chromatograms of m/z 118.065 correspond to retention times of 8.82 for the standard used (chromatograms shown in the top panel), while a retention time of 9.50 is shown in the bottom panel for the pooled serum sample. The molecule present in the pooled serum sample (bottom panel) has the same retention time as the indole. There are some other small peaks shown in the bottom panel that represent some other molecules/ features in the spectrum and their corresponding m/z mass do not match with that of the indole.

5.4.6 Carnitine

Carnitine is an endogenous molecule involved in fatty acid metabolism. It is synthesized by using l-lysine and l-methionine as substrates. The main function of carnitine is the transportation of the chain of fatty acids into the mitochondria. This provision of fatty acids is utilized by the cell to obtain energy by the breakdown of fat. Carnitine identification was also subjected to confirmation as under.

Table 5. 6 represents the chemical formula, m/z mass and retention time for carnitine of each of the samples examined.

Sample	Formulae	m/z mass	RT (*min*)	Delta ppm	Mode
Standard	$C_7H_{16}O_3N$	162.1124	10	-0.123	Positive
Pooled serum sample	$C_7H_{16}O_3N$	162.1123	9.95	-0.616	Positive

Table shows the detailed description of carnitine extracted from Thermo Xcalibur qual browser. The chemical formula of carnitine is $C_{10}H_{15}O_3N$. It is detected in the positive mode, so there is a gain of proton reflected in the chemical formula shown in the table above. The *m/z mass* for the standard sample and the pooled samples was 162.1124 and 162.1123, respectively with a delta ppm of -0.123 and -0.616 as shown in the table above. The retention times is shown in the following chromatograms taken from the thermo Xcalibur qual browser (Figure 5.8).

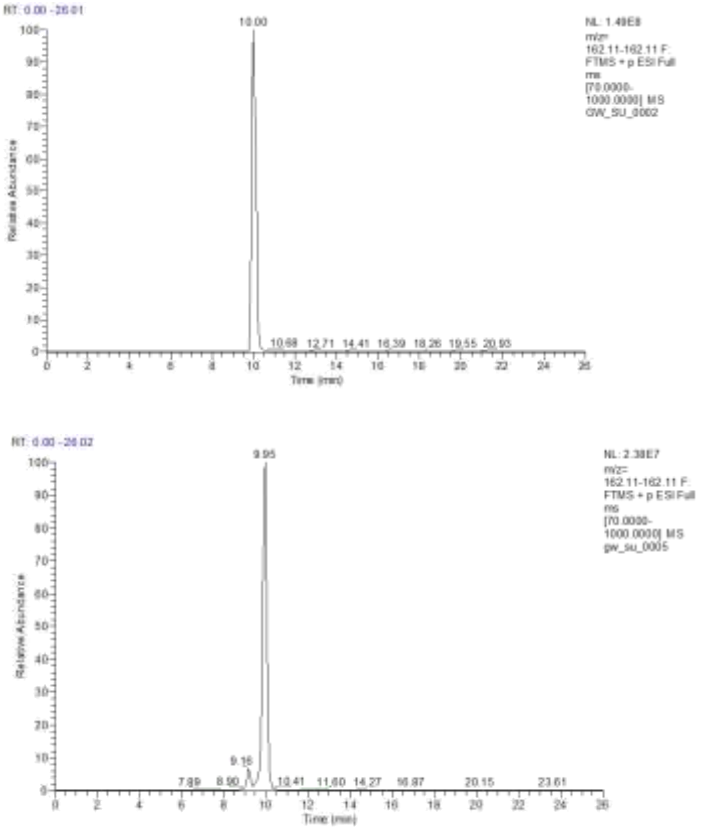

Figure 5. 8 Retention time information of carnitine. Two panels showing plots of relative abundance against time. The extracted ion chromatograms of m/z 160.09 correspond to retention times of 10 for the standard used (chromatograms shown in the top panel) while a retention time of 9.95 is shown in the bottom panel for the pooled serum sample. The molecule in the pooled serum sample (bottom panel) has the same retention time as the carnitine.

5.4.7 Urate

Purine metabolism was found to be significantly disrupted in the maternal serum with evidence of degradation of purines and the accumulation of urate. However, these intermediates were not seen to be significantly depleted in the foetal samples, and no evidence of urate accumulation was seen. These changes to purine metabolism and the accumulation of urate could have adverse effects on pregnancy as high urate levels have been associated with gestational hypertension and pre-eclampsia in humans (Martell Claros, 2017). Table 5.7 shows some of the features/ chemical properties to confirm its identification.

Table 5. 7 represents the chemical formula, m/z mass, retention time along with delta ppm for urate of each of the samples examined.

Sample	Formulae	m/z mass	RT (*min*)	Delta ppm	Mode
Standard	$C_5H_3O_3N_4$	167.0212	10.5	0.819	Negative
Pooled serum sample	$C_5H_3O_3N_4$	167.0212	10.2	1.058	Negative

The table shows the detailed description of the urate extracted from Thermo Xcalibur qual browser. The chemical formula of urate is $C_5H_4O_3N_4$ and is detected in the negative mode, so there is a loss of proton reflected in the chemical formula shown in the table above. The *m/z* mass of both the standard sample and the pooled samples was 167.0212 with a delta ppm of 0.819 and 1.058, respectively. The retention times is shown in the following chromatograms taken from the Thermo Xcalibur qual browser (Figure 5.9).

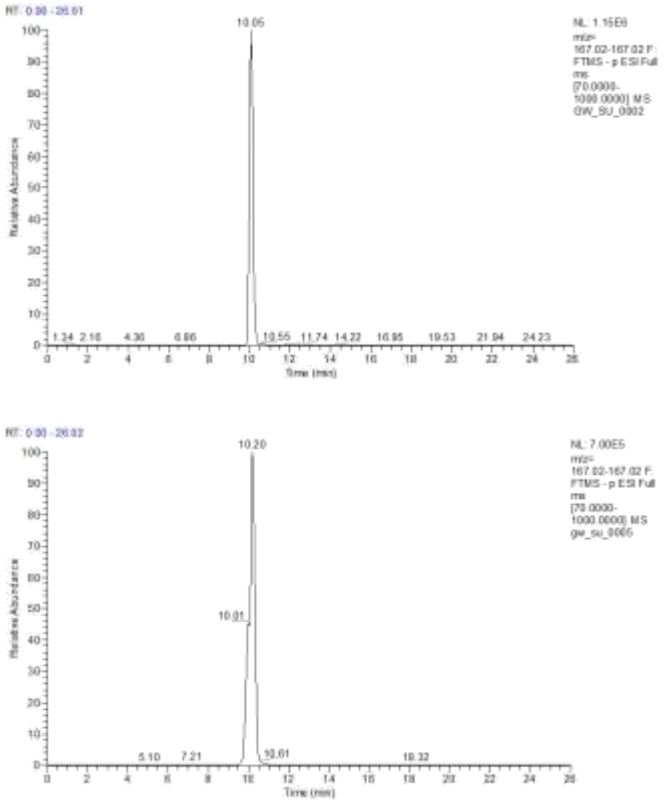

Figure 5. 9 Retention time information of urate. The extracted ion chromatograms of m/z 167.02 correspond to retention times of 10.05 for the standard used (chromatograms shown in the top panel), while a retention time of 10.20 is shown in the bottom panel for the pooled serum sample. The molecule in the pooled serum sample (bottom panel) has the same retention time as the urate.

It is worth mentioning that other than the RT and m/z mass comparison shown here, a few of the metabolites selected also got additional information regarding their fragmentation data derived from Glasgow polyomics. These metabolites include kynurenine and carnitine. This information tells us about the different fragments of metabolites formed along with their mass and formulae. Identification of a molecule can be confirmed by looking into the formulas of different fragments formed. Here, kynurenine fragmentation analysis from the software PiMP is an additional level of support to the true identification carried out based on the RT comparison in this study.

5.5 Conclusion

As discussed in section 5.1, there were many techniques used in the past to identify the true metabolites. However, those identification methods presented some bottlenecks, as described in the introduction section 5.1 of the current chapter. RTs prediction is the only technique in the current era getting attention and authenticity to identify different metabolites (Witting and Böcker, 2020). Although these RTs can be different in different experimental conditions, time scales and instruments used, it is still considered to be the most reliable technique for valid identifications of the metabolites. However, it is unlikely for any laboratory to buy all of the authentic standards for the confirmation of all the putatively identified metabolites. In reality as described here a reasonable compromise is to retrospectively use authentic standards to confirm those metabolites of greatest importance and where important conclusions can be made. Based on different authentic standards compared with the annotated metabolites detected from the extracts of the developing foetus and the maternal serum, these metabolites are now confirmed for their accurate identifications based on the combination of *m/z* mass and RT values.

There are many metabolomic data repositories like Metabolights, Metabolomics workbench and Global Natural Products Social Molecular Networking (GNPS); hence there is more and more training data for RT prediction is available. Therefore, it is strongly believed that RT prediction and incorporating this into metabolite identification will have a bright future (Wang et al., 2016), and another study showed optimism that new techniques will be introduced in the future that will make retention time in combination with MS^2 spectrum, a precious asset in untargeted metabolomics (Witting and Böcker, 2020).

6- Comparison of the metabolomics profile of the developing foetus with the brains of adult mice born to the infected mothers

Abstract

In the previous chapters (Chapter 4), detailed metabolomics profiles of the maternal serum and the developing foetus obtained from the mothers infected with *T. gondii* were discussed. The results obtained showed that maternal infection induces various significant metabolomic changes. Here, the effects of *T. gondii* infection on the metabolome of the brain from the adult mice born to the infected mothers was compared with that of the metabolomics profile of the developing foetus. It is worth mentioning here that the data from the brain was previously obtained in the same laboratory by (Abdelsalam, 2019). The primary objective of this chapter is to compare the expression trends of various important metabolites that were observed in the previous chapters. A potential limitation of this comparison is the previous data set from the brain extracts and the current data set from the developing foetus were processed and analysed in the same manner, however, at different systems, different time points and different soft wares were used for analysis. The data set obtained from the brain of the mice born to the infected mothers was mainly analysed on a software named BioCyc. For comparison, only the peaks detected with the pHILIC column from both data set were selected. The process of peak selection was the same as described in the section 4.3 of chapter 4. The number of metabolites detected in the extracts from the developing foetus were large as compared to the number of metabolites detected in the extracts from brain of mice born to the mothers infected with *T. gondii*. However, there are still 41 metabolites which are found common in both of these tissues compared. Other metabolites, including citrulline, proline, ornithine, tryptophan, 1-methylnictiinamide and 4-guanidinobutanoate were found to be significantly reduced in foetuses from infected mothers, while in the extracts from brain, citrulline and ornithine were reduced, but not with a statistical significance. Similarly, 1-methyl nicotinamide was statistically increased in the brain extracts from mice infected during adulthood. Urate was found to increase in the brain; however, this is not detected in the foetus. Degradation of

tryptophan and a resultant increase in kynurenine has been linked previously with the *T. gondii* infection. Kynurenine was found to be significantly raised in the brain and foetuses from infected mothers compared with the control group. It is worth noting that increased level of kynurenine has been suggested to exert serious consequences of developing schizophrenia. Guanidinobutanoate, but not indoxylsulfate was the only microbial metabolite detected in the brain of mice born to infected mothers. Different methodologies used in the 2 studies means that caution needs to be exercised when interpreting results. However, it can be concluded that changes to tryptophan metabolism as evident through kynurenine levels occur early in foetal life. As these changes were not seen in adult mice born to infected mothers, they are a likely consequence of the maternal immune response as seen in maternal serum. However, the increased levels of kynurenine seen in congenitally infected adult mice demonstrate that infection in utero has long term consequences for brain chemistry. The relative contributions that raised kynurenine levels have for the development of psychoneurological diseases in both of these circumstances, in the context of *T. gondii* infection merits further studies.

6.1 Introduction

The effects of *T. gondii* infection on the maternal-foetal interface and the developing foetus have been discussed in detail in the previous chapters. Various metabolites have been identified as being altered during *T. gondii* infection. These metabolites have been shown to play roles in pathways such as tryptophan degradation pathway, purine degradation pathway, arginine metabolism pathway as well as others. Changes to these metabolites have varied so far depending on whether it is the maternal-foetal interface, the developing foetus or serum. Now we have the information regarding those metabolites that change significantly along with disrupted metabolic pathways. As it is now known, if the primary infection with *T. gondii* occurs for the first time during late pregnancy, it may result in the severe consequences of vertical transmission to the foetus, leading to congenital toxoplasmosis (Roberts and Alexander, 1992). There is a considerable volume of literature available describing how *T. gondii* contributes to neural and ocular toxoplasmosis in both adult and congenital acquired disease. In conjunction with this, a previous study in the same laboratory by (Abdelsalam, 2019) detailed the metabolomics profiling of the brain extracted from the adult mice born to the infected mothers as well as of the brain from mice infected during adulthood. So now we have the data of the metabolomics profiles of the brain, the developing foetus and the maternal serum.

Here in this chapter, a comparison was made between the data obtained from the developing foetus with the data set previously obtained from the brain extracts taken from adult mice originally born to mothers infected with *T. gondii* during pregnancy. This comparison will give an insight into how the metabolic pathways and various metabolites vary between tissues at these selected times of infection. Monitoring these changes in the metabolomics profile will provide insight into whether these metabolites and their associated pathways can be targeted to help combat *T. gondii* infection.

6.2 Aims and Objectives

The aims of the studies described herein are to understand if metabolic changes that occur in foetuses in utero when their mother is infected with *T. gondii* during pregnancy are perpetuated into adult hood. Therefore, the objective of this chapter is to compare the metabolic changes induced by maternal *T. gondii* infection occurring in the foetuses from chapter 4 are evident in the brain of adult mice (14 weeks of age) with congenital infection.

6.3 Comparative analysis of metabolic profiles of the brain of mice born to mothers infected with *T. gondii* with that of the developing foetus.

The Venn diagram (Figure 6.1) below displays a comparison and overlap of the metabolites amongst the brain from the adult mice born to infected mothers and the developing foetus.

Overall, number of metabolites detected were large in the developing foetus as compared to the extracts from the brain of mice born to the infected mothers. After manual curation, the number of peaks selected from the foetuses to include in the analysis were 359, while 127 peaks were selected from the brain. The figure indicates an overlap of 37 metabolites were found common between the developing foetus and infected brain of the mice born to infected mothers. 322 metabolites were found detected only in the developing foetus while the number of metabolites detected only in the brain from the mice born to the infected mothers were 90 (figure 6.1). The detail of the metabolites found in common between the developing foetus and the brain are shown in table 6.1.

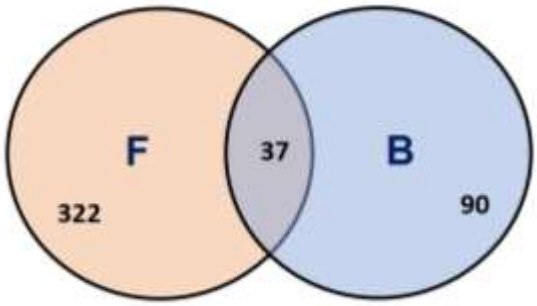

Figure 6. 1 Venn diagram showing the overlap of the metabolites detected between the developing foetus and the brain from mice born to the infected mothers. F= developing foetus, B= brain from the mice born to infecetd mothers.

Table 6. 1 Metabolites present in common in all of the tissues compared. A threshold of 1.5 of Log2 fold-change was set to identify metabolites that showed well-defined changes in abundance and a Log10 P of less than -1.3 was set to define statistical significance (unpaired T-test, 2-tailed). Significantly increased metabolites marked as red (dark red and light red) and significantly decreased metabolites represented by blue colour (dark blue and light blue).

		Foetus		Brain	
Putative metabolite	**Pathway**	**Log2- FC**	**Log10 P**	**Log2- FC**	**Log10 P**
4-Guanidinobutanoate	Arginine and proline metabolism	-0.87	-2.66	0.07	-0.22
5-6-Dihydrouridine	0	-0.60	-2.74	0.25	-1.52
5-Acetamidopentanoate	Lysine degradation	-0.05	-0.15	0.58	-2.40
6-Phospho-D-gluconate	Pentose phosphate pathway	-0.77	-2.10	0.30	-0.70
Allantoin	Purine metabolism	-0.28	-0.94	0.70	-3.70
Ascorbate	Ascorbate, aldarate metabolism	-0.30	-1.54	0.29	-1.70
CDP	Pyrimidine metabolism	-0.17	-0.38	0.48	-1.05
Creatinine	Arginine and proline metabolism	0.02	-0.03	0.08	-0.70
Deoxyadenosine	Purine metabolism	0.09	-0.09	-0.32	-2.00
Deoxyinosine	Purine metabolism	0.03	-0.06	-0.14	-0.52
Dethiobiotin	Biotin metabolism	-0.28	-1.47	-0.43	-1.52
Ergothioneine	Histidine metabolism	-0.73	-1.46	0.56	-3.30
Ethanolamine phosphate	Serine and threonine metabolism	-0.21	-0.61	0.19	-1.70
GDP	Purine metabolism	-0.22	-0.42	0.52	-2.00
Glutarylcarnitine	0	0.02	-0.03	-0.43	-1.30
Glutathione disulfide	Glutamate metabolism	-0.32	-0.42	0.60	-2.00
Guanosine	Purine metabolism	-0.10	-0.12	-0.30	-1.70
Hydroxybutyrylcarnitine	0	0.82	-3.09	0.44	-2.00
Hydroxymethylphosphonate	Aminophosphonate metabolism	-0.74	-0.82	0.34	-1.00
Hypoxanthine	Purine metabolism	-0.40	-2.28	-0.04	-0.22
IMP	Purine metabolism	0.26	-0.46	0.30	-2.00
Inosine	Purine metabolism	-0.11	-0.09	-0.14	-0.70
L-2-Aminoadipate	Lysine biosynthesis	0.02	-0.03	-0.17	-0.70
L-Aspartate	Alanine and aspartate metabolism	-0.38	-1.27	0.01	-0.05
L-Carnitine	Lysine degradation	-0.58	-4.29	0.40	-3.40
L-Citrulline	Arginine and proline metabolism	-1.39	-2.68	0.38	-3.30
L-Cystathionine	Serine and threonine metabolism	-0.70	-2.64	0.31	-1.70
L-Kynurenine	Tryptophan metabolism	0.67	-3.63	1.70	-2.05
L-Phenylalanine	Phenylalanine metabolism	0.28	-0.98	0.36	-1.52
L-Proline	Arginine and proline metabolism	-0.09	-0.41	0.31	-3.00
L-Serine	Serine and threonine metabolism	-0.45	-1.03	-0.12	-0.52
L-Tyrosine	Tyrosine metabolism	-0.12	-0.42	0.42	-2.40
L-Valine	Valine, leucine degradation	-0.13	-1.09	0.28	-1.30
N-(L-Arginino)succinate	Arginine and proline metabolism	-0.45	-1.01	0.29	-1.70
N(pi)-Methyl-L-histidine	Histidine metabolism	0.61	-2.91	0.48	-2.22
N4-Acetylcytidine	0	0.23	-0.78	0.31	-0.52
Trimethylamine N-oxide	Methane metabolism	-1.67	-6.02	0.15	-0.40

Log2 FC Threshold 2	Increase	≥ 1.0
Log2 FC Threshold 1.5	Increase	≥ 0.6
Log2 FC Threshold 1.5	Decrease	≤ -0.6
Log2 FC Threshold 2	Decrease	≤ -1.0

There are many metabolites in common (Table 6.1) but very few of these show a significant change. By looking into the metabolites showing significant alterations, it was noted that the kynurenine is the only single metabolite displaying a significant increase both in the developing foetuses as well as in the infected brain extracts. A similar consistent increase in the levels of kynurenine was also noted in the foetuses from infected mothers in an independent experiment discussed in chapter 3.

6.3.1 Comparison of metabolites associated with the purine degradation pathway

The metabolomics profiles of the brain from adult mice born to the infected mothers showed a disruption in purine metabolism. The metabolites detected associated with the purine metabolism were allantoin and urate. Regarding allantoin, increased levels were detected compared to uninfected control in the brain ($p<0.05$), while there was no change observed in the developing foetus. Regarding urate, the brain derived from the mice born to the mothers infected with *T. gondii* displayed statistically significant increased levels compared to their uninfected controls ($p<0.05$). However, urate was not detected in the developing foetus (Figure 6.2).

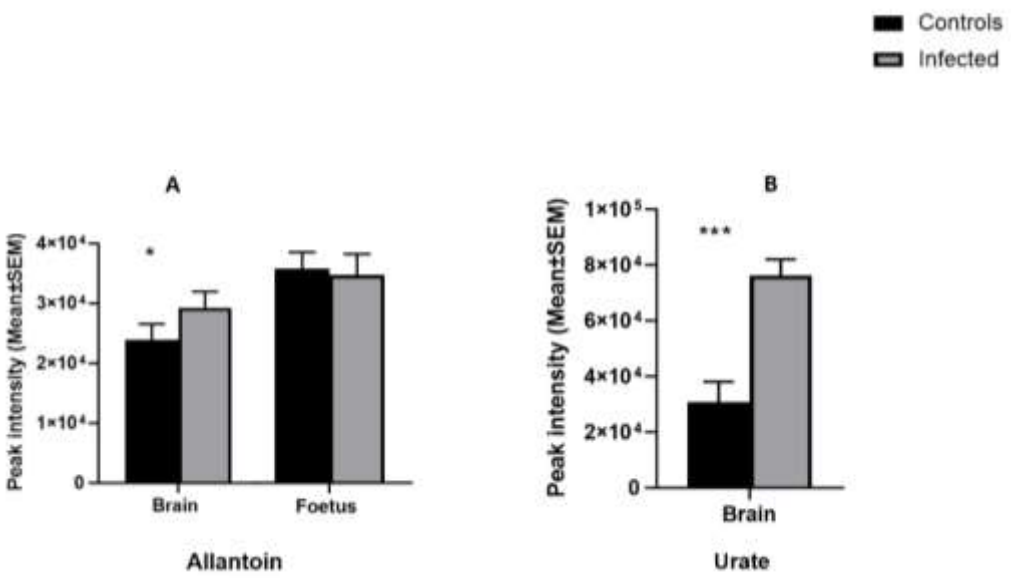

Figure 6. 2 represents metabolites detected in purine degradation pathway. Foetal extracts (n= 24 and 21 for uninfected and infected, respectively). Brain extracts from the adult mice born to infected mothers (n= 19 for infected and n=10 for uninfected controls). Student´s t-test was performed to determine significance ($p < 0.05$) where *$p < 0.05$, **$p < 0.001$ ***$p < 0.0001$ are significant compared to the control uninfected.

A- shows peak intensity value (Mean± SEM) of allantoin in the brain and developing foetus

B- shows peak intensity value (Mean± SEM) of urate detected only in the brain.

6.3.2 Comparison of metabolites associated with the arginine metabolism pathway

A comparison of the arginine metabolic pathway of the brain from mice born to mothers infected with *T. gondii* with the developing foetus revealed significant change in citrulline levels in the infected foetuses compared with the uninfected control foetuses, however, the levels of citrulline in the brain showed no significant change in the infected brain extracts compared with the uninfected control group (Figure 6.3).

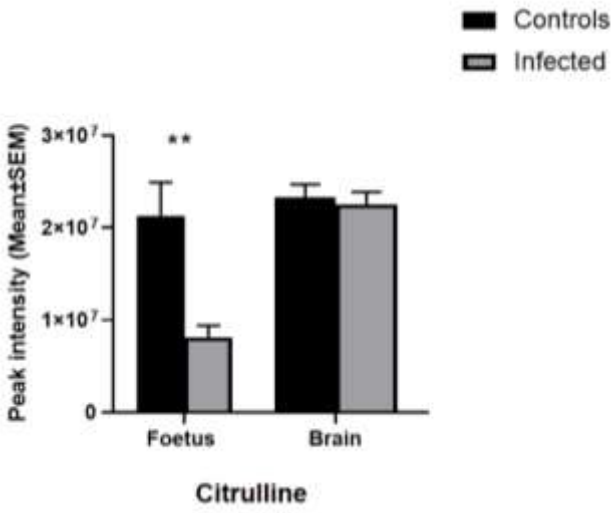

Figure 6. 3 represents peak intensity values (Mean± SEM) of citrulline in the developing foetus and the brain of the mice born to infected mothers. Foetal extracts (n= 24 and 21 for uninfected and infected, respectively). Brain extracts from the adult mice born to infected mothers (n= 19 for infected and n=10 for uninfected controls). Student´s t-test was performed to determine significance ($p < 0.05$) where *$p < 0.05$, **$p < 0.001$ ***$p < 0.0001$ are significant compared to the control uninfected.

6.3.3 Comparison of metabolites associated with the tryptophan degradation pathway

Kynurenine, produced in tryptophan degradation pathway, was identified as being increased in both of the tissues, the brain from the mice born to the infected mothers and the developing foetus infected with *T. gondii* compared with the uninfected control group ($p<0.05$).

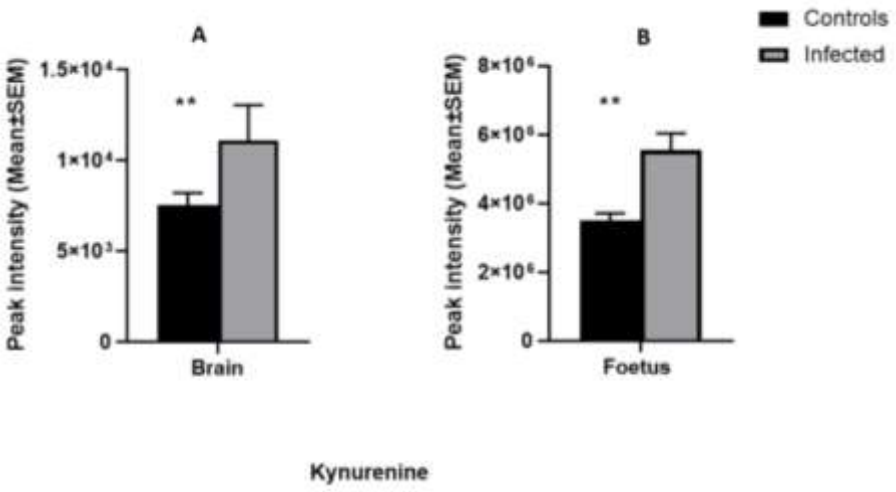

Figure 6. 4 showing kynurenine detected in tryptophan degradation pathway in both of the tissues. Foetal extracts (n= 24 and 21 for uninfected and infected, respectively). Brain extracts from the adult mice born to infected mothers (n= 19 for infected and n=10 for uninfected controls). Student´s t-test was performed to determine significance ($p <0.05$) where *$p <0.05$, **$p <0.001$ ***$p <0.0001$ are significant compared to the control uninfected.

A- shows peak intensity value (Mean± SEM) of kynurenine in the brain.

B- shows peak intensity value (Mean± SEM) of kynurenine in the foetal extracts.

6.3.4 Comparison of metabolites associated with the microbial metabolism

In the previous chapters (Ch.3 & 4) detailing the metabolomics profiles of the developing foetus and the maternal serum, some microbial metabolites were detected and discussed in detail. Those metabolites were searched for in the data from the brain extracts of mice born to the mothers infected with *T. gondii*, revealed that only one of the microbial metabolites, 4-guanidinobutanoate, was detected with a no change (non-significant change) in the expression level when compared infected with the uninfected control group. However, significantly reduced levels of 4-guanidinobutanoate were noted in the extracts from the developing foetus ($p<0.05$).

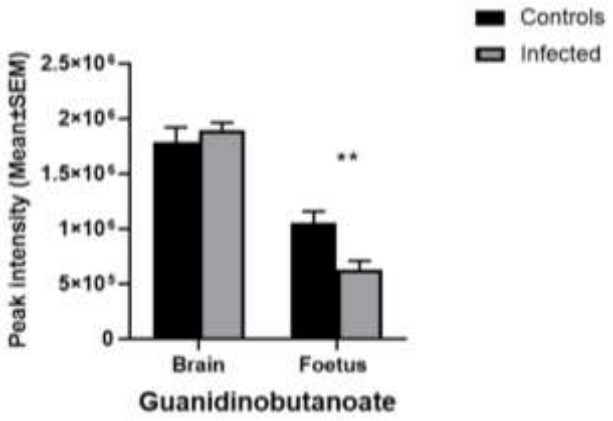

Figure 6. 5 showing microbial metabolite 4-guanidinobutanoate in both of the tissues. Foetal extracts (n= 24 and 21 for uninfected and infected, respectively). Brain extracts from the adult mice born to infected mothers (n= 19 for infected and n=10 for uninfected controls). Student´s t-test was performed to determine significance ($p <0.05$) where *$p <0.05$, **$p <0.001$ ***$p <0.0001$ are significant compared to the control uninfected.

6.4 Conclusion

The comparative analysis of the metabolomics profiles of the data set from the brain with developing foetus showed distinct changes in various metabolites. Some of the important metabolic changes observed in the brains of adult mice with congenital infection such as increased purine metabolism (evident through increased urate and allantoin levels) were not evident in the developing foetus. Conversely, citrulline levels were reduced in foetal tissue derived from infected mothers, but not in the brains of adult mice with congenital infection although the reasons could be many the biological significance of this not clear.

Another observation is that the reduced levels of the microbial product, 4-guanidinobutanoate noted in the foetuses from infected mothers was not evident in the brains of adult mice with congenital *T. gondii* infection. Thus we find no evidence that changes to the maternal microbiome experienced by the mother infected during pregnancy are evident long term at least in the brain tissue.

The most important findings of this study was the levels of kynurenine were consistently found to be significantly increased both in the infected developing foetuses and in the brain extracts from adult mice born to infected mothers. This is a highly important metabolite of tryptophan degradation, as kynurenine has been already implicated for the development of neuro-psychological diseases in life (Clark et al., 2019). Maternal kynurenine administration has been shown to increase the levels of kynurenine levels in the foetal brain as well as plasma, suggesting the ability of this important metabolite to cross the placenta, hence leading to the increased levels of kynurenine in the foetal brain (Goeden et al., 2017).

This is indicative of the fact that the foetuses are directly affected by the maternal infection during gestation. These data along with the results of previous chapters demonstrate changes to brain chemistry taking place during early foetal life and likely subsequently in adulthood.

7- Metagenomic analysis to evaluate the effects of *T. gondii* infection to the microbiome

Abstract

Work performed in the previous chapters demonstrate that infection of pregnant mice with *T. gondii* altered levels of 4-guanidinobutoanate and indoxylsulfate in their serum, decidua, placenta and foetuses. This study was conducted to determine the effects of the parasite exerted on the host intestinal microbiota in adult mice. BALB/c mice were infected with *T. gondii* cysts and fecal pellets were collected at the days 0,7, 14 and 21 post infection. Long term changes in the microbiota were investigated with high-throughput sequencing technology. Relative abundance from the top phylum to the genus level were analysed statistically. Despite the observed changes in metabolites discussed in the previous chapters, no significant changes to the relative abundance of host microbiota were found. This apparent contradiction might be due to the differences in the infection models used.

7.1 Introduction

In previous chapters, various pathways and their relevant metabolites were discovered to be altered in maternal foetal interface, the developing foetus and the maternal serum infected with *T. gondii*. These included 4-guanidinobutanoate and indoxylsulfate which are dependent on host microbiota for their production. Indoxylsulfate is altered by the action of tryptophanase expressing bacteria present in the gut (Sári et al., 2020). while 4-guanidinobutoanate, a metabolite of arginine, is altered significantly by the activity of *Pseudomonas aeruginosa*. This suggested that *T. gondii* infection is capable of altering the host microbiome. The following study was undertaken to determine if *T. gondii* infection alters the microbiome of the infected mice. Insight into the change in microbiome population/prevalence during *T. gondii* infection might have implications for the pathogenesis of *T. gondii* infection and also reveal some unknown facts about host-microbiome-infection triangle.

To do this, the prevalence of gut microbial population was evaluated to see the differences if any. DNA from the faecal pellets were extracted for downstream sequencing of prokaryotic prevalence or any changes taking place in the gut. Prokaryotes are rich in 16S rRNA gene that is used to differentiate between microbial phylogenies. The 16S ribosomal RNA sequence is composed of nine hypervariable regions (V1-V9) ranging from 30-100 base pairs long (Janda and Abbott, 2007).

For taxonomic classification, it is sufficient to sequence individual hypervariable regions instead of the entire gene. Additionally, the 16S gene contains highly conserved sequences between hypervariable regions, that enables the design of universal primers (Yang et al., 2016). With the development of high-throughput sequencing platforms, sequence variation in the 16S gene is widely used to characterize diverse microbial communities.

7.2 Aims and objectives

The aim of this study is to understand how *T. gondii* infection affects the intestinal microbiome of mice. If *T. gondii* is found to affect this microbiome of adult mice this could support the hypothesis that the differences in microbial products seen in the foetuses from *T. gondii*-infected mothers is due to *T. gondii*-induced, immune-mediated changes to the maternal intestinal microbiome. Therefore, the objective of this study was to use 16S rRNA sequencing to determine effects of infection with *T. gondii* on the murine intestinal microbiota.

7.3 Workflow of data analysis

Male BALB/c mice were randomly assigned to 3 groups. Group A were left non-infected, Group B were infected with 10 cysts of *T. gondii* type-II Beverley Strain by the oral route and Group C were administered brain homogenate from non-infected mice. This infection model was chosen because of its mild severity to allow collection of faecal samples at different time points. Faecal pellets were collected from each group on days 0, 7, 14 and 21 post infection. DNA was extracted from faecal pellets and all the samples were quantified for the purity and concentration of DNA extracted. The DNA samples were sent off for sequencing analysis to a commercial company called Novogene. From raw DNA samples to final data involved PCR, library preparation and sequencing, to keep the reliability of the data, quality control (QC) was performed at each of these steps by Novogene to generate raw data. These data were further processed and analysed in the laboratory.

The workflow of the data analysis to determine whether there is any change in the bacterial population when mice are infected with *T. gondii* is detailed in Figure 7.1.

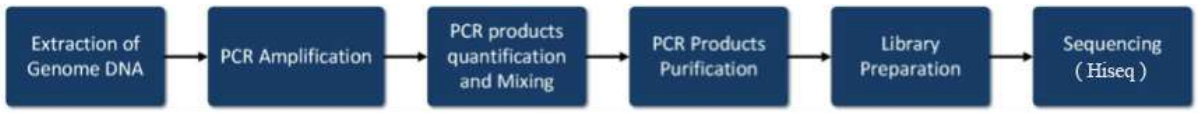

Figure 7. 1 Workflow diagram for the processing of DNA sequencing.

7.4 Results

7.4.1 Taxons relative abundance

The top 10 taxons in the different taxonomic ranks were selected to form the distribution histogram of relative abundance. The distribution in phylum was shown in figure 7.2 A & B. No statistical difference was observed between the groups of mice and considerable variation seen within each group.

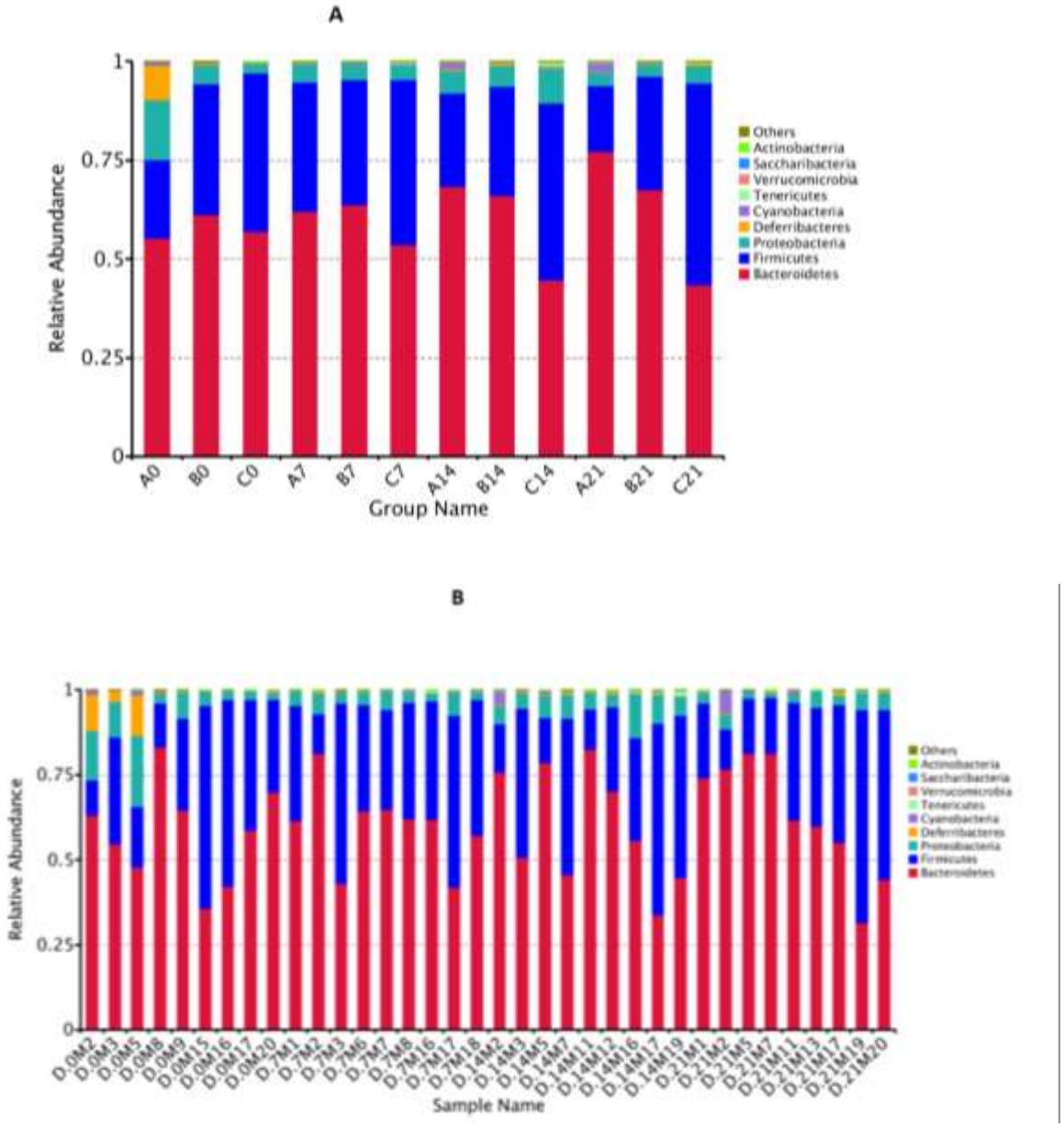

Figure 7. 2 Species relative abundance in phylum. (A) Plotted by the "Relative Abundance" on the Y-axis and "Group Name" on the X-axis. "Others" represents a total relative abundance of the rest of the phyla. (B) "Relative Abundance" on the Y-axis and "Sample Name" on the X-axis. "Others" represents a total relative abundance of the rest of the phyla besides the top 10 phyla. A= control group, B= infected group, C= control brain group. 0,7,14,21 represents DPI. Samples range 1-5= group A, 6-15= group B, 16-20 =group C.

An increased abundance of deferribacteres phylum can be seen in group A0 that represents samples from day 0, prior to infection relative to the other groups (A). However, this difference is not seen at later time points in this group of mice. So there appears to be variations regarding prevalence of this phylum in individual mice and over the time points sampled despite this being an untreated control group of mice. This can be further evaluated by sample wise distribution, as each group represented above contains three samples each (B). The distribution indicated that the said phylum was abundant mainly in two samples (D0-M2 and D0-M5) from day-0, those samples were not having any kind of effects of infection at this stage or at any of the later days (DPI). Further numerical relative abundance is shown in the following table 7.1.

Table 7. 1 showing relative abundance of top phyla.

		% relative abundance			
	Group	**Bacteroidetes**	**Proteobacteria**	**Firmicutes**	**Others**
0-DPI	A	**55**	**15**	**20**	**10**
	B	**61.33**	**5**	**33.23**	**0.44**
	C	**57**	**2.33**	**40**	**0.66**
7-DPI	A	**61.66**	**4.3**	**33**	**1.04**
	B	**63.6**	**4.01**	**31.09**	**1.3**
	C	**53**	**3.3**	**41**	**2.7**
14-DPI	A	**68**	**5.3**	**23.6**	**3**
	B	**66**	**3.3**	**27.7**	**3**
	C	**45**	**8.9**	**45**	**1.1**
21-DPI	A	**77.3**	**3**	**16.7**	**3**
	B	**67.7**	**3**	**29**	**0.3**
	C	**43.3**	**4.3**	**51.3**	**1.1**

The table 7.1 showed no significant change in relative abundance at any time point. However, few observations to note regardless of the infection are, the relative abundance of the phylum bacteroidetes showed an increase in the uninfected control group (A) (55 %, 61.66%, 68% and 77.3%) and infected group (B) (61.33%, 63.6%, 66% and 67.7%), while the control brain group (C) showed a decreasing % relative abundance of the said phylum as the days progress (57%, 53%, 45% and 43%).

Similarly, when comparison of the microbiome was carried out at the genus level by relative abundance, one of the genus lachnospiraceaUCG-001, from lachnospiracea family was found to be decreased in infected group when compared only during the progression of the disease. However, when compared with the uninfected control at different time points, a non-significant difference was observed. Lachnospiracea is a part of the core microbiome, found in the intestinal lumen from birth and it tends to increase during life of the host (Vacca et al., 2020). The results obtained from this study showed a decreased abundance in infected group from

day-0 through day-14, however, start to increase again at day-21. Control brain group showed an increase in the abundance of this genus as the days progress (Table 7.2).

Table 7. 2 showing relative abundance of lachnospiraceae-UCG-001.

	Relative abundance (%)			
	Day-0	Day-7	Day-14	Day-21
A (Uninfected control)	2	0.6	1.16	1.3
B (Infected)	8	2.2	1.5	2.7
C (Control brain)	1.5	2.8	2.3	4.9

7.4.2 Principal component analysis (PCA)

To assess the variations amongst samples in terms of composition similarity/differences, principal component analysis (PCA) was performed. The more similar the composition of community among the samples are, the closer the distance of their corresponding data points on the PCA graph are. The analysis shows that samples from each group of mice at each time point tend to cluster. However, samples from even non-infected mice at each time point do not cluster. Overall, the data indicate that the time point analysed and cage from which the mouse was housed in is the largest predictor of the microbiome composition, rather than infection status. The result of PCA analysis based on OTUs is shown in figure 7.3.

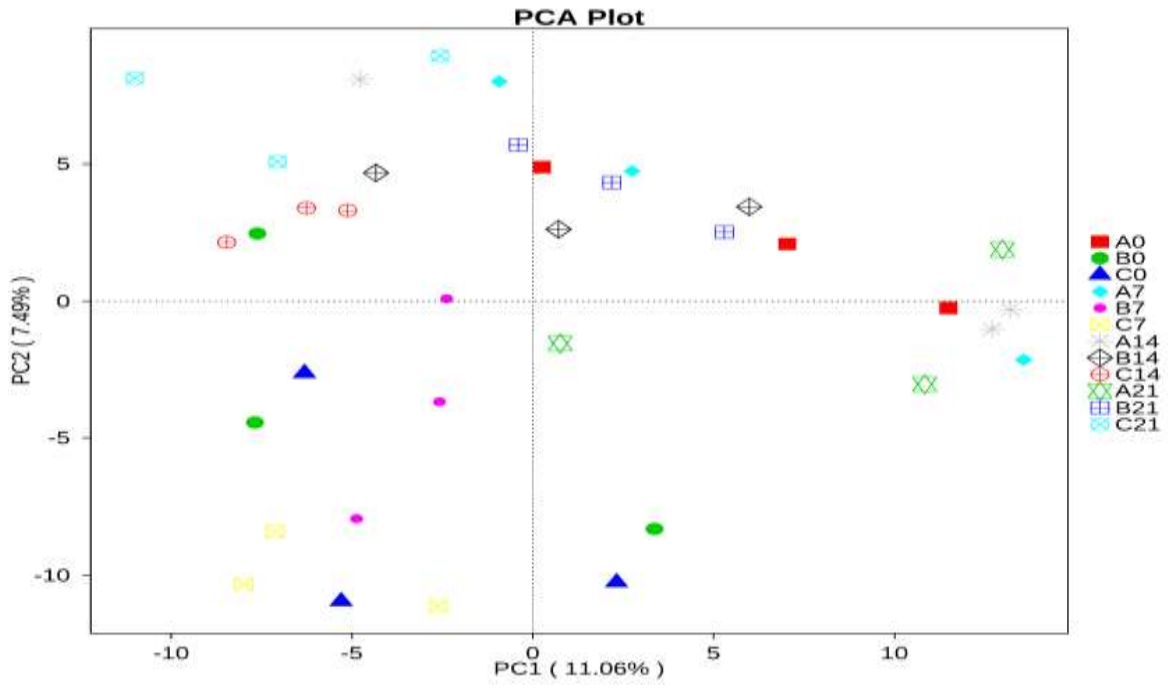

Figure 7. 3 PCA plot showing all of the groups in terms of similarity/ difference in composition of the bacterial population.

7.4.3 Taxonomic abundance heatmap

The abundance distribution of dominant 35 genera among all samples were displayed in the taxonomic abundance heat map. As seen below (Fig. 7.4), mice infected and sampled on day 7 post infection (B7) have a high abundance of genus *Rikenellaceae_RC9_gut_group*. However, on a detailed statistical analysis, this was found not to be a statistically significant change (Figure 7.5 a). Similarly, A0 apparently showed an increased abundance of the genus *Mucispirillum-schaedleri*, was found not to be a statistically significant change (Figure 7.5 b)

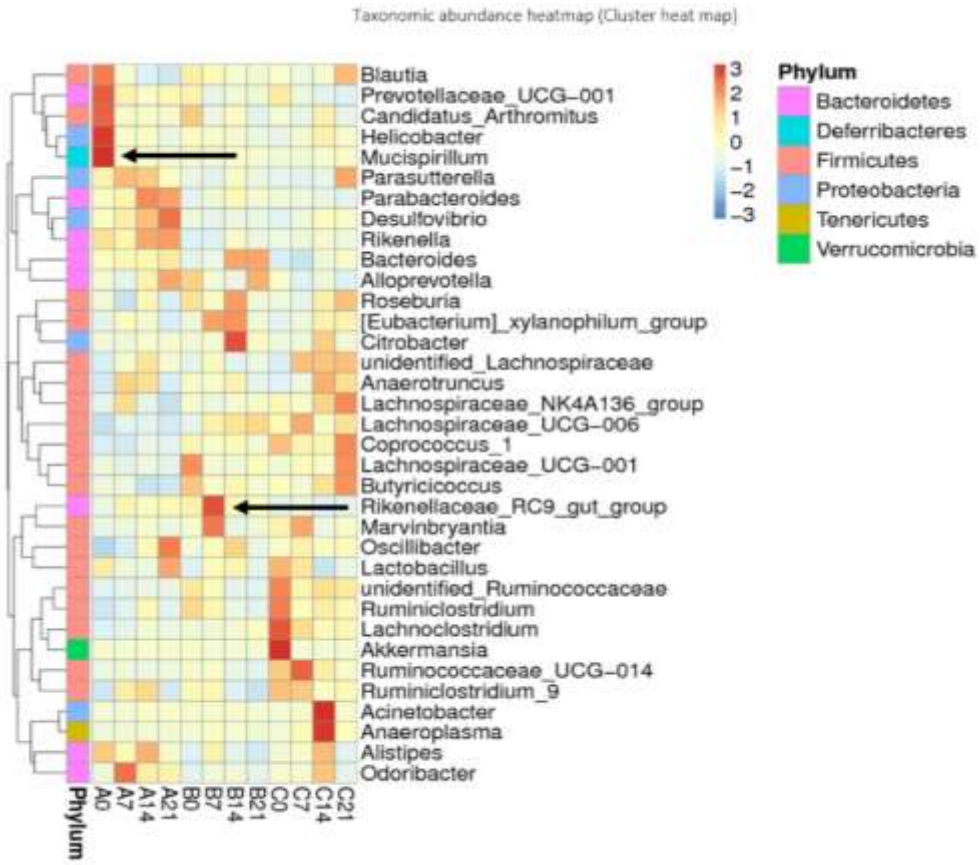

Figure 7. 4 Taxonomic abundance heat map showing relative abundance in genus level. Plotted by sample name on the X-axis and the Y-axis represents the genus.

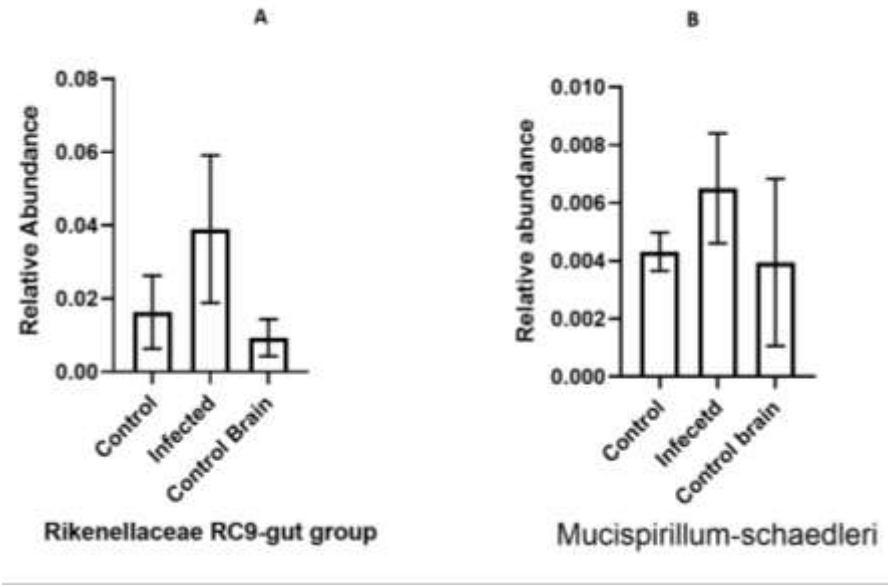

Figure 7. 5 showing relative abundance of two genus indicated in the heat map shown in figure 7.4. Figure shows relative abundance Mean±SD, Control (n= 5) Infected (n=5) Uninfected (n=5). Student´s t-test was performed to determine significance ($p < 0.05$) where *$p < 0.05$, **$p < 0.001$ ***$p < 0.0001$ are significant compared to the control uninfected.

A- shows relative abundance of genus *Rikenellaceae RC9-gut group*

B- shows relative abundance of genus *Mucispirillum-schaedleri*

7.5 Conclusion

Overall, the data in this chapter does not support that *T. gondii* infection alters the fecal microbiome of mice. However, there are a number of important caveats. Firstly, considerable variation was seen between groups of mice examined and between these groups over time. This means that potentially *T. gondii*-induced small changes to the microbiome could be masked by this variation. Secondly, the infection model used here (orally administered cysts) was designed to be mild to allow multiple time points to be examined. In contrast the infection model that prompted this study and used in the previous chapter is much more severe as it involves intraperitoneal injection of tachyzoites.

Overall, the intra-group differences observed in the relative abundance of phylum through genus showed many variations, however when the microbiome of the infected group is compared with that of uninfected, there is no significant change observed at any time point. The variations observed in different groups for Bacteroidetes phylum, are larger between the control group given nothing and the control group given uninfected brain homogenate than between the control group and the infected group. However, the relative difference between these groups are likely due to the initial varying individual composition of the microbiome of each group. The infected group of mice showed only small variations in microbiome over the course of the study.

A previously published study carried out on female BALB/c mice infected with *T. gondii* showed an increase in the phylum proteobacteria at day 13 post infection (Shao et al., 2020). Notably this study used oocysts, rather than tissue cysts to initiate infection. A further study Using C57BL/6 mice infected orally with the ME49 strain of *T. gondii*, found that increased levels of *Clostridia* in their intestinal microbiome throughout chronic disease. The authors noted that these mice also developed cachexia, but that this was not linked to the observed dysbiosis as mice housed with chronically infected mice developed similar microbiomes but

not cachexia (Hatter et al., 2018). The apparent difference between these published studies and the current study is hard to reconcile, but it is likely that the large intra and inter group differences as well as the temporal differences observed in the current study, mask any difference induced by *T. gondii* infection.

Overall, the data presented in this chapter is does not support that *T. gondii* infection alters the microbiome of mice. However, the weight of evidence from the previous studies suggests otherwise. Future studies should use the same infection model as used in the earlier chapters to determine if the microbiome is affected by that specific model. This still seems the most likely explanation as to why *T. gondii* infection affects 4-guanidinobutoanate and indoxylsulfate in their serum, decidua, placenta and foetuses.

8- Discussion

Studying the effect of *T. gondii* infection on the foetal maternal interface is important as it could contribute to our understanding of maternal and foetal outcomes due to *T. gondii* infection and ultimately the development of treatments to minimise their impact. Furthermore, elucidation of early events in the foetus to lead to treatments to reduce the effects of congenital infection. Although some recent studies have concentrated on studying the immune events at the maternal foetal interface using the murine model (PrabhuDas et al., 2015). However, no studies to date have examined changes to metabolism. Metabolism is now known to be bi-directionally linked to the immune response, but the study of this at the maternal foetal interface where regulation of the immune response is critical for the success of pregnancy is recognised to be 'lagging' (Wei et al., 2021). However, it is known that at least some aspects of metabolism, for example tryptophan metabolism is essential for successful pregnancy. How infectious diseases affect metabolism at the maternal foetal interface is even less well studied. Logically the interplay of the immune response and metabolism at the maternal interface could be disrupted directly by the metabolic demands of microbes or indirectly by the immune response they induce. Consequences could range from disruption of pregnancy or developmental disorders due to disruption of nutritional needs of transplacental transfer of toxic metabolites. The studies described in this thesis demonstrate that *T. gondii* infection not only affects the metabolism at the maternal foetal interface, but also the metabolites found in the developing foetus. The full consequences of these observations are not yet clear.

Arginine and citrulline

Initially, a global LC-MS based metabolomics approach was used to determine how metabolites are altered in the maternal foetal interface and the developing foetus extracted from the mothers infected with *T. gondii* infection. Sources of biological tissues exploited in pregnancy were placenta, decidua and the developing foetus. The results obtained indicated various changes in the metabolomics profile of these tissues taken from the mothers infected with *T. gondii.*

Significantly, the metabolites that showed a significant decrease were citrulline, arginine succinate, while spermine and spermidine were increased significantly. However, proline was significantly reduced in the decidua and placenta, L-arginine was significantly reduced in the decidual extracts while no change was noted in the foetal extracts taken from the mothers infected with *T. gondii* infection. During pregnancy, dietary intake of arginine is essential owing to it being a semi-essential amino acid (Hsu and Tain, 2019). Other than being used as a building block for the synthesis of protein, arginine is also used as a substrate for important metabolic pathways affecting macrophages, dendritic cells and T cells immune characters

Arginine acts as a precursor for some important biologically active compounds including nitric oxide (NO), polyamines, creatine and phosphocreatine (Martí and Reith, 2021). The results from the chapter 3 are suggestive of maternal arginine degradation being utilised for the synthesis of polyamines as increased levels of polyamines were noted following infection. Another possibility to explain the decreased levels of maternal arginine and citrulline during infection might be a change to the intestinal-renal axis where de novo synthesis of citrulline takes place from glutamate (Dhanakoti et al., 1990), as there were decreased levels of L-glutamate and N-acetyl-glutamate (they ultimately converts into the citrulline) were also recorded. Reduced intake of arginine/citrulline due to protein malnutrition and depletion of

endogenous L-arginine due to the maternal infection e.g., malaria have been associated with pre-eclampsia and poor pregnancy outcomes. Conversely arginine and citrulline supplementation has been shown to be beneficial for the pregnancy outcome. Thus, the observation that *T. gondii* infection also reduces arginine levels raises that possibility that similar treatment during pregnancy might alleviate some of the detrimental effects of infection.

Tryptophan metabolism

Tryptophan metabolism can be categorised into endogenous and bacterial. Kynurenine is one of the endogenous metabolites of kynurenine pathway (KP) of tryptophan degradation. Kynurenine pathway is initiated by the IDO and TDO enzymes that are stimulated by inflammatory cytokines and IFN-γ.

Evaluation of tryptophan degradation pathway indicated some of the metabolites which were changed including kynurenine and tryptophan. While kynurenine was downregulated in the decidua and placenta of infected mice relative to control mice, it was upregulated in the foetal extracts. L-tryptophan was decreased only in the decidual extracts of infected mice relative to control mice. Interaction of the tryptophan degradation pathway with the nicotinate pathway resulted in a significant decrease of 1-methylnicotinamide in all of the tissues examined from infected mice relative to control mice. Notably, levels of tryptophan were decreased in the foetus and maternal serum of *T. gondii* infected mice. These results demonstrate that *T. gondii* infection increases tryptophan degradation pathway towards the kynurenine pathway rather than serotonin pathway. This results in increased levels of kynurenine in developing foetuses. Notably, kynurenine has been found to cross the placenta and therefore the increased levels noted in the foetuses could be derived from the maternal immune response to *T. gondii* which is known to induce indolamine deoxygenase expression and degradation of tryptophan. This

could have implications for the health of the offspring as foetal exposure to kynurenine has been linked with increased risk of psychoneurological disease later in life (Goeden et al., 2017).

Administration of polyIC in the early stage of pregnancy has been used as a model of maternal immune activation that induces kynurenine in the foetus and results in pyschoneurological disease in later life (Clark et al., 2019). Examining the metabolomic profiles of the brain taken from adult mice born to infected mothers during pregnancy, raised levels of kynurenine were also noted in the brain. This demonstrates that kynurenine levels are at the very least raised from early foetal life through to adult life. However, these changes were not seen in uninfected adult mice born to infected mothers, suggesting they are maternally derived and short lived. Increased levels of kynurenine are also seen in congenitally infected adult mice demonstrate that infection in utero results in long term consequences for brain chemistry.

Overall, all these changes observed allowed us to conclude that the maternal infection with *T. gondii* has the ability to affect the foetus at very early stage and some of the changes taking place during early foetal life persist or mirror those evident in adulthood.

Tryptophan has been shown to display anti-inflammatory effects in mammals and has been shown to be a modulator of inflammatory responses (Gao et al., 2018). Mice with a low tryptophan diet had been shown to be more susceptible to chemically induced inflammation. While mice with sufficient tryptophan levels had decreased inflammation, mice with tryptophan depleted diets have been shown to result in more severe central nervous system inflammation (Gao et al., 2018). Here, tryptophan levels are reduced in the maternal foetal interface, developing foetus and maternal serum of infected mice relative to control mice. Neurological problems occurring as a result of *T. gondii* infection could also be attributed to the fact that lower tryptophan levels would be expected to result in increased inflammation leading to release of pro-inflammatory cytokines and damage to the brain.

The studies described here also find that *T. gondii* infection results in alteration of bacterial tryptophan metabolism. Thus, one of the metabolites of bacterial origin from tryptophan degradation**,** indole was altered in infected mice. Lactobacilli/tryptophanase producing bacterial species can metabolize tryptophan to produce indole (Roager and Licht, 2018). Levels of indole were increased in the foetal extracts from the infected mothers and their maternal serum, whereas in the decidua and placenta, decreased levels of indole were noted.

Indole is a ligand of aryl hydrocarbon receptors (AhR), which mediate regulation of intestinal immunity by the endogenous and bacterial metabolites of tryptophan degradation, thus AhR plays a role in immune homeostasis (Hubbard et al., 2015).AhR signalling influences the microbial composition in the small intestine as well as some genes targeted in the intestine or liver. In addition to this mechanism, AhR also acts as a regulator of host-microbiome communication, thus it affects the host metabolism and the immune system (Gao et al., 2018). Other than this, AhR itself plays an important role in regulating IDO1 and TDO1 levels (Bessede et al., 2014). In another study it was concluded that most strains of *P. aeruginosa* isolated from the cystic fibrosis patients produce increased levels of kynurenine, that support microbial survival and let bacteria avoid the innate immune response by scavenging reactive oxygen species (ROS) by neutrophil (Genestet et al., 2014). The raised levels of kynurenine might explain this immune modulation.

Further elaborating, this study also covered some of the metabolite changes associated with the microbiome, mainly indoxylsulfate and guanidinobutanoate. Levels of indoxylsulfate were noted as decreased following *T. gondii* infection with a statistical significance in all of the tissues examined throughout this study except brain. Cytochrome P450 enzymes are responsible for the oxidation of indole to indoxyl (detected in this study chapter 3, but not consistently found in the data described in chapter 4) that acts as an intermediate for the formation of indoxylsulfate (Banoglu et al., 2001). This is a protein bound uremic toxin that

is a metabolite of the microbiome produced from protein fermentation of the microbial population residing in the gut microbiota. A considerable amount of literature is available associating the high concentrations of indoxylsulfate in renal insufficiency and it is considered an important biomarker for chronic kidney disease (Tan et al., 2017). Some of the toxic effects of indoxylsulfate includes stimulation of inflammation and immune responses by upregulation of the MCP-1 and leukocyte interactions (Sun et al., 2013). In another study to determine the inflammatory response to indoxylsulfate, carried out on renal tubular cells, decreased serum levels of IS were correlated with a decreased oxidative stress in the kidney leading to better functioning and less histological injury (Palm et al., 2010). Decreased level of indoxylsulfate in the maternal serum as well as developing foetus were also noted in our study, however, association of indoxylsulfate during *T. gondii* infection with the developing foetus or pregnancy outcome is yet to be explored. It may be carried out with the help of metagenomics evaluation with same strain of *T. gondii* used for infection. Another potential future exploration could be the effects of *T. gondii* infection on the host hepatic metabolism.

4-Guanidinobutanoate (4-GB) levels were found to be decreased in all of the examined tissues of infected animals relative to control animals (developing foetus, decidua, placenta and maternal serum) in this study. It is produced by two pathways including D-arginine dehydrogenase pathway in *P. aeruginosa* and is a metabolite of GABA formed by the transfer of the guanidine group from arginine. In other studies, some indications of GABAergic effects of this metabolite have been reported and it is presumably considered an important metabolite for neural functions (Adkins et al., 2013, Watson et al., 2020). In another study, higher levels of 4-Guanidinobutanoate were detected with an increased level of GABA under the treatment of antiepileptic drugs including vigabatrin (Adkins et al., 2013). In a study carried out on the birth to weaning serum metabolomics profiling of grey seals, decreased levels of 4-Guanidinobutanoate were observed, however there was not any potential reason/hypothesis

given for this change (Watson et al., 2020). The result in the current study suggests some *T. gondii* induced changes in the microbiome, however the implications of this change for the outcome of pregnancy are still unknown, and future studies can be carried out to reach any conclusion.

To further investigate the in vitro effects of these microbial metabolites to the immune response, they were co-cultured with the mouse macrophages. Initial studies examined the effect of these metabolites on the pro-inflammatory cytokine IL-6 (see appendix 1). Ultimately it would have been desirable to test the effect of these metabolites on *T. gondii* induced cytokines and *T. gondii* multiplication. However, these studies for both metabolites were cut short due to the arising pandemic situation and non-availability of alternate resources. However, due to incomplete results, the available data obtained from in-vitro experiment is shown in appendix section (Appendix 1).

The ability of *T. gondii* infection to induce changes in metagenomics, was also evaluated. The results showed no change in the faecal microbiome of mice following *T. gondii* infection, however variations in microbiome were noted between groups with time. However, a previous study in BALB/c mice infected with *T. gondii*, showed a significant change in the relative abundance of the phylum proteobacteria at day 13 post infection (Shao et al., 2020). This could be due to the use of different models of infection between these studies or due the large intragroup/temporal variation disguising inter group variations.

Overall, the studies described in this thesis demonstrate for the first time, *T. gondii* induced changes to metabolites at the maternal foetal interface and the developing foetus. More widely the model used and these initial findings lay the ground work for further studies that could focus on the implication of these findings for pregnancy and life-long health of foetus and ultimately adult offspring. The most striking finding is that kynurenine, a metabolite that has been associated with development of pyschoneurological disease is raised in the foetus at early/mid stages of gestation and this finding could have practical use as it suggests that developing treatments to alleviate kynurenine production and their application early in life could have an impact on prevention of psychoneurological diseases later in life.

Future work

- Future work is required to study the consequences of the changes observed in various metabolites for their post-natal health and development of the foetus
- *T. gondii* alters the microbiome or the infection affects liver metabolism to convert indole to indoxylsulfate, an exclusive study on host hepatic metabolism to be studied in future
- Metagenomics evaluation regarding *T. gondii* should be carried out with the same infection model

References

ABBASI, M., KOWALEWSKA-GROCHOWSKA, K., BAHAR, M. A., KILANI, R. T., WINKLER-LOWEN, B. & GUILBERT, L. J. 2003. Infection of placental trophoblasts by Toxoplasma gondii. *The Journal of infectious diseases,* 188**,** 608-616.

ABDELSALAM, A. A. A. 2019. *A Systems Approach to Determine how Toxoplasma Gondii Infection Causes Neuropsychiatric Disease,* University of Strathclyde.

ABRAHAMS, V. M., KIM, Y. M., STRASZEWSKI, S. L., ROMERO, R. & MOR, G. 2004a. Macrophages and apoptotic cell clearance during pregnancy. *Am J Reprod Immunol,* 51**,** 275-82.

ABRAHAMS, V. M., STRASZEWSKI-CHAVEZ, S. L., GULLER, S. & MOR, G. 2004b. First trimester trophoblast cells secrete Fas ligand which induces immune cell apoptosis. *Mol Hum Reprod,* 10**,** 55-63.

ADKINS, D. E., MCCLAY, J. L., VUNCK, S. A., BATMAN, A. M., VANN, R. E., CLARK, S. L., SOUZA, R. P., CROWLEY, J. J., SULLIVAN, P. F., VAN DEN OORD, E. J. & BEARDSLEY, P. M. 2013. Behavioral metabolomics analysis identifies novel neurochemical signatures in methamphetamine sensitization. *Genes Brain Behav,* 12**,** 780-91.

AFONSO, E., THULLIEZ, P. & GILOT-FROMONT, E. 2010. Local meteorological conditions, dynamics of seroconversion to Toxoplasma gondii in cats (Felis catus) and oocyst burden in a rural environment. *Epidemiology & Infection,* 138**,** 1105-1113.

AL-WARID, H. S. & AL-QADHI, B. N. 2012. Evaluation of progesterone and estrogen hormonal levels in pregnant women with toxoplasmosis. *European Journal of Scientific Research,* 91**,** 515-519.

AREVALO, M.-A., SANTOS-GALINDO, M., BELLINI, M.-J., AZCOITIA, I. & GARCIA-SEGURA, L. M. 2010. Actions of estrogens on glial cells: implications for neuroprotection. *Biochimica et Biophysica Acta (BBA)-General Subjects,* 1800**,** 1106-1112.

AREVALO, M. A., AZCOITIA, I. & GARCIA-SEGURA, L. M. 2015. The neuroprotective actions of oestradiol and oestrogen receptors. *Nat Rev Neurosci,* 16**,** 17-29.

ARMSTRONG, C. T., MASON, P. E., ANDERSON, J. & DEMPSEY, C. E. 2016. Arginine side chain interactions and the role of arginine as a gating charge carrier in voltage sensitive ion channels. *Scientific reports,* 6**,** 1-10.

AWOKE, K., NIBRET, E. & MUNSHEA, A. 2015. Sero-prevalence and associated risk factors of Toxoplasma gondii infection among pregnant women attending antenatal care at Felege Hiwot Referral Hospital, northwest Ethiopia. *Asian Pacific journal of tropical medicine,* 8**,** 549-554.

BABAN, B., CHANDLER, P. R., SHARMA, M. D., PIHKALA, J., KONI, P. A., MUNN, D. H. & MELLOR, A. L. 2009. IDO activates regulatory T cells and blocks their conversion into Th17-like T cells. *The Journal of Immunology,* 183**,** 2475-2483.

BADAWY, A. A. 2015. Tryptophan metabolism, disposition and utilization in pregnancy. *Biosci Rep,* 35.

BANOGLU, E., JHA, G. G. & KING, R. S. 2001. Hepatic microsomal metabolism of indole to indoxyl, a precursor of indoxyl sulfate. *Eur J Drug Metab Pharmacokinet,* 26**,** 235-40.

BARBOSA, B. F., LOPES-MARIA, J. B., GOMES, A. O., ANGELONI, M. B., CASTRO, A. S., FRANCO, P. S., FERMINO, M. L., ROQUE-BARREIRA, M. C., IETTA, F. & MARTINS-FILHO, O. A. 2015. IL10, TGF beta1, and IFN gamma modulate intracellular signaling pathways and cytokine production to control Toxoplasma gondii infection in BeWo trophoblast cells. *Biology of reproduction,* 92**,** 82, 1-13.

BARBOSA, B. F., PAULESU, L., IETTA, F., BECHI, N., ROMAGNOLI, R., GOMES, A. O., FAVORETO-JUNIOR, S., SILVA, D. A., MINEO, J. R., MINEO, T. W. & FERRO, E. A. 2014. Susceptibility to Toxoplasma gondii proliferation in BeWo human trophoblast cells is dose-dependent of macrophage migration inhibitory factor (MIF), via ERK1/2 phosphorylation and prostaglandin E2 production. *Placenta,* 35**,** 152-62.

BARDOT, E. S. & HADJANTONAKIS, A. K. 2020. Mouse gastrulation: Coordination of tissue patterning, specification and diversification of cell fate. *Mech Dev,* 163**,** 103617.

BEHNKE, M. S., WOOTTON, J. C., LEHMANN, M. M., RADKE, J. B., LUCAS, O., NAWAS, J., SIBLEY, L. D. & WHITE, M. W. 2010. Coordinated progression through two subtranscriptomes underlies the tachyzoite cycle of Toxoplasma gondii. *PLoS One,* 5**,** e12354.

BERDOY, M., WEBSTER, J. P. & MACDONALD, D. W. 2000. Fatal attraction in rats infected with Toxoplasma gondii. *Proceedings of the Royal Society of London. Series B: Biological Sciences,* 267**,** 1591-1594.

BERGER, F., GOULET, V., LE STRAT, Y. & DESENCLOS, J.-C. 2009. Toxoplasmosis among pregnant women in France: risk factors and change of prevalence between 1995 and 2003. *Revue d'epidemiologie et de sante publique,* 57**,** 241-248.

BESSEDE, A., GARGARO, M., PALLOTTA, M. T., MATINO, D., SERVILLO, G., BRUNACCI, C., BICCIATO, S., MAZZA, E. M., MACCHIARULO, A., VACCA, C., IANNITTI, R., TISSI, L., VOLPI, C., BELLADONNA, M. L., ORABONA, C., BIANCHI, R., LANZ, T. V., PLATTEN, M., DELLA FAZIA, M. A., PIOBBICO, D., ZELANTE, T., FUNAKOSHI, H., NAKAMURA, T., GILOT, D., DENISON, M. S., GUILLEMIN, G. J., DUHADAWAY, J. B., PRENDERGAST, G. C., METZ, R., GEFFARD, M., BOON, L., PIRRO, M., IORIO, A., VEYRET, B., ROMANI, L., GROHMANN, U., FALLARINO, F. & PUCCETTI, P. 2014. Aryl hydrocarbon receptor control of a disease tolerance defence pathway. *Nature,* 511**,** 184-90.

BESTEIRO, S. 2019. The role of host autophagy machinery in controlling Toxoplasma infection. *Virulence,* 10**,** 438-447.

BLACKWELL, J. M., ROBERTS, C. W. & ALEXANDER, J. 1993. Influence of genes within the MHC on mortality and brain cyst development in mice infected with Toxoplasma gondii: kinetics of immune regulation in BALB H-2 congenic mice. *Parasite Immunol,* 15**,** 317-24.

BLISS, S. K., MARSHALL, A. J., ZHANG, Y. & DENKERS, E. Y. 1999. Human polymorphonuclear leukocytes produce IL-12, TNF-α, and the chemokines macrophage-inflammatory protein-1α and-1β in response to Toxoplasma gondii antigens. *The Journal of Immunology,* 162**,** 7369-7375.

BLOIS, S. M., KLAPP, B. F. & BARRIENTOS, G. 2011. Decidualization and angiogenesis in early pregnancy: unravelling the functions of DC and NK cells. *Journal of reproductive immunology,* 88**,** 86-92.

BOLLANI, L., STROCCHIO, L. & STRONATI, M. 2013. Congenital toxoplasmosis. *Early human development,* 89**,** S70-S72.

BORGES, M., MAGALHÃES SILVA, T., BRITO, C., TEIXEIRA, N. & ROBERTS, C. W. 2019. How does toxoplasmosis affect the maternal-foetal immune interface and pregnancy? *Parasite Immunol,* 41**,** e12606.

BOZZACCO, L., TRUMPFHELLER, C., SIEGAL, F. P., MEHANDRU, S., MARKOWITZ, M., CARRINGTON, M., NUSSENZWEIG, M. C., PIPERNO, A. G. & STEINMAN, R. M. 2007. DEC-205 receptor on dendritic cells mediates presentation of HIV gag protein to CD8+ T cells in a spectrum of human MHC I haplotypes. *Proc Natl Acad Sci U S A,* 104**,** 1289-94.

BRADLEY, P. J., WARD, C., CHENG, S. J., ALEXANDER, D. L., COLLER, S., COOMBS, G. H., DUNN, J. D., FERGUSON, D. J., SANDERSON, S. J., WASTLING, J. M. &

BOOTHROYD, J. C. 2005. Proteomic analysis of rhoptry organelles reveals many novel constituents for host-parasite interactions in Toxoplasma gondii. *J Biol Chem,* 280**,** 34245-58.

BRINKMANN, M. M., SPOONER, E., HOEBE, K., BEUTLER, B., PLOEGH, H. L. & KIM, Y.-M. 2007. The interaction between the ER membrane protein UNC93B and TLR3, 7, and 9 is crucial for TLR signaling. *The Journal of cell biology,* 177**,** 265-275.

BRITO, C., T, M. S., M, M. C., WYRWAS, W., OLIVEIRA, B., B, M. F., OLIVEIRA, P., C, W. R., TEIXEIRA, N. & BORGES, M. 2020. Toxoplasma gondii infection reduces serum progesterone levels and adverse effects at the maternal-foetal interface. *Parasite Immunol,* 42**,** e12690.

BROEKHUIZEN, M., DANSER, A. H. J., REISS, I. K. M. & MERKUS, D. 2021. The Function of the Kynurenine Pathway in the Placenta: A Novel Pharmacotherapeutic Target? *Int J Environ Res Public Health,* 18.

CARLIER, Y., TRUYENS, C., DELORON, P. & PEYRON, F. 2012. Congenital parasitic infections: a review. *Acta Trop,* 121**,** 55-70.

CHABTINI, L., MFARREJ, B., MOUNAYAR, M., ZHU, B., BATAL, I., DAKLE, P. J., SMITH, B. D., BOENISCH, O., NAJAFIAN, N., AKIBA, H., YAGITA, H. & GULERIA, I. 2013. TIM-3 regulates innate immune cells to induce fetomaternal tolerance. *J Immunol,* 190**,** 88-96.

CHAUDHRY, S. A., GAD, N. & KOREN, G. 2014. Toxoplasmosis and pregnancy. *Canadian Family Physician,* 60**,** 334-336.

CIRELLI, K. M. 2016. *Rodent inflammasome activation by Toxoplasma gondii*. Massachusetts Institute of Technology.

CLARK, S. M., NOTARANGELO, F. M., LI, X., CHEN, S., SCHWARCZ, R. & TONELLI, L. H. 2019. Maternal immune activation in rats blunts brain cytokine and kynurenine pathway responses to a second immune challenge in early adulthood. *Prog Neuropsychopharmacol Biol Psychiatry,* 89**,** 286-294.

CLOUGH, B., WRIGHT, J. D., PEREIRA, P. M., HIRST, E. M., JOHNSTON, A. C., HENRIQUES, R. & FRICKEL, E. M. 2016. K63-Linked Ubiquitination Targets Toxoplasma gondii for Endo-lysosomal Destruction in IFNγ-Stimulated Human Cells. *PLoS Pathog,* 12**,** e1006027.

COLLINS, M. K., TAY, C. S. & ERLEBACHER, A. 2009. Dendritic cell entrapment within the pregnant uterus inhibits immune surveillance of the maternal/fetal interface in mice. *J Clin Invest,* 119**,** 2062-73.

COOK, A., HOLLIMAN, R., GILBERT, R., BUFFOLANO, W., ZUFFEREY, J., PETERSEN, E., JENUM, P., FOULON, W., SEMPRINI, A. & DUNN, D. 2000. Sources of toxoplasma infection in pregnant women: European multicentre case-control studyCommentary: Congenital toxoplasmosis—further thought for food. *Bmj,* 321**,** 142-147.

CREEK, D. J., JANKEVICS, A., BURGESS, K. E. V., BREITLING, R. & BARRETT, M. P. 2012. IDEOM: an Excel interface for analysis of LC–MS-based metabolomics data. *Bioinformatics,* 28**,** 1048-1049.

CROY, B. A., CHEN, Z., HOFMANN, A. P., LORD, E. M., SEDLACEK, A. L. & GERBER, S. A. 2012. Imaging of vascular development in early mouse decidua and its association with leukocytes and trophoblasts. *Biology of reproduction,* 87**,** 125, 1-11.

CROY, B. A., HE, H., ESADEG, S., WEI, Q., MCCARTNEY, D., ZHANG, J., BORZYCHOWSKI, A., ASHKAR, A. A., BLACK, G. P. & EVANS, S. S. 2003. Uterine natural killer cells: Insights to their cellular and molecular biology from mouse modelling. *Reproduction (Cambridge, England),* 126**,** 149.

DA SILVA, R. R., DORRESTEIN, P. C. & QUINN, R. A. 2015. Illuminating the dark matter in metabolomics. *Proc Natl Acad Sci U S A,* 112**,** 12549-50.

DEGRANDI, D., KONERMANN, C., BEUTER-GUNIA, C., KRESSE, A., WÜRTHNER, J., KURIG, S., BEER, S. & PFEFFER, K. 2007. Extensive characterization of IFN-induced GTPases mGBP1 to mGBP10 involved in host defense. *J Immunol,* 179**,** 7729-40.

DHANAKOTI, S. N., BROSNAN, J. T., HERZBERG, G. R. & BROSNAN, M. E. 1990. Renal arginine synthesis: studies in vitro and in vivo. *Am J Physiol,* 259**,** E437-42.

DUBEY, J., HILL, D., JONES, J., HIGHTOWER, A., KIRKLAND, E., ROBERTS, J., MARCET, P., LEHMANN, T., VIANNA, M. C. B. & MISKA, K. 2005. Prevalence of viable Toxoplasma gondii in beef, chicken, and pork from retail meat stores in the United States: risk assessment to consumers. *Journal of Parasitology,* 91**,** 1082-1093.

DUBEY, J., KOTULA, A., SHARAR, A., ANDREWS, C. & LINDSAY, D. 1990. Effect of high temperature on infectivity of Toxoplasma gondii tissue cysts in pork. *The Journal of parasitology***,** 201-204.

DÜHRKOP, K., SHEN, H., MEUSEL, M., ROUSU, J. & BÖCKER, S. 2015. Searching molecular structure databases with tandem mass spectra using CSI:FingerID. *Proc Natl Acad Sci U S A,* 112**,** 12580-5.

DUMÈTRE, A., LE BRAS, C., BAFFET, M., MENECEUR, P., DUBEY, J., DEROUIN, F., DUGUET, J.-P., JOYEUX, M. & MOULIN, L. 2008. Effects of ozone and ultraviolet radiation treatments on the infectivity of Toxoplasma gondii oocysts. *Veterinary parasitology,* 153**,** 209-213.

DUNAY, I. R., GAJUREL, K., DHAKAL, R., LIESENFELD, O. & MONTOYA, J. G. 2018. Treatment of Toxoplasmosis: Historical Perspective, Animal Models, and Current Clinical Practice. *Clin Microbiol Rev,* 31.

DUNCANSON, P., TERRY, R. S., SMITH, J. E. & HIDE, G. 2001. High levels of congenital transmission of Toxoplasma gondii in a commercial sheep flock. *International journal for parasitology,* 31**,** 1699-1703.

DUNN, D., WALLON, M., PEYRON, F., PETERSEN, E., PECKHAM, C. & GILBERT, R. 1999. Mother-to-child transmission of toxoplasmosis: risk estimates for clinical counselling. *The Lancet,* 353**,** 1829-1833.

DZITKO, K., DZIADEK, B., GATKOWSKA, J. & DŁUGOŃSKA, H. 2013. Toxoplasma gondii binds sheep prolactin. *Experimental parasitology,* 134**,** 216-219.

DZITKO, K., LAWNICKA, H., GATKOWSKA, J., DZIADEK, B., KOMOROWSKI, J. & DŁUGOŃSKA, H. 2012. Inhibitory effect of prolactin on Toxoplasma proliferation in peripheral blood mononuclear cells from patients with hyperprolactinemia. *Parasite Immunol,* 34**,** 302-11.

FERGUSON, D. J., PARMLEY, S. F. & TOMAVO, S. 2002. Evidence for nuclear localisation of two stage-specific isoenzymes of enolase in Toxoplasma gondii correlates with active parasite replication. *International journal for parasitology,* 32**,** 1399-1410.

FISCH, D., YAKIMOVICH, A., CLOUGH, B., WRIGHT, J., BUNYAN, M., HOWELL, M., MERCER, J. & FRICKEL, E. 2019. Defining host-pathogen interactions employing an artificial intelligence workflow. *Elife,* 8.

FLOC'H, L., OTTEN, W. & MERLOT, E. 2011. Tryptophan metabolism, from nutrition to potential therapeutic applications. *Amino acids,* 41**,** 1195-1205.

FOULK, R. A. 2001. From fertilization to implantation. *Early Pregnancy,* 5**,** 61-2.

FREDRIKSSON, G., BUXTON, D., UGGLA, A., KINDAHL, H. & EDQVIST, L. E. 1990. The Effect of Toxoplasma gondii Infection in Unvaccinated and Iscom-Vaccinated Pregnant Ewes as Monitored by Plasma Levels of 15-Ketodihydroprostaglandin F2α, Progesterone, and Oestrone Sulphate. *Journal of Veterinary Medicine Series A,* 37**,** 113-122.

FRICKEL, E. M. & HUNTER, C. A. 2021. Lessons from Toxoplasma: Host responses that mediate parasite control and the microbial effectors that subvert them. *J Exp Med,* 218.

GAO, J., XU, K., LIU, H., LIU, G., BAI, M., PENG, C., LI, T. & YIN, Y. 2018. Impact of the Gut Microbiota on Intestinal Immunity Mediated by Tryptophan Metabolism. *Front Cell Infect Microbiol,* 8**,** 13.

GARCÍA-VÁZQUEZ, F. A., GADEA, J., MATÁS, C. & HOLT, W. V. 2016. Importance of sperm morphology during sperm transport and fertilization in mammals. *Asian J Androl,* 18**,** 844-850.

GAVINET, M., ROBERT, F., FIRTION, G., DELOUVRIER, E., HENNEQUIN, C., MAURIN, J., TOURTE-SCHAEFER, C. & DUPOUY-CAMET, J. 1997. Congenital toxoplasmosis due to maternal reinfection during pregnancy. *Journal of clinical microbiology,* 35**,** 1276-1277.

GAY-ANDRIEU, F., COZON, G. J., FERRANDIZ, J. & PEYRON, F. 2002. Progesterone fails to modulate Toxoplasma gondii replication in the RAW 264· 7 murine macrophage cell line. *Parasite immunology,* 24**,** 173-178.

GAZZINELLI, R. T., HAKIM, F. T., HIENY, S., SHEARER, G. M. & SHER, A. 1991. Synergistic role of CD4+ and CD8+ T lymphocytes in IFN-gamma production and protective immunity induced by an attenuated Toxoplasma gondii vaccine. *J Immunol,* 146**,** 286-92.

GAZZINELLI, R. T., WYSOCKA, M., HIENY, S., SCHARTON-KERSTEN, T., CHEEVER, A., KÜHN, R., MÜLLER, W., TRINCHIERI, G. & SHER, A. 1996. In the absence of endogenous IL-10, mice acutely infected with Toxoplasma gondii succumb to a lethal immune response dependent on CD4+ T cells and accompanied by overproduction of IL-12, IFN-gamma and TNF-alpha. *J Immunol,* 157**,** 798-805.

GENESTET, C., LE GOUELLEC, A., CHAKER, H., POLACK, B., GUERY, B., TOUSSAINT, B. & STASIA, M. J. 2014. Scavenging of reactive oxygen species by tryptophan metabolites helps Pseudomonas aeruginosa escape neutrophil killing. *Free Radic Biol Med,* 73**,** 400-10.

GOEDEN, N., NOTARANGELO, F. M., POCIVAVSEK, A., BEGGIATO, S., BONNIN, A. & SCHWARCZ, R. 2017. Prenatal Dynamics of Kynurenine Pathway Metabolism in Mice: Focus on Kynurenic Acid. *Dev Neurosci,* 39**,** 519-528.

GUEVARA, R. B., FOX, B. A. & BZIK, D. J. 2021. A Family of Toxoplasma gondii Genes Related to GRA12 Regulate Cyst Burdens and Cyst Reactivation. *mSphere,* 6.

HAMPTON, M. M. 2015. Congenital toxoplasmosis: a review. *Neonatal Network,* 34**,** 274-278.

HARGRAVE, K. E., WOODS, S., MILLINGTON, O., CHALMERS, S., WESTROP, G. D. & ROBERTS, C. W. 2019. Multi-Omics Studies Demonstrate Toxoplasma gondii-Induced Metabolic Reprogramming of Murine Dendritic Cells. *Front Cell Infect Microbiol,* 9**,** 309.

HENRIQUEZ, S. A., BRETT, R., ALEXANDER, J., PRATT, J. & ROBERTS, C. W. 2009. Neuropsychiatric disease and Toxoplasma gondii infection. *Neuroimmunomodulation,* 16**,** 122-33.

HILL, D., COSS, C., DUBEY, J., WROBLEWSKI, K., SAUTTER, M., HOSTEN, T., MUÑOZ-ZANZI, C., MUI, E., WITHERS, S. & BOYER, K. 2011. Identification of a sporozoite-specific antigen from Toxoplasma gondii. *The Journal of parasitology,* 97**,** 328-337.

HILL, D. & DUBEY, J. 2002. Toxoplasma gondii: transmission, diagnosis and prevention. *Clinical microbiology and infection,* 8**,** 634-640.

HSU, C. N. & TAIN, Y. L. 2019. Impact of Arginine Nutrition and Metabolism during Pregnancy on Offspring Outcomes. *Nutrients,* 11.

HUBBARD, T. D., MURRAY, I. A. & PERDEW, G. H. 2015. Indole and Tryptophan Metabolism: Endogenous and Dietary Routes to Ah Receptor Activation. *Drug Metab Dispos,* 43**,** 1522-35.

HUNTER, C. A. & SIBLEY, L. D. 2012. Modulation of innate immunity by Toxoplasma gondii virulence effectors. *Nat Rev Microbiol,* 10**,** 766-78.

JANDA, J. M. & ABBOTT, S. L. 2007. 16S rRNA gene sequencing for bacterial identification in the diagnostic laboratory: pluses, perils, and pitfalls. *J Clin Microbiol,* 45**,** 2761-4.

JOHNSON, L. L. 1992. SCID mouse models of acute and relapsing chronic Toxoplasma gondii infections. *Infection and immunity,* 60**,** 3719-3724.

JOHNSON, L. M., ATKINS, C. E., KEENE, B. W. & BAI, S. A. 1996. Pharmacokinetic and pharmacodynamic properties of conventional and CD-formulated diltiazem in cats. *J Vet Intern Med,* 10**,** 316-20.

JONES, J. & DUBEY, J. 2010. Waterborne toxoplasmosis–recent developments. *Experimental parasitology,* 124**,** 10-25.

KIM, K. & WEISS, L. M. 2004. Toxoplasma gondii: the model apicomplexan. *Int J Parasitol,* 34**,** 423-32.

KITTAS, C. & HENRY, L. 1979. Effect of gonadectomy and oestrogen administration on the response of lymph-node post-capillary venules to infection with Toxoplasma gondii. *The Journal of Pathology,* 127**,** 129-136.

KODJIKIAN, L., HOIGNE, I., ADAM, O., JACQUIER, P., AEBI-OCHSNER, C., AEBI, C. & GARWEG, J. G. 2004. Vertical transmission of toxoplasmosis from a chronically infected immunocompetent woman. *The Pediatric infectious disease journal,* 23**,** 272-274.

KOGA, K., CARDENAS, I., ALDO, P., ABRAHAMS, V. M., PENG, B., FILL, S., ROMERO, R. & MOR, G. 2009. Activation of TLR3 in the trophoblast is associated with preterm delivery. *Am J Reprod Immunol,* 61**,** 196-212.

KRAUTKRAMER, K. A., FAN, J. & BÄCKHED, F. 2021. Gut microbial metabolites as multi-kingdom intermediates. *Nature Reviews Microbiology,* 19**,** 77-94.

LEE, K. Y., JEONG, J. W., TSAI, S. Y., LYDON, J. P. & DEMAYO, F. J. 2007. Mouse models of implantation. *Trends Endocrinol Metab,* 18**,** 234-9.

LEE, S. K., KIM, J. Y., LEE, M., GILMAN-SACHS, A. & KWAK-KIM, J. 2012. T h17 and regulatory t cells in women with recurrent pregnancy loss. *American Journal of Reproductive Immunology,* 67**,** 311-318.

LIMA, T. S., MALLYA, S., JANKEEL, A., MESSAOUDI, I. & LODOEN, M. B. 2021. Toxoplasma gondii Extends the Life Span of Infected Human Neutrophils by Inducing Cytosolic PCNA and Blocking Activation of Apoptotic Caspases. *mBio,* 12.

LIU, Q., WEI, F., GAO, S., JIANG, L., LIAN, H., YUAN, B., YUAN, Z., XIA, Z., LIU, B. & XU, X. 2009. Toxoplasma gondii infection in pregnant women in China. *Transactions of the Royal Society of Tropical Medicine and Hygiene,* 103**,** 162-166.

LIU, X., ZHAO, M., YANG, X., HAN, M., XU, X., JIANG, Y. & HU, X. 2014. Toxoplasma gondii infection of decidual CD1c(+) dendritic cells enhances cytotoxicity of decidual natural killer cells. *Inflammation,* 37**,** 1261-70.

LUDVIK, J. V. 1958. Morphology of Toxoplasma gondii in electron microscope. *Vestnik Ceskoslovenske Zoologicke Spolecnosti,* 22**,** 130-36.

LYONS, R. E., MCLEOD, R. & ROBERTS, C. W. 2002a. Toxoplasma gondii tachyzoite-bradyzoite interconversion. *Trends Parasitol,* 18**,** 198-201.

LYONS, R. E., MCLEOD, R. & ROBERTS, C. W. 2002b. Toxoplasma gondii tachyzoite–bradyzoite interconversion. *Trends in parasitology,* 18**,** 198-201.

MAHIEU, N. G. & PATTI, G. J. 2017. Systems-Level Annotation of a Metabolomics Data Set Reduces 25 000 Features to Fewer than 1000 Unique Metabolites. *Anal Chem,* 89**,** 10397-10406.

MAMMARI, N., HALABI, M. A., YAACOUB, S., CHLALA, H., DARDÉ, M.-L. & COURTIOUX, B. 2019a. Toxoplasma gondii modulates the host cell responses: an overview of apoptosis pathways. *BioMed research international,* 2019.

MAMMARI, N., HALABI, M. A., YAACOUB, S., CHLALA, H., DARDÉ, M. L. & COURTIOUX, B. 2019b. Toxoplasma gondii Modulates the Host Cell Responses: An Overview of Apoptosis Pathways. *Biomed Res Int,* 2019**,** 6152489.

MANY, A. & KOREN, G. 2006. Toxoplasmosis during pregnancy. *Can Fam Physician,* 52**,** 29-30, 32.

MARTELL CLAROS, N. 2017. [Gestational hypertension]. *Hipertens Riesgo Vasc,* 34 Suppl 2**,** 22-25.

MARTÍ, I. L. A. A. & REITH, W. 2021. Arginine-dependent immune responses. *Cell Mol Life Sci,* 78**,** 5303-5324.

MEGLI, C. J. & COYNE, C. B. 2021. Infections at the maternal-fetal interface: an overview of pathogenesis and defence. *Nat Rev Microbiol***,** 1-16.

MILLS, C. D. 2001. Macrophage arginine metabolism to ornithine/urea or nitric oxide/citrulline: a life or death issue. *Crit Rev Immunol,* 21**,** 399-425.

MONCADA, P. A. & MONTOYA, J. G. 2012. Toxoplasmosis in the fetus and newborn: an update on prevalence, diagnosis and treatment. *Expert review of anti-infective therapy,* 10**,** 815-828.

MONDRAGON, R., HOWE, D. K., DUBEY, J. & SIBLEY, L. D. 1998. Genotypic analysis of Toxoplasma gondii isolates from pigs. *The Journal of parasitology***,** 639-641.

MOR, G., ALDO, P. & ALVERO, A. B. 2017. The unique immunological and microbial aspects of pregnancy. *Nat Rev Immunol,* 17**,** 469-482.

MOR, G. & KWON, J.-Y. 2015. Trophoblast-microbiome interaction: a new paradigm on immune regulation. *American journal of obstetrics and gynecology,* 213**,** S131-S137.

MORRIS JR, S. M. 2007. Arginine metabolism: boundaries of our knowledge. *The Journal of nutrition,* 137**,** 1602S-1609S.

NARUSE, K., LASH, G. E., BULMER, J. N., INNES, B. A., OTUN, H. A., SEARLE, R. F. & ROBSON, S. C. 2009. The urokinase plasminogen activator (uPA) system in uterine natural killer cells in the placental bed during early pregnancy. *Placenta,* 30**,** 398-404.

NEGISHI, Y., TAKAHASHI, H., KUWABARA, Y. & TAKESHITA, T. 2018. Innate immune cells in reproduction. *J Obstet Gynaecol Res,* 44**,** 2025-2036.

NISHIMURA, M., UMEDA, K., SUWA, M., FURUOKA, H. & NISHIKAWA, Y. 2017. CCR5 Is Involved in Interruption of Pregnancy in Mice Infected with Toxoplasma gondii during Early Pregnancy. *Infect Immun,* 85.

PALM, F., NANGAKU, M., FASCHING, A., TANAKA, T., NORDQUIST, L., HANSELL, P., KAWAKAMI, T., NISHIJIMA, F. & FUJITA, T. 2010. Uremia induces abnormal oxygen consumption in tubules and aggravates chronic hypoxia of the kidney via oxidative stress. *Am J Physiol Renal Physiol,* 299**,** F380-6.

PAPPAS, G., ROUSSOS, N. & FALAGAS, M. E. 2009. Toxoplasmosis snapshots: global status of Toxoplasma gondii seroprevalence and implications for pregnancy and congenital toxoplasmosis. *Int J Parasitol,* 39**,** 1385-94.

PAQUET, C. & YUDIN, M. H. 2018. No. 285-Toxoplasmosis in Pregnancy: Prevention, Screening, and Treatment. *J Obstet Gynaecol Can,* 40**,** e687-e693.

PARIA, B. C., SONG, H. & DEY, S. K. 2001. Implantation: molecular basis of embryo-uterine dialogue. *Int J Dev Biol,* 45**,** 597-605.

PARKER, S. J., ROBERTS, C. W. & ALEXANDER, J. 1991. CD8+ T cells are the major lymphocyte subpopulation involved in the protective immune response to Toxoplasma gondii in mice. *Clin Exp Immunol,* 84**,** 207-12.

PFAFF, A. W., MOUSLI, M., SÉNÉGAS, A., MARCELLIN, L., TAKIKAWA, O., KLEIN, J. P. & CANDOLFI, E. 2008. Impact of foetus and mother on IFN-gamma-induced indoleamine 2,3-dioxygenase and inducible nitric oxide synthase expression in murine placenta following Toxoplasma gondii infection. *Int J Parasitol,* 38**,** 249-58.

PIFER, R. & YAROVINSKY, F. 2011. Innate responses to Toxoplasma gondii in mice and humans. *Trends Parasitol,* 27**,** 388-93.

PRABHUDAS, M., BONNEY, E., CARON, K., DEY, S., ERLEBACHER, A., FAZLEABAS, A., FISHER, S., GOLOS, T., MATZUK, M., MCCUNE, J. M., MOR, G., SCHULZ, L., SOARES, M., SPENCER, T., STROMINGER, J., WAY, S. S. & YOSHINAGA, K. 2015. Immune mechanisms at the maternal-fetal interface: perspectives and challenges. *Nat Immunol,* 16**,** 328-34.

PUJAL, J.-M., ROURA, S., MUÑOZ-MARMOL, A. M., MATE, J.-L. & BAYES-GENIS, A. 2012. Fetal-maternal interface: A chronicle of allogeneic coexistence. *Chimerism,* 3**,** 18-23.

PUNG, O. J. & LUSTER, M. I. 1986. Toxoplasma gondii: decreased resistance to infection in mice due to estrogen. *Experimental parasitology,* 61**,** 48-56.

PUTIGNANI, L., MANCINELLI, L., DEL CHIERICO, F., MENICHELLA, D., ADLERSTEIN, D., ANGELICI, M., MARANGI, M., BERRILLI, F., CAFFARA, M. & DI REGALBONO, D. F. 2011. Investigation of Toxoplasma gondii presence in farmed shellfish by nested-PCR and real-time PCR fluorescent amplicon generation assay (FLAG). *Experimental parasitology,* 127**,** 409-417.

RED-HORSE, K., ZHOU, Y., GENBACEV, O., PRAKOBPHOL, A., FOULK, R., MCMASTER, M. & FISHER, S. J. 2004. Trophoblast differentiation during embryo implantation and formation of the maternal-fetal interface. *J Clin Invest,* 114**,** 744-54.

REMINGTON, J. S. & KLEIN, J. O. 2001. *Infectious diseases of the fetus and newborn infant*, London: WB Saunders, 2001.

REZENDE-OLIVEIRA, K., SILVA, N. M., MINEO, J. R. & RODRIGUES JUNIOR, V. 2012. Cytokines and chemokines production by mononuclear cells from parturient women after stimulation with live Toxoplasma gondii. *Placenta,* 33**,** 682-7.

RIDDER, L., VAN DER HOOFT, J. J., VERHOEVEN, S., DE VOS, R. C., VAN SCHAIK, R. & VERVOORT, J. 2012. Substructure-based annotation of high-resolution multistage MS(n) spectral trees. *Rapid Commun Mass Spectrom,* 26**,** 2461-71.

ROAGER, H. M. & LICHT, T. R. 2018. Microbial tryptophan catabolites in health and disease. *Nat Commun,* 9**,** 3294.

ROBBINS, J. R., ZELDOVICH, V. B., POUKCHANSKI, A., BOOTHROYD, J. C. & BAKARDJIEV, A. I. 2012. Tissue barriers of the human placenta to infection with Toxoplasma gondii. *Infect Immun,* 80**,** 418-28.

ROBERT-GANGNEUX, F. & DARDÉ, M.-L. 2012. Epidemiology of and diagnostic strategies for toxoplasmosis. *Clinical microbiology reviews,* 25**,** 264-296.

ROBERTS, C. & ALEXANDER, J. 1992. Studies on a murine model of congenital toxoplasmosis: vertical disease transmission only occurs in BALB/c mice infected for the first time during pregnancy. *Parasitology,* 104**,** 19-23.

ROBERTS, C., BREWER, J. & ALEXANDER, J. 1994. Congenital toxoplasmosis in the Balb/c mouse: prevention of vertical disease transmission and fetal death by vaccination. *Vaccine,* 12**,** 1389-1394.

ROBERTS, C. W., WALKER, W. & ALEXANDER, J. 2001. Sex-associated hormones and immunity to protozoan parasites. *Clinical microbiology reviews,* 14**,** 476-488.

ROBERTSON, S. A., MAU, V. J., TREMELLEN, K. P. & SEAMARK, R. F. 1996. Role of high molecular weight seminal vesicle proteins in eliciting the uterine inflammatory response to semen in mice. *J Reprod Fertil,* 107**,** 265-77.

ROBINSON, D. P. & KLEIN, S. L. 2012. Pregnancy and pregnancy-associated hormones alter immune responses and disease pathogenesis. *Hormones and behavior,* 62**,** 263-271.

ROJAS-PIRELA, M., MEDINA, L., ROJAS, M. V., LIEMPI, A. I., CASTILLO, C., PÉREZ-PÉREZ, E., GUERRERO-MUÑOZ, J., ARANEDA, S. & KEMMERLING, U. 2021. Congenital Transmission of Apicomplexan Parasites: A Review. *Front Microbiol,* 12**,** 751648.

RUDZKI, E. N., ANDER, S. E., COOMBS, R. S., ALRUBAYE, H. S., CABO, L. F., BLANK, M. L., GUTIÉRREZ-MELO, N., DUBEY, J. P., COYNE, C. B. & BOYLE, J. P. 2021. Toxoplasma gondii GRA28 Is Required for Placenta-Specific Induction of the Regulatory Chemokine CCL22 in Human and Mouse. *mBio***,** e0159121.

RUTTKIES, C., SCHYMANSKI, E. L., WOLF, S., HOLLENDER, J. & NEUMANN, S. 2016. MetFrag relaunched: incorporating strategies beyond in silico fragmentation. *J Cheminform,* 8**,** 3.

SA, Q., WOODWARD, J. & SUZUKI, Y. 2013. IL-2 produced by CD8+ immune T cells can augment their IFN-γ production independently from their proliferation in the secondary response to an intracellular pathogen. *Journal of immunology (Baltimore, Md. : 1950),* 190**,** 2199-2207.

SAITO, S., NAKASHIMA, A., SHIMA, T. & ITO, M. 2010. Th1/Th2/Th17 and regulatory T-cell paradigm in pregnancy. *American journal of reproductive immunology,* 63**,** 601-610.

SAITO, S., SHIMA, T., NAKASHIMA, A., INADA, K. & YOSHINO, O. 2016. Role of Paternal Antigen-Specific Treg Cells in Successful Implantation. *Am J Reprod Immunol,* 75**,** 310-6.

SÁRI, Z., MIKÓ, E., KOVÁCS, T., BORATKÓ, A., UJLAKI, G., JANKÓ, L., KISS, B., URAY, K. & BAI, P. 2020. Indoxylsulfate, a Metabolite of the Microbiome, Has Cytostatic Effects in Breast Cancer via Activation of AHR and PXR Receptors and Induction of Oxidative Stress. *Cancers (Basel),* 12.

SATPATHY, A. T., WU, X., ALBRING, J. C. & MURPHY, K. M. 2012. Re(de)fining the dendritic cell lineage. *Nat Immunol,* 13**,** 1145-54.

SCHWARTZMAN, J., MAFFIA, A., CRUSIUS, M. E. & BRUNHOFFER, A. 1948. Congenital toxoplasmosis. *The Journal of Pediatrics,* 33**,** 66-73.

SELLECK, E. M., ORCHARD, R. C., LASSEN, K. G., BEATTY, W. L., XAVIER, R. J., LEVINE, B., VIRGIN, H. W. & SIBLEY, L. D. 2015. A Noncanonical Autophagy Pathway Restricts Toxoplasma gondii Growth in a Strain-Specific Manner in IFN-γ-Activated Human Cells. *mBio,* 6**,** e01157-15.

SHAO, D. Y., BAI, X., TONG, M. W., ZHANG, Y. Y., LIU, X. L., ZHOU, Y. H., LI, C., CAI, W., GAO, X., LIU, M. & YANG, Y. 2020. Changes to the gut microbiota in mice induced by infection with Toxoplasma gondii. *Acta Trop,* 203**,** 105301.

SHEPARDSON, L. B., YOUNGNER, S. J., SPEROFF, T. & ROSENTHAL, G. E. 1999. Increased risk of death in patients with do-not-resuscitate orders. *Medical care,* 727-737.

SHIADEH, M. N., NIYYATI, M., FALLAHI, S. & ROSTAMI, A. 2016. Human parasitic protozoan infection to infertility: a systematic review. *Parasitol Res,* 115**,** 469-77.

SICA, A. & MANTOVANI, A. 2012. Macrophage plasticity and polarization: in vivo veritas. *J Clin Invest,* 122**,** 787-95.

SKARIAH, S., MCINTYRE, M. K. & MORDUE, D. G. 2010. Toxoplasma gondii: determinants of tachyzoite to bradyzoite conversion. *Parasitol Res,* 107**,** 253-60.

SNYDER, A. G. & OBERST, A. 2021. The Antisocial Network: Cross Talk Between Cell Death Programs in Host Defense. *Annu Rev Immunol,* 39**,** 77-101.

STAHL, W., KANEDA, Y. & NOGUCHI, T. 1994. Reproductive failure in mice chronically infected withToxoplasma gondii. *Parasitology research,* 80**,** 22-28.

SUMAN, P., MALHOTRA, S. S. & GUPTA, S. K. 2013. LIF-STAT signaling and trophoblast biology. *Jakstat,* 2**,** e25155.

SUMNER, L. W., AMBERG, A., BARRETT, D., BEALE, M. H., BEGER, R., DAYKIN, C. A., FAN, T. W., FIEHN, O., GOODACRE, R., GRIFFIN, J. L., HANKEMEIER, T., HARDY, N., HARNLY, J., HIGASHI, R., KOPKA, J., LANE, A. N., LINDON, J. C., MARRIOTT, P., NICHOLLS, A. W., REILY, M. D., THADEN, J. J. & VIANT, M. R. 2007. Proposed minimum reporting standards for chemical analysis Chemical Analysis Working Group (CAWG) Metabolomics Standards Initiative (MSI). *Metabolomics,* 3**,** 211-221.

SUN, C. Y., HSU, H. H. & WU, M. S. 2013. p-Cresol sulfate and indoxyl sulfate induce similar cellular inflammatory gene expressions in cultured proximal renal tubular cells. *Nephrol Dial Transplant,* 28**,** 70-8.

SVENSSON-ARVELUND, J., MEHTA, R. B., LINDAU, R., MIRRASEKHIAN, E., RODRIGUEZ-MARTINEZ, H., BERG, G., LASH, G. E., JENMALM, M. C. &

ERNERUDH, J. 2015. The human fetal placenta promotes tolerance against the semiallogeneic fetus by inducing regulatory T cells and homeostatic M2 macrophages. *J Immunol,* 194**,** 1534-44.

TAN, X., CAO, X., ZOU, J., SHEN, B., ZHANG, X., LIU, Z., LV, W., TENG, J. & DING, X. 2017. Indoxyl sulfate, a valuable biomarker in chronic kidney disease and dialysis. *Hemodial Int,* 21**,** 161-167.

THULLIEZ, P. 2001. Commentary: efficacy of prenatal treatment for toxoplasmosis: a possibility that cannot be ruled out. *International Journal of Epidemiology,* 30**,** 1315-1316.

TORRES-NAGEL, N., KRAUS, E., BROWN, M. H., TIEFENTHALER, G., MITNACHT, R., WILLIAMS, A. F. & HÜNIG, T. 1992. Differential thymus dependence of rat CD8 isoform expression. *Eur J Immunol,* 22**,** 2841-8.

TORRES, J. A., PASQUARELLI, R. R., BACK, P. S., MOON, A. S. & BRADLEY, P. J. 2021. Identification and Molecular Dissection of IMC32, a Conserved Toxoplasma Inner Membrane Complex Protein That Is Essential for Parasite Replication. *mBio,* 12.

TRAQUETE, F., LUZ, J., CORDEIRO, C., SOUSA SILVA, M. & FERREIRA, A. E. N. 2021. Binary Simplification as an Effective Tool in Metabolomics Data Analysis. *Metabolites,* 11.

VACCA, M., CELANO, G., CALABRESE, F. M., PORTINCASA, P., GOBBETTI, M. & DE ANGELIS, M. 2020. The Controversial Role of Human Gut Lachnospiraceae. *Microorganisms,* 8.

VACCA, P., MONTALDO, E., VITALE, C., CROXATTO, D., MORETTA, L. & MINGARI, M. C. 2015. MSC and innate immune cell interactions: A lesson from human decidua. *Immunol Lett,* 168**,** 170-4.

VELICKY, P., KNÖFLER, M. & POLLHEIMER, J. 2016. Function and control of human invasive trophoblast subtypes: Intrinsic vs. maternal control. *Cell adhesion & migration,* 10**,** 154-162.

WANG, M., CARVER, J. J., PHELAN, V. V., SANCHEZ, L. M., GARG, N., PENG, Y., NGUYEN, D. D., WATROUS, J., KAPONO, C. A., LUZZATTO-KNAAN, T., PORTO, C., BOUSLIMANI, A., MELNIK, A. V., MEEHAN, M. J., LIU, W. T., CRÜSEMANN, M., BOUDREAU, P. D., ESQUENAZI, E., SANDOVAL-CALDERÓN, M., KERSTEN, R. D., PACE, L. A., QUINN, R. A., DUNCAN, K. R., HSU, C. C., FLOROS, D. J., GAVILAN, R. G., KLEIGREWE, K., NORTHEN, T., DUTTON, R. J., PARROT, D., CARLSON, E. E., AIGLE, B., MICHELSEN, C. F.,

JELSBAK, L., SOHLENKAMP, C., PEVZNER, P., EDLUND, A., MCLEAN, J., PIEL, J., MURPHY, B. T., GERWICK, L., LIAW, C. C., YANG, Y. L., HUMPF, H. U., MAANSSON, M., KEYZERS, R. A., SIMS, A. C., JOHNSON, A. R., SIDEBOTTOM, A. M., SEDIO, B. E., KLITGAARD, A., LARSON, C. B., P, C. A. B., TORRES-MENDOZA, D., GONZALEZ, D. J., SILVA, D. B., MARQUES, L. M., DEMARQUE, D. P., POCIUTE, E., O'NEILL, E. C., BRIAND, E., HELFRICH, E. J. N., GRANATOSKY, E. A., GLUKHOV, E., RYFFEL, F., HOUSON, H., MOHIMANI, H., KHARBUSH, J. J., ZENG, Y., VORHOLT, J. A., KURITA, K. L., CHARUSANTI, P., MCPHAIL, K. L., NIELSEN, K. F., VUONG, L., ELFEKI, M., TRAXLER, M. F., ENGENE, N., KOYAMA, N., VINING, O. B., BARIC, R., SILVA, R. R., MASCUCH, S. J., TOMASI, S., JENKINS, S., MACHERLA, V., HOFFMAN, T., AGARWAL, V., WILLIAMS, P. G., DAI, J., NEUPANE, R., GURR, J., RODRÍGUEZ, A. M. C., LAMSA, A., ZHANG, C., DORRESTEIN, K., DUGGAN, B. M., ALMALITI, J., ALLARD, P. M., PHAPALE, P., et al. 2016. Sharing and community curation of mass spectrometry data with Global Natural Products Social Molecular Networking. *Nat Biotechnol,* 34**,** 828-837.

WARNING, J. C., MCCRACKEN, S. A. & MORRIS, J. M. 2011. A balancing act: mechanisms by which the fetus avoids rejection by the maternal immune system. *Reproduction,* 141**,** 715-24.

WATSON, D. G., POMEROY, P. P., AL-TANNAK, N. F. & KENNEDY, M. W. 2020. Stockpiling by pups and self-sacrifice by their fasting mothers observed in birth to weaning serum metabolomes of Atlantic grey seals. *Sci Rep,* 10**,** 7465.

WECKMAN, A. M., MCDONALD, C. R., BAXTER, J. B., FAWZI, W. W., CONROY, A. L. & KAIN, K. C. 2019. Perspective: L-arginine and L-citrulline Supplementation in Pregnancy: A Potential Strategy to Improve Birth Outcomes in Low-Resource Settings. *Adv Nutr,* 10**,** 765-777.

WEI, Y., DING, J., LI, J., CAI, S., LIU, S., HONG, L., YIN, T., ZHANG, Y. & DIAO, L. 2021. Metabolic Reprogramming of Immune Cells at the Maternal-Fetal Interface and the Development of Techniques for Immunometabolism. *Front Immunol,* 12**,** 717014.

WHITLEY, G. S. & CARTWRIGHT, J. E. 2009. Trophoblast-mediated spiral artery remodelling: a role for apoptosis. *J Anat,* 215**,** 21-6.

WILLIAMS, A. J. 2008. Public chemical compound databases. *Curr Opin Drug Discov Devel,* 11**,** 393-404.

WISHART, D. S., FEUNANG, Y. D., MARCU, A., GUO, A. C., LIANG, K., VÁZQUEZ-FRESNO, R., SAJED, T., JOHNSON, D., LI, C., KARU, N., SAYEEDA, Z., LO, E., ASSEMPOUR, N., BERJANSKII, M., SINGHAL, S., ARNDT, D., LIANG, Y., BADRAN, H., GRANT, J., SERRA-CAYUELA, A., LIU, Y., MANDAL, R., NEVEU, V., PON, A., KNOX, C., WILSON, M., MANACH, C. & SCALBERT, A. 2018. HMDB 4.0: the human metabolome database for 2018. *Nucleic Acids Res,* 46**,** D608-d617.

WITOLA, W. H., MUI, E., HARGRAVE, A., LIU, S., HYPOLITE, M., MONTPETIT, A., CAVAILLES, P., BISANZ, C., CESBRON-DELAUW, M. F., FOURNIÉ, G. J. & MCLEOD, R. 2011. NALP1 influences susceptibility to human congenital toxoplasmosis, proinflammatory cytokine response, and fate of Toxoplasma gondii-infected monocytic cells. *Infect Immun,* 79**,** 756-66.

WITTING, M. & BÖCKER, S. 2020. Current status of retention time prediction in metabolite identification. *J Sep Sci,* 43**,** 1746-1754.

WOLF, S., SCHMIDT, S., MÜLLER-HANNEMANN, M. & NEUMANN, S. 2010. In silico fragmentation for computer assisted identification of metabolite mass spectra. *BMC Bioinformatics,* 11**,** 148.

WUJCICKA, W., WILCZYŃSKI, J. & NOWAKOWSKA, D. 2014. Do the placental barrier, parasite genotype and Toll-like receptor polymorphisms contribute to the course of primary infection with various Toxoplasma gondii genotypes in pregnant women? *Eur J Clin Microbiol Infect Dis,* 33**,** 703-9.

XU, X., WANG, Q., DENG, B., WANG, H., DONG, Z., QU, X. & KONG, B. 2012. Monocyte chemoattractant protein-1 secreted by decidual stromal cells inhibits NK cells cytotoxicity by up-regulating expression of SOCS3. *PLoS One,* 7**,** e41869.

YANG, B., WANG, Y. & QIAN, P. Y. 2016. Sensitivity and correlation of hypervariable regions in 16S rRNA genes in phylogenetic analysis. *BMC Bioinformatics,* 17**,** 135.

YAP, G. S. & SHER, A. 1999. Cell-mediated immunity to Toxoplasma gondii: initiation, regulation and effector function. *Immunobiology,* 201**,** 240-247.

YU, L. L., ZHANG, Y. H. & ZHAO, F. X. 2017. Expression of indoleamine 2,3-dioxygenase in pregnant mice correlates with CD4+CD25+Foxp3+ T regulatory cells. *Eur Rev Med Pharmacol Sci,* 21**,** 1722-1728.

ZHANG, D., SUN, X., REN, L., YANG, C., LIU, X., ZHANG, H., JIANG, Y. & HU, X. 2018. Proteomic profiling of human decidual immune proteins during Toxoplasma gondii infection. *J Proteomics,* 186**,** 28-37.

ZHANG, Y., LAI, B. S., JUHAS, M. & ZHANG, Y. 2019. Toxoplasma gondii secretory proteins and their role in invasion and pathogenesis. *Microbiol Res*, 227**,** 126293.

Appendix

Appendix 1

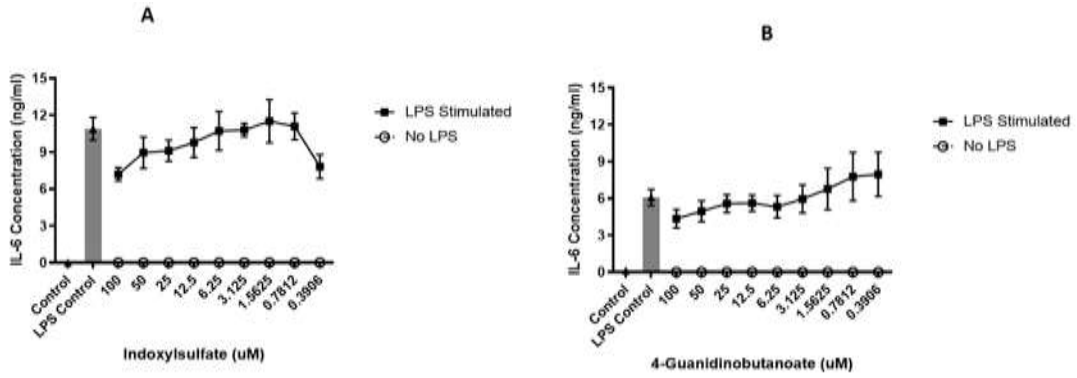

Figure 1. Effects of indoxylsulfate (A) and 4-guanidinobutanoate (B) on the induction of proinflammatory cytokine IL-6.

Table 2.1 List of standards used for the metabolomics analysis chapter 3

Compound Name (MW 70 to 400)	**RT (*min*)**	**Calculated RT (*min*)**
Bilirubin	3.82	5.18
Succinate	8.44	11.83
6-Hydroxydopamine	7.94	11.33
L-Noradrenaline	7.92	11.17
Melatonin	4.64	6.28
Lipoate	4.69	6.21
2-Hydroxybutanoic acid	7.82	10.33
Cis-4-Hydroxy-D-Proline	14.45	20.95
L-Aspartate	14.51	20.06
Lithocholate	4.28	5.17
Betaine	8.54	11.51
Nicotinate	7.53	9.31
L-Proline	12.40	16.53
Uracil	8.32	10.22
Ribothymidine	8.26	10.12
Theobromine	7.23	8.94
Thymidine	7.33	8.83
Hippurate	7.24	8.47
2-Indolecarboxylicacid	7.23	8.46
Creatinine	9.50	11.45
(R)-2-Hydroxyglutarate	11.16	12.79
Kynurenate	7.26	8.43
N6-(L-1,3-Dicarboxypropyl)-L-lysine	15.21	19.00
D-ribose	11.16	13.07
Sarcosine	14.01	17.55
Adenosine	8.85	10.35
N-Formyl-L-methionine	7.23	8.16
Galactarate	16.34	18.34
L-Glutamate	14.27	17.15
creatine	14.20	17.66
Pantothenate	8.52	9.46
Pyridoxamine	11.11	13.48
N-Acetyl-D-Glucosamine	11.45	13.13
Ectoine	12.76	15.81

1,7-Dimethylxanthine	7.23	8.17
Picolinic acid	7.94	8.91
D-Glucuronate	15.16	17.12
Uridine	9.51	10.61
Indolelactate	7.53	8.12
D-Glucosamine	14.05	15.93
D-Glucose 1-phosphate	15.24	17.31
D-Fructose 1,6-bisphosphate	17.22	19.57
D-Ribose 1,5-bisphosphate	16.89	19.35
beta-Alanine	14.79	17.50
D-galactose 1-phosphate	15.35	17.31
Choline	18.87	24.11
5'-Methylthioadenosine	7.26	7.86
ATP	15.62	18.32
glutathione disulfide	16.80	17.58
L-Alanine	14.28	16.31
CTP	17.37	20.30
N-Acetyl-D-glucosamine 6-phosphate	14.60	16.10
6-Phospho-D-gluconate	16.86	17.90
indole-3-acetate	7.53	7.91
L-Serine	15.31	16.54
UDP-N-acetyl-D-glucosamine	14.46	16.00
L-Threonine	14.07	15.23
Malonate	12.18	12.58
2-Phospho-D-glycerate	15.91	16.79
L-Ornithine	22.57	27.38
Xylitol	12.53	12.79
L-Homoserine	14.59	15.74
2-Phospho-D-glycerate	15.98	16.79
Dihydrobiopterin	10.42	10.87
5-methylcytidine	10.33	10.88
D-mannose	13.74	14.40
D-glucose 6-phosphate	16.19	17.27
O-Acetylcarnitine	10.78	11.88
Homogentisate	8.89	8.88

UTP	16.89	18.61
Adenine	9.38	9.69
UDP-glucose	15.62	16.73
3-Phosphoglycerate	16.16	16.47
L-Leucine	10.57	11.04
L-Homocysteine	12.76	13.24
L-Valine	12.22	12.89
D-Sorbitol	13.47	13.00
4-Coumarate	7.88	7.61
D-Glucosamine 6-Phosphate	15.81	16.14
Mannitol	13.57	13.00
Cystathionine	16.58	17.34
Cytidine	11.54	11.43
D-galactose	14.63	14.40
L-isoleucine	11.01	11.14
Homoarginine	25.80	28.81
4-Hydroxyphenylacetaldoxime	7.23	6.87
L-Glutamine	14.59	14.60
ADP	14.49	14.59
L-Phenylalanine	10.07	9.97
Cytosine	10.90	10.57
(R)-Malate	15.24	14.31
CDP	16.25	16.29
Citrate	17.26	15.80
Inosine	10.53	9.97
Isocitrate	17.61	16.08
Citramalate	14.13	13.06
Pyridoxal	7.94	7.30
AMP	13.31	12.80
N-Acetyl-L-aspartate	14.04	12.92
Guanosine	12.10	11.45
Biotin	8.62	7.82
d-rhamnose	13.47	12.75
N-Acetyl-D-mannosamine	13.95	13.13
N(pi)-Methyl-L-histidine	12.64	12.34

L-Methionine	11.33	10.92
Allantoin	13.08	12.00
beta-D-Fucose	13.57	12.75
L-Histidine	14.39	13.86
Riboflavin	8.39	7.47
UDP	15.67	14.99
alloxanthine	10.22	9.20
CMP	15.24	14.24
GDP	17.07	16.12
N-Acetyl-L-glutamate	13.51	11.83
L-Cystine	15.80	14.71
L-Kynurenine	10.67	9.61
Acetylcysteine	11.83	10.37
dAMP	12.36	11.14
UMP	14.57	13.14
L-Tryptophan	11.25	10.20
Phosphoenolpyruvate	16.67	14.87
Taurine	14.33	13.20
D-fructose 6-phosphate	15.34	13.35
Sucrose	14.63	12.75
D-Xylulose 5-phosphate	15.12	13.11
GMP	16.06	14.27
D-Ribulose 5-phosphate	15.16	13.11
Hypoxanthine	9.87	8.41
L-Lysine	24.08	23.71
L-Citrulline	15.45	13.50
carnosine	15.24	13.35
Cis-Aconitate	18.08	14.93
Xanthine	10.98	9.18
FAD	11.01	9.16
Glycerone phosphate	14.75	12.51
S-Adenosyl-L-homocysteine	13.26	11.34
N6-Methyl-L-lysine	22.85	21.66
Xanthosine	11.65	9.62
Imidazole-4-acetate	12.85	10.42

IMP	14.88	12.28
Biopterin	11.09	8.85
5-Hydroxyindoleacetate	10.55	8.32
L-Tyrosine	12.60	10.24
dAMP	13.95	11.14
L-Arginine	25.51	22.39
Mesaconate	14.52	11.12
Caffeate	10.86	8.17
Phthalate	13.07	9.81
5-Aminolevulinate	13.36	10.03
D-3-hydroxy-butyrate	14.52	10.86
N6-Acetyl-L-Lysine	14.65	11.22
Thiamin	19.42	16.09
D-Glucuronolactone	15.62	11.80
Acetoacetate	13.47	9.40
Ne,Ne dimethyllysine	20.95	16.14
Ethanolamine phosphate	15.45	10.37
N6,N6,N6-Trimethyl-L-lysine	21.57	15.69
Amphetamine	17.07	10.45
1-(4-Hydroxyphenyl)-2-aminoethanol	19.05	10.86
1H-Imidazole-4-ethanamine	25.61	14.88
L-Metanephrine	17.50	9.64
Folate	15.89	7.82
1-Phenylethylamine	19.71	10.90

Table 2.2 List of standards used for the metabolomics analysis chapter 4

Compound Name (MW 70 to 400)	**RT (*min*)**	**Calculated RT (*min*)**
Phenylhydrazine	4.62	6.55
L-Aspartate	12.06	17.31
trans-4-Hydroxy-L-proline	11.73	16.25
Phenylpyruvate	4.56	6.26
Melatonin	4.09	5.38
Taurocholate	4.15	5.41
pyrophosphate	13.24	17.23
Mercaptoethanol	6.23	8.01
2-Oxoglutarate	7.68	10.03
Lipoate	4.36	5.59
Glutathione disulfide	12.70	15.92
Phenylacetylglycine	5.50	6.96
L-Glutamate	11.84	14.82
D-Glucono-1,4-lactone	7.77	9.50
D-Galactarate	13.33	16.53
2-phospho-D-glycerate	12.75	15.66
2-Aminobutan-4-olide	6.40	7.77
Orthophosphate	12.44	15.06
L-Proline	10.72	13.00
meso-2,6-Diaminoheptanedioate	13.51	16.24
L-Ornithine	16.40	19.46
3-Phospho-D-glycerate	12.87	15.39
thymine	6.77	7.85
lipoamide	4.35	5.00
Thymidine	6.26	7.20
Betaine	8.54	9.99
D-glucose 6-phosphate	12.80	14.60
(R)-Lactate	9.13	10.47
Glycine	12.56	14.24

Cis-4-Hydroxy-D-Proline	14.45	16.25
Orotate	9.64	10.89
5'-Methylthioadenosine	5.85	6.45
Creatinine	8.70	9.72
L-Cystathionine	12.90	14.19
D-Galacturonate	12.93	14.30
D-Gluconic acid	11.69	12.75
Nicotinamide	6.29	6.84
D-ribose 5-phosphate	12.25	13.30
L-Alanine	12.02	13.12
D-Threose	9.20	9.93
N6-(L-1,3-Dicarboxypropyl)-L-lysine	15.21	16.32
L-Serine	12.62	13.58
Nicotinate	7.44	8.07
L-2-Aminoadipate	11.89	12.85
(R)-3-Hydroxybutanoate	8.73	9.36
Isonicotinic acid	7.52	8.07
cis-Aconitate	13.66	14.92
L-Threonine	11.83	12.48
Pyruvate	8.14	8.65
L-homoserine	12.10	12.70
N-Acetylneuraminate	11.11	11.65
5-Oxoproline	9.49	10.05
Phosphoenolpyruvate	13.25	13.98
2-Methylcitrate	13.25	14.16
Ala-Gly	10.47	10.94
gamma-L-Glutamyl-L-cysteine	11.52	11.97
Pyridoxine	7.25	7.48
Adenosine	7.98	8.18
pyrazinoate	8.48	8.78
L-Rhamnose	9.84	10.04
3-(4-Hydroxyphenyl)pyruvate	6.81	6.97
Betaine	9.66	9.99
L-Cysteate	12.80	13.22
Orotidine	10.88	11.15

(S)-Malate	12.74	13.17
CMP	11.94	11.97
Deoxyadenosine	7.25	7.27
N-Acetyl-D-glucosamine	10.13	10.13
Deoxyuridine	7.49	7.51
6-Methylaminopurine	7.07	7.09
sn-Glycerol 3-phosphate	11.77	11.75
Glycylglycine	11.61	11.68
D-Glucosamine	12.14	12.09
O-Acetylcarnitine	9.28	9.22
UMP	11.37	11.34
4-(beta-Acetylaminoethyl)imidazole	6.52	6.49
Pantothenate	8.13	8.08
AMP	10.96	10.88
GMP	12.26	12.12
L-Valine	10.55	10.48
L-Cystine	12.53	12.42
L-Lysine	17.42	16.93
Thymidine	7.33	7.20
D-Ribose	10.46	10.25
D-Erythrose	10.12	9.93
Oxalate	13.87	13.91
4-Aminobutanoate	12.25	11.97
Thiopurine S-methylether	5.79	5.66
L-Leucine	9.33	9.09
L-Glutamine	12.02	11.67
MOPS	7.01	6.82
Choline	16.61	15.83
Eflornithine	11.00	10.41
(R)-2-Hydroxyglutarate	12.19	11.75
Uridine	8.94	8.48
4-Trimethylammoniobutanoate	10.77	10.16
D-Arabinose	11.60	10.93
Homocystine	12.53	11.74
Maleic acid	11.50	11.04

N(pi)-Methyl-L-histidine	10.62	9.97
N-Acetylornithine	11.95	11.13
N-Acetylglutamine	9.50	8.88
D-Glucuronolactone	9.92	9.27
L-Phenylalanine	8.89	8.30
N-acetyl-L-glutamate	11.43	10.78
dAMP	10.35	9.59
Picolinic acid	8.29	7.77
D-Fructose 6-phosphate	12.35	11.33
L-Asparagine	12.24	11.36
Selenomethionine	9.77	9.02
Methylcysteine	10.24	9.47
Adenine	8.52	7.86
L-Carnitine	10.89	10.01
Malonate	12.63	11.72
dCMP	11.57	10.50
D-glucose	12.32	11.15
L-isoleucine	10.07	9.15
L-Methionine	9.88	8.92
dUMP	11.11	9.97
Fumarate	12.86	11.76
D-Fructose	11.53	10.22
Acetylcholine	12.84	11.32
N2-Acetyl-L-lysine	11.77	10.35
FMN	9.54	8.44
Choline phosphate	11.51	10.08
Succinate	12.22	10.96
L-Arginine	18.79	16.26
L-Citrulline	12.52	10.90
riboflavin	7.54	6.59
Imidazole-4-acetate	10.23	8.97
succinate semialdehyde	9.26	8.10
Inosine	9.58	8.30
Pyridoxal	7.52	6.52
Cytidine	10.34	8.89

L-Kynurenine	9.40	8.09
4-Coumarate	7.97	6.91
dIMP	11.31	9.77
cytosine	9.99	8.57
Taurine	12.52	10.73
S-Adenosyl-L-homocysteine	10.68	9.03
Itaconate	12.23	10.59
Adenosine 2',5'-bisphosphate	12.35	10.83
Maltose	12.59	10.53
Methylmalonate	12.13	10.39
Phenolsulfonphthalein	5.61	4.68
L-Gulono-1,4-lactone	11.45	9.50
3-Hydroxyphenylacetate	8.75	7.33
allantoin	12.41	10.33
Guanosine	10.91	8.99
sucrose	12.11	9.69
Hypoxanthine	9.23	7.33
L-Tyrosine	11.06	8.71
1-Aminopropan-2-ol	17.29	13.37
sn-glycero-3-Phosphocholine	11.36	8.70
O-Acetyl-L-serine	11.46	8.89
Phthalate	11.82	9.21
HEPES	9.38	7.17
Ethanolamine phosphate	12.20	9.21
5-Aminolevulinate	11.29	8.54
Xanthine	10.39	7.87
Guanine	10.87	8.15
3,4-Dihydroxyphenylacetate	11.72	7.93
Folate	12.82	7.80